

LIVING SHORELINES REEF BALL DESIGN: SHELL COVER, RUGOSITY, AND TIDAL ELEVATION IMPACT FAUNAL RECRUITMENT IN SOUTHERN CALIFORNIA, USA

A Thesis By

BRYCE PEROG

ORCID ID: 0000-0002-8239-7982

California State University, Fullerton
Spring, 2021

In partial fulfillment of the degree:

Master of Science, Biology

Department:

Department of Biological Science

Committee:

Danielle C. Zacherl, Department of Biological Science, Chair
Douglas J. Eernisse, Department of Biological Science
Ryan P. Walter, Department of Biological Science

DOI:

10.5281/zenodo.4750817

Keywords:

living shoreline, eco-engineering, reef ball, *Ostrea lurida*, *Crassostrea gigas*, rugosity

Abstract:

Estuaries have been armored with artificial habitat to protect coastal infrastructure from erosion, but armoring may have negative ecological impacts. Other shoreline protection strategies, such as eco-engineered seawalls and living shorelines, offer more natural, rugose substrata to native species while limiting coastal erosion. The Port of San Diego plans to build a living shoreline using concrete reef balls that recruit the native oyster, *Ostrea lurida*, but the Port wants to avoid recruitment of non-indigenous species (NIS), especially the non-indigenous oyster, *Crassostrea gigas*. I modified concrete tiles that acted as proxies for reef balls with added shell cover and rugosity to determine if there is a treatment that can achieve these goals. I deployed six treatment types embedded into 15 x 15 cm concrete tiles: two with surface shell (100% cover of crushed or large shell fragments), two without shell (smooth or rough concrete), and two reference treatments (50% shell cover and terracotta). Seven replicates per treatment were deployed at two sites in San Diego Bay and one site in Newport Bay, California, USA, at 0 and 0.6 m Mean Lower Low Water (MLLW) from May to September 2018. I used three-way ANOVAs, ANCOVAs, and PERMANOVAs to test for the effects of tile orientation, tidal elevation, shell cover, and rugosity on the recruitment of oysters and other fauna. *O. lurida* recruited in higher abundance and generally higher percent cover than *C. gigas* onto all treatments across all sites at 0 m MLLW and treatments that combined 100% shell cover with high rugosity at two of three sites at 0.6 m MLLW, a tidal elevation to which *O. lurida* rarely recruits. Some NIS recruited in lower abundance to 100% shell treatments and/or rugose treatments, although the effects were not consistent across species. Recruitment strength of both native and NIS varied across sites and treatments and should be tested on a site-specific basis prior to reef ball deployment, but I suggest projects that utilize reef balls in living shoreline designs in southern California should generally add shell cover and rugosity to the concrete to favor native species and discourage NIS.

TABLE OF CONTENTS

ACKNOWLEDGMENTS.....	iv
Chapter	
1. NATIVE AND NON-INDIGENOUS OYSTER RECRUITMENT	1
Introduction	1
Impact to Estuaries Over Time	1
Shoreline Armoring Alternatives	1
Living Shorelines Using Oyster Habitat.....	2
Southern California.....	3
Shell Cover.....	5
Rugosity.....	5
Surface Orientation	6
Tidal Elevation	7
Research Gap	7
Aim	8
Materials and Methods	8
Experimental Design	8
Tile Deployment and Collection.....	9
Statistical Analysis.....	12
Results.....	13
Summary	13
Settlement, Growth, and Survival.....	14
Mud Accretion	14
Effects of Tile Orientation, Tidal Elevation, and Treatment.....	15
Effects of Tidal Elevation, Shell Cover, and Rugosity	17
Discussion.....	23
Tile Orientation	24
Tidal Elevation	25
Shell Cover and Rugosity	27
Other Considerations	29
Management Implications	31
2. NATIVE AND NON-INDIGENOUS SPECIES RECRUITMENT.....	32
Introduction	32
Estuarine Ecosystems.....	32
Non-indigenous Species	32
Southern California.....	34
Methods	35
Soft-bodied Fauna	35
Canopy-forming Algae and Fauna	35
Presence/absence.....	36
Identification of Sessile Fauna	37
Space-dominating Fauna	38
Statistical Analysis.....	38
Results.....	40
Species Richness.....	40
Community Composition	42
Tunicate Abundance	44

Biomass.....	45
Major Space Occupiers Summary.....	46
Cryptogenic Space Occupier.....	46
NIS Space Occupiers	47
Native Space Occupier.....	48
Discussion.....	48
Tidal Elevation	49
Shell Cover	50
Rugosity.....	51
Other Considerations	53
Management Implications	55
APPENDICES	56
A: TABLES AND FIGURES	56
B: SUPPLEMENTARY MATERIAL.....	118
REFERENCES.....	140

ACKNOWLEDGMENTS

This master's thesis is a culmination of the work of a large team of students, volunteers, and technical advisors that helped me to generate this large and fascinating dataset. Their contributions were key in the progression of this project and are listed in table format below. I am grateful for my committee members for their advice and support, my fellow Zacherl lab members for their friendship and encouragement, and I especially thank my advisor, Dr. Danielle Zacherl, for her mentorship in leading me to not only complete this degree, but to serve as a key contributor to provide me with opportunities to grow personally and professionally. Funding was provided via a subcontract with Merkel & Associates, Inc, with flow-through funds provided by Port of San Diego. Scholarships were awarded by the California State University, Fullerton (CSUF) Biology Department from Coppel Graduate Science Award, A. James Diefenderfer Memorial Scholarship, and the Rachel Carson Scholarship in Conservation Biology.

Name	Affiliation	Acknowledgement
Tyffany Alli	Mt. San Antonio College	Processing data
Kelvin Barwick	Orange County Sanitation District	Taxonomic expertise
Chelsea Bowers	CSUF	Processing data
Kelly Donovan	CSUF	Building map of sites
Katheryn Eckholdt	CSUF	Processing data
Doug Eernisse	CSUF	Committee member
Ben Ferraro	Orange County Sanitation District	Taxonomic expertise
Ty Frantz	CSUF	Thesis peer review
Ruth Gatica	Cypress College	Processing data
Salvador Gutierrez	Mt. San Antonio College, Project RAISE	Processing data
Leslie Harris	Natural History Museum of Los Angeles County	Taxonomic expertise
Chris Hong	Troy High School (internship)	Processing data
Skyler Keyes	CSUF	Processing data
Gretchen Lambert	Southern California Association of Marine Invertebrate Taxonomists	Taxonomic expertise
Ryan Lee	Troy High School (internship)	Processing data
Sabrina Li	Walnut High School (SCAS Junior Scholar)	Processing data
Carmen Lopez	CSUF	Processing data

Name	Affiliation	Acknowledgement
Fernando Marquez	CSUF	Processing data
Megan McCuller	North Carolina Museum of Natural Sciences	Taxonomic expertise
Marie Nydam	Soka University	Taxonomic expertise
Bruno Pernet	California State University, Long Beach	Taxonomic expertise
Leeza-Marie Rodriguez	CSUF	Processing data
Mayra Rodriguez	CSUF	Processing data
Sara Sadek	CSUF	Processing data
Nick Salgado-Stanley	Troy High School (internship)	Processing data
Sabina Simjee	CSUF	Processing data
Eric Stucker	CSUF	Processing data
Hallie Takenaga	CSUF	Processing data
Jesus Torres	Cypress College, Project RAISE	Processing data
Rick Torres	CSUF	Processing data
Thomas Turner	University of California, Santa Barbara	Taxonomic expertise
Sean Walker	CSUF	Statistics expertise
Ryan Walter	CSUF	Committee member
Christine Whitcraft	California State University, Long Beach	Statistics expertise
Marah Wolf	CSUF	Processing data
Danielle Zacherl	CSUF	Advisor

CHAPTER 1

NATIVE AND NON-INDIGENOUS OYSTER RECRUITMENT

Introduction

Impact to Estuaries Over Time

Coastal development and rising sea levels have caused estuarine shorelines to rapidly erode. When strong El Niño-Southern Oscillation storms damaged shorelines in the late 1900s, resource managers in California, USA, increased their use of hard armor to protect the coastline from erosion (Griggs, 2009). Shoreline armoring (e.g., via seawalls, rip rap, groins, and revetments) is a popular method to protect coastal infrastructure (Gittman et al., 2015), but can have negative repercussions on the environment. Hard armor is deployed to stop erosion but, perversely, accelerates down-shore erosion (Bozek & Burdick, 2005), reduces species richness and abundance (Seitz et al., 2006), and may allow non-indigenous species to establish (Airoidi et al., 2015; Glasby et al., 2007; Tyrrell & Byers, 2007). Today in southern California, as much as 33% of the open-coast shoreline is armored in urbanized counties (Griggs & Patsch, 2019), and the percentage of shoreline armored is even higher in sheltered areas such as estuaries (75-100%) (Gittman et al., 2015).

Shoreline Armoring Alternatives

There are more environmentally friendly alternatives than hard armor when building infrastructure to protect shorelines from erosion. One alternative to hard armoring is to utilize a natural habitat, such as an eelgrass bed or an oyster reef, to mitigate for erosion while also provisioning more habitat to native species; this solution is called a “living shoreline” (NOAA, 2015). There is little published information about the long-term success of living shorelines since most projects are less than 5 years old (Smith et al., 2020). A living shoreline can be built using materials ranging from all-natural material, termed “green” (e.g., planting cordgrass), to a mix of both man-made and natural material, termed “green/grey hybrid” (e.g., rock sills below cordgrass) (SAGE, n.d.).

There is also an effort to “green” the “grey” traditional hard armoring infrastructure (e.g., seawalls, rip rap) (NOAA, 2015) through ecological engineering, or “eco-engineering.” Project

managers aim to make existing hard armor or newly deployed hard armor more environmentally friendly to recruit algae, invertebrates, and fish while maintaining its integrity. Some eco-engineering examples include adding water retention features (e.g., tide pools) to hard armor to improve habitat value (Chapman & Blockley, 2009; Firth et al., 2016, Ostalé-Valriberas et al., 2018, Perkol-Finkel & Sella, 2015), adding surface complexity, or rugosity, to hard armor so that it better represents natural habitat (Morris et al., 2017; Perkol-Finkel & Sella, 2015; Strain et al., 2021), and changing the composition of concrete to reduce the carbon footprint (Dennis et al., 2018) and attract more native larvae (Latta & Boyer, 2015; Perkol-Finkel & Sella, 2014). Projects that use green/grey living shoreline approaches can be even more “greened” by incorporating concepts from eco-engineering research to better recruit native species.

Living Shorelines Using Oyster Habitat

Oyster habitat is often chosen in living shorelines designs (Smith et al., 2020) because oyster reef habitat is severely diminished globally (Beck et al., 2011), oysters may have the ability to outpace sea level rise (Rodriguez et al., 2014), and oysters provide an additional ecosystem function of filtering water. Traditional oyster restoration techniques use stacked oyster shell bags or loose oyster shell piled onto the mudflat as habitat to recruit oysters (Chauvin, 2018; Chowdhury et al., 2019; Scyphers et al., 2015). There are green/grey hybrid models that also recruit oysters, such reef balls (concrete molded into domes with holes to allow for recruitment of fauna) (Latta & Boyer, 2015; Scyphers et al., 2015, Smith et al., 2018), that have other benefits, such as a stronger ability to protect shorelines from wave action and storms (Smith et al., 2018) and conserve limited oyster shell (Henderson et al., unpublished data).

Coastal managers on the U.S. West Coast are exploring building living shorelines using a variety of techniques ranging from placing loose (Groth, 2010) or bagged oyster shell (Fuentes et al. 2020, Latta & Boyer, 2015, Zacherl et al., 2015) on mudflats or by placing reef balls (Latta & Boyer, 2015); each technique is meant to target the recruitment of native Olympia oysters, *Ostrea lurida*, to restore its populations and ecosystem benefits. *O. lurida* are the only native oyster to the U.S. West

Coast and once existed in such high abundances that they built beds on the shorelines of estuaries (Bonnot, 1935; Dimick et al., 1941; Gilbert, 1889; Hittell, 1882). Culling *O. lurida* in the 1800s and early 1900s for aquaculture degraded the low-relief oyster beds (MacKenzie, 1997) because *O. lurida* populations could not keep pace with demand due to its small size, thin body, and slow growth (Barrett, 1963). Significant declines in harvestable *O. lurida* led to the introduction of *Crassostrea virginica* from the U.S. East Coast and *Crassostrea gigas* from Japan to supplement the U.S. West Coast aquaculture industry (Bonnot, 1935; Barrett, 1963; MacKenzie, 1997). *O. lurida* beds never recovered, and *O. lurida* today are considered “functionally extinct” (Zu Ermgassen et al., 2012). Remnant populations are present in most estuaries along its historic range and feral or otherwise introduced *C. gigas* are found in most estuaries along their distribution (Polson & Zacherl, 2009) and can exist in high abundances, especially in the Pacific Northwest and southern California (Kornbluth et al., unpublished data). *C. gigas* are global non-indigenous species and are often considered invasive; they cohabituate estuaries with native foundation species, including seagrass (Wagner et al., 2012), worms (Dubois et al., 2006; Green & Crowe, 2013), mussels (Diederich, 2005, Eschweiler & Christensen, 2011; Green & Crowe, 2014; Markert et al., 2009) and other oyster species (Tronske et al., 2018; Vozzo et al., 2021). Their impact on the various estuarine communities has been documented as positive (Green & Crowe, 2014; Markert et al., 2009), negative (Green & Crowe, 2013; Guy et al., 2018; Wilkie et al., 2012), or negligible (Zwerschke et al., 2016; Wagner et al., 2012). *C. gigas* impact on native *O. lurida* populations and overall community structure remains unknown in California.

Southern California

San Diego Bay, the largest estuary in southern California and the site of the largest naval base in the world (USDN/NFECS & Port of San Diego, 2013), has 75.5% grey infrastructure along its coastline (Perog et al., unpublished data). The U.S. Department of the Navy, Naval Facilities Engineering Command Southwest (USDN/NFECS) and Port of San Diego determined that climate change and invasive species were the newest drivers of change in San Diego Bay, and defined goals

in their Natural Resource Plan (2013) to limit the impact of these factors. Their highest priorities for the future of San Diego Bay include improving the habitat value of infrastructure without sacrificing efficacy, planning for sea level rise, restoring native species, and limiting the spread of invasive species. In 2013, the Port of San Diego initiated planning to build a living shoreline in San Diego Bay, California, using reef balls that target native *O. lurida* recruitment at sites that have erosional profiles and consistent settlement of *O. lurida*, but were cautious about providing habitat to non-indigenous species, especially *C. gigas*.

Henderson et al. (2015, 2018) completed studies that investigated the efficacy of a living shoreline using different materials at different tidal elevations to meet the project goals to limit shoreline erosion by attenuating wind-driven wave action while simultaneously recruiting *O. lurida*. Reef balls were determined the best option since shell is limited in San Diego, heavy natural cobble and man-made rock were less desired, and reef balls made of baycrete (concrete mixed with native material, including locally sourced sand and shell) have been successful in San Francisco (Henderson et al., unpublished data; Latta & Boyer, 2015). However, *C. gigas* has been eradicated in San Francisco Bay (Cohen & Weinstein, 2008) while estuaries in southern California have established *C. gigas* populations (Crooks et al., 2015; Polson & Zacherl, 2009), making their recruitment onto living shorelines structures of significant concern.

Living shorelines using a green/grey hybrid concrete reef ball design can be eco-engineered by adding rugosity to the surface or by changing the concrete composition via oyster shell additions. These modifications may improve recruitment of native estuarine organisms, including native oysters, by mimicking natural substrata. For example, addition of shell cover may make unnatural substrata more natural and attract larvae. Recruitment dynamics of larvae on shell compared to other substrata is largely unknown; epifaunal diversity has been quantified on the shells of living species, but the findings are often not compared directly to other habitats (Bell, 2005; Guy et al., 2018; Summerhayes et al., 2009; Wilkie et al., 2012; Zwerschke et al., 2016). The few studies that have compared shell to

artificial substrata document different community assemblages (Aikins & Kikuchi, 2011; Connell, 2001) and bivalve recruitment (Hanlon et al., 2018).

Shell Cover

Oysters are aggregating species and may prefer to settle on oyster shell over other hard substrata. *O. lurida* does not show a preference settling onto live or dead *O. lurida* or *C. gigas* shell (Sawyer, 2011), but *O. lurida* recruits in higher abundances to shell compared to gravel (White et al., 2009), so it is a viable alternative to use *C. gigas* shell procured from the aquaculture industry in an *O. lurida* living shoreline context. *C. gigas* settlers prefer to settle onto conspecifics over mussel shell and settle in the same high abundance onto live or dead shell (Diederich, 2005). Both oyster species may therefore recruit in higher abundances to shelled treatments compared to unshelled treatments. In a living shoreline study within San Francisco Bay, CA, *O. lurida* initially recruited in higher densities to bags of *C. gigas* shell compared to reef balls made of baycrete (concrete mixed with natural material from the bay), but the densities on both substrata were >1,000 oysters/m², which is significantly higher compared to *O. lurida* background densities in California (Latta & Boyer, 2015).

Rugosity

Rugosity is another feature that can be manipulated on reef balls. The effect of rugosity on recruitment of marine species has been explored in multiple communities, including estuaries (Pomerat & Weiss, 1946), breakwaters (Burt et al., 2011), coral habitats (Carleton & Sammarco, 1987; Luckhurst & Luckhurst, 1978; Whalan et al., 2015), and oyster reefs (Hill & Weissburg, 2013). Crevices from rugose structures in the intertidal zone can provide protection from predators (Dittel et al., 1996), more surface available for recruitment, a lower maximum temperature, shaded area, and higher humidity compared to flat surfaces (Strain et al., 2020). Sessile invertebrates recruit in higher abundances to rugose tiles (Hanlon et al., 2018; Strain et al., 2021). Mussel, tunicate, hydroid, and barnacle larvae prefer to settle onto more rugose substrata (Crisp & Barnes, 1954; Dean, 1981; Walters & Wetthey, 1996), but this preference may vary across species. For example, while some

barnacles prefer rugose surfaces, *Balanus improvisus*, a global fouler in estuaries (Fofonoff et al., 2018), prefers to settle onto smooth substrata (Berntsson et al., 2000).

Oysters may also prefer to settle onto more rugose surfaces. Hopkins (1935) speculated that greater *O. lurida* settlement onto concrete spat collectors versus glass plates may be due to the irregular surfaces of the concrete. Schaefer (1937) repeated Hopkins' experiment with *C. gigas* and also found that the rougher surface of concrete may have encouraged *C. gigas* settlement, although both researchers were merely speculating. Rugose live barnacles facilitate *Crassostrea sp.* settlement (Barnes et al., 2010), specifically *C. gigas* (Diederich, 2005), but the first study to directly study the effect of rugosity on *C. gigas* recruitment was Vozzo et al. (2021); researchers tested concrete tiles in a full factorial design with rugosity (high, low) and seeded oysters (present, absent) and found that *C. gigas* recruited in higher abundance to all seeded and rugose treatments compared to smooth concrete tiles. Based upon its large size on smooth seawalls and boulders, however, flat surfaces may allow adult *C. gigas* to maximize its ability to grow large and still adhere to the substratum, while *O. lurida* can have a small attachment to the surface and may grow best on rougher substrata (personal observation). Limited existing experimental evidence exploring the effects of rugosity on these two oyster species leaves open the question whether rugosity might be manipulated in a way that could favor *O. lurida* recruitment relative to *C. gigas*. In southern California specifically, the effect of substratum rugosity on the recruitment of oysters, particularly relative to one another, and on the recruitment of their associated communities remains completely unexplored.

Surface Orientation

Reef balls have multiple orientations of the substratum available for larvae to settle upon, including horizontal (upperside and underside) and vertical orientations, both with varying degrees. Orientation of the substratum is an important factor in larval recruitment (Holliday, 1996; McKinney & McKinney, 2002), including for oysters (Hopkins, 1935; Schaefer, 1937). *O. lurida* larvae settle in higher abundances to the underside of surfaces and rarely settle on surfaces facing upward (Hopkins, 1935; Sawyer, 2011; Torres et al., unpublished data). Past recruitment studies reflect this pattern

(Latta & Boyer, 2015; Torres et al., unpublished data). *C. gigas* also settles (Schaefer, 1937) and recruits (Sawyer 2011; Torres et al., unpublished data data) in higher abundances to the underside of substrata, but Schaefer (1937) concluded that this preference by *C. gigas* was not as strong as for *O. lurida*. Sedimentation stress is thought to be the biggest stressor in the estuarine intertidal for *O. lurida* (Wasson et al., 2016), so recruitment to the underside of surfaces may allow oysters and other larvae to escape this stressor.

Tidal Elevation

O. lurida and *C. gigas* in San Diego Bay, CA settle and recruit in a zonation pattern across tidal elevations (Torres et al., unpublished data) that is also reflected in adult population distributions (Tronske et al., 2018). *O. lurida* settles in highest abundances to terracotta tiles deployed lower in the intertidal (approximately -0.3 m to +0.3 m) while *C. gigas* settles in highest abundances to terracotta tiles deployed higher in the intertidal (approximately +0.3 m to +0.6 m Mean Lower Low Water (MLLW) (Torres et al., unpublished data). The prospective Port of San Diego living shorelines design includes baycrete reef balls deployed in the intertidal zone that are approximately 0.6 m high and thus would span across a range of intertidal elevations. If reef balls are placed lower in the intertidal zone, it would recruit mostly *O. lurida*, while a reef ball at a higher tidal elevation would recruit mostly *C. gigas*. It is critical to understand the effect of various baycrete designs at multiple tidal elevations under consideration prior to deployment to maximize the recruitment success of native oysters while minimizing that of the non-indigenous oyster species.

Research Gap

Both oyster species have recruited higher abundance to rugose surfaces (Barnes et al., 2010; Vozzo et al., 2021) and shell cover (Sawyer, 2011; Diederich, 2005; White et al., 2009), but it is unknown if a combination of these factors will benefit one species more than the other. For example, *O. lurida* settles in much higher abundances to the underside of tiles than the upperside of tiles (Hopkins, 1935), but the preference for the underside is not as strong for *C. gigas* (Schaefer, 1937). Therefore, on the uppersides of surfaces, *C. gigas* can dominate the space even though it is not its

preferred habitat. Recruitment of larvae can be context-dependent, and recruitment patterns found may not persist across estuaries (Strain et al., 2021). Furthermore, there is little research on the U.S. West Coast of *O. lurida* and *C. gigas* recruitment onto substrata of varying shell cover and rugosity, and information about their recruitment to these surfaces on a local scale can help inform local projects.

Aim

I explored modifying the surface of concrete tiles that act as proxies for reef balls by adding shell and rugosity in various combinations to identify treatments that encourage *O. lurida* recruitment and discourage *C. gigas* recruitment in San Diego Bay, CA. Additionally, I aimed to uncover a treatment that favors *O. lurida* recruitment to higher tidal elevations compared to that which they would typically recruit to understand the effect of reef balls deployed at higher tidal elevations (as outlined in the Study Design in Henderson et al., 2015). I tested the hypotheses that (1) *O. lurida* and *C. gigas* will recruit in higher percent cover to the underside of tiles compared to the upperside of tiles, (2) *O. lurida* will recruit in higher abundance and percent cover compared to *C. gigas* at lower tidal elevations, and the pattern will be reversed at higher tidal elevations, (3) *O. lurida* and *C. gigas* will recruit in higher abundances and percent cover to substrata with oyster shell cover compared to substrata with no shell cover, and (4) onto rugose surfaces versus smoother surfaces.

Materials and Methods

Experimental Design

I worked with Merkel & Associates, Inc., to construct concrete tiles of varying rugosity (high, low) and shell cover (0%, 100%) in a full factorial design with seven replicates per treatment and two reference treatments (50% cover, terracotta tile, Figure 1). Low rugosity with 0% shell cover is hereinafter referred to as “Smooth,” low rugosity with 100% shell cover is referred to as “Fine,” high rugosity with 0% shell cover is referred to as “Rough,” and high rugosity with 100% shell cover is referred to as “Full.” The 50% shell treatment is referred to as “Half” and serves as an intermediate of rugosity and shell cover, and terracotta is referred to as “Tile” and allows comparison of results from

this study with archived oyster recruitment data on terracotta tiles from the same location from 2015-2018 in San Diego Bay, California, USA. Terracotta tiles were glued together using marine epoxy with the smooth side facing outwards and plastic mesh in-between the tiles. Marine epoxy holding terracotta tiles together failed twice (one bottom tile was lost at E Street at 0 m MLLW, one top tile was lost at E Street). Subsequent results reflect the reduction in sample size for Tile. Cleaned *C. gigas* shell was procured from Carlsbad Aquafarm, Carlsbad, California, USA, to build the shelled treatments. All tiles were built with Portland cement and reinforced with fiberglass by Merkel & Associates, Inc. Shelled treatments were built by pouring concrete over crushed shell (finely crushed for low rugosity treatment versus larger shell fragments for high rugosity treatment and Half) and shell was pressed into the exposed side. Rugose concrete was built by raking the surface with approximately 3 mm wide crests and 3 mm deep troughs (Figure 1). Plastic mesh was integrated in the middle of the concrete so tiles would suspend freely from PVC pipe using zip ties (Figure 2). Tiles suspended horizontally simulated habitat provided by reef balls because the sides of the interior of the reef ball provide a protected surface from sun exposure and sediment accretion, similar to the habitat provided by the bottom of tiles, and the inverse is true for the top of reef balls and tiles.

Prior to deployment, we measured rugosity on the top and bottom of each tile by using a 1 mm chain to follow the contour of the surface across a fixed length of tile. The chain would then be stretched out to measure the final length. A relative rugosity was measured by dividing the measured length over the standard length. Shelled treatments were photographed on the top and bottom before deployment. Percent cover of shell was measured by superimposing a 100-point grid in Image J, counting the number of points that were shell, and converting counts to percent cover.

Tile Deployment and Collection

Tiles were deployed at three sites across two bays (San Diego Bay and Newport Bay) in southern California, USA (Figure 3). Coney Island (hereinafter CI) is a site containing a natural cobble field in Newport Bay, located adjacent to a public boat launch (33°37'10.4"N, 117°53'32.5"W). Grand Caribe (hereinafter GC) and E Street (hereinafter ES) are sites in San Diego Bay. ES is a large,

gently grading mudflat (32°37'59.6"N, 117°06'27.4"W) that was identified as a possible location for planned reef ball deployment (Henderson et al., 2015). GC has rip rap in the upper intertidal zone that grades to a sandy beach in the mid to low intertidal zone, then transitions to a mudflat in the low intertidal zone. It is located 2 km across bay from ES (32°37'37.4"N, 117°07'47.1"W).

Tile treatments were deployed at two tidal elevations that reflected the distribution patterns of the native (0 m MLLW) and non-native oysters (0.6 m MLLW) (Henderson et al., 2015; Tronske et al. 2018), as well as planned deployments of reef balls. Tiles were deployed on May 21, 2018 and were collected September 6 – 10, 2018. The tile deployment coincided with the recruitment season of *O. lurida* (Coe, 1931; Seale & Zacherl, 2009) and *C. gigas* (Zacherl, D.C., unpublished data). Tiles were suspended 12 – 15 cm above the surface from PVC pipes (called “PVC tees”) that were inserted into the sediment (Figure 2), adapted from Seale and Zacherl (2009). The base of the PVC tee was deployed at 0 m MLLW and 0.6 m MLLW according to the National Oceanic and Atmospheric Administration (NOAA) Tides and Currents (accessed by <https://tidesandcurrents.noaa.gov>) for San Diego Bay (Station ID 9410152) and Newport Bay (Station ID 9410580) along the contour of the water. The adjusted tidal height of the hanging tiles was approximately 0.12 – 0.15 m (hereinafter “0 m”) MLLW, and 0.72 – 0.75 m (hereinafter “0.6 m”) MLLW. In 2020, the heights of the PVC tees were checked at ES and were found to be approximately 0.18 m higher than the target elevations, so results at ES may vary compared to CI and GC. Oyster settlement was studied simultaneously by suspended 15 x 15 cm terracotta tiles in cages from PVC tees intermixed between PVC tees with concrete treatments. Terracotta tiles were replaced every tidal cycle for the duration of the study to monitor settlement of *O. lurida* and *C. gigas*. Oyster settlers were identified and quantified on the undersides of tiles using a stereomicroscope. Oyster recruitment to terracotta tiles in a cage of plastic mesh were deployed alongside settlement tiles that were deployed from March 26 – September 6 – 10, 2018. In this study, “settlement” was defined as larvae censused within two weeks following metamorphosis that had secreted shell and attached to a tile surface and “recruitment” was defined as oyster settlers that survived and grew to be ≥ 5 mm; recruitment was censused at the end of their

recruitment season in mid-September. These additional settlement tiles were used to compare the settlement strength among cohorts of oysters across years.

Prior to retrieval in September, mud that accreted on the top of the treatment tiles was measured (in mm) using a graduated periodontal probe, then the tiles were transported to the laboratory at CSU Fullerton, CA in labeled Ziploc bags. Tiles were rinsed in freshwater to collect mobile epifauna and remove mud and canopy-forming organisms so the underlying fauna could be photographed (Figure 2). Mobile epifauna were preserved in formalin, are archived for future study, and are beyond the scope of this thesis. Canopy-forming organisms were kept with the respective plastic bag and later quantified for biomass. The tiles were photographed on upper and undersides, then solitary soft-bodied animals were removed, relaxed in menthol, and preserved in formalin. Methods and results for quantifying biomass and soft-bodied animals on tile treatments are discussed in Chapter 2. Tiles were stored at -80 °C and defrosted in warm water before processing.

To understand the major space competitors on the tiles, we quantified percent cover of fauna by using a 100-point grid superimposed upon the tile. We referenced the photos to quantify the percent cover of soft-bodied animals that were removed and preserved in formalin. Any faunal organism that was first touched by the probe was recorded even if it was not the primary recruit (e.g., *O. lurida* recruited to the top of *C. gigas* would be recorded as *O. lurida*) to determine the habitat available to subsequent larvae. All oysters were checked internally for presence of tissue to determine if it was live when the tiles were collected. Number of points were extrapolated to percent cover. Post-deployment rugosity was recorded prior to processing oysters. Then, for each tile orientation (tile surface facing upward when deployed, hereinafter “top”, or facing the substratum when deployed, hereinafter “bottom”), we recorded number of oysters, their length (mm) and width (mm). Oysters that were less than 5 mm in length and width were not quantified. Additionally, we counted the number of dead oysters to determine the percent survival of each oyster species ($\% \text{ survival} = \text{count of live oysters (L)} / \text{the number of live oysters} + \text{dead oysters (D)}$ and multiplying by 100%, or $\% \text{ survival} = L / (L + D) * 100\%$). All oysters were identified externally, and the

first 25 were also identified internally to ensure identification accuracy using internal morphological characters, particularly the presence or absence of chomata, a generic-level trait, as in Polson et al. (2009) and Raith et al. (2015). Any external identifications that were questioned were also identified internally. Tiles at 0 m MLLW were heavily fouled from San Diego Bay sites, so only a randomly chosen quarter of the tile was processed for oyster counts and measurements. Tiles at 0.6 m MLLW and all tiles from Newport Bay were processed completely. Some tiles from GC 0.6 m MLLW had heavy recruitment of oysters, so half of the tile was sampled if there were more than 50 oysters on 50% of the tile. When tiles were subsampled, oyster counts were extrapolated to one full tile for statistical comparisons.

Statistical Analysis

To test whether *O. lurida* and *C. gigas* will recruit in higher percent cover on the bottom of the tiles compared to the top of the tiles, we examined the effects of tile orientation, tidal elevation, treatment and all of their interactions on percent cover of *O. lurida* and *C. gigas* separately, as well as on the difference between percent cover of *O. lurida* and *C. gigas* (*O. lurida* - *C. gigas*) using three-way Analysis of Variance (ANOVA) tests in JMP 14. Differencing showcases where there was higher abundance or percent cover of an oyster species relative to the other species. Heteroscedasticity was checked by visually examining residuals in predicted, studentized and normal quantile plots for all ANOVAs. Data that did not meet the assumptions of the ANOVA were log transformed ($\log(x+1)$ or $\log(x/y)$ for differencing between species), square root transformed, or rank-averaged. Transformations are noted in table captions listing the statistical results. Once it was established that percent cover was generally higher for both species on the bottom of the tiles of all treatments, I moved forward with all subsequent hypothesis testing (see below) using only data from the bottoms of the tiles on the species separately and by differencing between the species. Mud accretion to the top of tiles was explored using a three-way ANOVA in the same manner.

Note that in this first set of analyses, treatment included all six unique treatments including the reference treatments, which did not allow me to test explicitly for the effects of rugosity and shell

cover in the full factorial design. Subsequent analyses eliminated the reference treatments and tested for the effects of tidal elevation, shell cover, and rugosity on oyster recruitment. Importantly, Analysis of Covariance (ANCOVA) tests were used, with rugosity as a continuous factor as opposed to a categorical factor, because pre-deployment rugosity did not match the intended full factorial design (three-way ANOVA, three-way interaction, site*tidal elevation*treatment, $p < 0.05$, Tables S1 – 2, Figures A1 – 2). For example, Full and Rough treatments were significantly different from one another when the intention was for them to be approximately equivalent in rugosity. Further, while Full and Half differed in shell cover, rugosity was sometimes statistically equivalent. Shell cover was kept as a categorical factor because while it did not reach the target 100% and 50% for Full, Fine, and Half treatments, the shell intended to cover the full surface treatments (Full and Fine) were statistically different compared to Half (three-way ANOVA, three-way interaction, site*tidal elevation*treatment, $p < 0.05$, Tables S3 – 4, Figures A3 – 4). Full and Fine treatments across all sites averaged > 80% shell cover while Half averaged between 20-30% shell cover (Figures A3 – 4). Full and Fine are still referred to as “100% shell” in the text. We examined the effects of tidal elevation (0 m MLLW versus 0.6 m MLLW, categorical factor), shell cover (0% versus 100%, categorical factor), and rugosity (continuous factor), and all of their interactions on number and percent cover of *O. lurida* and *C. gigas* separately and on their difference (*O. lurida* - *C. gigas*) using three-way ANCOVAs.

Heteroscedasticity was checked and data were transformed with the same method as described previously for ANOVAs.

Results

Summary

More *O. lurida* individuals recruited to tiles compared to *C. gigas* at CI (797 *O. lurida* versus 9 *C. gigas*) and GC (2,918 *O. lurida* versus 2,033 *C. gigas*), but more *C. gigas* recruited to tiles at ES compared to *O. lurida* (797 *O. lurida* versus 1,210 *C. gigas*). Effects of shell cover, and rugosity differed as a function of tidal elevation, tile orientation, and oyster species, often with factors interacting. Oysters generally recruited in highest percent cover to the bottom of the tiles. External

identification was 99.99% accurate (just 33/4,653 oysters internally identified were incorrectly identified externally). Marine epoxy holding terracotta tiles together failed for one tile at E Street at 0 m MLLW and the bottom of the tile was lost before the tile was processed. Subsequent results reflect this decrease in sample size.

Settlement, Growth, and Survival

O. lurida settlement rate on terracotta tiles was 2x higher at 0 m MLLW in 2018 compared to 2017, and 8x higher compared to 2016 at ES (Figure 4). *C. gigas* settlement rate was 5x higher in 2018 at 0.6 m MLLW compared to 2017 (Figure 4). In 2018, *O. lurida* settled in 5x higher densities to 0 m MLLW compared to 0.6 m MLLW and *C. gigas* in 10x higher densities to 0.6 m MLLW compared to 0 m MLLW (Figure 4). In 2018, ES experienced 2 – 3x higher recruitment of *O. lurida* and *C. gigas* compared to past years (Figure 5). *O. lurida* recruits were > 500x more abundant on tiles at 0 m MLLW compared to 0.6 m MLLW, while *C. gigas* recruits were just 2x more abundant on tiles at 0.6 m MLLW compared to 0 m MLLW (Figure 5).

On recruitment tiles deployed from May-September 2018, *O. lurida* recruit median length ranged from 3 mm to 15.5 mm while *C. gigas* recruits had a much larger median length that ranged from 8 mm to 40.5 mm (Figure A5). *O. lurida* median survival ranged from 0-100%, which differed and was often lower compared to *C. gigas* median survival that ranged from 50-100% (Figure A6). There was generally a positive but weak correlation between pre-deployment rugosity and post-deployment rugosity at most treatments across sites and the correlation was generally strongest at ES (Figure A7).

Mud Accretion

Mud accretion was 1.1 mm higher on Rough compared to Tile across tidal elevations (average of 2.1 ± 0.3 mm versus 1.0 ± 0.1 mm) but was not significantly different from other concrete treatments (three-way ANOVA, one-way interaction, treatment, $p = 0.0094$, Table 1, Figure 6). CI at 0 m MLLW accreted the most mud across sites and tidal elevations (average of 2.8 ± 0.3 mm) and accumulated 2 mm more mud on average than CI at 0.6 m MLLW and ES at either tidal elevation

(three-way ANOVA, two-way interaction, site*tide, $p < 0.0001$, Table 1, Figure 6). GC accreted the same amount of mud across tidal elevations and did not significantly differ from CI at 0 m MLLW (Figure 6).

Effects of Tile Orientation, Tidal Elevation, and Treatment

Across sites, *O. lurida* generally recruited in highest percent cover to the bottom versus the top of the tiles at 0 m MLLW. At CI, average *O. lurida* percent cover ranged from an average of $0.0 \pm 0.0\%$ on the top of tiles at either tidal elevation on Fine and Full to $8.6 \pm 3.3\%$ on the bottom of tiles at 0 m MLLW on Half (Figure 7). *O. lurida* recruited in similar percent cover to Full across tidal elevations, but otherwise recruited in highest percent cover at 0 m MLLW compared to 0.6 m MLLW (average of $5.0 \pm 1.0\%$ at 0 m MLLW compared to $5.1 \pm 0.9\%$; three-way ANOVA, three-way interaction, tile orientation*tidal elevation*treatment, $p = 0.0325$, Table 2, Figure 7). At 0.6 m MLLW, *O. lurida* did not recruit to Half, Smooth, and Tile at 0.6 m MLLW and recruited in highest percent cover to the bottom of Full relative to any other treatment or tile orientation at that tidal elevation, and its cover was equivalent to many of the lower elevation treatments (Figure 7). At CI, there were very few *C. gigas* that recruited to the bottom (6/84 tiles recruited eight *C. gigas* individuals) or the top (1/84 tiles recruited one *C. gigas* individual) of tiles and data did not meet the assumptions of ANOVA even when transformed so an ANOVA could not be run to test the effects of tile orientation, tidal elevation, and treatment on *C. gigas* percent cover but is displayed in Figure 8. *O. lurida* - *C. gigas* percent cover reflected the same patterns as *O. lurida* alone (three-way ANOVA, three-way interaction, tile orientation*tidal elevation*treatment, $p = 0.0115$, Table 3, Figure 9).

At ES, average *O. lurida* percent cover ranged from $0.0 \pm 0.0\%$ on the top of Fine, Half, Rough, and Tile at 0.6 m MLLW to $30.0 \pm 4.5\%$ on the bottom of Smooth at 0 m MLLW, with cover that was substantially higher compared to at CI (Figure 7 versus Figure 10). *O. lurida* percent cover was 10 – 30x higher on the bottom versus top of the tiles at 0 m MLLW, but at 0.6 m MLLW, percent cover was universally low, always below 2% (three-way ANOVA, three-way interaction, tile orientation*tidal elevation*treatment, $p = 0.0137$, Table 4, Figure 10). *O. lurida* percent cover was on

average 12% higher on Smooth compared to Fine on the bottom of tiles at 0 m MLLW and was on average 2.5% higher on Full at 0.6 m MLLW compared to other treatments (Figure 10). Additionally, treatments with shell and/or rugosity (Fine, Full, Half, and Rough) recruited on average 2x higher percent cover of *O. lurida* to the top of tiles at 0 m MLLW compared to Smooth and Tile (Figure 10). *C. gigas* average percent cover was higher on the bottom of tiles compared to the top of tiles across treatments and tidal elevations ($27.9 \pm 10.1\%$ versus $10.1 \pm 1.1\%$; three-way ANOVA, one-way interaction, tile orientation, $p < 0.0001$, Table 5, Figure 11). *C. gigas* percent cover ranged from an average of $5.2 \pm 2.1\%$ on Tile at 0.6 m MLLW to $34.6 \pm 5.1\%$ on Rough at 0 m MLLW (Figure 11). *C. gigas* percent cover was about 2x higher on concrete treatments, Smooth and Rough, at 0 m MLLW compared to Fine and Full, and Half recruited an intermediate percent cover of *C. gigas* and did not differ from all other treatments (average of $25.3 \pm 2.1\%$; three-way ANOVA, two-way interaction, tidal elevation*treatment, $p < 0.0001$, Table 5, Figure 11). Average percent cover of *O. lurida* never surpassed percent cover of *C. gigas* on either side of the tile at either tidal elevation, which is indicated by a negative difference in *O. lurida* - *C. gigas* (Figure 12). The bottom of tiles at 0.6 m MLLW yielded the largest negative difference in *O. lurida* - *C. gigas* percent cover (three-way ANOVA, two-way interaction, tile orientation*tidal elevation, $p < 0.0001$, Table 6, Figure 12). Percent cover of *O. lurida* - *C. gigas* was less negative on Fine and Full compared to Rough at 0 m MLLW (three-way ANOVA, two-way interaction, treatment*tidal elevation, $p = 0.0405$, Table 6, Figure 12). *O. lurida* percent cover surpassed *C. gigas* percent cover on only 10 of the 83 tiles deployed at ES, and only occurred on the bottom of tiles at 0 m MLLW.

GC tiles yielded the highest average percent cover of *O. lurida* compared to CI or ES on the bottom of Half at 0 m MLLW ($65.9 \pm 2.0\%$; Figures 7, 10, and 13). *O. lurida* percent cover was on average one order of magnitude greater on the bottom versus top of the tiles at 0 m MLLW across treatments (three-way ANOVA, three-way interaction, tile orientation*tidal elevation*treatment, $p = 0.0001$, Table 7, Figure 13). On the bottom of tiles at 0 m MLLW, Full recruited 50% less percent cover of *O. lurida* compared to other shelled treatments, although percent cover was still higher on

Full at 0 m MLLW at GC compared to CI or ES (average of $36.9 \pm 5.5\%$; Figures 7, 10, and 13). On the bottom of tiles at 0.6 m MLLW, Full recruited on average at least 5x higher percent cover of *O. lurida* compared to Half, Rough, Smooth, and Tile, but only 1.5x higher percent cover compared to Fine (Figure 13). *C. gigas* percent cover ranged on average $0.0 \pm 0.0\%$ on the top of Tile at 0.6 m MLLW to $78.8 \pm 3.6\%$ on the bottom of Smooth at 0.6 m MLLW (Figure 14). *C. gigas* percent cover was approximately 30x higher on the bottom versus top of the tiles at 0.6 m MLLW, but at 0 m MLLW, *C. gigas* percent cover never exceeded 5% and recruitment to the bottom of the tile was not statistically different from the top of the tile (three-way ANOVA, three-way interaction, tile orientation*tidal elevation*treatment, $p = 0.0069$, Table 8, Figure 14). *C. gigas* percent cover was suppressed to an average of $26.3 \pm 10.0\%$ cover on the bottom of Full compared to other treatments at 0.6 m MLLW that recruited on average 2x more percent cover of *C. gigas* (Figure 14). Percent cover of *O. lurida* was always higher compared to *C. gigas* on bottom of tiles at 0 m MLLW, and at 0.6 m MLLW, *C. gigas* was always higher than *O. lurida* on the bottom of tiles (three-way ANOVA, three-way interaction, tile orientation*tidal elevation*treatment, $p < 0.0001$, Table 9, Figure 15). *O. lurida* and *C. gigas* recruited in equally low percent cover to the top of tiles at both tidal elevations, so their difference was close to 0% cover (Figure 15). On the bottom of tiles at 0 m MLLW, Full recruited a smaller difference in percent cover compared to other shelled treatments (Fine and Half), and at 0.6 m MLLW, Full recruited a smaller difference in percent cover compared to all other treatments (Figure 15).

Effects of Tidal Elevation, Shell Cover, and Rugosity

Across sites, *O. lurida* recruited in higher number of individuals compared to percent cover on the tiles while the opposite was true for *C. gigas*. Metric of measurement (abundance or percent cover) changed the results for all sites and factoring in percent cover dead shell of oysters into analyses changed the results for differencing *O. lurida* and *C. gigas* at one site, ES. The effect of rugosity and shell cover depended on site and tidal elevation.

At CI, *O. lurida* recruited in highest abundance to 0 m MLLW (average of 12.3 ± 1.4 oysters) compared to 0.6 m MLLW (average of 4.8 ± 1.5 oysters) and to 100% shell treatments (average of 10.9 ± 1.6 oysters) compared to 0% shell treatments (average of 6.2 ± 1.5 oysters; three-way ANCOVA, one-way interaction, tidal elevation, $p = 0.0008$; one-way interaction, shell cover, $p = 0.0086$, Table 10, Figure 16). Abundance of *C. gigas* was exceedingly low at CI and did not meet the assumptions of an ANCOVA even when transformed, so the effect of tidal elevation, shell cover and rugosity on number of *C. gigas* is displayed in Figure 17. *C. gigas* individuals never recruited on the bottom of tiles at 0 m MLLW but recruited in highest abundance to 0.6 m MLLW on treatments with high rugosity and 100% shell (average of 0.3 ± 0.3 individuals). Number of *O. lurida* - *C. gigas* reflected the same trend as number of *O. lurida* alone (three-way ANCOVA, one-way interaction, shell cover, $p = 0.0181$, one-way interaction, tidal elevation, $p = 0.0007$, Table 11, Figure 18).

O. lurida percent cover at CI varied across tidal elevations and as a function of shell cover, ranging from an average of $0.3 \pm 0.2\%$ on tiles with 0% shell cover at 0.6 m MLLW to $4.9 \pm 1.0\%$ on tiles with 100% shell at 0 m MLLW (three-way ANCOVA, two-way interaction, tidal elevation*shell cover, $p = 0.0136$; Table 12, Figure 19). *O. lurida* only differed by an average of $< 1\%$ across 0 and 100% shell at 0 m MLLW and across tidal elevations at 0.6 m MLLW on 100% shell (Figure 19). *O. lurida* percent cover was higher at 0 m MLLW than 0.6 m MLLW but was similar across tidal elevations on high rugosity treatments (three-way ANCOVA, two-way interaction, tidal elevation*rugosity, $p = 0.0420$, Table 12, Figure 20). Despite the significant interaction effect, the explanatory power of rugosity on *O. lurida* percent cover was exceedingly low for both tidal elevations ($R^2 = 0.03 - 0.04$ across elevations; Figure 20). *O. lurida* percent cover was weakly positively correlated with rugosity on 100% shell treatments ($R^2 = 0.14$) and there was no correlation on tiles without shell cover ($R^2 = 0.00$; three-way ANCOVA, two-way interaction, shell cover*rugosity, $p = 0.0488$, Table 12, Figure 21). There was very low percent cover of *C. gigas* on tiles at CI (5/84 tiles recruited a maximum of 2% cover of *C. gigas*), so data did not fit the assumptions of the ANCOVA test even when transformed. The effects of tidal elevation, shell cover, and rugosity on *C. gigas*

recruitment are displayed in Figure 22. Percent cover of *O. lurida* - *C. gigas* matched the trends found in percent cover of *O. lurida* alone (Figures 19-20), but the effect of rugosity on tiles with shell cover was lost (three-way ANCOVA, two-way interaction, tidal elevation*shell cover, $p = 0.0124$, Table 13, Figure 23; two-way interaction, tidal elevation*rugosity, $p = 0.0454$, $R^2 = -0.03 - 0.06$ across elevations, Table 13, Figure 24). Percent cover of live and dead *O. lurida* - *C. gigas* reflected the same patterns as percent cover of live *O. lurida* - *C. gigas* (three-way ANCOVA, two-way interaction, tidal elevation*shell cover, $p = 0.0061$, Table 14, Figure 25; two-way interaction, tidal elevation*rugosity, $p = 0.0310$, $R^2 = -0.03 - 0.07$ across elevations, Table 14, Figure 26).

At ES, *O. lurida* abundance was positively correlated with rugosity on 100% shell treatments at 0.6 m MLLW ($R^2 = 0.53$), but there was no other correlation between rugosity and shell cover at either tidal elevation (0% shell cover: $R^2 = 0.00 - 0.01$ across elevations; 100% shell cover: $R^2 = 0.01$ at 0 m MLLW; three-way ANCOVA, three-way interaction, tidal elevation*shell cover*rugosity, $p = 0.0039$, Table 15, Figure 27). At ES, *O. lurida* and *C. gigas* both recruited in highest abundances to 0 m MLLW (Figures 27 and 28). *C. gigas* recruited 1.8x higher abundance to tiles at 0 m MLLW compared to 0.6 m MLLW, and there was no effect of treatment (three-way ANCOVA, one-way interaction, tidal elevation, $p = 0.0015$, Table 16, Figure 28). Number of *O. lurida* - *C. gigas* reflected the same positive correlation with rugosity on 100% shell treatments at 0.6 m MLLW as number of *O. lurida* alone (Figure 27; $R^2 = 0.40$; three-way ANCOVA, three-way interaction, tidal elevation*shell cover*rugosity, $p = 0.0319$, Table 17, Figure 29). Rugosity was negatively correlated with *O. lurida* - *C. gigas* abundance on 0% shell cover treatments at 0.6 m MLLW ($R^2 = 0.21$), which indicated that there were more *C. gigas* than *O. lurida* individuals (Figure 29). At 0 m MLLW, there were always more *O. lurida* than *C. gigas* individuals and there was no effect of treatment ($R^2 = 0.00$ for both 0 and 100% shell cover treatments; Figure 29)

At ES, patterns found in abundance analyses of oyster recruitment did not always match the patterns found in percent cover analyses. Percent cover of *O. lurida* at ES ranged from an average of $0.1 \pm 0.5\%$ on 0% shell cover treatments at 0.6 m MLLW to $25.0 \pm 3.3\%$ on 0% shell cover treatments

at 0 m MLLW (Figure 30). There were multiple significant two-way interactions for percent cover of *O. lurida* (three-way ANCOVA, two-way interaction, tidal elevation*shell cover*rugosity, $p < 0.05$; Table 18), but not a three-way interaction like the one found for *O. lurida* abundance (Table 15). *O. lurida* recruited in statistically similar high percent cover to 0 m MLLW to tiles with 0% and 100% shell (on average 25.1 ± 3.3 and 21.7 ± 3.3 , respectively) and was much higher than tiles at 0.6 m MLLW (average of $0.9 \pm 0.5\%$ cover on 100% shell cover treatments; three-way ANCOVA, two-way interaction, tidal elevation*shell cover, $p = 0.0002$, Table 18, Figure 30). At 0.6 m MLLW, *O. lurida* recruited 9x higher percent cover on 100% shell treatments compared to 0% shell treatments (Figure 30). There was a significant interaction effect between tidal elevation and rugosity on the percent cover of *O. lurida*, but the explanatory power of rugosity on *O. lurida* percent cover was exceedingly low for both tidal elevations ($R^2 = 0.00 - 0.04$ across tidal elevations; three-way ANCOVA, two-way interaction, tidal elevation*rugosity, $p = 0.0062$, Table 18, Figure 31). At low rugosities, *O. lurida* recruited equivalent percent cover on 100% shell and 0% shell treatments, but *O. lurida* percent cover was positively correlated with rugosity on tiles with 100% shell cover, similar to the pattern found at CI for the percent cover of *O. lurida* (Figure 21; $R^2 = 0.46$; three-way ANCOVA, two-way interaction, shell cover*rugosity, $p = 0.0005$, Table 18, Figure 32). Percent of *C. gigas* ranged on average from $20.0 \pm 3.0\%$ on tiles at 0 m MLLW to $44.7 \pm 3.8\%$ on tiles at 0 m MLLW and both extremes were found on 0% shell cover treatments (Figure 33). *C. gigas* recruited on average about 2x higher percent cover on 0% shell tiles compared to 100% shells at 0 m MLLW and tiles at 0.6 m MLLW with and without shell cover (three-way ANCOVA, two-way interaction, tidal elevation*shell cover, $p = 0.0015$, Table 19, Figure 33), which differed from *C. gigas* abundance where there was no effect of treatment on *C. gigas* recruitment at either tidal elevation (Figure 28). Unlike *O. lurida* - *C. gigas* abundance (Figure 29), percent cover did not vary by tidal elevation, shell cover, or rugosity, and *C. gigas* percent cover was generally higher compared to *O. lurida* at both tidal elevations (three-way ANCOVA, tidal elevation*shell cover, $p > 0.05$, Table 20, Figure 34). There was a higher percent cover of *O. lurida* compared to *C. gigas* when dead shell was factored into percent cover analyses,

and this effect was found at 0 m MLLW with 100% shell (three-way ANCOVA, two-way interaction, tidal elevation*shell cover, $p = 0.0007$, Table 21, Figure 35). *C. gigas* still had on average at least 15% higher cover compared to *O. lurida* on treatments with 0% shell at 0 m MLLW and on both 100% shell and 0% shell treatments at 0.6 m MLLW (Figure 35).

GC recruited the most *O. lurida* and *C. gigas* individuals overall. *O. lurida* and *C. gigas* abundances were maximized at different tidal elevations, while at ES, both species recruited in highest abundances to the same tidal elevation (Figures 27 and 28 versus 36 and 37). *O. lurida* recruited in higher abundances to tiles at GC at 0 m MLLW compared to tiles at 0.6 m MLLW and the effect of rugosity on number of *O. lurida* per tile was dependent on shell cover and tidal elevation (three-way ANCOVA, three-way interaction, tidal elevation*shell cover*rugosity, $p < 0.0001$, Table 22, Figure 36). *O. lurida* abundance at 0 m MLLW was strongly negatively correlated with rugosity on tiles with 100% shell cover ($R^2 = -0.62$) but at 0.6 m MLLW, *O. lurida* abundance was positively correlated with rugosity on tiles with 100% shell cover ($R^2 = 0.24$), similar to ES (Figures 27 and 36). Rugosity did not correlate with *O. lurida* abundance on tiles with 0% shell cover at either tidal elevation ($R^2 = 0.05 - 0.04$ across elevations; Figure 36). *C. gigas* recruited in higher abundances to tiles at 0.6 m MLLW compared to tiles at 0 m MLLW, and at both tidal elevations generally recruited in higher abundances to 0% shell treatments (three-way ANCOVA, three-way interaction, tidal elevation*shell cover*rugosity, $p = 0.0451$, Table 23, Figure 37). At 0 m MLLW, *C. gigas* abundance was negatively correlated with rugosity on 0% shell cover treatments ($R^2 = -0.40$) and was not correlated with rugosity on 100% shell treatments ($R^2 = 0.03$; Figure 37). *C. gigas* only recruited to 4/14 tiles with 100% shell at 0 m MLLW. At 0.6 m MLLW, there was a positive correlation between rugosity and *C. gigas* abundance on 0% shell treatments ($R^2 = 0.16$) and a negative correlation on 100% shell cover treatments ($R^2 = -0.13$; Figure 37). Number of *O. lurida* - *C. gigas* at GC reflected the same patterns as *O. lurida* alone (Figure 36; on 0% shell cover, $R^2 = 0.13 - 0.00$ across tidal elevations; on 100% shell, $R^2 = -0.63 - 0.22$ across tidal elevations; three-way ANCOVA, three-way interaction, tidal elevation*shell cover*rugosity, $p < 0.0001$, Table 24, Figure 38). *O. lurida* outnumbered *C. gigas* on

all treatments at 0 m MLLW and on treatments with high rugosity on 100% shell cover treatments at 0.6 m MLLW, indicated by a positive number (Figure 38).

Unlike CI and ES, patterns found at GC in analysis of abundance (Figures 36 – 38) persisted in analyses of percent cover for *O. lurida* (three-way ANCOVA, two-way interaction, tidal elevation*shell cover, $p < 0.0001$, Table 25, Figure 39), generally for *C. gigas* (three-way ANCOVA, three-way interaction, tidal elevation*shell cover*rugosity, $p = 0.0009$, Table 26, Figure 40), and *O. lurida - C. gigas* (three-way ANCOVA, three-way interaction, tidal elevation*shell cover*rugosity, $p < 0.0001$, Table 27, Figure 41) at GC. Similar to *O. lurida* abundance (Figure 36), *O. lurida* percent cover was strongly negatively correlated with rugosity at 0 m MLLW on 100% shell treatments ($R^2 = -0.73$), but at 0.6 m MLLW, *O. lurida* percent cover was positively correlated with rugosity ($R^2 = 0.14$; Figure 39). Unlike *C. gigas* abundance (Figure 37), *C. gigas* percent cover was negatively correlated with rugosity on all treatments and tidal elevations (for 0% shell cover, $R^2 = -0.64 - -0.34$ across tidal elevations; for 100% shell cover, $R^2 = -0.11 - -0.58$ across tidal elevations; Figure 40). Similar to *O. lurida - C. gigas* abundance (Figure 38), percent cover of *O. lurida - C. gigas* was positively correlated with rugosity on 0% shell treatments at 0 m MLLW ($R^2 = 0.40$) but unlike *O. lurida - C. gigas* abundance, percent cover of *O. lurida - C. gigas* was also positively correlated with rugosity at 0.6 m MLLW ($R^2 = 0.34$; Figure 41). Percent cover of *O. lurida - C. gigas* at 0.6 m MLLW was positively correlated with rugosity on 0% and 100% shell cover treatments ($R^2 = 0.34 - 0.52$, respectively), the overall value was always positive for 100% shell treatments, which indicated that there was higher percent cover of *O. lurida* compared to *C. gigas*, but the opposite was true for 0% shell cover treatments (Figure 41), similar to *O. lurida - C. gigas* abundance (Figure 38). The trends found for percent cover of *O. lurida - C. gigas* persisted when percent cover of dead oysters was factored into analyses (on 0% shell, $R^2 = 0.42 - 0.32$ across tidal elevations; on 100% shell, $R^2 = -0.32 - 0.48$ across tidal elevations; three-way ANCOVA, three-way interaction, tidal elevation*shell cover*rugosity, $p < 0.0001$, Table 28, Figure 42). The negative effect of rugosity on 100% shell cover

treatments at 0 m MLLW on percent cover of *O. lurida* - *C. gigas* was weakened when dead shell was included in analyses (Figures 41 and 42; $R^2 = -0.69$ compared to -0.32 , respectively).

Discussion

This is the first study to identify conditions that allow the native species, *O. lurida*, to recruit at higher densities outside of its optimal tidal elevation range. This native foundation species outcompetes the non-indigenous space occupier, *C. gigas*, in both abundance and percent cover on concrete with full shell cover and high rugosity at a tidal elevation where *C. gigas* normally dominates the space (Torres et al., unpublished). Additionally, I found that shell cover discourages the recruitment of this global NIS, and the effect can sometimes be exacerbated by also adding rugosity. Importantly, the deployment of substratum in the orientation and tidal elevation preferred by oysters (Hopkins, 1935; Schaefer, 1937; Torres et al., unpublished) recruited a high percent cover of the species in San Diego Bay that is rarely seen in adult density surveys (Perog et al., 2021), supporting that reef balls would successfully recruit oysters in this estuary. I examined recruitment onto concrete structures used in a living shorelines context, but the notion that grey structures can be manipulated for more desirable outcomes (such as recruiting more oysters of a particular species) is one that can transfer to multiple contexts. Perkol-Finkel & Sella provided some key first steps in this direction by changing the composition of concrete and adding rugosity to vertical concrete infrastructure by eco-engineering (Perkol-Finkel et al., 2018; Perkol-Finkel & Sella, 2014, 2015; Sella & Perkol-Finkel, 2015), but here, for the first time, I also manipulate shell cover as another technique to target the growth of a native community to horizontal surfaces. This study addresses a research gap identified by Morris et al. (2019) to study different materials to improve the living shoreline design in different contexts. We expanded knowledge of a living shoreline design to southern California, at two sites, two tidal elevations, and with varying substrata and rugosities.

After one recruitment season, the substratum available at low tidal elevations was replaced with native, rugose *O. lurida* live and dead shell at San Diego sites and some native habitat at higher tidal elevations. This replacement of concrete surface with animals that build calcium carbonate shells

is referred to as “bioprotection” and it may increase the longevity of the concrete (Coombes et al., 2017). This study builds upon the small collection of published projects that explore differential *O. lurida* recruitment to various substrata (Sawyer, 2011; White et al., 2009) and can now be applied to a living shorelines design.

Results from this study were also strongly context-dependent, with site, tidal elevation, tile orientation, shell cover, and rugosity all playing significant roles in determining oyster recruitment but in varied combinations and only partially supporting my hypotheses. GC and ES are sites that are only approximately 2 km apart but experienced vastly different densities of *O. lurida* and *C. gigas* recruitment to the tiles. Context-dependency is well-explored in the literature in different marine environments, such as estuaries (Bracewell et al., 2013; Ellis et al., 2017; Robinson et al., 2017; Strain et al., 2021), lagoons (Thomsen et al., 2006) and the rocky intertidal (Bulleri et al., 2012; Russell et al., 2006, but see Foster et al., 2003). Coastal managers should exercise caution when making decisions about a living shorelines design based on effects observed at different sites or in different bays. Repeating this experiment at the target site prior to the installation of a large-scale living shorelines project would be beneficial to ensure that project goals are met.

Tile Orientation

Orientation of substratum significantly impacted oyster recruitment of both species. Living shorelines using reef balls should maximize the underside and minimize the upperside of surfaces available for larvae. Large shells that jut out of the structure may be added to the reef ball to add additional horizontal underside surface for *O. lurida* recruitment, especially on the outside and top of reef balls. Additionally, all tile orientations should be coated with shell to discourage *C. gigas* recruitment. My findings agreed with seminal literature on settlement preferences of *O. lurida* and *C. gigas* onto underside of horizontal surfaces (Hopkins, 1935; Schaefer, 1937) and with previous research in San Diego Bay (Torres et al., unpublished). Reef balls have a considerable amount of substratum that is vertically oriented that was not addressed in this study; an additional set of concrete tiles (Fine, Full, Half, Rough, Smooth; n = 3) were deployed to ES at 0 m MLLW from June

2019 – June 2020 to compare vertical orientation to horizontal orientation (Marques et al., unpublished data). Researchers found that there was no treatment effect, but oysters recruited in higher abundance to the underside of tiles with a horizontal orientation (Marques et al., unpublished data) and supports the addition of shell to the reef balls to increase the horizontal underside surface available for *O. lurida* recruitment. Oysters may recruit to the shaded undersides of tiles because their growth may be negatively impacted by solar radiation (Zacherl, D.C., CSUF, personal communication, April 9, 2021); these shaded surfaces are similar to the shaded interior of the reef balls and support that the recruitment patterns in this study would persist on a deployed reef ball. Alternatively, oyster larvae may prefer to settle onto the underside of substrata because they travel in the water column with their velum upwards, attach their foot and secrete shell from the velum, and can better escape sedimentation (Hopkins, 1935; Schaefer, 1937). Concrete with added rugosity affixed to vertical seawalls have been successful in recruiting a higher abundance of native oysters (Perkol-Finkel et al., 2018; Strain et al., 2020; Vozzo et al., 2021) perhaps due to the increased horizontal space available to settlers. Pre-deployment rugosity and percent cover of shell differed between the upperside and underside of the tiles (Figures A1 – A4), but the effect of tile orientation was so strong on percent cover of both oyster species that it is likely that patterns found for oyster recruitment would persist if the treatments were equal in predeployment rugosity and shell cover.

Tidal Elevation

The hypothesis that *O. lurida* would recruit in higher abundances to lower tidal elevations and that the inverse would be true for *C. gigas* was supported at GC, rejected at ES, and was partially supported for CI. At ES, the tidal height of the base of the PVC tees from this experiment was checked in 2020 and found to be approximately 0.18 m higher compared to the target tidal elevations, which may capture more *C. gigas* settlers (Figure 4). ES is a mudflat with a gradual slope and shallow pools that have high water retention, unlike the other sites that have a steeper slope and low water retention. When deploying PVC tees, it can be difficult to discern the correct tidal elevation because of the many pools that form near the waterline. In 2020, following this study, new PVC tees with

smooth concrete recruitment tiles were deployed to the correct tidal elevation at ES (Perog et al., unpublished data). Researchers found that *C. gigas* still recruited in relatively high percent cover to 0 m MLLW, which suggests that treatment effects found at ES in this project would persist even at lower tidal elevations (Perog et al., unpublished data). *C. gigas* at 0 m MLLW recruited many *O. lurida* onto the top of their shells in this study (personal observation), so even if reef balls recruit *C. gigas*, *O. lurida* may still have higher abundance and percent cover and meet the project goals. If the reef balls are culled, live *C. gigas* may be cracked open but the intact shell should remain to allow the *O. lurida* to survive and provide additional rugose habitat for subsequent *O. lurida* larvae.

The mudflat at ES does not have hard habitat with the exception of a few boulders at very high tidal elevations (> 0.6 m MLLW) and scattered anthropogenic litter (personal observation), so larvae may have recruited to the only hard substratum available at the time of settlement. There is some evidence that introduction of hard substrata to a previously soft-bottomed habitat can recruit opportunistic species, or species that can grow and colonize quickly (Vaselli et al., 2008). Specifically, non-indigenous species can be opportunistic (Bracewell et al., 2013; Kerckhof et al., 2009) because they can colonize new artificial structures more quickly than native fauna that may be slower growing. *C. gigas* is a non-indigenous species and grows larger and faster than *O. lurida* and may have recruited to the only hard habitat available at ES even though it recruited outside of its tidal elevation range. The zonation pattern of the oyster species observed at GC may be influenced by the availability of hard substratum available offered by nearby rip rap. Structures deployed at lower tidal elevations would likely successfully recruit *O. lurida*, but the results may be site-specific and may be more successful if there are other substrata available. Although there was no clear treatment to encourage native oyster recruitment to 0 m MLLW, restoration practitioners can seed the structure by adding live specimens to encourage gregarious settlement (Strain et al., 2020, Tamburri et al., 2007). Reef balls with shell cover and rugosity deployed at a higher tidal elevation would successfully provide habitat to native species and better attenuate wave action and reduce shoreline erosion (Henderson et al., unpublished data). At CI, the best scenario was found where *O. lurida* recruited in

equally high abundances to tiles across tidal elevations to tiles with high rugosity and 100% shell cover with little competition with *C. gigas*. More pilot studies should explore the settlement and recruitment dynamics of *C. gigas* in Newport Bay and determine if there is interannual variation before deploying reef balls at the site.

Shell Cover and Rugosity

The most important factor in the tile design that impacted oyster recruitment was shell; it encouraged *O. lurida* recruitment when the treatment was coupled with rugosity and allowed recruitment to a tidal elevation to which *O. lurida* rarely recruits. Additionally, shell cover discouraged *C. gigas* recruitment at sites with high recruitment of the non-indigenous oyster, but the effects were tidal-elevation dependent. Shell cover can attract oyster spat (Tamburri et al., 2007), and rugosity may allow the oysters to survive because microhabitat is provided (Strain et al., 2020).

Oysters were observed on the undersurfaces of shell and in the deep crevices near the attachment point of the shell fragment and concrete that were not captured by measuring rugosity with a 1 mm chain (Figure 43). The umbo of *O. lurida* often was wedged in the crevices of Rough tiles at CI, showing that they first settled in the rugose part of the tile (Figure 43). At 0 m MLLW, the tidal elevation where *O. lurida* abundance was generally maximized, there was generally no effect of shell cover or rugosity, except at GC. *O. lurida* recruited in highest percent cover and abundance to 100% shell cover treatments with low rugosity and lowest percent cover and abundances to tiles with 100% shell cover and high rugosity. Crushed shell used to build the low rugosity shelled treatments may provide micro-rugosity, or rugose habitat that is large on the scale of larvae but small on the scale of the human eye, that *O. lurida* larvae may prefer over macro-rugosity provided by larger shell fragments. Current studies that investigate oyster recruitment to shells do not account for the effect of macro- or micro-rugosity on oyster recruitment (Sawyer, 2011; White et al., 2009). Nonetheless, percent cover of *O. lurida* at GC was higher on all treatments compared to other sites, and the implementation of 100% shell cover with high rugosity would discourage the recruitment of *C. gigas* and should be considered when building reef balls. The effect of rugosity on concrete tiles with 0%

shell cover on *C. gigas* abundance were site and tidal elevation dependent. At ES, there was no effect of treatment, but at GC, there was a negative impact of rugosity at 0 m MLLW, but a positive impact of rugosity at 0.6 m MLLW. Vozzo et al. (2021) completed a study in Australia of the effect of rugosity on concrete tiles affixed to seawalls on faunal recruitment and found that non-indigenous *C. gigas* recruited in higher abundances to rugose tiles compared smooth tiles across sites, but the study was only deployed at one tidal elevation. Further research should investigate the differential recruitment of *C. gigas* across sites and rugosities. Planned reef balls in San Diego Bay will use baycrete instead of Portland cement, but addition of shell cover and rugosity is still recommended to provide more suitable habitat for *O. lurida* at higher tidal elevations and discourage *C. gigas* recruitment.

Oysters from San Diego may not have responded to rugosity alone because the predation pressure was not high. Dead oysters were found gaping without tissue and with the shell often still attached to the hinge, which is not indicative of a death from predation (cracked shells, holes in shells). When predation pressure is high, oysters may have greater survival in the crevices of rugose concrete tiles (Strain et al., 2018). If the tiles were deployed longer, there may have been a more significant effect of rugosity on oyster recruitment (Strain et al., 2020), although preliminary data from a follow-up study using the same concrete treatments as this project at ES reveal that there are no effects of rugosity or shell cover on oyster abundance or percent cover after one year (Marques et al., unpublished data).

Dead, gaping oysters can provide additional rugosity to larvae and other fauna, and dead oyster shell can still serve an ecosystem engineering function (Jones et al., 1994) including providing habitat for subsequent larvae and shelter for other species by providing increased rugosity on the substratum surface. Shore crabs were found inside these gaping oysters that were not removed during a freshwater rinse, presumably searching for refuge as the tiles froze in the laboratory. *O. lurida* generally had a lower survival rate compared to *C. gigas*, which may explain the differences in *O. lurida* - *C. gigas* findings when dead oysters were factored into the analyses. There could be

additional ecological benefits to substratum that has both live and dead oysters, including recruiting a higher abundance of epifauna (Sheehan et al., 2015) and a more diverse community structure (Bell, 2005; Tolley & Volety, 2005; Summerhayes et al., 2009) because different niches can be filled.

Additionally, oysters recruit to shell, and native oysters settle on conspecifics, regardless of if they are alive or dead (Sawyer, 2011).

Other Considerations

O. lurida and *C. gigas* settlement in San Diego Bay was abnormally high in 2018 compared to compared to the previous three years, although the dataset is relatively small and past years actually may have been abnormally low settlement years. Nonetheless, repeating this experiment may yield different results depending on the abundance of larvae that year. There are no prior settlement data for *C. gigas* in Newport Bay, so it is unknown if low recruitment of *C. gigas* was due to particularly poor larvae supply in 2018 or if *C. gigas* larvae supply is always low in Newport Bay.

Mud deposition on the top of tiles over four months (maximum average of 2.8 ± 0.3 mm at CI at 0 m MLLW) was just 1 mm less compared to mud deposited onto oyster restoration beds after six months built by using shell in coir bags in the low intertidal in Newport Bay, CA (Wood, 2018). Mud accretion was highest on the top of the most rugose treatment, which agreed with the findings of a similar experiment (Hanlon et al., 2018). Mud accretion may not only help slow shoreline erosion and deposit sediment back to the shoreline, but it may also increase the prevalence of tube-forming species over time (Hanlon et al., 2018), which would reduce the bare space on top of reef balls. Mud sedimentation was only studied on the top of horizontal tiles in this experiment, but this tile orientation may accrete more mud on average compared to vertical orientations (Marques et al., unpublished data). Mud accretion on the reef balls via increasing the surface roughness is one way that a living shorelines project can capture even more suspended sediment from the water column. Reef balls are already expected to attenuate wave action and accrete mud landward of the reef ball (Chowdhury et al., 2019; Henderson et al., unpublished data), but adding surface roughness may strengthen this positive effect.

O. lurida were generally smaller compared to *C. gigas* across treatments and tidal elevations, which contributed to the discrepancy in findings when the response variable was abundance versus percent cover. At ES, *O. lurida* showed better success on tiles compared to *C. gigas* when abundances were considered, but the results changed when percent cover of the oysters were analyzed; *C. gigas* occupied more space compared to *O. lurida*. This disparity between results using different quantification methods may be explained by oyster growth patterns. *O. lurida* are a smaller oyster in general, and, in addition, were observed to grow in crevices that were not captured by percent cover quantification techniques. Additionally, *O. lurida* often had a much smaller attachment to the surface and grew away from the substratum while *C. gigas* grew flatter to the surface. Restoration practitioners should set expectations by specifically considering whether the goal is to recruit higher percent cover or, rather, higher abundance of the target fauna and adjust their expectations accordingly.

Caged terracotta tiles have been used to study oyster settlement and recruitment in Newport Bay for over 15 years and San Diego Bay for four years (Zacherl, D.C., unpublished data). In this study, caged terracotta tiles recruited fewer *O. lurida* at 0.6 m MLLW and fewer *C. gigas* at 0 m MLLW compared to what was observed on concrete tile treatments. In this experiment, oysters on caged terracotta tiles were small, numerous, and created more three-dimensional habitat than uncaged terracotta tiles (personal observation). Oysters that recruited to terracotta tiles were easily dislodged and were found with scars of oysters that had presumably fallen off, whereby oysters that recruited to concrete or shelled tiles were more difficult and never had these scars, which indicated that oysters had better adhesion to the substratum. Concrete and shell may offer micro-rugosity, which supports Hopkins (1935) and Schaefer (1937) speculations that the difference in textures of concrete and glass caused more oysters to settle onto the rougher surfaces. This study exposes the difference in oyster recruitment across caged terracotta, uncaged terracotta, and concrete substrata and future research on the differential recruitment onto these materials would benefit future oyster monitoring efforts.

Management Implications

Though a reef ball deployed at a higher tidal elevation may provide better shoreline erosion, the substratum may recruit more *C. gigas* compared to a reef ball at a lower tidal elevation. If a reef ball is deployed at a higher tidal elevation, restoration practitioners should add shell cover and rugosity to deter *C. gigas* recruitment and provide a more suitable habitat for *O. lurida*. A reef ball deployed at a low tidal elevation would recruit more *O. lurida* and addition of shell could be added to discourage *C. gigas* recruitment. Restoration practitioners should replicate the experiment at the chosen site to determine the best site-specific treatment to meet the goals of the project.

CHAPTER 2

NATIVE AND NON-INDIGENOUS SPECIES RECRUITMENT

Introduction

Estuarine Ecosystems

Shoreline armoring built to protect coastal infrastructure from erosion has changed the estuarine ecosystem drastically. Not only can hard armor result in habitat loss (Lai et al., 2015; Masucci & Reimer, 2019), recruit different communities, reduce taxon richness (Loke et al., 2017), and negatively impact species abundance (Kornis et al., 2018), but it may also facilitate the spread and persistence of non-indigenous species (NIS) (Kerckhof et al., 2009).

Non-indigenous Species

NIS introductions have increased over time because most invasive species can travel via shipping activity (70%) (Molnar et al., 2008; Ruiz et al., 2000) through ballast water (Bailey et al., 2005) and the hulls (Chapman & Carlton, 1991) of both transglobal ships (Keller et al., 2011) and recreational boats (Murray et al., 2011). These invasive species can have spillover effects to nearby harbors and expand their range and impact (Wasson et al., 2001). Invasions from shipping are accidental, but other introductions of invasive species have occurred intentionally through aquaculture (41%) (Molnar et al., 2008). For example, in the 1900s, the Eastern oyster (*Crassostrea virginica*) from the U.S. East Coast and the Pacific oyster, *Crassostrea gigas*, from Japan were planted directly into multiple estuaries in the Pacific Northwest and California (Bonnot, 1935; Dimick et al., 1941). Not only can the oysters “escape” aquaculture by reproducing and establishing wild populations, but they can carry other NIS attached to their shells; Eastern oyster drills, *Urosalpinx cinerea*, and the slipper shell, *Crepidula fornicata*, were introduced from planting Eastern oysters that were not inspected prior to shipping (Bonnot, 1935). Even when aquaculture of oysters failed, these oysters and hitchhikers successfully colonized and reproduced in the estuaries long after their introduction (Buhle & Ruesink, 2009; Wasson et al., 2001). Eastern oyster drills prey on oysters and are one of the reasons that

native Olympia oyster populations have remained in low abundances in some portions of their range, even while the harvesting of wild populations had discontinued (Buhle & Ruesink, 2009).

NIS establishment success (Thomsen et al., 2011) and impacts (Robinson et al., 2017) are context-dependent, but they are reported in high abundances on artificial structures (Airoidi et al., 2015; Chapman & Carlton, 1991; Lambert & Lambert, 1998). Species association with artificial structures has even been described as a characteristic to identify NIS (Chapman & Carlton, 1991). NIS are opportunistic and can grow rapidly after disturbance or installation of a new structure (Bracewell et al., 2013, Viola et al., 2018); both native and NIS recruit to artificial structures, but NIS show higher survival rates on the artificial versus natural habitats (Tyrrell & Byers, 2007).

Hard armor fundamentally alters natural habitat (Morley et al., 2012). It is usually made of unnatural material to an estuarine ecosystem (e.g., plastic docks, granite boulders, or concrete pilings) and typically has a smooth texture. Coastal managers are interested in improving the design of existing hard armor through eco-engineering because native species may prefer substrata that are more rugose or offer tide pool habitat similar to natural substrata, while NIS may not have a preference. There is a recent interest in understanding the recruitment dynamics of native and NIS onto newly deployed structures with modified substratum composition and/or surface complexity meant to target native species recruitment (Perkol-Finkel et al., 2018; Strain et al., 2020; Strain et al., 2021; Vozzo et al., 2021), but these studies are limited in their focus to recruitment onto vertical seawalls.

Coastal managers also experiment with nature-based erosion control methods, called “living shorelines,” that have more natural slope; they deploy natural habitats such as oyster reefs, eelgrass beds and cordgrass that restore target species and their ecosystem functions while continuing to protect coastal infrastructure (NOAA, 2015). Living shoreline designs range from use of completely natural habitat (“green” designs) to hybrid designs (“green/grey”) that mix natural and human-constructed habitats (e.g., concrete reef balls). Eco-engineering techniques developed for seawalls can also be applied to these green/grey hybrid designs to discourage the recruitment of NIS. For

example, on reef balls, oyster shell added to the surface may add rugosity and better mimic natural habitat and result in higher recruitment of native species. Deployment tidal elevation may also be a factor that impacts the recruitment of NIS (Bracewell et al., 2012); structures with longer submersion time at a lower tidal elevation may recruit more NIS (Leclerc et al., 2020).

Southern California

NIS in southern California have increased over time, and introduction and establishment rates are higher compared to in neighboring states (Cohen et al., 2005). One possible explanation for these higher rates is that the incidence of invasions from shipping and aquaculture in the Southern California Bight, USA, is higher compared to global averages (81% and 71%, respectively) (Molnar et al., 2008). Further, estuaries in southern California are highly modified; San Diego Bay has lost 84% of its shallow subtidal habitat (USDN/NFECS and Port of San Diego, 2013) and now an estimated 64,000 pier pilings and 72 km of rip rap and seawall line the bay (Perog et al., unpublished data). San Diego Bay had the second highest NIS richness (53) just after the Ports of Los Angeles and Long Beach (quantified as one harbor, NIS richness was 57) compared to other bays in southern California (CDFW et al., 2014). The U.S. Department of the Navy, Naval Facilities Engineering Command Southwest (USDN/NFECS) and Port of San Diego have identified invasive species one of the largest drivers of change in San Diego Bay and have outlined goals to limit their impact in their most recent Natural Resources Management Plan (2013).

More recently, the Port of San Diego is proposing a living shoreline design to protect some of the remaining natural habitat by deploying reef balls that target the growth of native oyster habitat. Colonization of NIS is a significant concern for reef balls; removal may be required if the substratum develops a higher ratio of NIS to native species relative to comparable habitat in the bay (Henderson et al., unpublished data). The proposed reef balls would span across 0.6 m of intertidal elevation (Henderson et al., unpublished data), and previous recruitment studies (Torres et al., unpublished data) and field surveys (Zacherl, D.C., unpublished data) suggest reef balls at higher tidal elevations would capture mostly *Vaucheria* sp. (a native yellow-green algae), non-indigenous *Crassostrea gigas*,

and non-indigenous *Amphibalanus amphitrite*, but the recruitment dynamics of NIS species and native species onto concrete deployed at high tidal elevations compared to low tidal elevations remain unknown. It is crucial to understand if there is a treatment that discourages their recruitment and attains a higher percent cover of native to NIS that can be applied to a reef ball. In this project, I test the effects of concrete with modified substratum (shell cover and rugosity added to the surface) on native and NIS recruitment. I hypothesize that community composition will vary by tidal elevation, shell cover, and rugosity.

Methods

Sites and tile deployment and processing methods were discussed in. Additional methods to address Chapter 2 hypotheses are discussed below. Marine epoxy holding terracotta tiles together for Tile treatment failed on one tile at E Street at 0 m MLLW and the bottom of the tile was lost before the tile was processed. Subsequent results reflect this change.

Soft-bodied Fauna

Soft-bodied fauna, including sea anemones and solitary tunicates, were removed from the tiles prior to their preservation in the freezer. Soft-bodied fauna can lose their distinguishing characteristics when they are frozen, so they were instead relaxed using menthol crystals and preserved in formalin. In 2019 (one year after preservation), the soft-bodied fauna were transferred from formalin to 70% ethanol and were identified to the lowest taxonomic level under a stereomicroscope by external and internal characteristics from the keys in the Light and Smith Manual (2007) and Tracy et al. (2017) and with the help of local ascidian expert, Dr. Marie Nydam (Soka University, California). There was only one sea anemone and relatively few unidentifiable specimens, so they were removed from analyses. All species found in soft-body fauna samples were noted as present in “present/absent” surveys (see methods below).

Canopy-forming Algae and Fauna

Organisms that formed a canopy on the tiles create three-dimensional habitat for fauna on the tiles but had a small attachment to the substratum. To quantify their contribution to community

structure, we measured their biomass and compared the effects of site, tidal elevation, and treatment on recruitment of these species. Some of these organisms were separated from the tiles at the time of collection to better view sessile organisms for photographing the tiles (see Chapter 1), but additional removal of organisms occurred while processing the tiles for oysters. All removed samples were stored in labeled Ziploc bags at -80 °C. All species that were separated for biomass processing were noted as present in “present/absent” surveys (see methods below). Methods for gathering wet weight and dry weight were gathered from a non-comprehensive literature review that explored methods to measure biomass of algae and fauna together (Table A5). Prior to collecting biomass measurements, canopy-forming samples were defrosted and submerged in warm freshwater, then were cleaned of mobile epifauna, mud, and detritus. The species that comprised the majority of the sample was recorded. If two species comprised approximately equal halves of the sample, they were both scored as equal contributors to biomass. Fauna were identified to the lowest taxonomic level by stereoscope and algae were combined into one category. The organisms were patted dry by paper towel, and wet weight was measured. The samples were dried at 60 °C until they were a consistent weight (< 10% weight loss or maximum of 0.05 g loss between dry weights; all samples met these criteria at 18 hours). Dry weight was used for analyses.

Presence/absence

To understand sessile community composition, we recorded the presence/absence of all sessile species on the undersides of the tiles, including any soft-bodied species and canopy-forming species. All fauna were identified to the lowest taxonomic level and I determined if they were native or non-indigenous using the Light and Smith Manual (2007), online databases, and with assistance from local taxonomic experts (see below). Tiles at 0 m MLLW from San Diego Bay sites were heavily fouled, so for these sites, one quarter of the tile was randomly selected to be processed for presence of fauna and introduced a potential species-area effect that is addressed below. Tiles at 0.6 m MLLW and all tiles from Newport Bay were processed completely. After it was observed that the majority of organisms recruited to the undersides of tiles (see Chapter 1), the bottom tile orientation was used for

analyses of community composition. A species area curve for a subset of tiles from ES (Smooth at 0 m MLLW) revealed that subsampling the tile underestimated overall tile species richness on tiles at ES and GC at 0 m MLLW (Figure A8). I continued with analyses with the knowledge that sites and tidal elevations could not be directly compared.

Identification of Sessile Fauna

Sessile fauna, including sponges, polychaetes, bryozoans, bivalves, barnacles, and colonial tunicates were successfully identified to the lowest taxonomic level possible. Sponges were identified to species or family with the help of Dr. Thomas Turner (University of California, Santa Barbara, California). Bryozoans were identified to species when possible using the Light and Smith Manual (2007), but most were kept at genus or family level because they were young colonies < 3 mm in size (Ben Ferraro, Orange County Sanitation District, personal communication, January 2021) and identification was based on photographs (Megan McCuller, North Carolina Museum of Natural Sciences, personal communication, February 2021). Most serpulid worms in calcareous tubes from San Diego Bay were successfully identified to species based on operculum characteristics using Bastida-Zavala et al. (2017) with the assistance of Dr. Bruno Pernet (University of California, Long Beach, California). Reversed chama (*Pseudochama exogyra*) were identified using external and internal characteristics outlined in Light and Smith Manual (2007). Mussels were identified to species or family with the help of Kelvin Barwick (Orange County Sanitation District, California). Most barnacles were identified to species using the Light and Smith Manual (2007). Colonial tunicates were frozen on the tiles and consequently lost their distinguishing characteristics when defrosted so were identified using a combination of original photos of the tiles and photos after preservation and were confirmed by Dr. Marie Nydam and Gretchen Lambert (Southern California Association of Marine Invertebrate Taxonomists).

Some fauna were not successfully identified and were kept as groups of species or morphotypes. Species that were rare but distinct from known species identifications were grouped in an “other” category. Spirorbid worms were grouped to one category because of their cryptogenic

origins and difficulty in identification (Leslie Harris, Natural History Museum of Los Angeles, personal communication, September 2019). Polychaetes that built soft tubes on the tiles were poorly preserved after freezing (Kelvin Barwick, personal communication, January 2021) so they were grouped into one category with all tube-dwelling animals. Some polychaetes were found underneath oyster shell or shell embedded into the concrete and were separated into two morphotypes. All unidentified species have archived vouchers, photos, or both. Species richness for native species and NIS is conservative due to the level of taxonomic identification achieved.

Space-dominating Fauna

The top five fauna, excluding oysters, that occupied space on the bottom of tiles were identified as space-dominating fauna. These fauna occupied ≥ 50 points among tiles at a site ($50/8,400$ available points = 1% of available space was covered by the animal). Methods for collecting percent cover data is outlined in Chapter 1. Oysters and barnacles were reliably determined as live or dead during percent cover surveys; all other calcareous fauna and bryozoans were not separated into live or dead so resulting percent cover may include dead individuals. An in-depth exploration of oyster abundance and percent cover was explored in Chapter 1 and is not included in Chapter 2.

Statistical Analysis

Species Richness

Species richness was quantified by adding the number of unique species on the tile. Morphotypes that included unidentified species or species complexes were counted as one species. Overall, native, and non-indigenous species richness is underestimated due to limited ability to identify some fauna. Species richness was analyzed for each site and for each tidal elevation separately (due to uneven sampling effort) using one-way Analysis of Variance (ANOVA) to test the effect of treatment. Heteroscedasticity was checked by visually examining residuals in predicted, studentized and normal quantile plots for all ANOVAs. Data that did not meet the assumptions of the model were log transformed ($\log(x+ 1)$) or square root transformed. Transformations are noted in table captions listing the statistical results.

Community Composition

To test the hypotheses that community composition will differ across tidal elevations, shell cover, and rugosities, I built non-parametric multi-dimensional scaling plots (nMDS) plots from presence/absence data collected from the underside of tiles in Primer v7. I pre-treated the data with a presence/absence transformation and built the nMDS plots using 150 restarts. I conducted permutational analysis of variance (PERMANOVA) tests and post-hoc analyses with 9999 permutations on unrestricted permutation of raw data in PERMANOVA+ based on Euclidean distance to test the effects of site, tidal elevation, and treatment on overall community composition (all native, non-indigenous, and cryptogenic species included) on the bottom of tiles. I repeated these analyses for native and NIS communities separately. Tunicate abundance was analyzed in the same way based on Bray-Curtis similarity index using fourth root transformed data.

Tunicates and Biomass

I examined the effects of site, tidal elevation, and treatment on the recruitment of native and non-indigenous tunicates and canopy-forming algae and fauna that contributed to biomass using three-way ANOVAs in JMP 14. Heteroscedasticity and transformations were performed the same way as species richness ANOVAs. Transformations are noted in table captions listing the statistical results.

Cover of Major Space Occupiers

I examined the effects of tidal elevation, shell cover, rugosity, and their interactions on percent cover of major space occupiers at each site using three-way Analysis of Covariance (ANCOVA) tests in JMP 14. For some species, their recruitment was limited to one tidal elevation, so that factor was removed and replaced with a different factor (e.g. native sponge *Leucandra losangelensis* percent cover at 0.6 m MLLW was not detected, so effect of site, shell cover, and rugosity was tested instead of tidal elevation, shell cover, and rugosity) to complete the three-way ANCOVA. If the space occupier's recruitment was limited to one site and one tidal elevation, tidal elevation was removed and a two-way ANCOVA was run (e.g. *Botryllus schlosseri* only recruited in substantial percent cover

to CI and was not detected at 0.6 m MLLW, so analysis was limited to 0 m MLLW and included the factors shell cover and rugosity). The results for oysters are explored in-depth in Chapter 1. Heteroscedasticity was checked and transformations were performed in the same way as ANOVAs. Transformations are noted in table captions listing the statistical results.

Results

Species Richness

Overall species richness varied across sites, but generally higher shell cover and/or rugosity recruited higher overall and native species richness on the tiles at both tidal elevations (Figures 44 - 46). Native species richness was lower than non-indigenous species richness across sites. All native, non-indigenous, and cryptogenic species are listed in Table A6.

At CI at 0 m MLLW, Fine recruited four more species on average than Smooth (one-way ANOVA, one-way interaction, treatment, $p = 0.0002$, Table 29, Figure 44) and at 0.6 m MLLW, Full recruited at least four more species on average than other treatments (one-way ANOVA, one-way interaction, treatment, $p < 0.0001$, Table 29, Figure 44). At 0 m MLLW at CI, native species richness was on average 2x higher on Full and Half compared to Tile (one-way ANOVA, $p = 0.0053$, Table 29, Figure 44). Native species richness was on average 0.7 higher on Full compared to Fine and Half at 0.6 m MLLW at CI (1.1 ± 0.1 versus 0.4 ± 0.2 and 0.3 ± 0.2 species, respectively) but did not differ from Rough (one-way ANOVA, $p < 0.0001$, Table 29, Figure 44). Native species were not detected on Smooth and Tile at 0.6 m MLLW at CI (Figure 44). Non-indigenous species richness at CI at 0 m MLLW recruited two more species on average to Fine compared to Tile but did not differ among other concrete tile treatments (one-way ANOVA, $p = 0.0356$, Table 29, Figure 44). At CI at 0.6 m MLLW, non-indigenous species richness was highest on average on Full (2.7 ± 0.4 species) compared to all other treatments that always recruited less than an average of 1.5 species (one-way ANOVA, $p < 0.0001$, Table 29, Figure 44).

ES differed from CI at 0 m MLLW (Figure 44) because Fine recruited lower overall species richness compared to Rough (average of 8.3 ± 0.5 versus 11.7 ± 0.8 species, respectively; one-way

ANOVA, one-way interaction, treatment, $p = 0.0038$, Table 29, Figure 45), which corresponded with the treatment and tidal elevation that major space occupier, non-indigenous *Crassostrea gigas*, recruited in highest percent cover (Figure 11). There was no treatment effect on overall species richness at ES at 0.6 m MLLW (one-way ANOVA, $p > 0.05$, Table 29, Figure 45). At ES, patterns of native species richness across treatments mirrored patterns of overall species richness but Rough only recruited 1.5 more native species on average compared to Fine (one-way ANOVA, $p = 0.0011$, Table 29, Figure 45). At ES at 0.6 m MLLW, Full recruited the highest average native species richness (0.7 ± 0.2 species) compared to Fine (no native species were detected; one-way ANOVA, $p = 0.0405$, Table 29, Figure 45). ES at 0 m MLLW recruited the highest non-indigenous species richness on average to Rough (5.7 ± 0.3 species) compared to Full (3.9 ± 0.4 species) and Half (4.1 ± 0.4 species; one-way ANOVA, $p = 0.0011$, Table 29, Figure 45). At ES at 0.6 m MLLW, non-indigenous species richness highest on Fine (average of 4.0 ± 0.2 species) compared to Smooth (2.7 ± 0.7 species; one-way ANOVA, $p = 0.0106$, Table 29, Figure 45).

At GC at 0 m MLLW, Fine and Full recruited about four more species on average compared to Smooth (one-way ANOVA, one-way interaction, treatment, $p = 0.0003$, Table 29, Figure 46) and at 0.6 m MLLW, Fine recruited at least three more species on average than other treatments (one-way ANOVA, one-way interaction, treatment, $p = 0.0034$, Table 29, Figure 46). GC native species richness at 0 m MLLW was similar across Fine, Full, and Half, and Smooth and Rough, but Full was on average higher than Smooth (1.9 ± 0.3 versus 1.0 ± 0.0 species; one-way ANOVA, one-way interaction, treatment, $p = 0.0115$, Table 29, Figure 46). At GC at 0.6 m MLLW, there was no effect of treatment on native species richness (one-way ANOVA, $p > 0.05$, Table 29, Figure 46). At GC at 0 m MLLW, there was a significant effect of treatment on non-indigenous species richness, but post-hoc Tukey and Student t tests could not differentiate between treatments (one-way ANOVA, $p = 0.0491$, Table 29, Figure 46), but at 0.6 m MLLW, Full recruited two more species on average compared to Rough and Tile (one-way ANOVA, $p = 0.0189$, Table 29, Figure 46).

Community Composition

PERMANOVA analyses comparing species from presence/absence surveys across sites, tidal elevations, and treatments recruited different overall, native, and non-indigenous community composition (PERMANOVA, site*tidal elevation*treatment, three-way interaction, $p < 0.05$, Tables 30-32; Figures 47-49), but pair-wise comparisons were restricted to compare treatments within each site and tidal elevation since increasing proportion of tile searched resulted in more species found (Figure A8).

Community composition at CI in Newport Bay was different compared to ES or GC in San Diego Bay and at CI, communities differed across tidal elevations shown visually by more separation between samples in the nMDS plot (Figure 47). There was more overlap in community composition at ES and GC, both located in San Diego Bay, and among tidal elevations. PERMANOVA analyses revealed an interaction effect among site, tidal elevation, and treatment on overall community structure on the bottom of tiles (PERMANOVA, site*tidal elevation*treatment, three-way interaction, $p = 0.0003$, stress coefficient = 0.15; Table 30; Figure 47). All pair-wise comparisons across treatments within each site and tidal elevation are shown in Table A7. Differences in shell cover and rugosity impacted overall community composition at each site and within each tidal elevation (Table A7; Figure 47). At ES at 0 m MLLW, Rough recruited a different overall community compared to all other treatments, which also was the treatment and tidal elevation to recruit the highest percent cover of non-indigenous *Crassostrea gigas* reported in Chapter 1 (Figure 11), but at ES 0.6 m MLLW, the communities were similar regardless of rugosity (Table A7; Figure 47). At GC at 0 m MLLW, Full and Fine recruited similar communities, and Full and Rough recruited similar communities, but the treatments recruited different communities at 0.6 m MLLW (Table A7; Figure 47). At 0 m MLLW, Full and Fine recruited different communities compared to Smooth and Half (Table A7; Figure 47). At CI at both tidal elevations, Full recruited different communities compared to Fine, Smooth, and Rough (Table A7; Figure 47).

Native community structure at ES and GC overlapped across sites and tidal elevations, but the native community at CI at 0 m MLLW was distinct from the community at CI at 0.6 m MLLW and from the other sites shown visually by more separation between samples in the nMDS plot (Figure 48). PERMANOVA analyses revealed an interaction effect among site, tidal elevation, and treatment on native community structure on the bottom of tiles (PERMANOVA, site*tidal elevation*treatment, three-way interaction, $p = 0.0005$, stress coefficient = 0.04; Table 31; Figure 48). All pair-wise comparisons across treatments (within each site and elevation) are shown in Table A8. Native community structure was driven by the presence of the bryozoan, *Celleporaria brunnea* and the sponge, *Leucandra losangelensis* shown visually by biplot rays (Figure 49). Most treatment effects were observed only at 0 m MLLW across sites (Table A8; Figure 48) because most of the native species in analyses were found at 0 m MLLW (Table A6). There was little difference between native community structure across tidal elevations and treatments at ES at GC at 0.6 m MLLW, but GC at 0 m MLLW recruited different native communities on Fine compared to Half, Smooth, and Tile (Table A8; Figure 48).

NIS community structure was strongly tidally influenced at CI and ES, but GC at 0.6 was similar to 0 m MLLW and ES at both tidal elevations shown visually by more separation between samples in the nMDS plot (Figure 49). PERMANOVA analyses revealed an interaction effect among site, tidal elevation, and treatment on NIS community structure on the bottom of tiles (PERMANOVA, site*tidal elevation*treatment, three-way interaction, $p = 0.0061$, stress coefficient = 0.09; Table 32; Figure 49). All pair-wise comparisons across treatments (within each site and elevation) are shown in Table A9. NIS community structure was driven by the presence of the bryozoans, *Watersipora subtorquata* and *Amathia verticillata*, the barnacle, *Amphibalanus amphitrite*, the oyster, *Crassostrea gigas*, and the calcareous tube-dwelling polychaete, *Hydroides elegans* shown visually by biplot rays (Figure 49). Differences in shell cover and rugosity impacted NIS community composition (Table A9; Figure 49). Across all sites and tidal elevations, NIS communities did not differ between Smooth and Rough, nor did Fine and Full at ES and GC at 0 m MLLW (Table A9; Figure 49). At GC at 0.6 m MLLW and CI at either tidal elevation, NIS community composition differed on Fine and Full (Table

A9; Figure 49). At 0.6 m MLLW, Full and Rough recruited different NIS communities at CI and GC, which was the treatment that recruited the highest percent cover of native *Ostrea lurida* at 0.6 m MLLW (Figures 19-21, 39, and 49; Table A9).

Tunicate Abundance

Only one sea anemone was found on the bottom of Rough at Coney at 0 m MLLW and the rest of soft-bodied fauna were solitary tunicates (Table A10). The sea anemone was removed from analyses. Most tunicates recruited to the bottom of tiles, and no tunicates recruited to the top of tiles at 0.6 m MLLW, and at CI, no tunicates recruited to the top or bottom of tiles at 0.6 m MLLW (Table A11).

Tunicate abundance was distinct across tidal elevations at CI and ES shown visually by more separation between samples in the nMDS plot, and tunicate abundance at GC was similar to other sites and tidal elevations shown visually by less separation (Figure 50). PERMANOVA analyses revealed an interaction effect among site, tidal elevation, and treatment on tunicate abundance on the bottom of tiles (PERMANOVA, site*tidal elevation*treatment, three-way interaction, $p = 0.0002$, stress coefficient = 0.14; Table 33; Figure 50). All pair-wise comparisons across treatments (within each site and elevation) are shown in Table A12. Patterns in tunicate abundance were driven by the abundance of non-indigenous tunicates, including *Styela clava* and *Styela plicata*, *Ciona* sp., *Polyandrocarpa zorritensis*, and the native tunicate, *Ascidia ceratodes* shown visually by biplot rays (Figure 50). Treatment effect on tunicate abundance was tidal elevation dependent (Table A12; Figure 50). Across sites and tidal elevations, Smooth and Rough recruited similar tunicate abundances (Table A12; Figure 50). At ES at 0.6 m MLLW and GC and CI at 0 m MLLW, Fine and Full recruited different tunicate abundance (Table A12; Figure 50).

Native *Ascidia ceratodes* recruited to tiles across all sites at 0 m MLLW, and at 0.6 m MLLW, only was detected at GC (Table A6). *A. ceratodes* was most abundant on Full at GC at 0 m MLLW (average of 34.1 ± 16.8 individuals) compared to treatments that did not recruit any *A. ceratodes* (at 0 m MLLW, Fine and Tile at ES; Rough, Smooth, and Tile at CI; Half, Smooth, and Tile at GC) and

compared to all treatments at all sites at 0.6 m MLLW except Full and Tile at GC (three-way ANOVA, three-way interaction, site*tidal elevation*treatment, $p = 0.0171$, Table 34, Figure 51). Non-indigenous tunicate abundance was highest on Full at GC at 0 m MLLW (average of 62.6 ± 26.4 individuals) but was only significantly different from tiles with exceedingly low abundance, always less than 7 individuals, including Rough, Smooth, and Tile across sites at 0 m MLLW, and all treatments at 0.6 m MLLW except Full at ES (three-way ANOVA, three-way interaction, site*tidal elevation*treatment, $p = 0.0013$, Table 35, Figure 52). At GC, the majority of tunicates that recruited to Fine and Full were gregarious solitary tunicates attached by stolons (*Polyandrocarpa zorritensis* comprised 201/247 tunicates on Fine, or 81% of tunicates, and 383/451 tunicates on Full, or 85% of tunicates).

Biomass

A total of 127 biomass samples were collected from the sites, but the samples were not distributed equally across site, tidal elevation, and treatment (Table A13). Biomass samples collected from the tiles were primarily composed of algae and *Amathia* (formerly *Zoobotryon*) *verticillata*, a NIS commonly found in estuaries (Fofonoff et al., 2018). Other species were found in the biomass survey (Table A14) but were not included in analyses because of their low density in the sample and small contribution to biomass.

Biomass of canopy-forming algae that recruited to tiles was highest at GC on Full at 0.6 m MLLW (average of 1.0 ± 0.4 g) and recruited 2x more biomass compared to all other treatments across sites and tidal elevations except Rough at GC at 0.6 m MLLW (0.6 ± 0.1 g; three-way ANOVA, three-way interaction, site*tidal elevation*treatment, $p = 0.0176$, Table 36, Figure 53). Biomass of *Amathia verticillata* recruited in equal biomass across treatments and was highest at CI at 0 m MLLW (0.3 ± 0.0 g) compared to other sites and tidal elevations, which were always below 0.01 g (three-way ANOVA, two-way interaction, site*tidal elevation, $p < 0.0001$, Table 37, Figure 54). *Amathia verticillata* was not detected at GC at either tidal elevation (Table A6, Figure 54).

Major Space Occupiers Summary

Four species and one group of worms were major space occupiers on tiles in addition to oysters (Table 38). All species were strongly influenced by tidal elevation and some species were also impacted by shell, rugosity, or both factors. Analyses exploring oyster recruitment to tidal elevation, shell cover, and rugosity factors are explored in Chapter 1.

Cryptogenic Space Occupier

Spirorbid worms, common cryptogenic polychaetes (Leslie Harris, personal communication, August 2019) that grow calcareous shell, recruited in high percent cover to all sites (Table 38). Spirorbid worms recruited in highest percent cover to CI, which was 37x higher compared to ES and 20x higher compared to GC (Table 38). At CI, spirorbid worms recruited in highest percent cover to concrete treatments at 0 m MLLW (average of $18.6 \pm 4.2\%$) compared to 100% shell treatments (average of $10.7 \pm 0.8\%$) and tiles at 0 m MLLW with 0% shell were on average 6x higher compared to 0% shell and 100% shell treatments at 0.6 m MLLW (three-way ANCOVA, two-way interaction, tidal elevation*shell cover, $p = 0.0354$, Table 39, Figure 55). Percent cover of spirorbid worms was positively correlated with rugosity at 0 m MLLW ($R^2 = 0.21$), but there was no relationship between percent cover and rugosity at 0.6 m MLLW ($R^2 = -0.01$; three-way ANCOVA, two-way interaction, tidal elevation*rugosity, $p = 0.0144$, Table 39, Figure 56). There was a significant interaction of shell cover and rugosity, but the explanatory power of rugosity spirorbid worm percent cover was exceedingly low for both 0% shell and 100% shell treatments ($R^2 = 0.00 - 0.03$, respectively; three-way ANCOVA, two-way interaction, shell cover*rugosity, $p = 0.0497$, Table 39, Figure 57). At ES, there was a positive effect of rugosity on spirorbid worm percent cover on tiles with 0% shell cover ($R^2 = 0.22$) and no effect of rugosity on tiles with 100% shell cover ($R^2 = -0.07$; three-way ANCOVA, two-way interaction, shell cover*rugosity, $p = 0.0075$, Table 40, Figure 58). At GC, average spirorbid worm percent cover was maximized at 0.6 m MLLW, opposite to the findings at CI (Figure 56), but only reached a maximum average of $1.7 \pm 0.7\%$ at 0.6 m MLLW compared to $38.7 \pm 6.0\%$ at 0 m MLLW at CI (three-way ANCOVA, one-way interaction, tidal elevation, $p = 0.0323$, Table 41, Figure 59).

NIS Space Occupiers

At ES, one NIS recruited in high percent cover to tiles and at CI, two NIS recruited in high percent cover (Table 38). No NIS other than *Crassostrea gigas* recruited in high percent cover to GC. NIS in high percent cover were restricted to one site and one tidal elevation and the effect of shell and rugosity varied.

At ES, *Amphibalanus amphitrite*, a common hull fouling barnacle that has established in harbors (Fofonoff et al., 2018), recruited in high percent cover to tiles. *A. amphitrite* recruited in highest average percent cover to tiles at 0.6 m MLLW with 0% shell ($35.1 \pm 1.6\%$) compared to tiles at 0 m MLLW with 0% shell cover ($3.9 \pm 0.2\%$) or 100% shell cover ($0.6 \pm 0.1\%$; three-way ANCOVA, two-way interaction, tidal elevation*shell cover, $p = 0.0022$, Table 42, Figure 60). *A. amphitrite* recruited 5.5x higher percent cover to tiles at 0.6 m MLLW with 0% shell than 100% shell (Figure 60). *A. amphitrite* was negatively correlated with rugosity at 0.6 m MLLW ($R^2 = -0.20$) but was not correlated with rugosity at 0 m MLLW where it was in lowest percent cover (Figure 60; $R^2 = -0.01$; three-way ANCOVA, two-way interaction, rugosity*tidal elevation, $p = 0.0017$, Table 42, Figure 61). When dead *A. amphitrite* percent cover was added to the analyses, the average percent cover of *A. amphitrite* increased to an average of $1.9 \pm 0.1\%$ to tiles at 0 m MLLW with 100% shell to $50.9 \pm 1.2\%$ to tiles at 0.6 m MLLW with 0% shell (Figure 63). Percent cover of live and dead *A. amphitrite* reflected the same patterns as percent cover of live *A. amphitrite* (Figures 60 – 61; three-way ANCOVA, two-way interaction, tidal elevation*shell cover, $p = 0.0001$, Table 43, Figure 62; $R^2 = -0.02$ – -0.18 across tidal elevations; two-way interaction, rugosity*tidal elevation, $p = 0.0016$, Table 43, Figure 63). *A. amphitrite* was often seen dead underneath *Crassostrea gigas* and were subsequently not quantified in percent cover.

Watersipora subtorquata, a common non-indigenous bryozoan in the estuarine intertidal (Cohen et al., 2005), recruited in high percent cover to the bottom of tiles at CI (Table 38). Percent cover of *W. subtorquata* recruited in higher percent cover to tiles at 0 m MLLW (average of $7.9 \pm$

1.0%) compared to tiles at 0.6 m MLLW (average of $0.1 \pm 0.1\%$) and there was no effect of shell or rugosity (three-way ANCOVA, one-way interaction, tidal elevation, $p < 0.0001$, Table 44, Figure 64).

Botryllus schlosseri, a common non-indigenous colonial tunicate in estuaries (Lambert & Lambert, 1998), recruited in high abundances to CI (Table 38), but was never detected at 0.6 m MLLW and only recruited percent cover to the top of tiles three times. A two-way ANCOVA exploring the effects of shell and rugosity on percent cover of *B. schlosseri* to the bottom of tiles at 0 m MLLW was used to better meet the assumptions of the ANCOVA statistical test. There was a negative correlation between *B. schlosseri* percent cover and rugosity regardless of shell cover ($R^2 = -0.25$; two-way ANCOVA, one-way interaction, rugosity, $p = 0.0367$, Table 45, Figure 65).

Native Space Occupier

Leucandra losangelensis is a native sponge that recruited to the bottom of tiles at 0 m MLLW at all sites in the study (Table A6) in relatively high percent cover (Table 38). *L. losangelensis* was strongly tidally influenced – it was not detected in percent cover at 0.6 m MLLW. To understand the recruitment of the sponge and better meet the assumptions of the ANCOVA statistical test, the factors site, rugosity, and shell cover were investigated and tiles at 0.6 m MLLW were excluded from the analysis. *L. losangelensis* was found in highest percent cover on tiles deployed at CI and GC (average of $2.4 \pm 0.6\%$ and $1.7 \pm 0.4\%$) compared to ES (average of $0.8 \pm 0.3\%$) and on tiles with 100% shell cover (average of $2.1 \pm 0.4\%$) compared to tiles with 0% cover (average of $1.2 \pm 0.3\%$; three-way ANCOVA, one-way interaction, site, $p = 0.0004$; three-way ANCOVA, one-way interaction, shell cover, $p = 0.0018$, Table 46, Figure 66).

Discussion

This study reveals the positive impact that shell cover and rugosity have on community composition and species richness and the simultaneous negative impact on NIS recruitment that are major space occupiers on the substratum. Recruitment of NIS onto concrete tiles was site-specific and this highlights the need for site-specific planning for living shorelines and eco-engineering projects. This study adds to the growing body of literature that supports the use of rugose structures

to discourage NIS recruitment (Perkol-Finkel et al., 2018; Strain et al., 2020; Strain et al., 2021; Vozzo et al., 2021) and adds upon the small in living shorelines and eco-engineering literature base that remains relatively unexplored: tidal elevation. This study shows that the effect of treatment on community composition and on major space occupiers changes with tidal elevation and should be considered in living shoreline research projects. Additionally, this study supports the management implications presented in Chapter 1 to add shell cover and rugosity to green/grey hybrid living shorelines, especially for structures that span across multiple tidal elevations.

Tidal Elevation

There has been limited research on the recruitment of NIS to different tidal elevations (Aguilera, 2018; Perkol-Finkel et al., 2018; Strain et al., 2021; Torres et al., unpublished data), but there has not been a study designed specifically to test the community composition across different treatments with the intention to limit the recruitment of NIS onto newly deployed structures. In this study, tidal elevation strongly influenced the positive impact of rugose shelled tiles, which recruited a higher native species richness at CI at 0.6 m MLLW compared to other treatments, including native *Ascidia ceratodes* tunicates to 0.6 m MLLW.

Some NIS were found in highest percent cover at lower tidal elevations, including bryozoans and tunicates, which is supported in the literature; NIS are found in high abundances on structures that are constantly immersed, like floating buoys and subtidal fixed structures (Cohen et al., 2005; Lambert & Lambert, 1998), but other NIS, specifically *Amphibalanus amphitrite* and *Crassostrea gigas*, recruited in higher percent cover to higher tidal elevations at some sites. Certain characteristics of these species, such as a hard shell that can be sealed during low tide, may allow the animal to survive the abiotic stressors of desiccation stress and grow in higher tidal elevations where there are less biotic stressors, such as predators and competitors (Ruesink, 2007). In San Diego Bay, *C. gigas* recruited in higher abundance and percent cover to lower tidal elevations than observed in past recruitment surveys (Figure 5). *A. amphitrite* covered a majority of the tiles at 0.6 and may have limited the recruitment of *C. gigas*. Oyster growth at higher tidal elevations has been suggested to be

caused by growth of NIS (Wasson 2010) and suspension feeding invertebrates (Bishop & Peterson, 2006) at lower tidal elevations that the oyster may prefer in the absence of competitors. In Newport Bay, native *Ostrea lurida* may have recruited in high percent cover to a higher tidal elevation compared to it normally is found (Zacherl, D.C., unpublished data) to escape competition with other filter and suspension feeders, including tunicates, spirorbid worms, and bryozoans found in high percent cover at the lower tidal elevation. The bottom valve of *C. gigas* revealed overgrowth of *A. amphitrite*, and the bottom valve of *O. lurida* revealed overgrowth of the oyster over spirorbid worms and *Watersipora subtorquata*, which suggests that they can outcompete the NIS for space. However, foulers have been shown to negatively impact *O. lurida* growth overall (Trimble et al., 2009). Oyster shell deployed at higher tidal elevations has been referred to as a “recruitment sink” in Washington, USA, where oyster spat die from desiccation and freezing (Trimble et al., 2009), but in southern California’s temperate climate, native *O. lurida* may grow better at higher tidal elevations without the hinderance of other competitors and may survive abiotic stressors when microhabitat is offered by high rugosity and high shell cover.

Shell Cover

Results from this study support the notion that shell cover provides a more natural substratum that recruits native species and discourages NIS recruitment in some cases. Building upon findings from Chapter 1, shelled treatments supported native sponge growth, *Leucandra losangelensis* at the tidal elevation that it was found in highest percent cover, but did not help to recruit the sponge to higher tidal elevations as it did for *Ostrea lurida* when paired with the effect of rugosity. This sponge species was often observed as habitat for other species, including isopods and amphipods, and may be an additional ecosystem engineer (Jones et al., 1994) supported by reef balls with shell cover added to the surface. Shell cover also corresponded with other desired outcomes, including supporting increased overall species richness, native species richness, native tunicate abundance, and algal biomass, but also resulted in some undesired outcomes, including supporting higher non-indigenous species richness and non-indigenous tunicate abundance. Although provisioning habitat

to native species also increased NIS species richness, percent cover of NIS that occupied a high percent cover on the tiles did not recruit in higher cover to shelled treatments. At ES, recruitment of both NIS major space occupiers was discouraged by shell cover (*Crassostrea gigas* and *Amphibalanus amphitrite*), supporting the decision to add shell cover to artificial substratum to encourage native species recruitment (*L. losangelensis*) while discouraging NIS (*C. gigas*, *A. amphitrite*).

Rugosity

Although the highest rugosity concrete treatment recruited higher overall non-indigenous species richness at ES, and treatments with high rugosity and shell cover recruited higher overall non-indigenous species richness at CI and GC, NIS space occupiers were negatively impacted by increases in rugosity at other sites, which supports current literature from the eastern hemisphere (Perkol-Finkel et al., 2018; Strain et al., 2020; Vozzo et al., 2021) and adds upon literature available for the western hemisphere (Strain et al., 2021). Non-indigenous colonial tunicates, *Botryllus schlosseri*, were negatively impacted by rugosity and unaffected by shell cover, which agrees with the findings by Tyrrell and Byers (2007) where researchers found *B. schlosseri* recruit in low percent cover to rugose whole shell. *Amphibalanus amphitrite* recruited in highest percent cover to the lowest rugosity concrete treatment, Smooth. Other studies have found that barnacles, specifically *A. amphitrite*, settle in higher abundance to very smooth substrata (glass) compared to substrata with micro-rugosity, like concrete (Berntsson et al. 2000; Rittschof et al., 1984), so *A. amphitrite* may have recruited to the smoothest habitat available on the mudflat (Bracewell et al., 2013). Rugosity alone did not impact major space occupiers found in this study but may be added to reef balls to discourage the recruitment of NIS *B. schlosseri* and *A. amphitrite*.

Amphibalanus amphitrite may encourage the recruitment of oysters (Barnes et al., 2010; Diederich, 2005) by providing a settlement cue and additional rugosity to settlers (Figure A9). Micro-rugosity may encourage (Liversage, 2017) or discourage (Berntsson et al., 2000) species recruitment. Empty *A. amphitrite* tests were found underneath *Crassostrea gigas* recruits (Figure A9), and *C.*

gigas settlers were observed on the sides of the shell of *A. amphitrite* settlers on settlement tiles deployed for just two weeks (personal observation). At 0.6 m MLLW, native *Ostrea lurida* were found in lowest average percent cover where *A. amphitrite* was maximized (0% shell at 0.6 m MLLW; Figure 30 versus Figure 60), but tiles with high rugosity and high shell cover corresponded with the opposite effect, which indicates that that *C. gigas* may recruit to tiles with high *A. amphitrite* percent cover, but *O. lurida* does not. Choosing a treatment that decreases the percent cover of non-indigenous *A. amphitrite* may also decrease the abundance of *C. gigas* on reef balls.

Other species that may provide micro-rugosity for subsequent settlers include *Watersipora subtorquata* and spirorbid worms (Figure A9). In the present study, *W. subtorquata* did not recruit in higher percent cover to any treatment type. Other studies observed *Watersipora sp.* recruit relatively equally onto substrata with varying rugosities (concrete, wood, aluminum, and glass) (Anderson & Underwood, 1994) and facilitate fouler recruitment to smooth surfaces (Floerl et al., 2004). Spirorbid worms were often found underneath native *Ostrea lurida*, native *Leucandra losangelensis*, non-indigenous *Watersipora subtorquata*, non-indigenous *Botryllus schlosseri*, and non-indigenous *Amathia verticillatum*, which indicated that that they were used for attachment by both native and NIS species. Cryptogenic spirorbid worms may serve as an ecosystem engineer by modifying the habitat to have calcium carbonate shell and micro-rugosity available to subsequent larvae (Jones et al., 1994).

Spirorbid worms are common in estuaries globally, but there is a research gap on their taxonomic distinction. Spirorbid worm provenance is widely unknown and they are difficult to identify (Leslie Harris, personal communication, August 2019). Keys require dissection of the worms, sometimes a gravid individual, and shell morphology may change due to environmental factors (Knight-Jones et al., 2009; Rzhavsky, 1994). There are 14 possible species of spirorbid worms in Newport and San Diego Bays (see Figure 8 in Knight-Jones et al., 2009). Spirorbid worms were present at all sites on most treatments and tidal elevations (Table A6), but there were mixed effects of tidal elevation, shell cover, rugosity, and their interactions across sites. At CI, spirorbid worms percent

cover surpassed the percent cover of native species at 0 m MLLW, and microscopic spirorbid worms recruited in high abundances to CI at 0.6 m MLLW that were not captured by the percent cover method used in this study (Figure A9). Further research into the identification of spirorbid worm species and their ecological impacts on faunal growth would better inform living shorelines projects that undoubtedly recruit spirorbid worms.

Other Considerations

Due to sub-sampling tiles in presence/absence surveys, the species richness on tiles was underestimated at ES and GC at 0 m MLLW (Figure A8). Furthermore, small tunicates were missed on the tiles before freezing, so tunicate abundance was underestimated. Nonetheless, there were differences among treatments found in nMDS plots and differing effects of shell cover and rugosity at both tidal elevations on overall, native, and non-indigenous species recruitment and tunicate abundance.

Non-indigenous *Crassostrea gigas* compared to native *Ostrea lurida* epifaunal diversity has not been studied in southern California. This study suggests that *C. gigas* may have a positive impact on species richness, but the impact was site-specific. *C. gigas* recruited in highest percent cover to tiles at ES 0 m MLLW and to Rough (Figure 11), which corresponded to the highest overall, native, and non-indigenous species richness (Figure 45). *C. gigas* may have a positive impact on species richness at ES, but the inverse results were found at GC. At 0.6 m MLLW at GC, Full recruited the lowest percent cover of *C. gigas* compared to other treatments at that tidal elevation (Figure 14), which corresponded with the highest overall and non-indigenous species richness, and trended to recruit the highest native species richness, although the effect of treatment was insignificant (Figure 46). Differences between the impact of *C. gigas* on species richness can be due to the differences in habitat availability at the sites. Artificial structure placed in a previously soft-bottomed habitat, such as ES, may recruit both native and NIS (Bracewell et al., 2013, Thomsen et al., 2006; Viola et al., 2018). There was other hard habitat available at GC, so larvae may have selected habitat differently when more choices were available. It is unlikely that *C. gigas* may have offered more post-deployment

rugosity on Rough than other treatments larvae preferred (average of 1.5 ± 0.0 on Rough versus 1.4 ± 0.0 on other treatments; Figure A7), so larvae may prefer to recruit to the micro-rugosity of the foliations on the *C. gigas*, or there may be another cue that live oysters may have that recruits the larvae to the shells and the tiles (for example, Barnes et al., (2010) found that *C. gigas* larvae recruited in higher abundances to live barnacles versus dead or modeled barnacle tests offering the same rugosity). The impact of non-indigenous *C. gigas* to community structure in other areas of the world has been studied and the results have also been mixed. In Northeast Ireland, *C. gigas* recruited a lower species diversity to its shell compared to native oyster shell (Guy et al., 2018), in Australia, *C. gigas* recruited similar species diversity to its shell but had lower abundances of species compared to native oyster shells (Wilkie, et al., 2012), and in Northern Ireland had no difference in epibiont species diversity compared to native oyster shells (Zwerschke et al., 2016).

Further study of the settlement of other NIS identified in this study can help to inform when to best deploy reef balls to minimize NIS impacts (suggested by Airoidi & Bulleri, 2011 and Viola et al., 2018). For example, non-indigenous *Crassostrea gigas* settlement is highest in mid-summer, while native *Ostrea lurida* is in late spring, so reef balls will be deployed earlier in the year to capture *O. lurida* so they can establish on the tile before *C. gigas* larvae become abundant (Torres et al., unpublished data).

Recruitment studies that are aimed to understand the recruitment dynamics of native and NIS should consider the material of the tile. This study has shown that terracotta tile recruits a different community compared to concrete tiles, and concrete tiles recruit a different community to tiles with shell cover. Results focused on patterns found between concrete and shelled treatments because the research is meant to apply to concrete reef balls. Other researchers have studied the native and NIS recruitment onto plastic into estuaries (Blum et al., 2007; Leclerc et al., 2020; Marins et al., 2010; Robinson et al., 2017; Susick et al., 2020; Tracy & Reynolds, 2014) and this study exposes how substratum material matters in the recruitment of native and NIS and should be considered in future studies.

Management Implications

NIS responses to treatments can vary globally (Strain et al., 2021), and this project supports the notion that effects of substratum composition and rugosity on community composition and density of species can vary by site, even within the same bay. It is key for restoration practitioners to replicate a similar study to test NIS recruitment dynamics to introduced material before installing a living shoreline to determine the site-specific best treatment to meet the goals of the project. Shell and rugosity may be added to reef balls deployed at either 0 m MLLW or 0.6 m MLLW to decrease the recruitment of NIS percent cover on the substratum and increase the abundance and percent cover of native species.

APPENDIX A
TABLES AND FIGURES

		Rugosity	
		Low	High
Shell Cover	0%	 Smooth concrete	 Rough concrete
	100%	 Fine shell	 Full shell
Reference treatments		 Terracotta	 Half (50%) shell

Figure 1. Tile (15 x 15 cm) treatments with varying rugosity (low, high) and shell cover (0%, 100%) and two reference treatments (terracotta tile and 50% shell). Treatments were deployed from May – September 2018 in Newport and San Diego Bays, CA, USA, to test effects of side of tile, tidal elevation, shell cover, and rugosity on the recruitment of native and non-indigenous oysters.

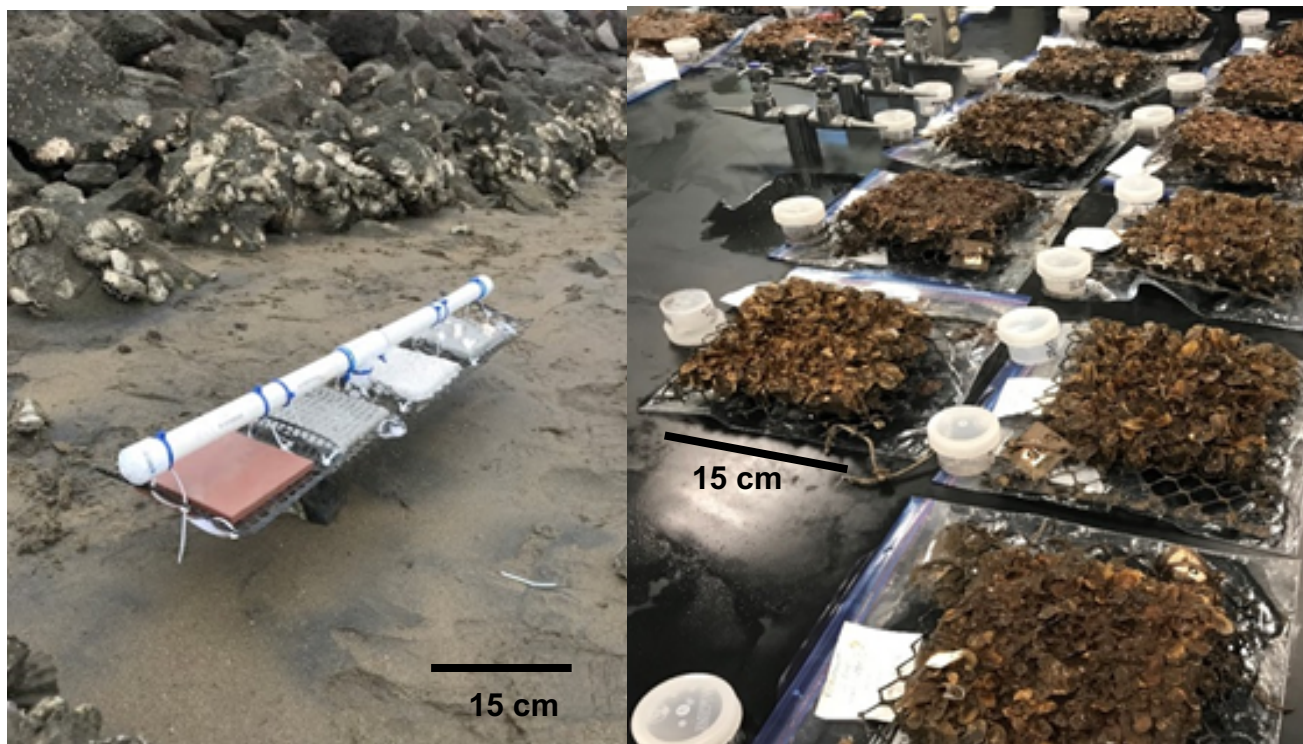


Figure 2. Left: Recently deployed tiles at GC hanging from PVC at 0.6 m MLLW on May 21, 2018. Adult *Crassostrea gigas* can be observed in the background on rip rap. Treatments shown from left to right are uncaged terracotta, rough, fine, and half shell. Right: Post-deployment tiles from GC at 0 m MLLW processed in the lab on September 8, 2018. *Ostrea lurida* is the dominant oyster species observed. Soft-bodied organism jar and mobile epifauna jar shown with each tile.

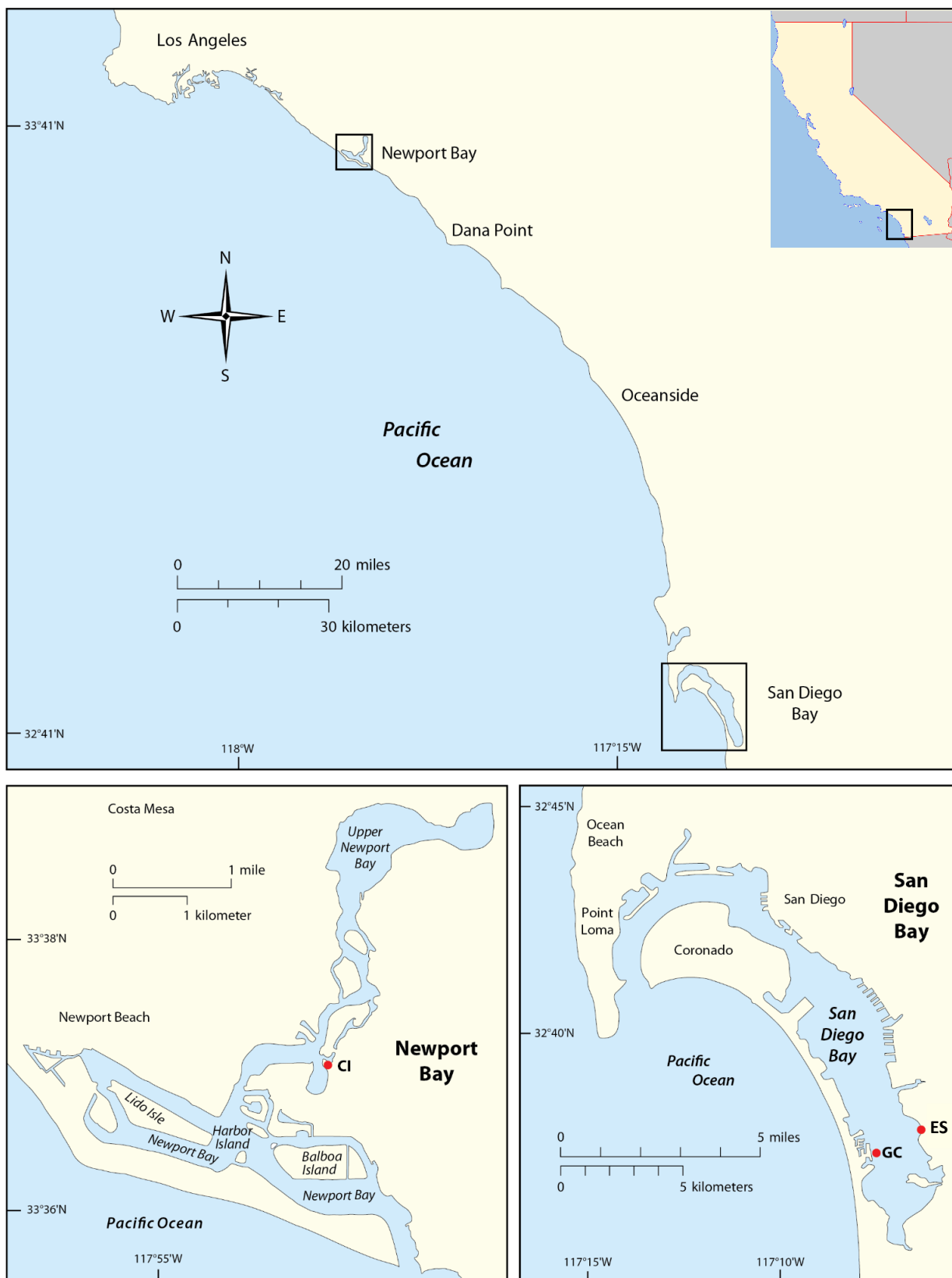


Figure 3. Map of study sites for settlement and recruitment study deployed from May – September 2018 in southern California, including Newport Bay and San Diego Bay, CA, USA (CI = Coney Island, GC = Grand Caribe, ES = E Street). Map produced by Kelly Donovan (California State University, Fullerton). Upper right map of California is open-sourced, the author is Angr, and site is Wikimedia Commons.

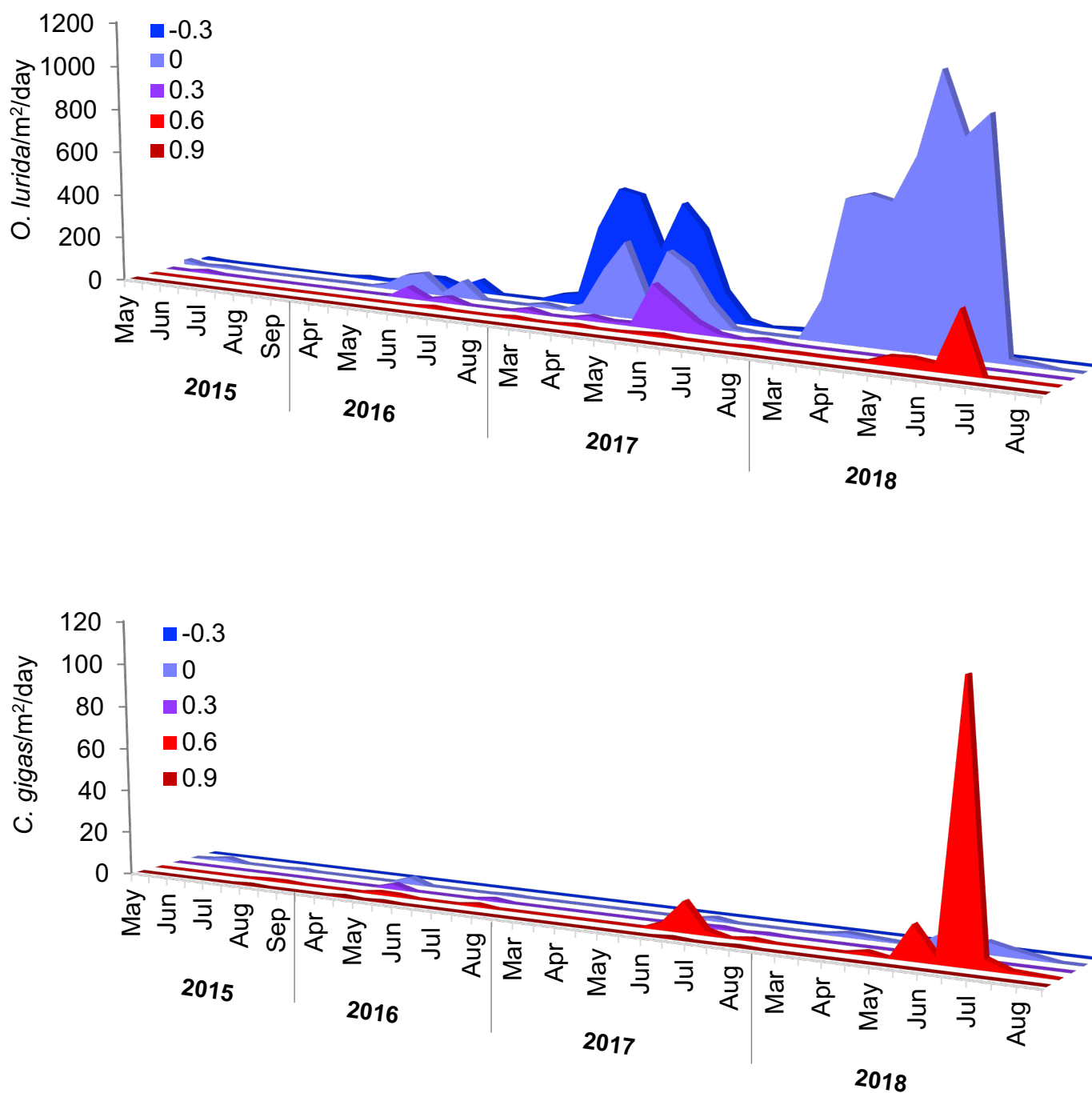


Figure 4. Oyster settlers per m² per day for *O. lurida* (top panel) and *C. gigas* (lower panel) across tidal elevations (-0.3, 0, +0.3, +0.6, and +0.9 m MLLW) on the undersides of tiles at ES during reproductive seasons from 2015-2017. In 2018, settlement at only two tidal elevations was recorded (0, 0.6 MLLW). Data for each two-week time period are averages (n = 5 replicate tiles). Note difference in scales on Y axes across panels. PVC tees were placed using the same methods in this project. Data from 2015-2017 incorporated into the figure are from Torres et al., unpublished data. Figure and caption from Zacherl & Perog, unpublished.

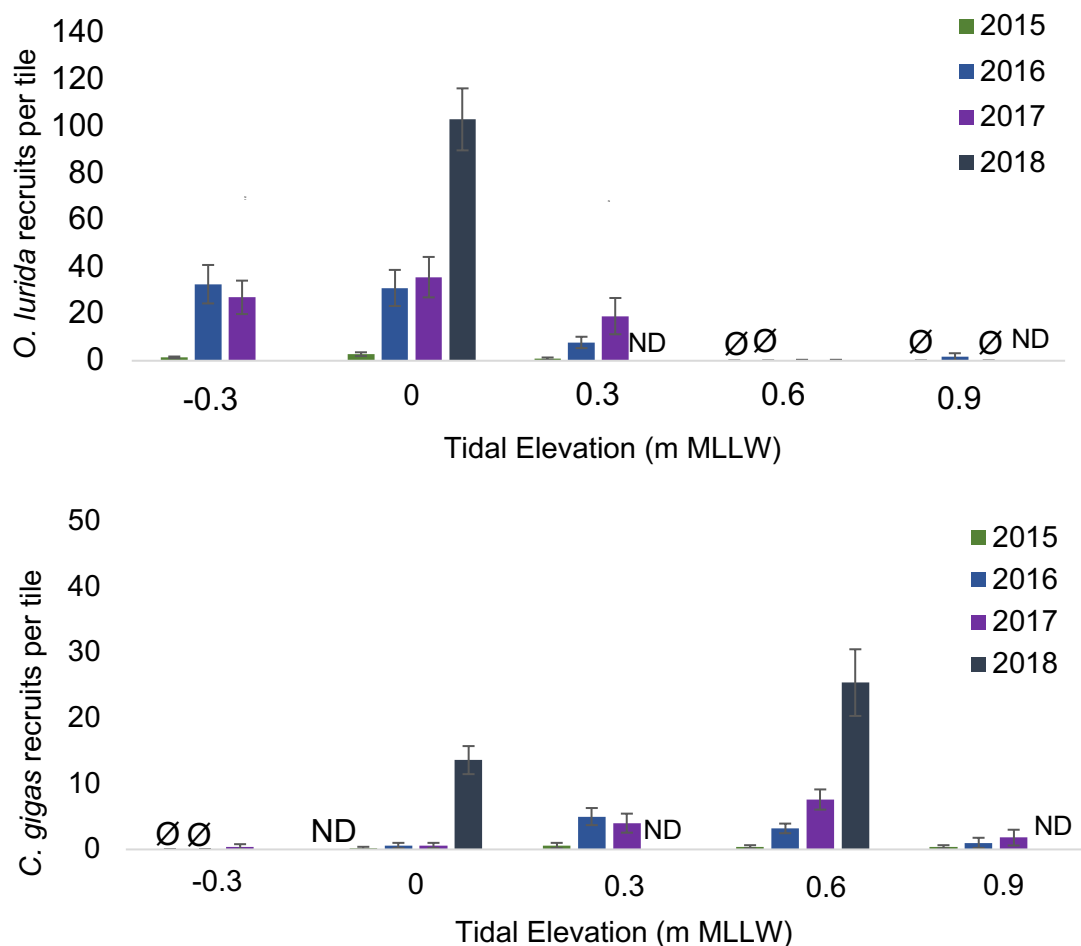


Figure 5. Average oyster recruits (± 1 SE) for *O. lurida* (top panel) and *C. gigas* (lower panel) across tidal elevations (-0.3, 0, + 0.3, + 0.6, and + 0.9 m MLLW) on the undersides of tiles at ES during reproductive seasons from 2015-2018, $n = 5$ replicate tiles per tidal elevation. ND = No data. Note difference in scales on Y axes across panels. PVC tees were placed using the same methods in this project. Data from 2015-2017 incorporated into the figure are from Torres et al., unpublished data. Figure and caption from Zacherl & Perog, unpublished.

Table 1. Three-way ANOVA test statistics for effects of site, tidal elevation, and treatment on square root-transformed mud accretion to the top of tiles deployed from May – September 2018 at all sites (CI in Newport Bay, ES and GC in San Diego Bay, CA, USA). Bold indicates significant difference.

Source	Nparm	DF	Sum of Squares	F Ratio	Prob > F
Site	2	2	17.869112	36.8322	<0.0001
Tidal elevation	1	1	9.110058	37.5557	<0.0001
Site*Tidal elevation	2	2	10.540170	21.7256	<0.0001
Treatment	5	5	3.800882	3.1338	0.0094
Site*Treatment	10	10	3.186108	1.3135	0.2245
Tidal elevation*Treatment	5	5	2.231489	1.8398	0.1063
Site*Tidal elevation*Treatment	10	10	1.908181	0.7866	0.6417

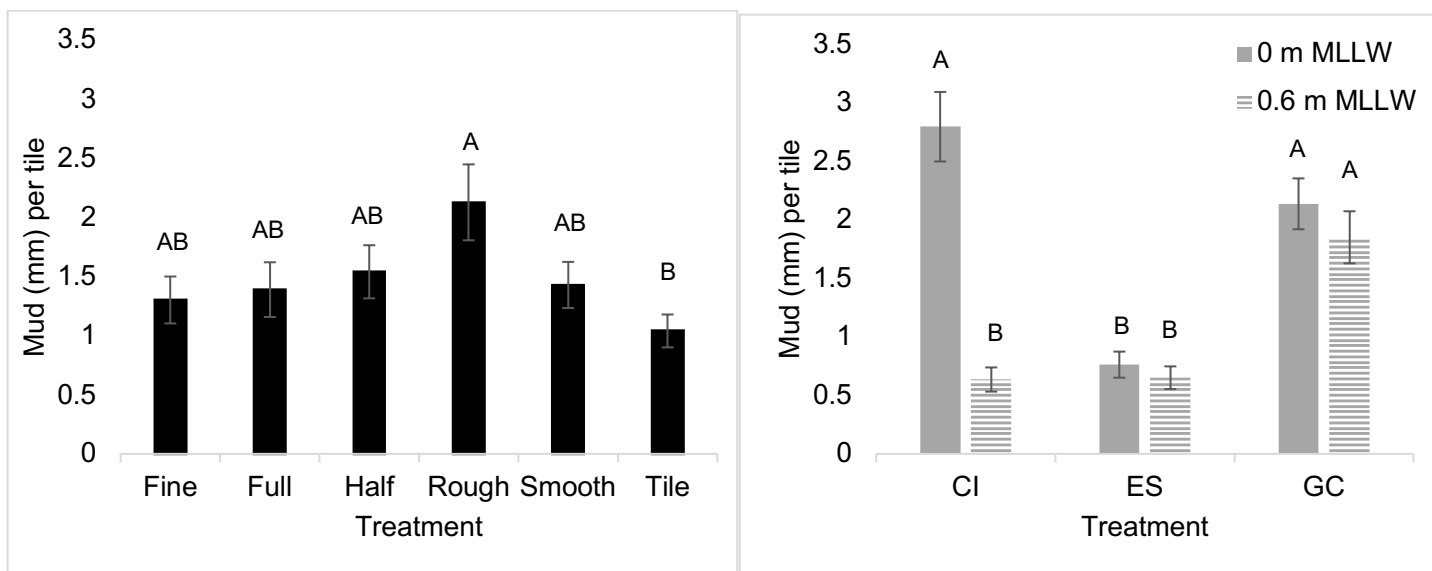


Figure 6. Mud accreted (mm) to the top of tiles deployed from May – September 2018 to Newport and San Diego Bays, CA, USA, as a function of site, tidal elevation, and treatment. Error bars = 1 SE. Different letters above bars indicate statistically significant differences based upon post-hoc Tukey HSD tests.

Table 2. Three-way ANOVA test statistics for effects of tile orientation, tidal elevation, and treatment on square root transformed percent cover of *O. lurida* per tile on tiles deployed from May – September 2018 at CI, Newport Bay, CA, USA. Bold indicates significant difference.

Source	Nparm	DF	Sum of Squares	F Ratio	Prob > F
Tile orientation	1	1	57.705485	109.5541	<0.0001
Tidal elevation	1	1	29.270745	55.5706	<0.0001
Tile orientation*Tidal elevation	1	1	15.662596	29.7355	<0.0001
Treatment	5	5	5.371519	2.0396	0.0765
Tile orientation*Treatment	5	5	11.974571	4.5468	0.0007
Tidal elevation*Treatment	5	5	8.635876	3.2791	0.0078
Tile orientation*Tidal elevation*Treatment	5	5	6.618103	2.5129	0.0325

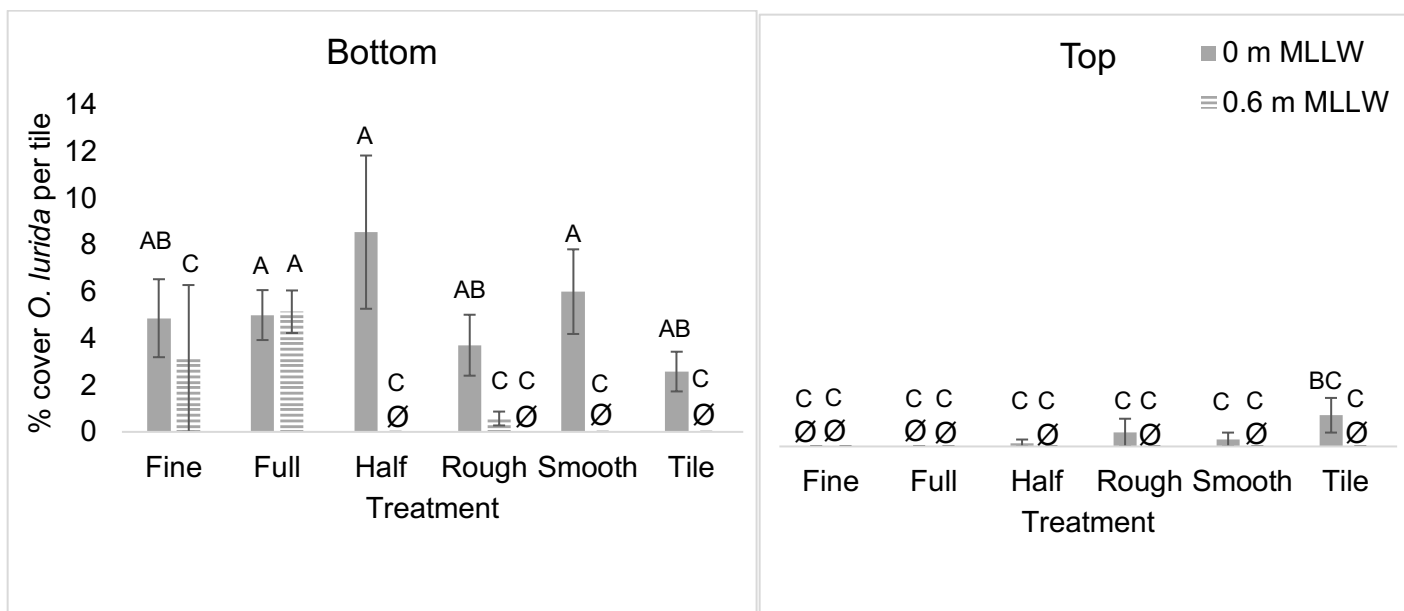


Figure 7. Percent cover of *O. lurida* per tile on tiles deployed from May – September 2018 at CI, Newport Bay, CA, USA as a function of tile orientation, tidal elevation, and treatment (solid = 0 m MLLW, striped = 0.6 m MLLW). Error bars = 1 SE. Different letters above bars indicate statistically significant differences based upon post-hoc Tukey HSD tests.

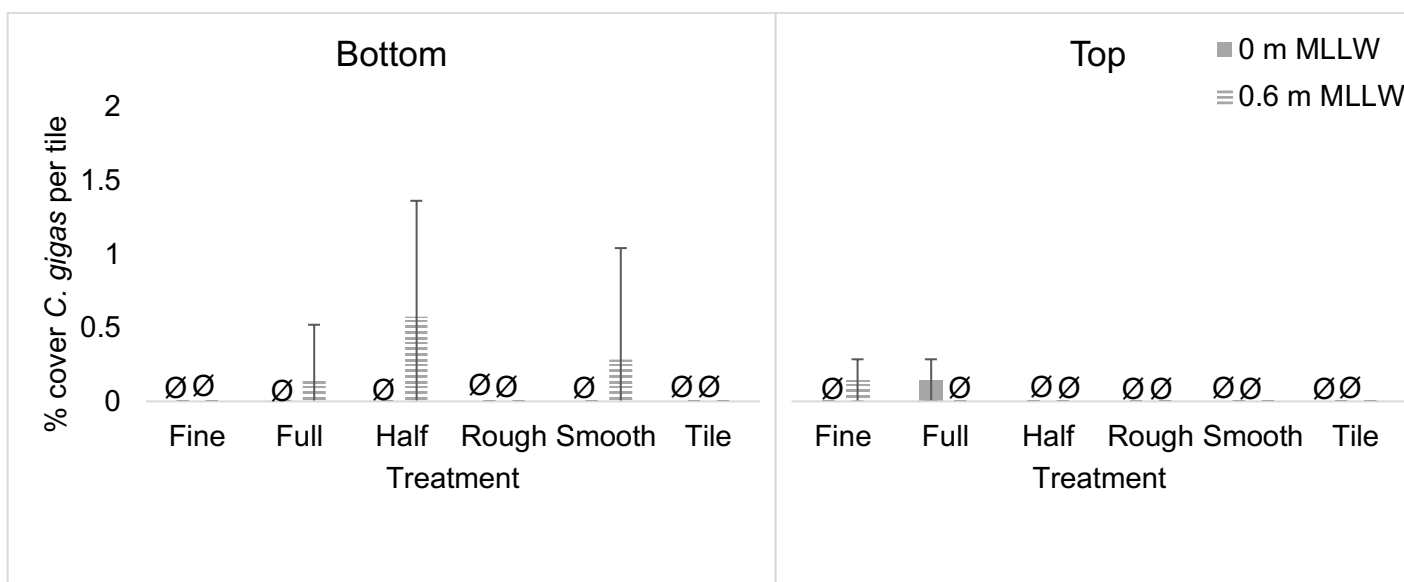


Figure 8. Percent cover of *C. gigas* per tile on tiles deployed from May – September 2018 at CI, Newport Bay, CA, USA as a function of tile orientation, tidal elevation, and treatment (solid = 0 m MLLW, striped = 0.6 m MLLW). Error bars = 1 SE. No statistical analyses were completed because data did not meet the assumptions of ANOVA.

Table 3. Three-way ANOVA test statistics for effects tile orientation, tidal elevation, and treatment on rank-averaged percent cover of *O. lurida* - *C. gigas* per tile on tiles deployed from May – September 2018 at CI, Newport Bay, CA, USA. Bold indicates significant difference.

Source	Nparm	DF	Sum of Squares	F Ratio	Prob > F
Tile orientation	1	1	74888.149	132.3343	<0.0001
Tidal elevation	1	1	53214.881	94.0356	<0.0001
Tile orientation*Tidal elevation	1	1	26777.625	47.3185	<0.0001
Treatment	5	5	10743.893	3.7971	0.0029
Tile orientation*Treatment	5	5	22883.815	8.0876	<0.0001
Tidal elevation*Treatment	5	5	16952.798	5.9914	<0.0001
Tile orientation*Tidal elevation*Treatment	5	5	8691.554	3.0718	0.0115

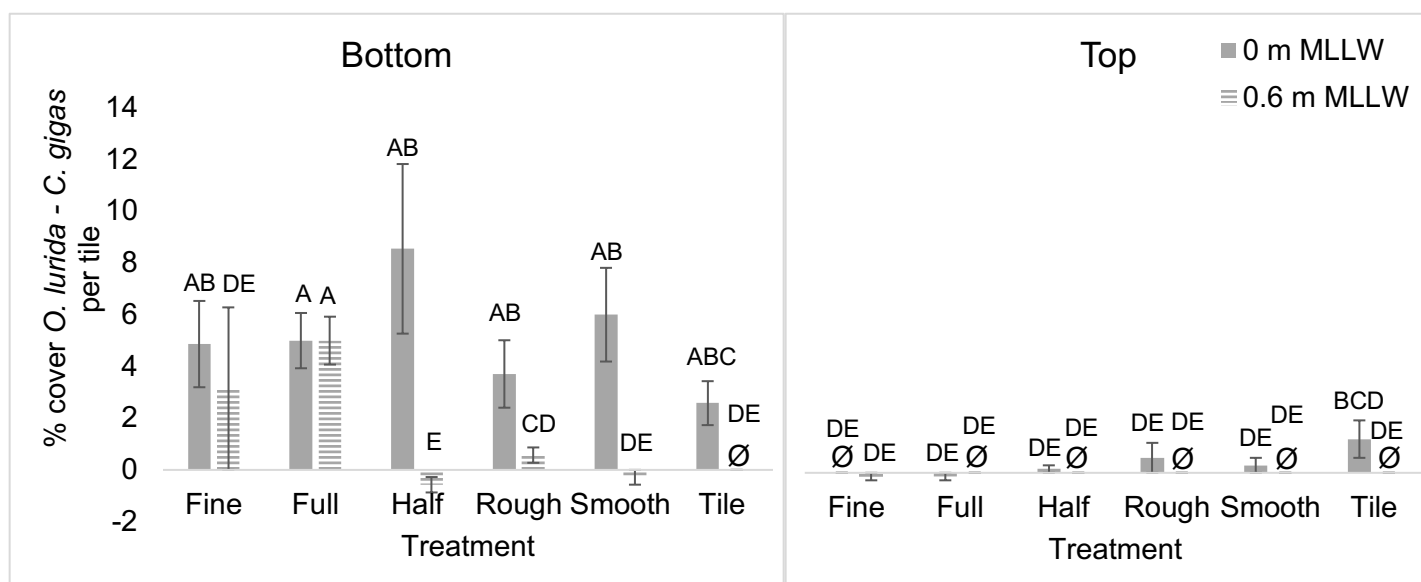


Figure 9. Percent cover of *O. lurida* - *C. gigas* per tile on tiles deployed from May – September 2018 at CI, Newport Bay, CA, USA as a function of tile orientation, tidal elevation, and treatment (solid = 0 m MLLW, striped = 0.6 m MLLW). Error bars = 1 SE. Different letters above bars indicate statistically significant differences based upon post-hoc Tukey HSD tests.

Table 4. Three-way ANOVA test statistics for effects of tile orientation, tidal elevation, and treatment on log transformed percent cover of *O. lurida* per tile on tiles deployed from May – September 2018 at ES, San Diego Bay, CA, USA. Bold indicates significant difference.

Source	Nparm	DF	Sum of Squares	F Ratio	Prob > F
Tile orientation	1	1	79.44907	405.2336	<0.0001
Tidal elevation	1	1	116.87075	596.1046	<0.0001
Tile orientation*Tidal elevation	1	1	60.02596	306.1652	<0.0001
Treatment	5	5	2.50002	2.5503	0.0304
Tile orientation*Treatment	5	5	1.05921	1.0805	0.3738
Tidal elevation*Treatment	5	5	0.36145	0.3687	0.8694
Tile orientation*Tidal elevation*Treatment	5	5	2.92190	2.9807	0.0137

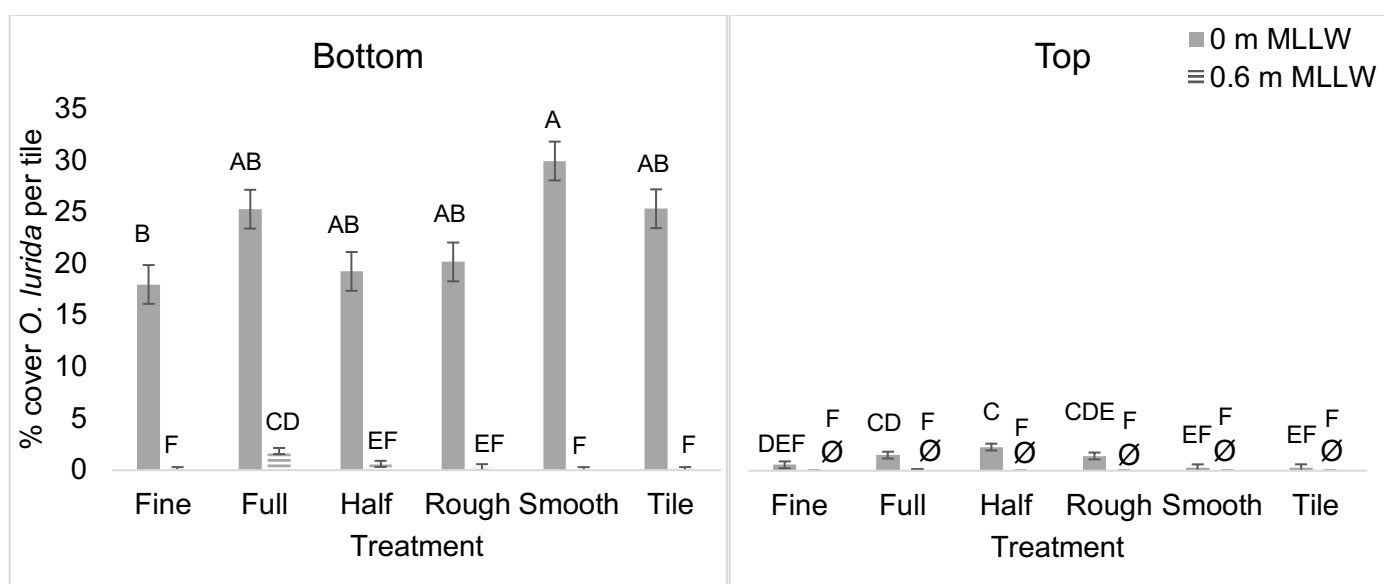


Figure 10. Percent cover of *O. lurida* per tile on tiles deployed from May – September 2018 at ES, San Diego Bay, CA, USA as a function of tile orientation, tidal elevation, and treatment (solid = 0 m MLLW, striped = 0.6 m MLLW). Error bars = 1 SE. Different letters above bars indicate statistically significant differences based upon post-hoc Tukey HSD tests.

Table 5. Three-way ANOVA test statistics for effects of tile orientation, tidal elevation, and treatment on square root transformed percent cover of *C. gigas* per tile on tiles deployed from May – September 2018 at ES, San Diego Bay, CA, USA. Bold indicates significant difference.

Source	Nparm	DF	Sum of Squares	F Ratio	Prob > F
Tile orientation	1	1	231.64735	202.2946	<0.0001
Tidal elevation	1	1	96.18026	83.9930	<0.0001
Tile orientation*Tidal elevation	1	1	0.01071	0.0094	0.9231
Treatment	5	5	74.45919	13.0048	<0.0001
Tile orientation*Treatment	5	5	9.06598	1.5834	0.1685
Tidal elevation*Treatment	5	5	43.86673	7.6616	<0.0001
Tile orientation*Tidal elevation*Treatment	5	5	12.84625	2.2437	0.0532

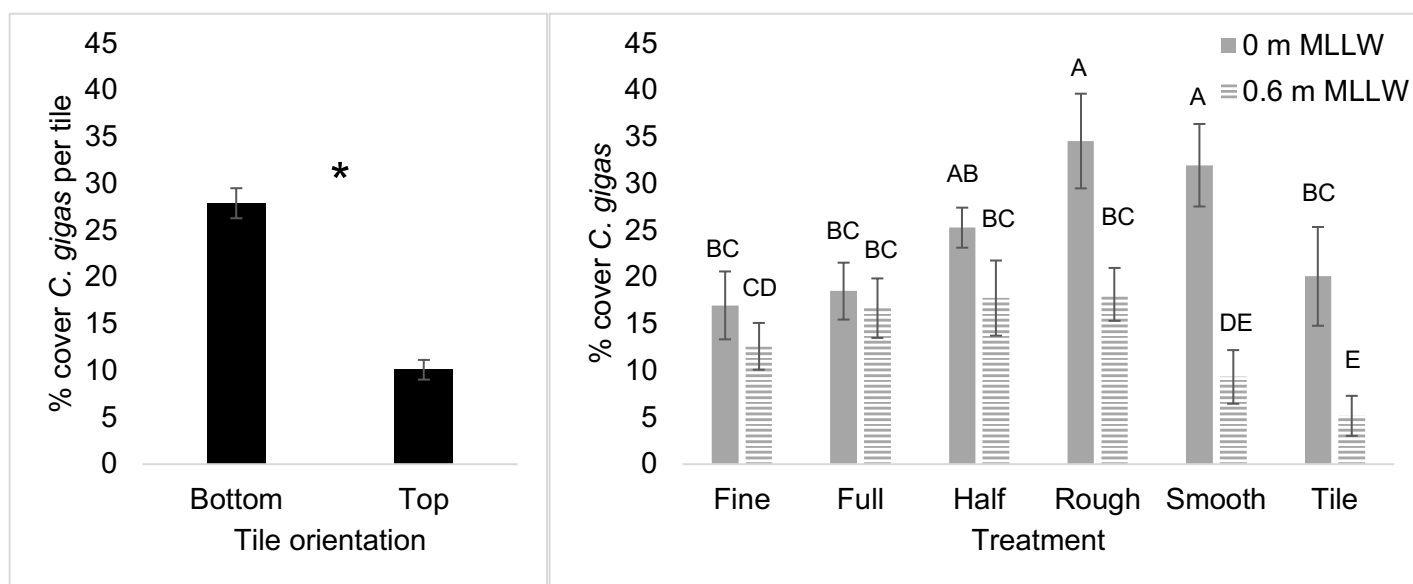


Figure 11. Percent cover of *C. gigas* per tile on tiles deployed from May – September 2018 at ES, San Diego Bay, CA, USA as a function of tile orientation, tidal elevation, and treatment (solid grey = 0 m MLLW, striped grey = 0.6 m MLLW). Error bars = 1 SE. Symbol between bars indicates statistically significant difference. Different letters above bars indicate statistically significant differences based upon post-hoc Tukey HSD tests.

Table 6. Three-way ANOVA test statistics for effects of tile orientation, tidal elevation, and treatment on percent cover of *O. lurida* - *C. gigas* per tile on tiles deployed from May – September 2018 at ES, San Diego Bay, CA, USA. Bold indicates significant difference.

Source	Nparm	DF	Sum of Squares	F Ratio	Prob > F
Tile orientation	1	1	1946.4024	13.5082	0.0003
Tidal elevation	1	1	2.4533	0.0170	0.8964
Tile orientation*Tidal elevation	1	1	2512.6936	17.4384	<0.0001
Treatment	5	5	3446.0068	4.7831	0.0005
Tile orientation*Treatment	5	5	379.4246	0.5266	0.7558
Tidal elevation*Treatment	5	5	1724.8902	2.3942	0.0405
Tile orientation*Tidal elevation*Treatment	5	5	1144.9178	1.5892	0.1669

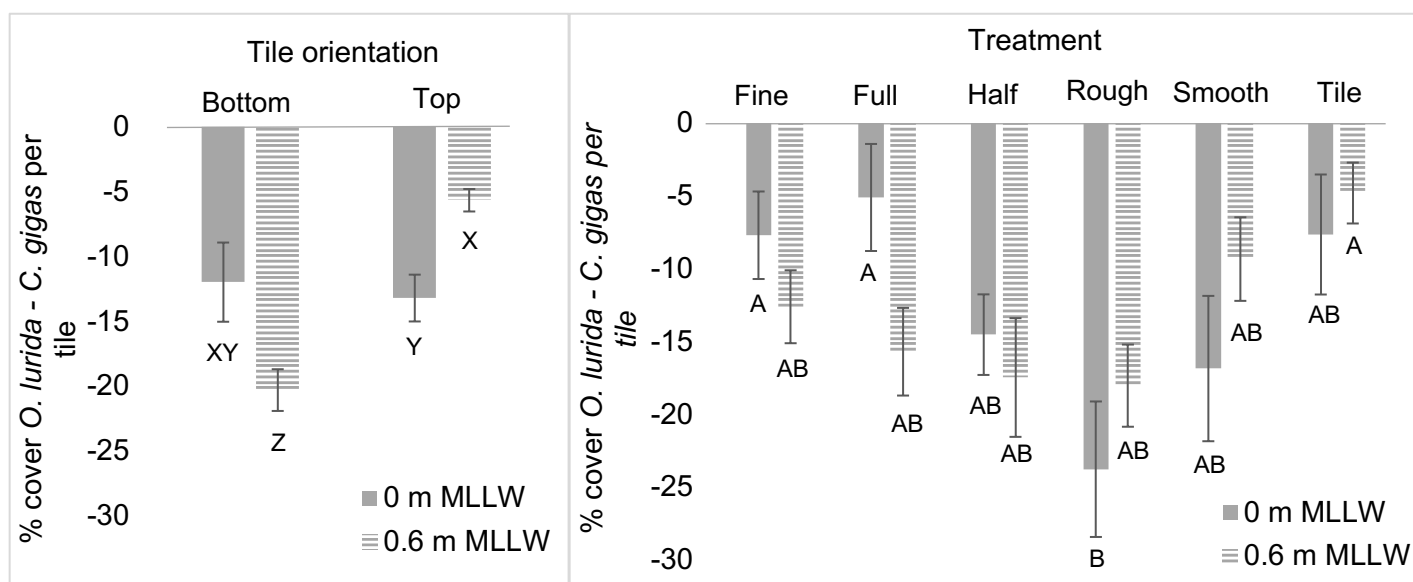


Figure 12. Percent cover of *O. lurida* - *C. gigas* per tile on tiles deployed from May – September 2018 at ES, San Diego Bay, CA, USA as a function of tile orientation, tidal elevation, and treatment (grey = 0 m MLLW, striped = 0.6 m MLLW). Error bars = 1 SE. Different letters below bars indicate statistically significant differences based upon post-hoc Tukey HSD tests.

Table 7. Three-way ANOVA test statistics for effects of tile orientation, tidal elevation, and treatment on square root transformed percent cover of *O. lurida* per tile on tiles deployed from May – September 2018 at GC, San Diego Bay, CA, USA. Bold indicates significant difference.

Source	Nparm	DF	Sum of Squares	F Ratio	Prob > F
Tile orientation	1	1	548.89965	727.0875	<0.0001
Tidal elevation	1	1	510.28523	675.9378	<0.0001
Tile orientation*Tidal elevation	1	1	186.66770	247.2651	<0.0001
Treatment	5	5	21.31341	5.6465	<0.0001
Tile orientation*Treatment	5	5	8.10359	2.1468	0.0633
Tidal elevation*Treatment	5	5	27.98469	7.4139	<0.0001
Tile orientation*Tidal elevation*Treatment	5	5	20.63898	5.4678	0.0001

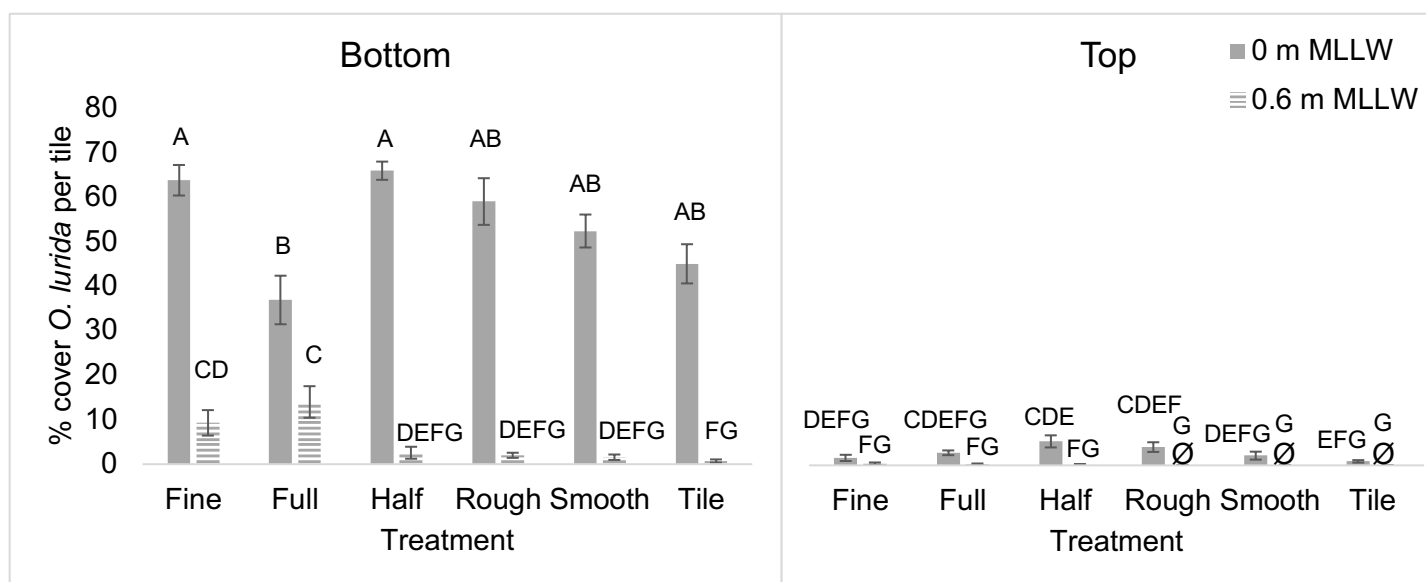


Figure 13. Percent cover of *O. lurida* per tile on tiles deployed from May – September 2018 at GC, San Diego Bay, CA, USA as a function of tile orientation, tidal elevation, and treatment (solid = 0 m MLLW, striped = 0.6 m MLLW). Error bars = 1 SE. Different letters above bars indicate statistically significant differences based upon post-hoc Tukey HSD tests.

Table 8. Three-way ANOVA test statistics for effects of tile orientation, tidal elevation, and treatment on percent cover of square root transformed *C. gigas* per tile on tiles deployed from May – September 2018 at GC, San Diego Bay, CA, USA. Bold indicates significant difference.

Source	Nparm	DF	Sum of Squares	F Ratio	Prob > F
Tile orientation	1	1	558.59922	441.0958	<0.0001
Tidal elevation	1	1	330.94099	261.3264	<0.0001
Tile orientation*Tidal elevation	1	1	347.73714	274.5894	<0.0001
Treatment	5	5	55.97586	8.8402	<0.0001
Tile orientation*Treatment	5	5	86.29489	13.6285	<0.0001
Tidal elevation*Treatment	5	5	20.20095	3.1903	0.0092
Tile orientation*Tidal elevation*Treatment	5	5	21.19156	3.3468	0.0069

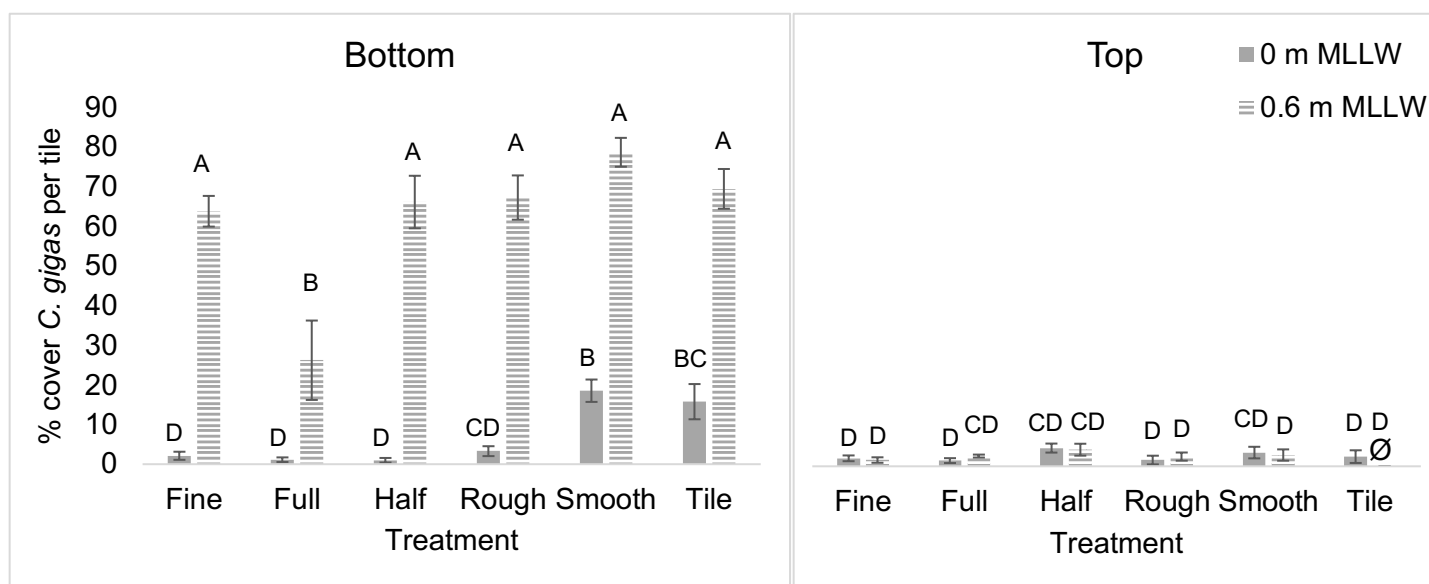


Figure 14. Percent cover of *C. gigas* per tile on tiles deployed from May – September 2018 at GC, San Diego Bay, CA, USA as a function of tile orientation, tidal elevation, and treatment (solid = 0 m MLLW, striped = 0.6 m MLLW). Error bars = 1 SE. Different letters above bars indicate statistically significant differences based upon post-hoc Tukey HSD tests.

Table 9. Three-way ANOVA test statistics for effects of tile orientation, tidal elevation, and treatment on percent cover of *O. lurida* - *C. gigas* per tile on tiles deployed from May – September 2018 at GC, San Diego Bay, CA, USA. Bold indicates significant difference.

Source	Nparm	DF	Sum of Squares	F Ratio	Prob > F
Tile orientation	1	1	803.39	5.4439	0.0210
Tidal elevation	1	1	118951.77	806.0307	<0.0001
Tile orientation*Tidal elevation	1	1	107554.21	728.7996	<0.0001
Treatment	5	5	6569.94	8.9037	<0.0001
Tile orientation*Treatment	5	5	5827.53	7.8976	<0.0001
Tidal elevation*Treatment	5	5	7602.78	10.3035	<0.0001
Tile orientation*Tidal elevation*Treatment	5	5	7429.65	10.0688	<0.0001

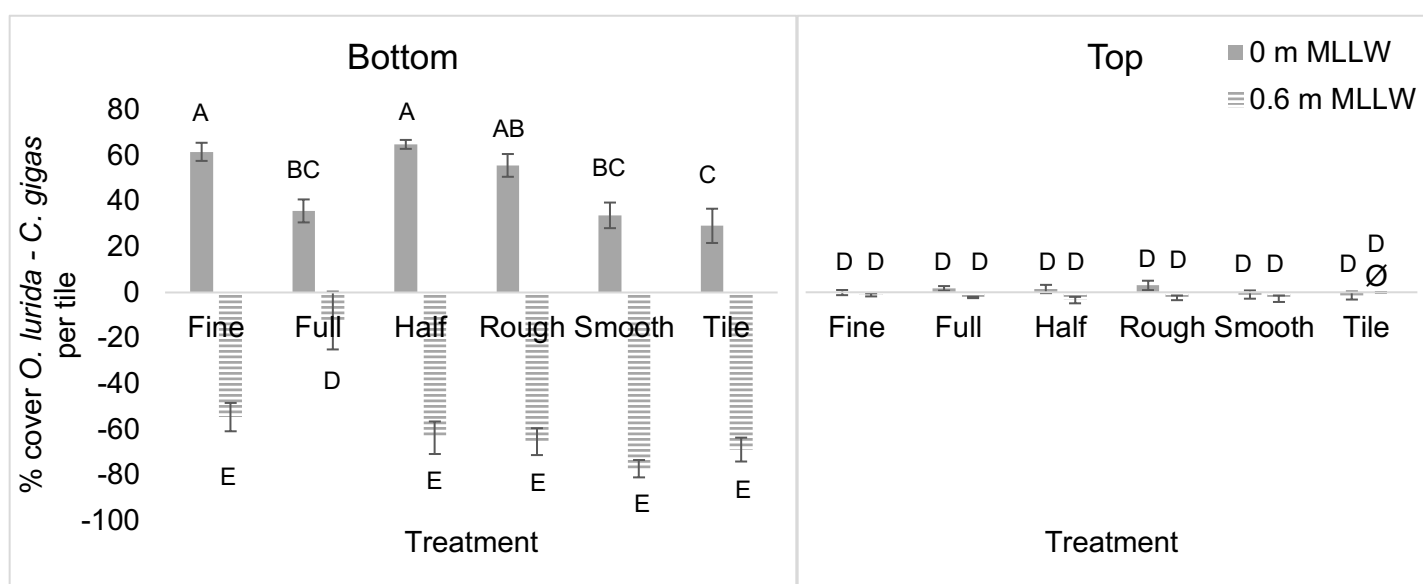


Figure 15. Percent cover of *O. lurida* - *C. gigas* per tile on tiles deployed from May – September 2018 at GC, San Diego Bay, CA, USA as a function of tile orientation, tidal elevation, and treatment (solid = 0 m MLLW, striped = 0.6 m MLLW). Error bars = 1 SE. Different letters above bars indicate statistically significant differences based upon post-hoc Tukey HSD tests.

Table 10. Three-way ANCOVA test statistics for effects of tidal elevation, shell cover, and rugosity on number of *O. lurida* per tile at CI, Newport Bay, CA, USA, deployed from May – September 2018. Bold indicates significant difference.

Source	Nparm	DF	Sum of Squares	F Ratio	Prob > F
Tidal elevation	1	1	661.23636	12.6873	0.0008
Shell cover	1	1	391.79696	7.5175	0.0086
Tidal elevation*Shell cover	1	1	152.29059	2.9220	0.0938
Rugosity	1	1	116.32048	2.2319	0.1417
Tidal elevation*Rugosity	1	1	46.51182	0.8924	0.3495
Shell cover*Rugosity	1	1	148.78836	2.8548	0.0976
Tidal elevation*Shell cover*Rugosity	1	1	7.93868	0.1523	0.6981

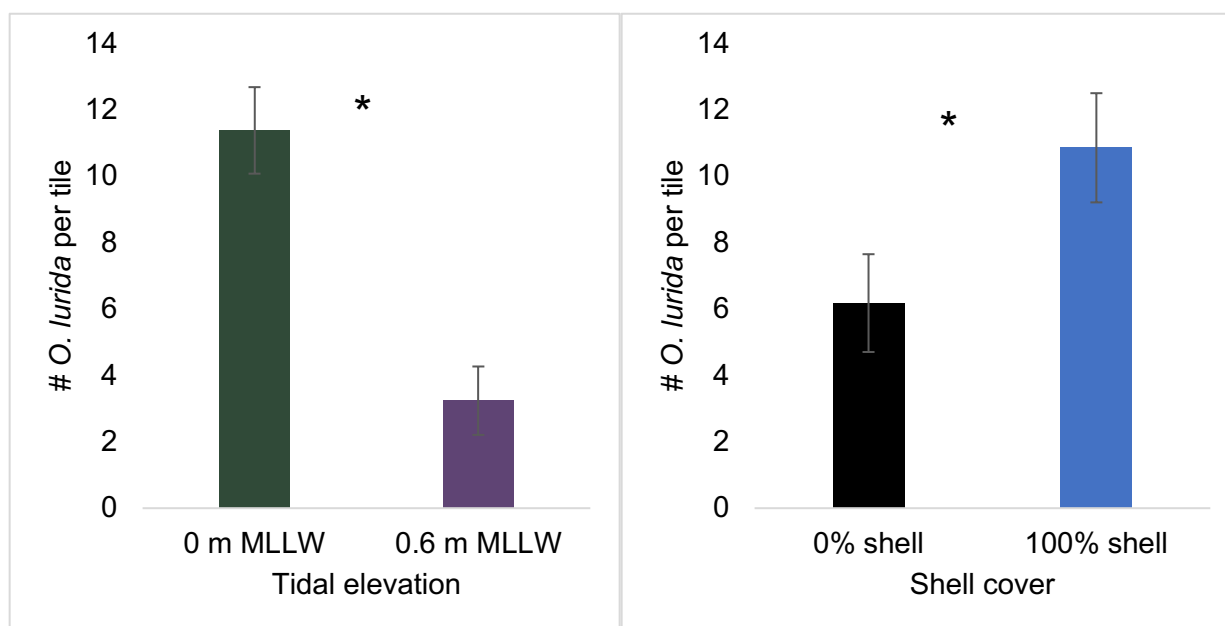


Figure 16. Number of *O. lurida* per tile on tiles deployed from May – September 2018 at CI, Newport Bay, CA, USA as a function of tidal elevation, shell cover, and rugosity. Error bars = 1 SE. Symbol between bars indicates statistically significant difference.

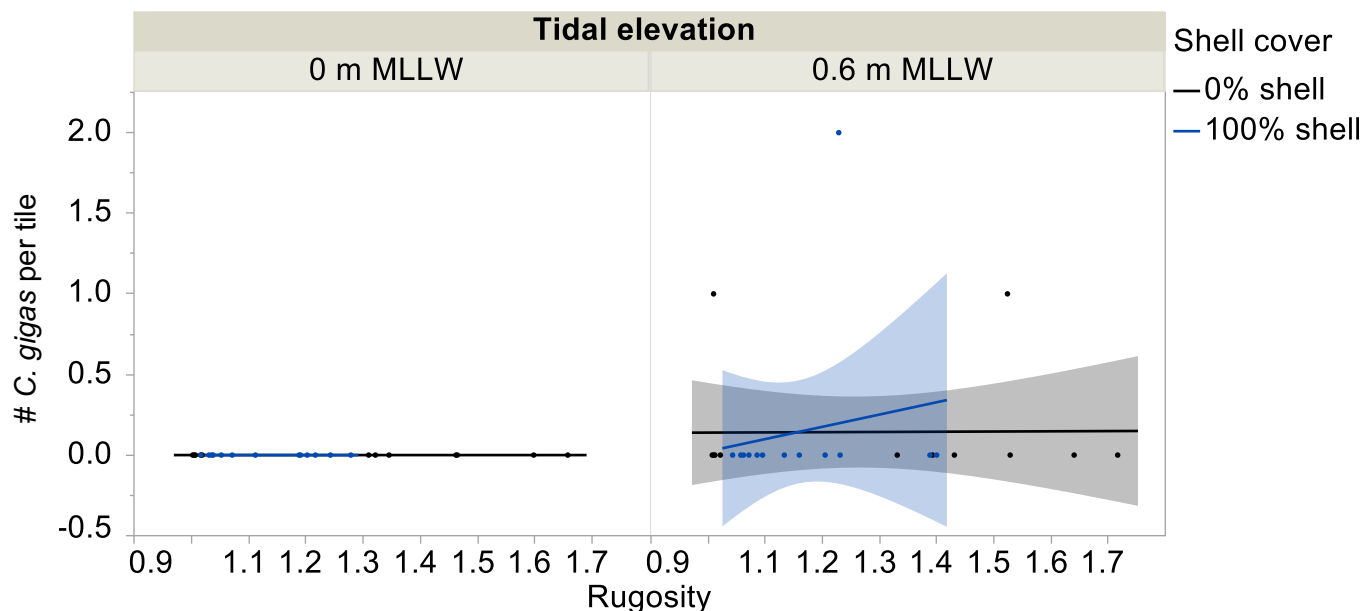


Figure 17. Number of *C. gigas* per tile on tiles deployed from May – September 2018 at CI, Newport Bay, CA, USA as a function of tidal elevation, shell cover, and rugosity (black = 0% shell, blue = 100% shell). Shaded regions represent 95% confidence fit. For 0 m MLLW, Y (0% shell) = $0 + 0x$, R^2 (0% shell) = 0.00, Y (100% shell) = $0 + 0x$, R^2 (100% shell) = 0.00. For 0.6 m MLLW, Y (0% shell) = $0.13 + 0.014x$, R^2 (0% shell) = 0.00; Y (100% shell) = $-0.74 + 0.76x$, R^2 (100% shell) = 0.03.

Table 11. Three-way ANCOVA test statistics for effects of tidal elevation, shell cover, and rugosity on number of *O. lurida* - *C. gigas* per tile at CI, Newport Bay, CA, USA, deployed from May – September 2018. Bold indicates significant difference.

Source	Nparm	DF	Sum of Squares	F Ratio	Prob > F
Tidal elevation	1	1	689.40400	13.2850	0.0007
Shell cover	1	1	389.77263	7.5110	0.0086
Tidal elevation*Shell cover	1	1	151.02949	2.9104	0.0945
Rugosity	1	1	112.29105	2.1639	0.1478
Tidal elevation*Rugosity	1	1	43.97689	0.8474	0.3619
Shell cover*Rugosity	1	1	144.38442	2.7823	0.1018
Tidal elevation*Shell cover*Rugosity	1	1	6.94686	0.1339	0.7161

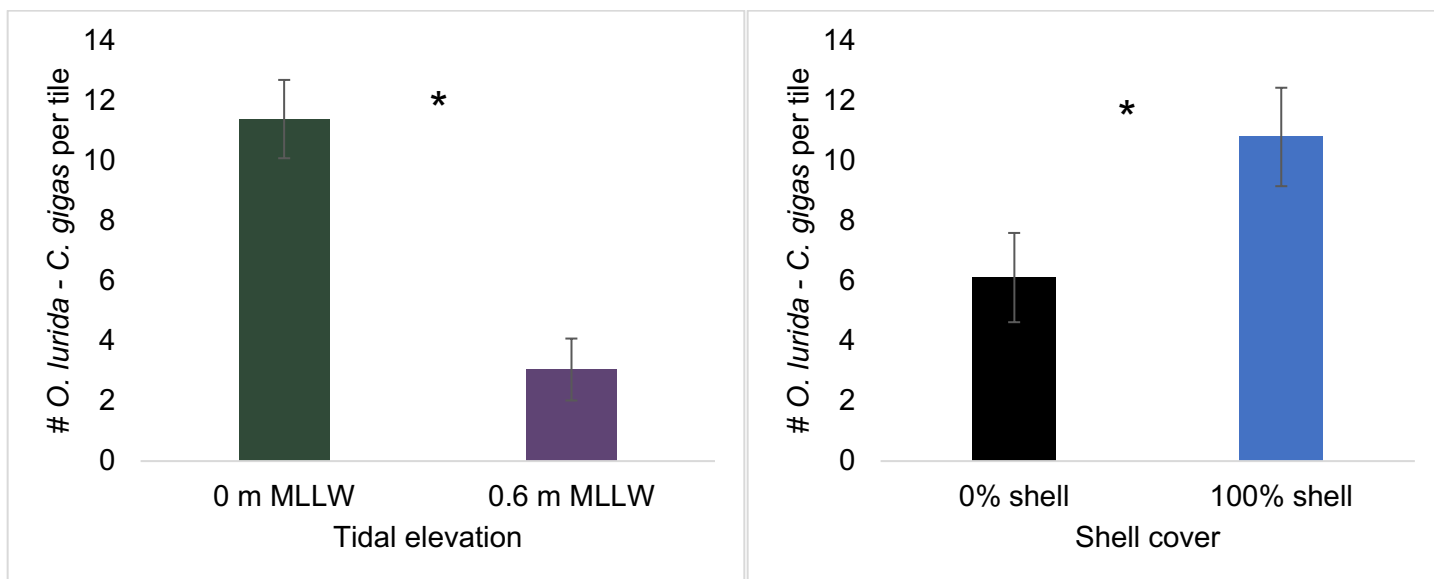


Figure 18. Number of *O. lurida* - *C. gigas* per tile on tiles deployed from May – September 2018 at CI, Newport Bay, CA, USA as a function of tidal elevation, shell cover, and rugosity. Error bars = 1 SE. Symbol between bars indicate statistically significant difference.

Table 12. Three-way ANCOVA test statistics for effects of tidal elevation, shell cover, and rugosity on log transformed percent cover of *O. lurida* per tile at CI, Newport Bay, CA, USA, deployed from May – September 2018. Bold indicates significant difference.

Source	Nparm	DF	Sum of Squares	F Ratio	Prob > F
Tidal elevation	1	1	9.2166617	18.0278	<0.0001
Shell cover	1	1	4.8827879	9.5507	0.0033
Tidal elevation*Shell cover	1	1	3.3529211	6.5583	0.0136
Rugosity	1	1	2.0962156	4.1002	0.0485
Tidal elevation*Rugosity	1	1	2.2311943	4.3642	0.0420
Shell cover*Rugosity	1	1	2.0887557	4.0856	0.0488
Tidal elevation*Shell cover*Rugosity	1	1	0.5178693	1.0130	0.3192

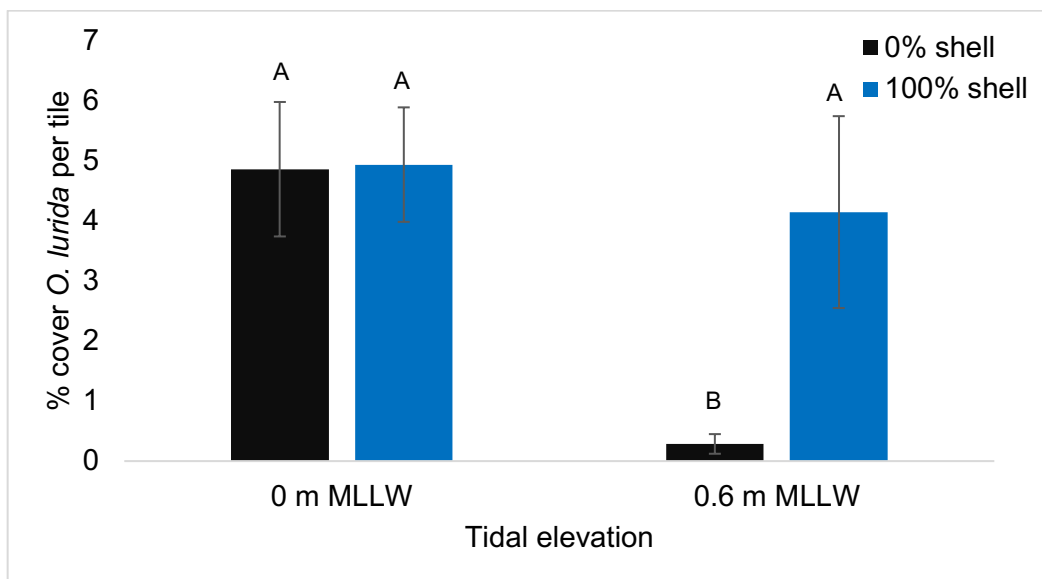


Figure 19. Percent cover of *O. lurida* per tile on tiles deployed from May – September 2018 at CI, Newport Bay, CA, USA as a function of tidal elevation, shell cover, and rugosity (black = 0% shell, blue = 100% shell). Error bars = 1 SE. Different letters above bars indicate statistically significant differences based upon post-hoc Tukey HSD tests.

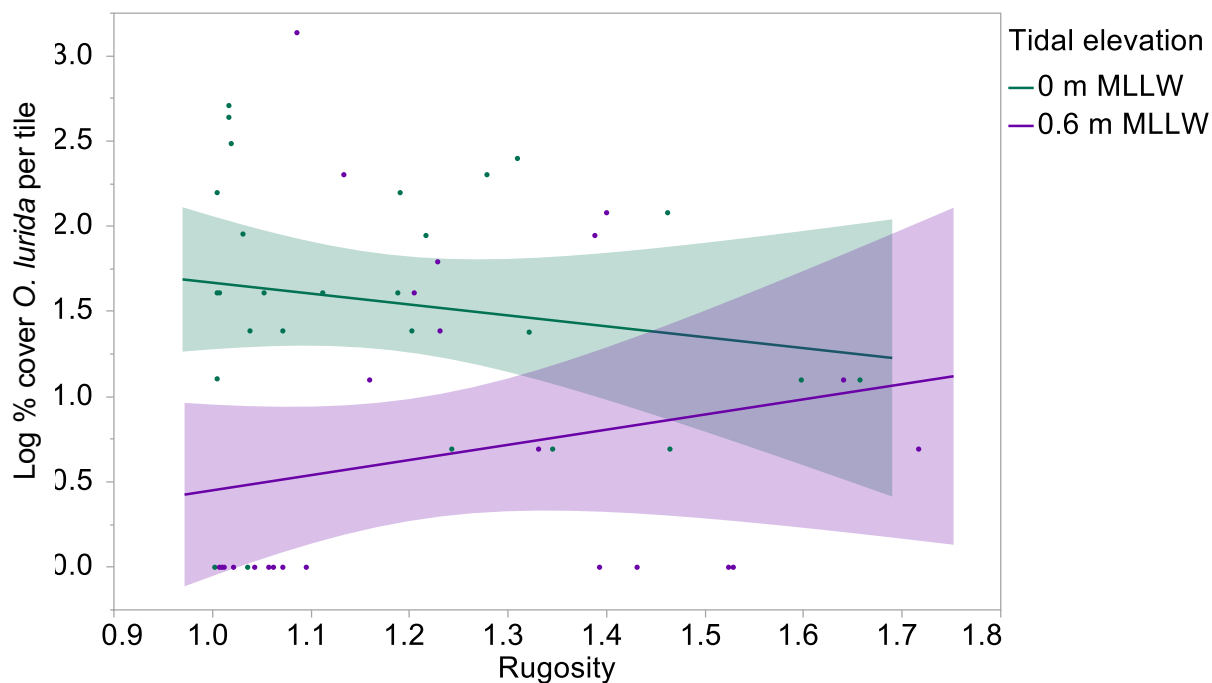


Figure 20. Log transformed percent cover *O. lurida* per tile on tiles deployed from May – September 2018 at CI, Newport Bay, CA, USA as a function of tidal elevation, shell cover, and rugosity (green = 0 m MLLW, purple = 0.6 m MLLW). Shaded regions represent 95% confidence fit. Y (0 m MLLW) = $2.31 - 0.64x$, R^2 (0 m MLLW) = 0.03; Y (0.6 m MLLW) = $-0.44 + 0.89x$, R^2 (0.6 m MLLW) = 0.04.

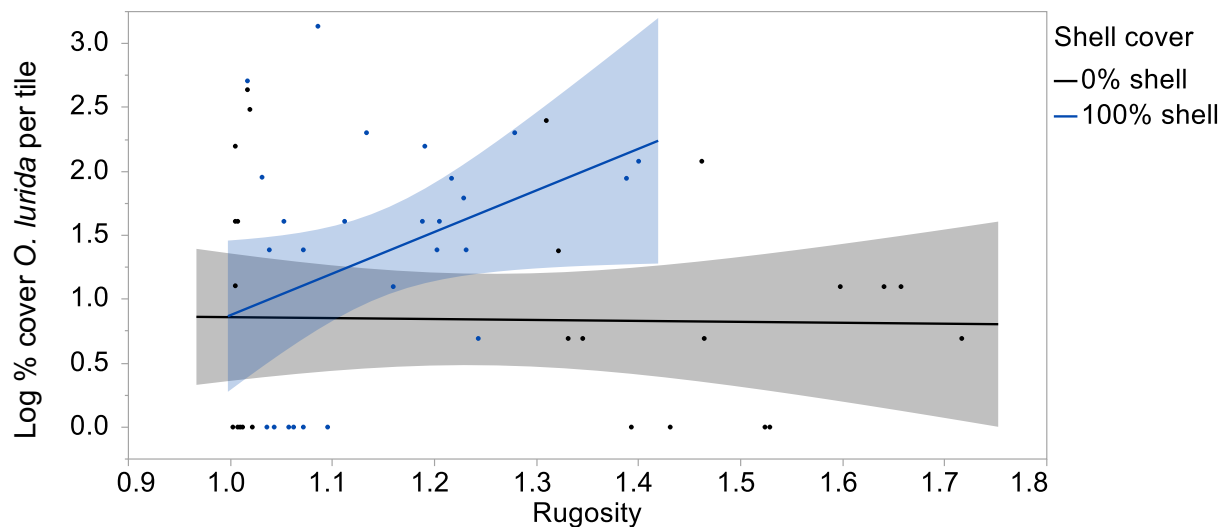


Figure 21. Log transformed percent cover *O. lurida* per tile on tiles deployed from May – September 2018 at CI, Newport Bay, CA, USA as a function of tidal elevation, shell cover, and rugosity (black = 0% shell, blue = 100% shell). Shaded regions represent 95% confidence fit. Y (0% shell) = $0.93 - 0.07x$, R^2 (0% shell) = 0.00; Y (100% shell) = $-2.38 + 3.25x$, R^2 (100% shell) = 0.14.

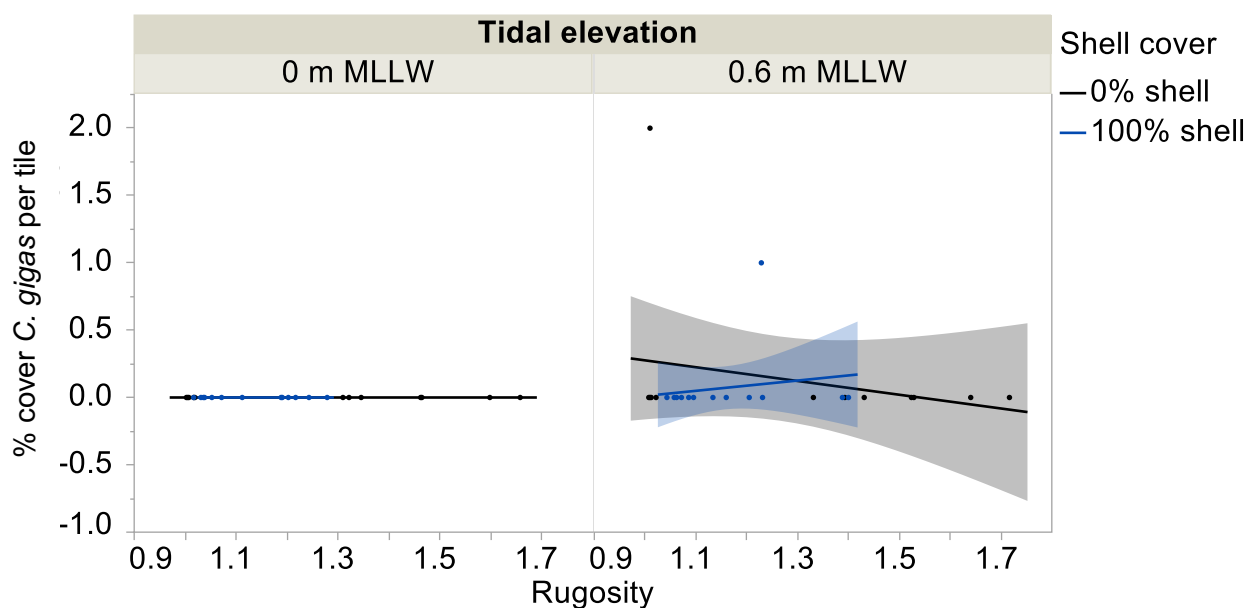


Figure 22. Percent cover *C. gigas* per tile on tiles deployed from May – September 2018 at CI, Newport Bay, CA, USA as a function of tidal elevation, shell cover, and rugosity (black = 0% shell, blue = 100% shell). Shaded regions represent 95% confidence fit. For 0 m MLLW, Y (0% shell) = $0 + 0x$, R^2 (0% shell) = 0; Y (100% shell) = $0 + 0x$, R^2 (100% shell) = 0. For 0.6 m MLLW, Y (0% shell) = $0.79 - 0.51x$, R^2 (0% shell) = 0.07; Y (100% shell) = $-0.37 + 0.38x$, R^2 (100% shell) = 0.03.

Table 13. Three-way ANCOVA test statistics for effects of tidal elevation, shell cover, and rugosity on log transformed percent cover of *O. lurida* – *C. gigas* per tile at CI, Newport Bay, CA, USA, deployed from May – September 2018. Bold indicates significant difference.

Source	Nparm	DF	Sum of Squares	F Ratio	Prob > F
Tidal elevation	1	1	10.928326	20.5535	<0.0001
Shell cover	1	1	5.171194	9.7258	0.0031
Tidal elevation*Shell cover	1	1	3.592621	6.7568	0.0124
Rugosity	1	1	2.107870	3.9644	0.0522
Tidal elevation*Rugosity	1	1	2.243218	4.2189	0.0454
Shell cover*Rugosity	1	1	1.723675	3.2418	0.0781
Tidal elevation*Shell cover*Rugosity	1	1	0.344882	0.6486	0.4246

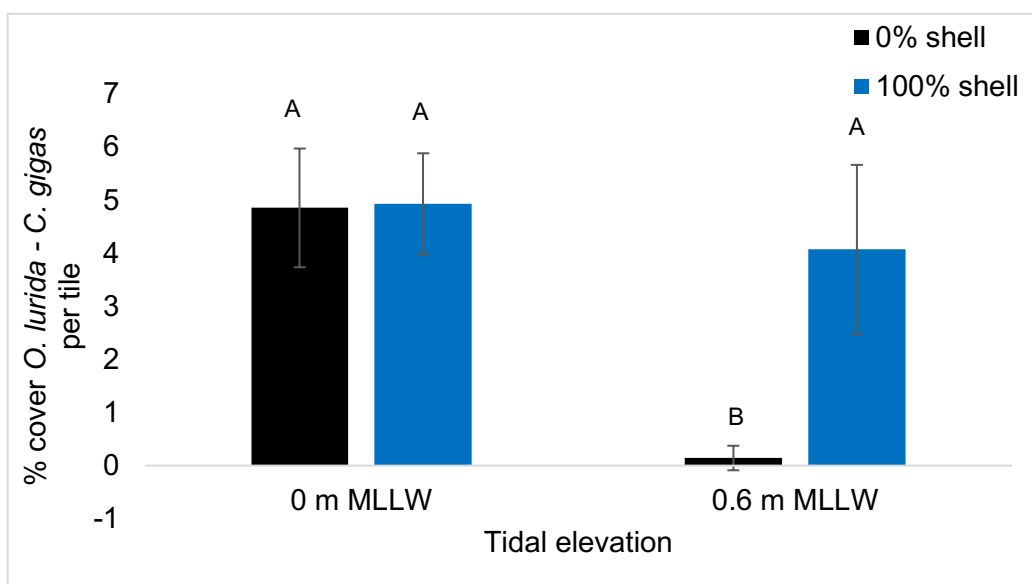


Figure 23. Percent cover of *O. lurida* - *C. gigas* per tile on tiles deployed from May – September 2018 at CI, Newport Bay, CA, USA as a function of tidal elevation, shell cover, and rugosity (black = 0% shell, blue = 100% shell). Error bars = 1 SE. Different letters above bars indicate statistically significant differences based upon post-hoc Tukey HSD tests.

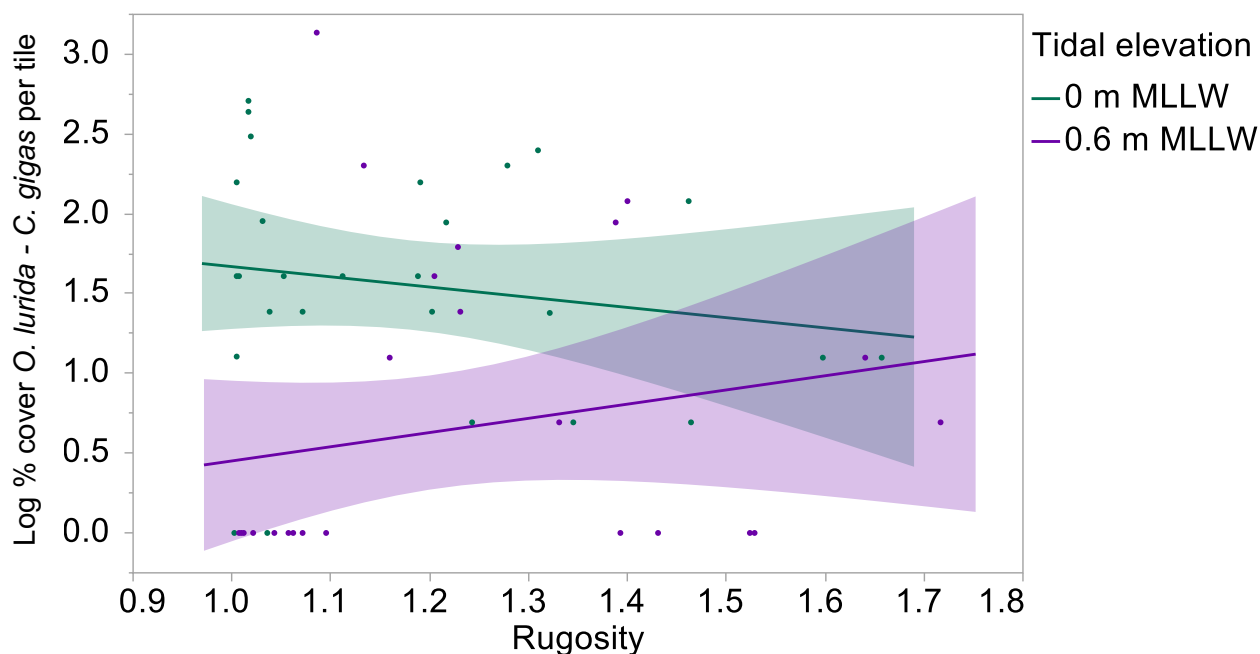


Figure 24. Log transformed percent cover of *O. lurida* - *C. gigas* per tile on tiles deployed from May – September 2018 at CI, Newport Bay, CA, USA as a function of tidal elevation, shell cover, and rugosity (green = 0 m MLLW, purple = 0.6 m MLLW). Shaded regions represent 95% confidence fit. Y (0 m MLLW) = $2.31 - 0.64x$, R^2 (0 m MLLW) = 0.03; Y (0.6 m MLLW) = $-0.70 + 1.06x$, R^2 (0.6 m MLLW) = 0.06.

Table 14. Three-way ANCOVA test statistics for effects of tidal elevation, shell cover, and rugosity on percent cover of live and dead *O. lurida* - *C. gigas* per tile at CI, Newport Bay, CA, USA, deployed from May – September 2018. Bold indicates significant difference.

Source	Nparm	DF	Sum of Squares	F Ratio	Prob > F
Tidal elevation	1	1	10.912903	20.2317	<0.0001
Shell cover	1	1	6.188214	11.4725	0.0014
Tidal elevation*Shell cover	1	1	4.447912	8.2461	0.0061
Rugosity	1	1	2.515279	4.6631	0.0358
Tidal elevation*Rugosity	1	1	2.662935	4.9369	0.0310
Shell cover*Rugosity	1	1	1.849965	3.4297	0.0702
Tidal elevation*Shell cover*Rugosity	1	1	0.402606	0.7464	0.3919

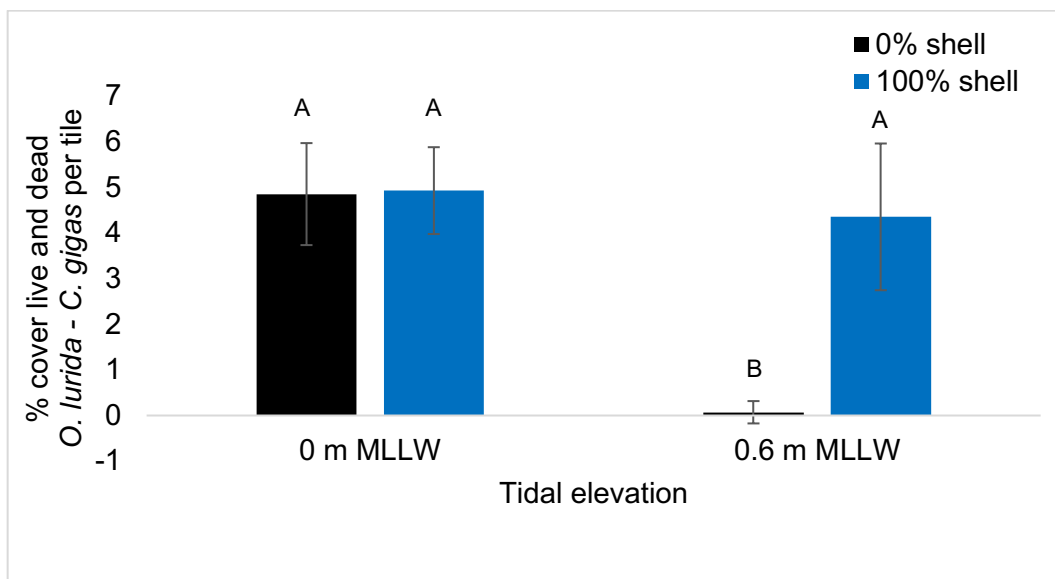


Figure 25. Percent cover of live and dead *O. lurida* - *C. gigas* per tile on tiles deployed from May – September 2018 at CI, Newport Bay, CA, USA as a function of tidal elevation, shell cover, and rugosity (black = 0% shell, blue = 100% shell). Error bars = 1 SE. Different letters above bars indicate statistically significant differences based upon post-hoc Tukey HSD tests.

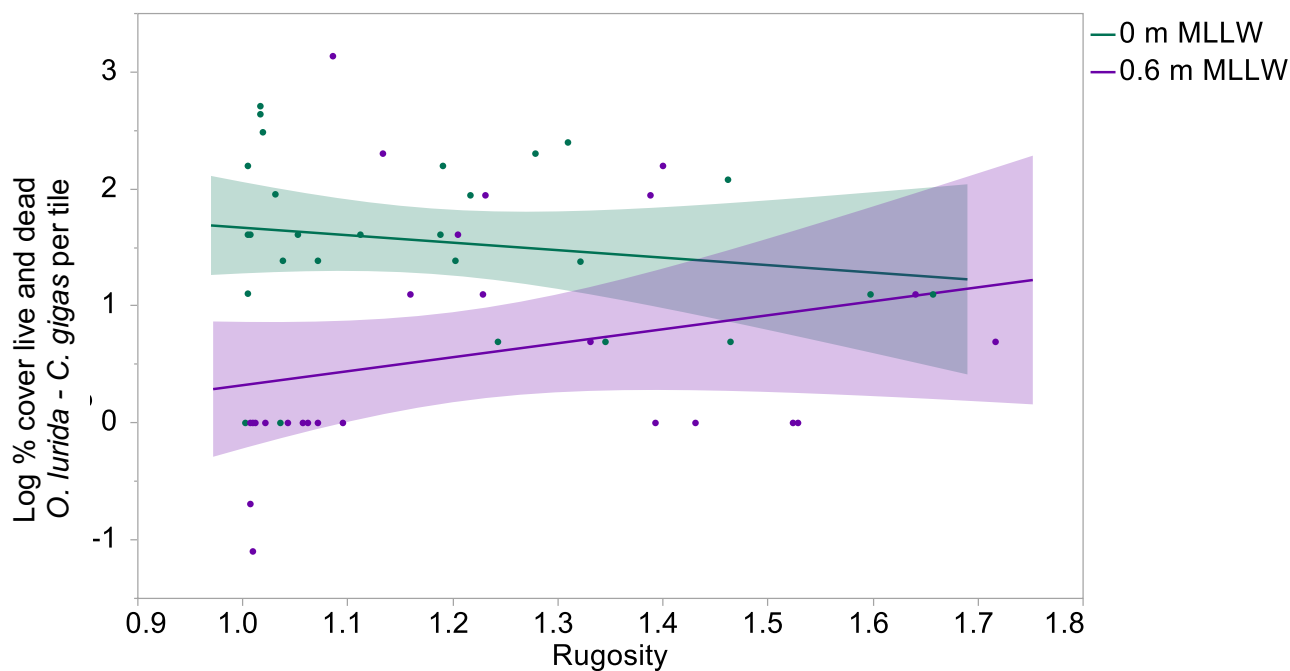


Figure 26. Log transformed percent cover of live and dead *O. lurida* - *C. gigas* per tile on tiles deployed from May – September 2018 at CI, Newport Bay, CA, USA as a function of tidal elevation, shell cover, and rugosity (green = 0 m MLLW, purple = 0.6 m MLLW). Shaded regions represent 95% confidence fit. Y (0 m MLLW) = $2.31 - 0.64x$, R^2 (0 m MLLW) = 0.03; Y (0.6 m MLLW) = $-0.87 + 1.20x$, R^2 (0.6 m MLLW) = 0.07

Table 15. Three-way ANCOVA test statistics for effects of tidal elevation, shell cover, and rugosity on log transformed number of *O. lurida* per tile on tiles deployed from May – September 2018 at ES, San Diego Bay, CA, USA. Bold indicates significant difference.

Source	Nparm	DF	Sum of Squares	F Ratio	Prob > F
Tidal elevation	1	1	116.48141	688.8687	<0.0001
Shell cover	1	1	1.33322	7.8847	0.0072
Tidal elevation*Shell cover	1	1	2.73377	16.1675	0.0002
Rugosity	1	1	1.88340	11.1384	0.0016
Tidal elevation*Rugosity	1	1	1.53364	9.0699	0.0041
Shell cover*Rugosity	1	1	1.68562	9.9687	0.0028
Tidal elevation*Shell cover*Rugosity	1	1	1.55412	9.1910	0.0039

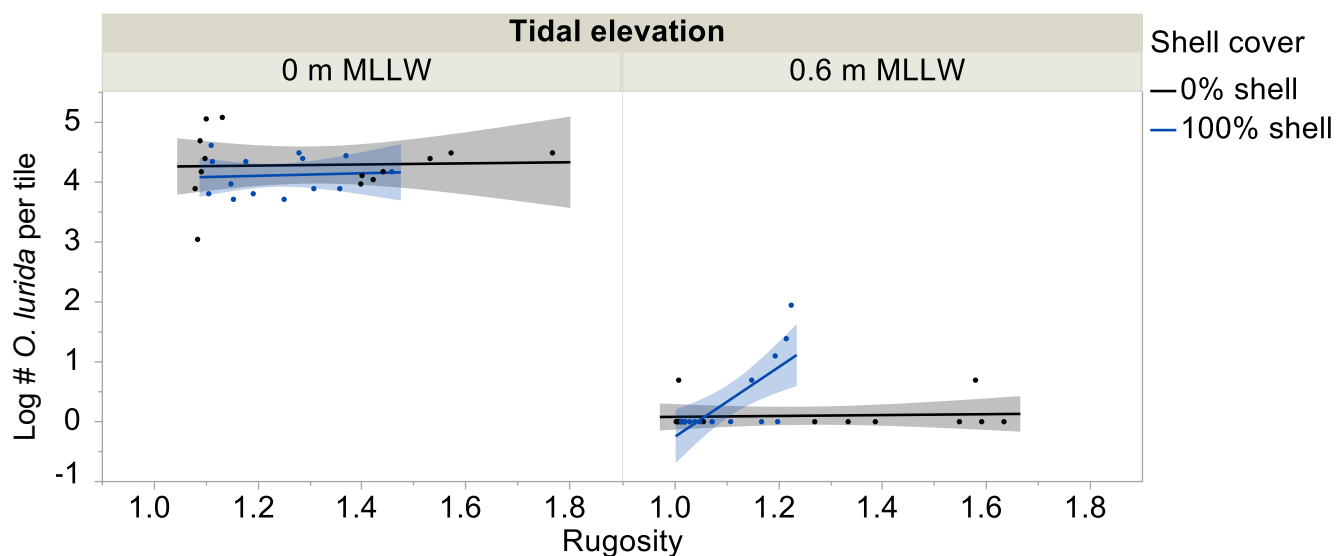


Figure 27. Log transformed number of *O. lurida* per tile on tiles deployed from May – September 2018 at ES, San Diego Bay, CA, USA as a function of tidal elevation, shell cover, and rugosity (black = 0% shell, blue = 100% shell). Shaded regions represent 95% confidence fit. At 0 m MLLW, Y (0% shell) = $4.17 + 0.09x$, R^2 (0% shell) = 0.00; Y (100% shell) = $3.86 + 0.21x$, R^2 (100% shell) = 0.01. At 0.6 m MLLW, Y (0% shell) = $0.01 + 0.07x$, R^2 (0% shell) = 0.01; Y (100% shell) = $-6.07 + 5.82x$, R^2 (100% shell) = 0.53.

Table 16. Three-way ANCOVA test statistics for effects of tidal elevation, shell cover, and rugosity on number of log transformed number of *C. gigas* per tile on tiles deployed from May – September 2018 at ES, San Diego Bay, CA, USA. Bold indicates significant difference.

Source	Nparm	DF	Sum of Squares	F Ratio	Prob > F
Tidal elevation	1	1	2.2074686	11.2882	0.0015
Shell cover	1	1	0.3615402	1.8488	0.1803
Tidal elevation*Shell cover	1	1	0.0028402	0.0145	0.9046
Rugosity	1	1	0.1446298	0.7396	0.3941
Tidal elevation*Rugosity	1	1	0.0322725	0.1650	0.6864
Shell cover*Rugosity	1	1	0.0293971	0.1503	0.6999
Tidal elevation*Shell cover*Rugosity	1	1	0.0101997	0.0522	0.8203

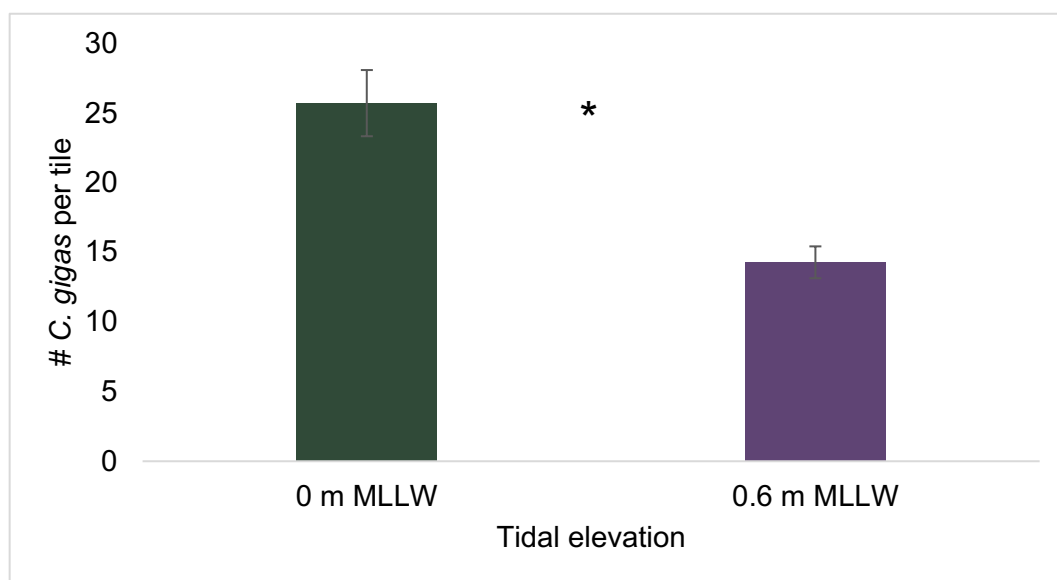


Figure 28. Number of *C. gigas* per tile on tiles deployed from May – September 2018 at ES, San Diego Bay, CA, USA as a function of tidal elevation, shell cover, and rugosity. Error bars = 1 SE. Symbol above bars indicate statistically significant difference.

Table 17. Three-way ANCOVA test statistics for effects of tidal elevation, shell cover, and rugosity on log transformed number of *O. lurida* - *C. gigas* per tile on tiles deployed from May – September 2018 at ES, San Diego Bay, CA, USA. Bold indicates significant difference.

Source	Nparm	DF	Sum of Squares	F Ratio	Prob > F
Tidal elevation	1	1	86.618392	233.0622	<0.0001
Shell cover	1	1	3.083310	8.2962	0.0059
Tidal elevation*Shell cover	1	1	2.560376	6.8891	0.0116
Rugosity	1	1	0.984200	2.6482	0.1102
Tidal elevation*Rugosity	1	1	1.120968	3.0162	0.0889
Shell cover*Rugosity	1	1	2.160221	5.8125	0.0198
Tidal elevation*Shell cover*Rugosity	1	1	1.816124	4.8866	0.0319

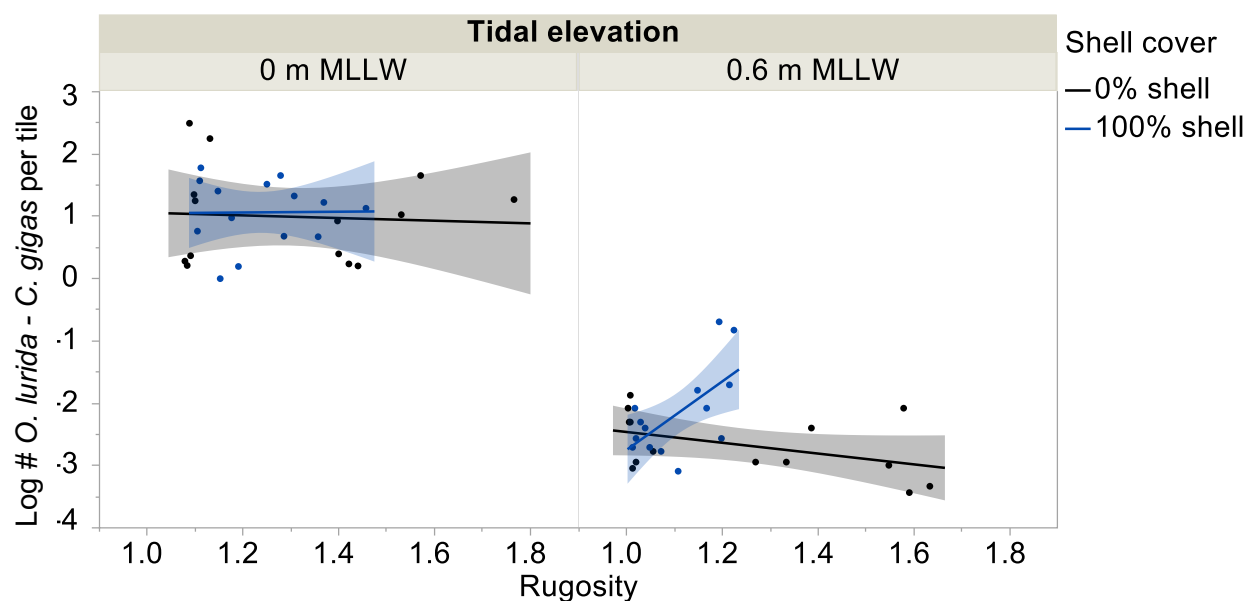


Figure 29. Log transformed number of *O. lurida* - *C. gigas* per tile on tiles deployed from May – September 2018 at ES, San Diego Bay, CA, USA as a function of tidal elevation, shell cover, and rugosity (black = 0% shell, blue = 100% shell). Shaded regions represent 95% confidence fit. At 0 m MLLW, Y (0% shell) = $1.271 - 0.2132x$, R^2 (0% shell) = 0.00; Y (100% shell) = $0.9866 + 0.0626x$, R^2 (100% shell) = 0.00. At 0.6 m MLLW, Y (0% shell) = $-1.596 - 0.8655x$, R^2 (0% shell) = 0.21; Y (100% shell) = $-8.242 + 5.496x$, R^2 (100% shell) = 0.40.

Table 18. Three-way ANCOVA test statistics for effects of tidal elevation, shell cover, and rugosity on log transformed percent cover of *O. lurida* per tile on tiles deployed from May – September 2018 at ES, San Diego Bay, CA, USA. Bold indicates significant difference.

Source	Nparm	DF	Sum of Squares	F Ratio	Prob > F
Tidal elevation	1	1	56.409747	305.9957	<0.0001
Shell cover	1	1	1.272831	6.9045	0.0115
Tidal elevation*Shell cover	1	1	3.111466	16.8782	0.0002
Rugosity	1	1	2.434074	13.2037	0.0007
Tidal elevation*Rugosity	1	1	1.511614	8.1998	0.0062
Shell cover*Rugosity	1	1	2.559578	13.8845	0.0005
Tidal elevation*Shell cover*Rugosity	1	1	0.735404	3.9892	0.0515

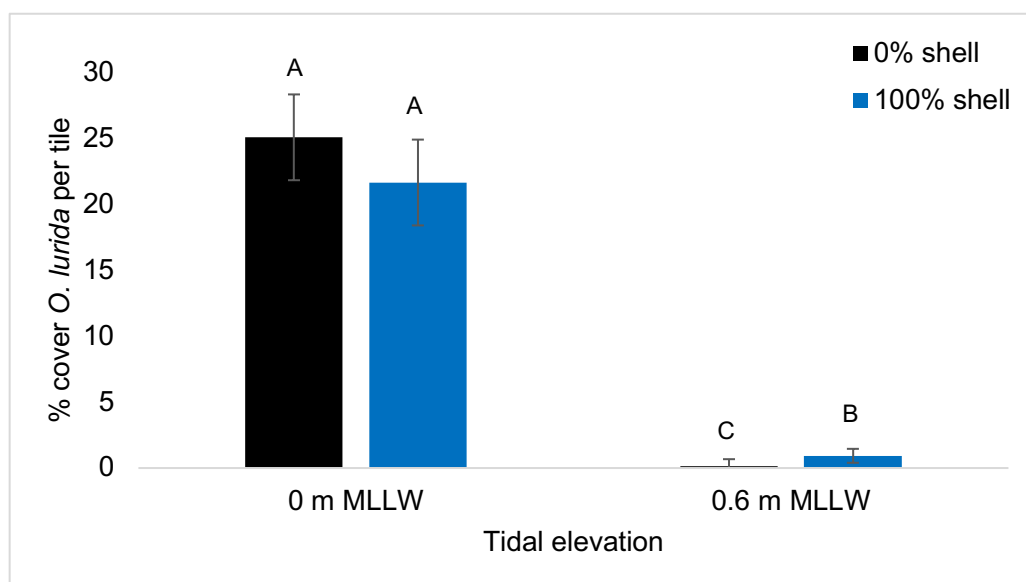


Figure 30. Percent cover of *O. lurida* per tile on tiles deployed from May – September 2018 at ES, San Diego Bay, CA, USA as a function of tidal elevation, shell cover, and rugosity (black = 0% shell, blue = 100% shell). Error bars = 1 SE. Different letters above bars indicate statistically significant differences based upon post-hoc Tukey HSD tests. Y-axis restricted to 0%.

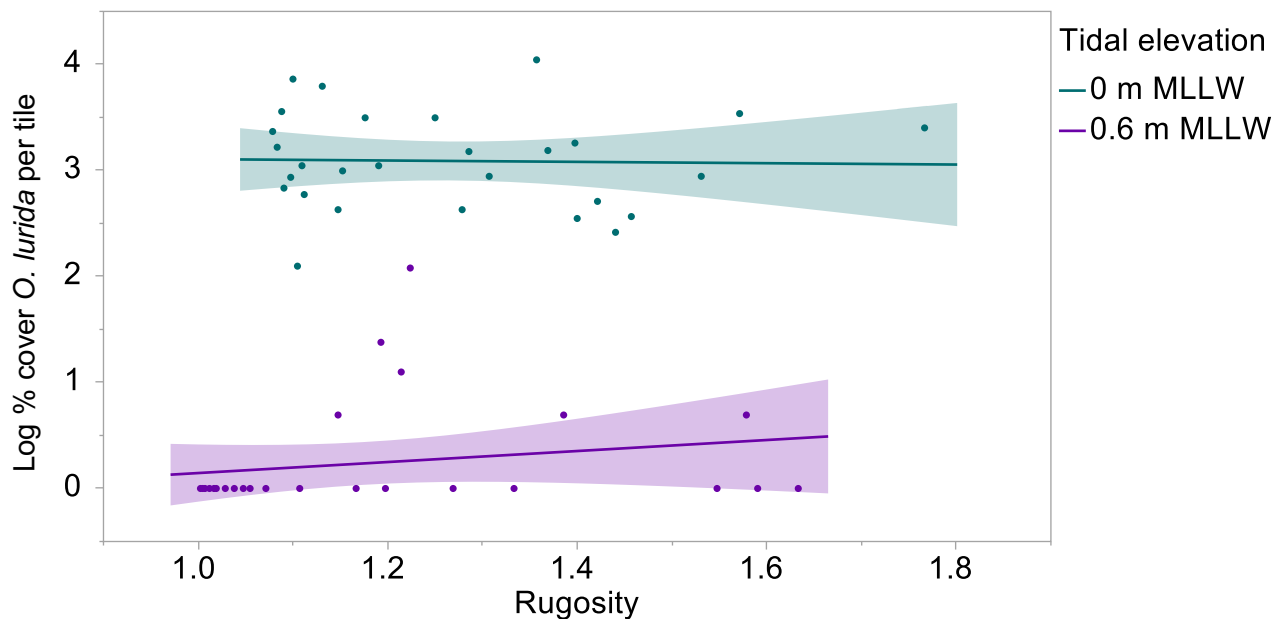


Figure 31. Log transformed percent cover of *O. lurida* per tile on tiles deployed from May – September 2018 at ES, San Diego Bay, CA, USA as a function of tidal elevation, shell cover, and rugosity (green = 0 m MLLW, purple = 0.6 m MLLW). Shaded regions represent 95% confidence fit. Y (0 m MLLW) = $3.17 - 0.06x$, R^2 (0 m MLLW) = 0.00; Y (0.6 m MLLW) = $-0.37 + 0.52x$, R^2 (0.6 m MLLW) = 0.04.

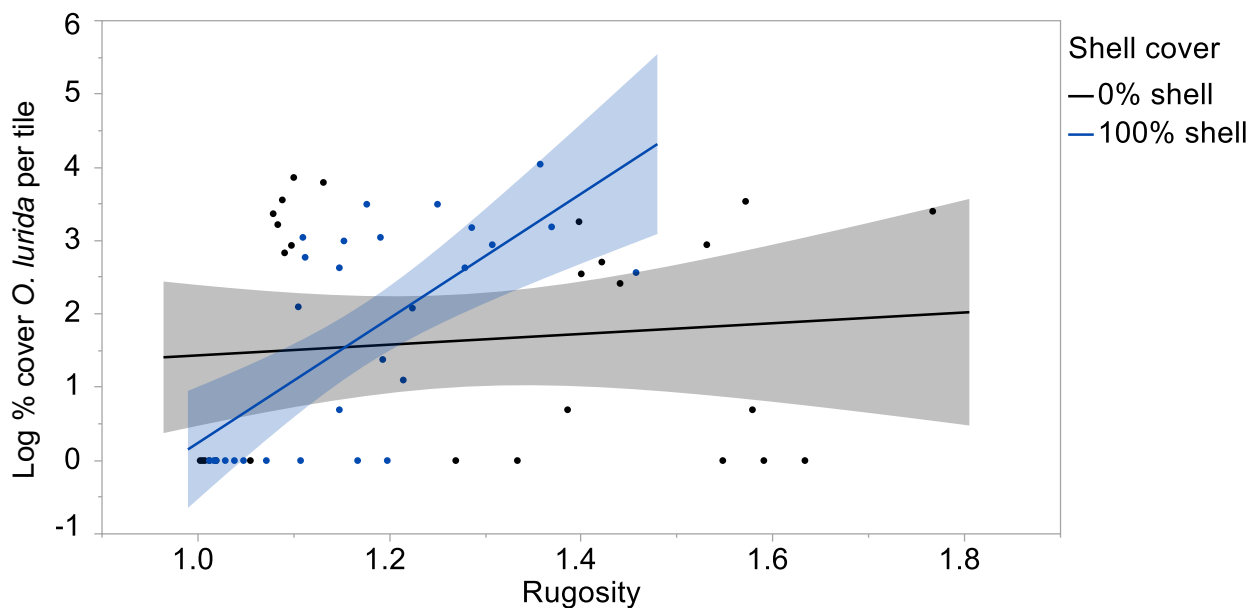


Figure 32. Log transformed percent cover of *O. lurida* per tile on tiles deployed from May – September 2018 at ES, San Diego Bay, CA, USA as a function of tidal elevation, shell cover, and rugosity (black = 0% shell, blue = 100% shell). Shaded regions represent 95% confidence fit. Y (0% shell) = $0.70 + 0.73x$, R^2 (0% shell) = 0.01; Y (100% shell) = $-8.265 + 8.51x$, R^2 (100% shell) = 0.46.

Table 19. Three-way ANCOVA test statistics for effects of tidal elevation, shell cover, and rugosity on percent cover of *C. gigas* per tile on tiles deployed from May – September 2018 at ES, San Diego Bay, CA, USA.

Source	Nparm	DF	Sum of Squares	F Ratio	Prob > F
Tidal elevation	1	1	1339.1211	10.6701	0.0020
Shell cover	1	1	181.0919	1.4429	0.2356
Tidal elevation*Shell cover	1	1	1430.2870	11.3965	0.0015
Rugosity	1	1	297.4778	2.3703	0.1302
Tidal elevation*Rugosity	1	1	140.8578	1.1224	0.2947
Shell cover*Rugosity	1	1	33.2359	0.2648	0.6092
Tidal elevation*Shell cover*Rugosity	1	1	5.8795	0.0468	0.8296

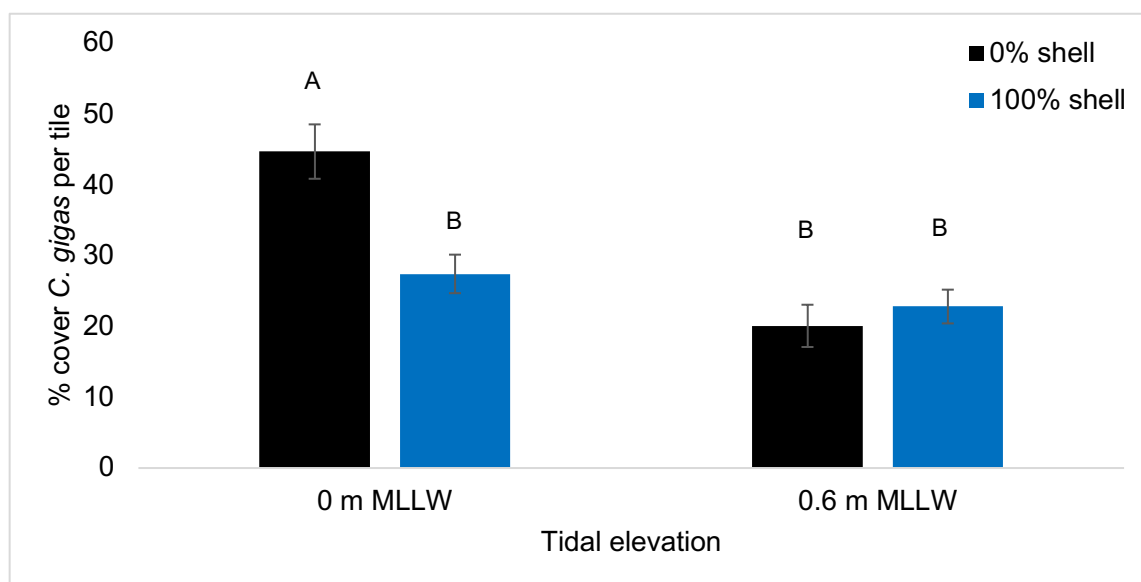


Figure 33. Percent cover of *C. gigas* per tile on tiles deployed from May – September 2018 at ES, San Diego Bay, CA, USA as a function of tidal elevation, shell cover, and rugosity (black = 0% shell, blue = 100% shell). Error bars = 1 SE. Different letters above bars indicate statistically significant differences based upon post-hoc Tukey HSD tests.

Table 20. Three-way ANCOVA test statistics for effects of tidal elevation, shell cover, and rugosity on percent cover of *O. lurida* - *C. gigas* per tile on tiles deployed from May – September 2018 at ES, San Diego Bay, CA, USA. Bold indicates significant difference.

Source	Nparm	DF	Sum of Squares	F Ratio	Prob > F
Tidal elevation	1	1	869.72596	3.2697	0.0768
Shell cover	1	1	102.04234	0.3836	0.5386
Tidal elevation*Shell cover	1	1	715.36453	2.6894	0.1076
Rugosity	1	1	85.60844	0.3218	0.5731
Tidal elevation*Rugosity	1	1	162.83697	0.6122	0.4378
Shell cover*Rugosity	1	1	56.65358	0.2130	0.6465
Tidal elevation*Shell cover*Rugosity	1	1	82.68821	0.3109	0.5797

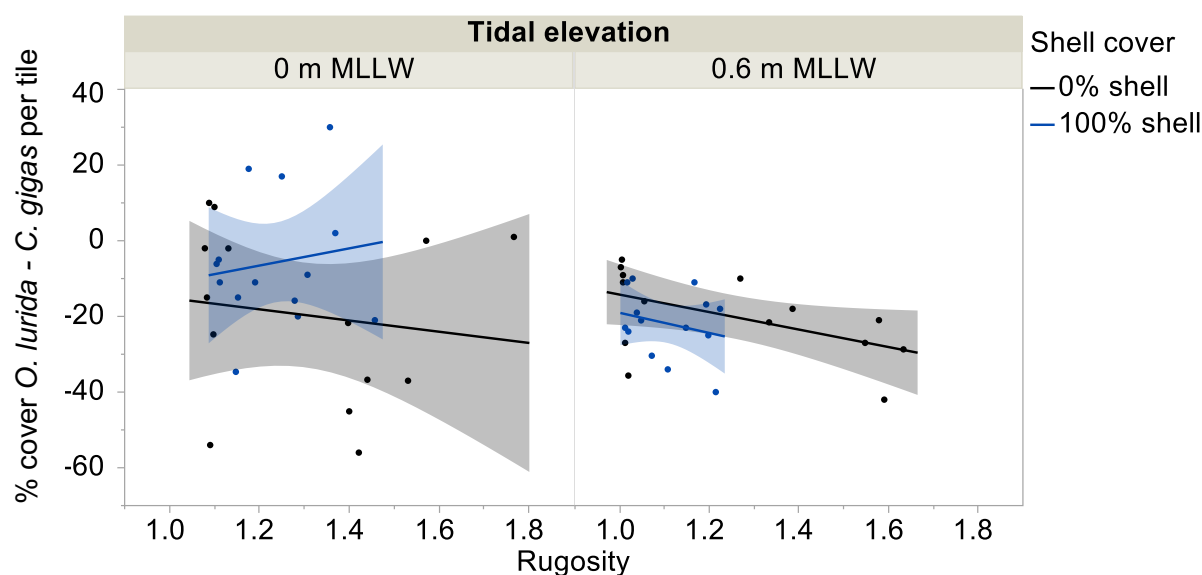


Figure 34. Percent cover of *O. lurida* - *C. gigas* per tile on tiles deployed from May – September 2018 at ES, San Diego Bay, CA, USA as a function of tidal elevation, shell cover, and rugosity (black = 0% shell, blue = 100% shell). Shaded regions represent 95% confidence fit. At 0 m MLLW, Y (0% shell) = $-0.36 - 14.8x$, R^2 (0% shell) = 0.02; Y (100% shell) = $-33.84 + 22.73x$, R^2 (100% shell) = 0.02. At 0.6 m MLLW, Y (0% shell) = $8.84 - 23.09x$, R^2 (0% shell) = 0.29; Y (100% shell) = $7.57 - 26.62x$, R^2 (100% shell) = 0.06.

Table 21. Three-way ANCOVA test statistics for effects of tidal elevation, shell cover, and rugosity on percent cover of *O. lurida* - *C. gigas* per tile live and dead on tiles deployed from May – September 2018 at ES, San Diego Bay, CA, USA. Bold indicates significant difference.

Source	Nparm	DF	Sum of Squares	F Ratio	Prob > F
Tidal elevation	1	1	7322.6064	24.0615	<0.0001
Shell cover	1	1	2949.0269	9.6903	0.0031
Tidal elevation*Shell cover	1	1	3973.0043	13.0550	0.0007
Rugosity	1	1	32.8783	0.1080	0.7438
Tidal elevation*Rugosity	1	1	0.3222	0.0011	0.9742
Shell cover*Rugosity	1	1	167.6969	0.5510	0.4615
Tidal elevation*Shell cover*Rugosity	1	1	6.1473	0.0202	0.8876

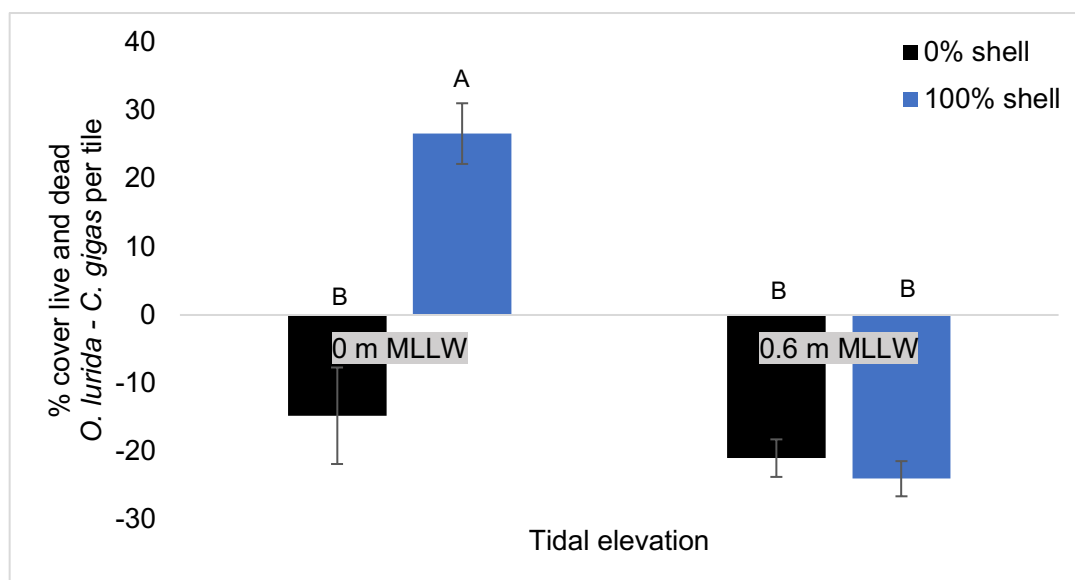


Figure 35. Percent cover of Live and dead *O. lurida* - *C. gigas* per tile on tiles deployed from May – September 2018 at ES, San Diego Bay, CA, USA as a function of tidal elevation, shell cover, and rugosity (black = 0% shell, blue = 100% shell). Error bars = 1 SE. Different letters above bars indicate statistically significant differences based upon post-hoc Tukey HSD tests.

Table 22. Three-way ANCOVA test statistics for effects of tidal elevation, shell cover, and rugosity on number of *O. lurida* per tile GC, San Diego Bay, CA, USA, deployed from May – September 2018. Bold indicates significant difference.

Source	Nparm	DF	Sum of Squares	F Ratio	Prob > F
Tidal elevation	1	1	213383.24	164.8966	<0.0001
Shell cover	1	1	4537.25	3.5063	0.0672
Tidal elevation*Shell cover	1	1	8146.63	6.2955	0.0155
Rugosity	1	1	8990.71	6.9478	0.0113
Tidal elevation*Rugosity	1	1	27268.77	21.0725	<0.0001
Shell cover*Rugosity	1	1	13760.84	10.6340	0.0020
Tidal elevation*Shell cover*Rugosity	1	1	32542.64	25.1480	<0.0001

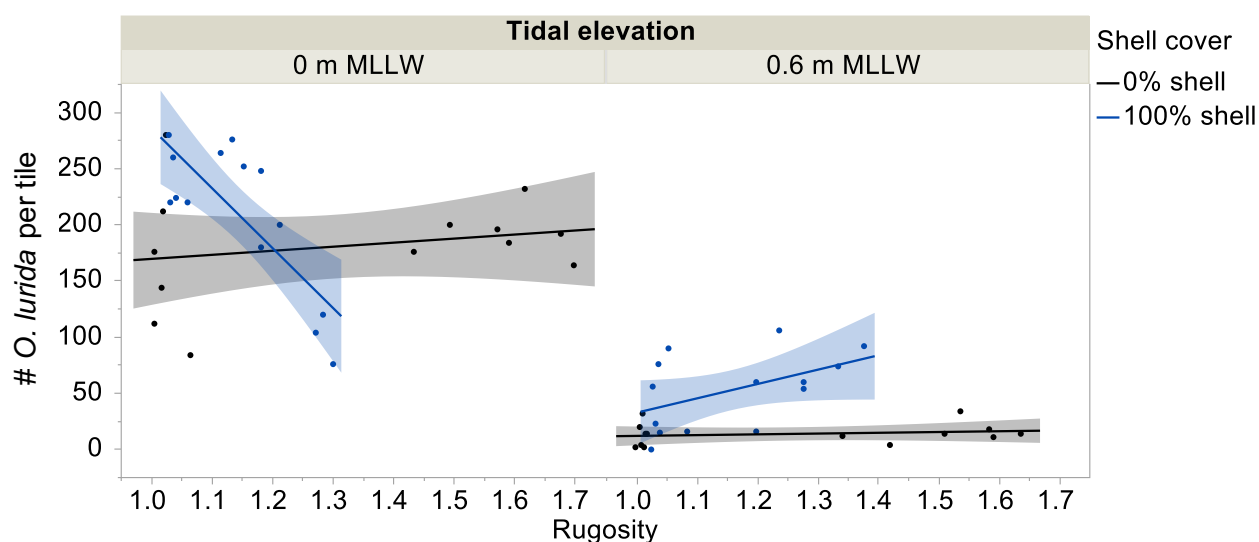


Figure 36. Number of *O. lurida* per tile on tiles deployed from May – September 2018 at GC, San Diego Bay, CA, USA as a function of tidal elevation, shell cover, and rugosity (black = 0% shell, blue = 100% shell). Shaded regions represent 95% confidence fit. At 0 m MLLW, Y (0% shell) = $133.6 + 35.12x$, R^2 (0% shell) = 0.05; Y (100% shell) = $819.5 - 533.6x$, R^2 (100% shell) = 0.62. At 0.6 m MLLW, Y (0% shell) = $5.20 + 6.91x$, R^2 (0% shell) = 0.04; Y (100% shell) = $-94.83 + 127.6x$, R^2 (100% shell) = 0.24.

Table 23. Three-way ANCOVA test statistics for effects of tidal elevation, shell cover, and rugosity on number of *C. gigas* per tile on tiles deployed from May – September 2018 at GC, San Diego Bay, CA, USA. Bold indicates significant difference.

Source	Nparm	DF	Sum of Squares	F Ratio	Prob > F
Tidal elevation	1	1	35226.422	234.1376	<0.0001
Shell cover	1	1	3006.499	19.9831	<0.0001
Tidal elevation*Shell cover	1	1	570.814	234.1376	0.0573
Rugosity	1	1	570.814	3.7940	0.1324
Tidal elevation*Rugosity	1	1	164.192	1.0913	0.4165
Shell cover*Rugosity	1	1	352.447	2.3426	0.3014
Tidal elevation*Shell cover*Rugosity	1	1	101.064	0.6717	0.0451

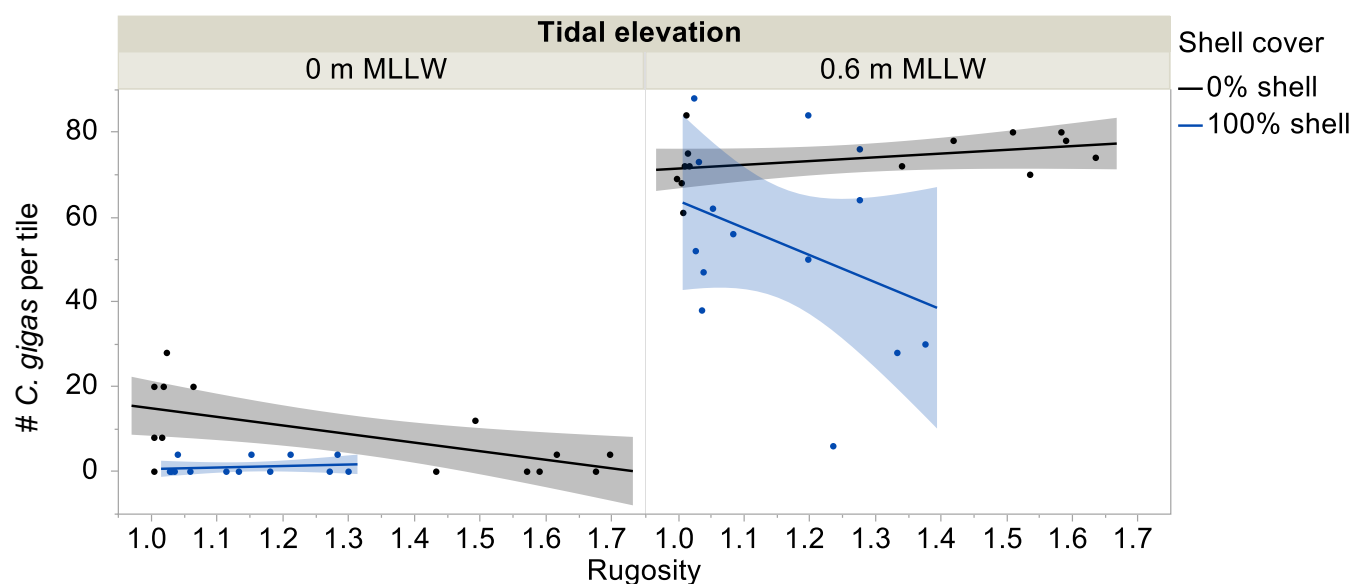


Figure 37. Number of *C. gigas* per tile on tiles deployed from May – September 2018 at GC, San Diego Bay, CA, USA as a function of tidal elevation, shell cover, and rugosity (black = 0% shell, blue = 100% shell). Shaded regions represent 95% confidence fit. At 0 m MLLW, Y (0% shell) = $35.18 - 20.23x$, R^2 (0% shell) = 0.40; Y (100% shell) = $-2.911 + 3.542x$, R^2 (100% shell) = 0.03. At 0.6 m MLLW, Y (0% shell) = $62.64 + 8.825x$, R^2 (0% shell) = 0.16; Y (100% shell) = $127.8 - 63.99x$, R^2 (100% shell) = 0.13.

Table 24. Three-way ANCOVA test statistics for effects of tidal elevation, shell cover, and rugosity on number of *O. lurida* - *C. gigas* per tile on tiles deployed from May – September 2018 at GC, San Diego Bay, CA, USA. Bold indicates significant difference.

Source	Nparm	DF	Sum of Squares	F Ratio	Prob > F
Tidal elevation	1	1	422007.80	266.0926	<0.0001
Shell cover	1	1	14930.57	9.4143	0.0035
Tidal elevation*Shell cover	1	1	13030.31	8.2161	0.0061
Rugosity	1	1	5782.96	3.6464	0.0622
Tidal elevation*Rugosity	1	1	30690.02	19.3513	<0.0001
Shell cover*Rugosity	1	1	10918.75	6.8847	0.0116
Tidal elevation*Shell cover*Rugosity	1	1	42284.45	26.6620	<0.0001

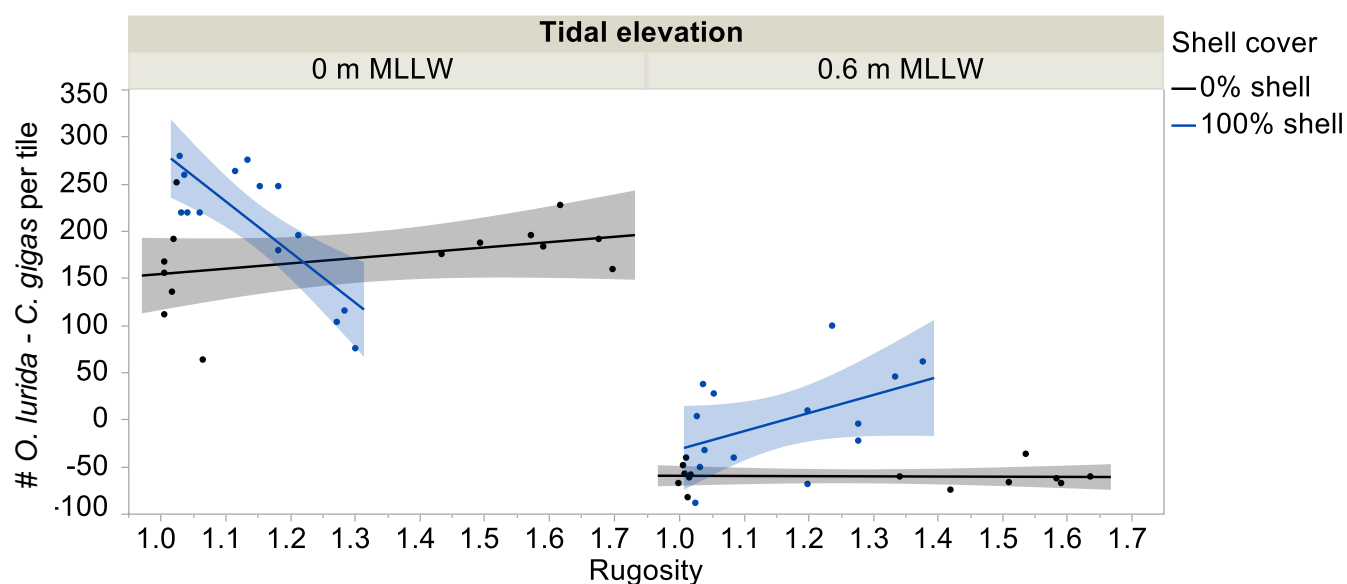


Figure 38. Number of *O. lurida* - *C. gigas* per tile on tiles deployed from May – September 2018 at GC, San Diego Bay, CA, USA as a function of tidal elevation, shell cover, and rugosity (black = 0% shell, blue = 100% shell). Shaded regions represent 95% confidence fit. At 0 m MLLW, Y (0% shell) = $98.39 + 56.35x$, R^2 (0% shell) = 0.13; Y (100% shell) = $822.5 - 537.1x$, R^2 (100% shell) = 0.63. At 0.6 m MLLW, Y (0% shell) = $-57.44 - 1.91x$, R^2 (0% shell) = 0.00; Y (100% shell) = $-222.7 + 191.6x$, R^2 (100% shell) = 0.22.

Table 25. Three-way ANCOVA test statistics for effects of tidal elevation, shell cover, and rugosity on percent cover of *O. lurida* per tile on tiles deployed from May – September 2018 at GC, San Diego Bay, CA, USA. Bold indicates significant difference.

Source	Nparm	DF	Sum of Squares	F Ratio	Prob > F
Tidal elevation	1	1	17636.736	226.4417	<0.0001
Shell cover	1	1	51.814	0.6652	0.4187
Tidal elevation*Shell cover	1	1	2079.639	26.7009	<0.0001
Rugosity	1	1	990.408	12.7161	0.0008
Tidal elevation*Rugosity	1	1	2032.777	26.0992	<0.0001
Shell cover*Rugosity	1	1	1452.845	18.6534	<0.0001
Tidal elevation*Shell cover*Rugosity	1	1	2557.784	32.8399	<0.0001

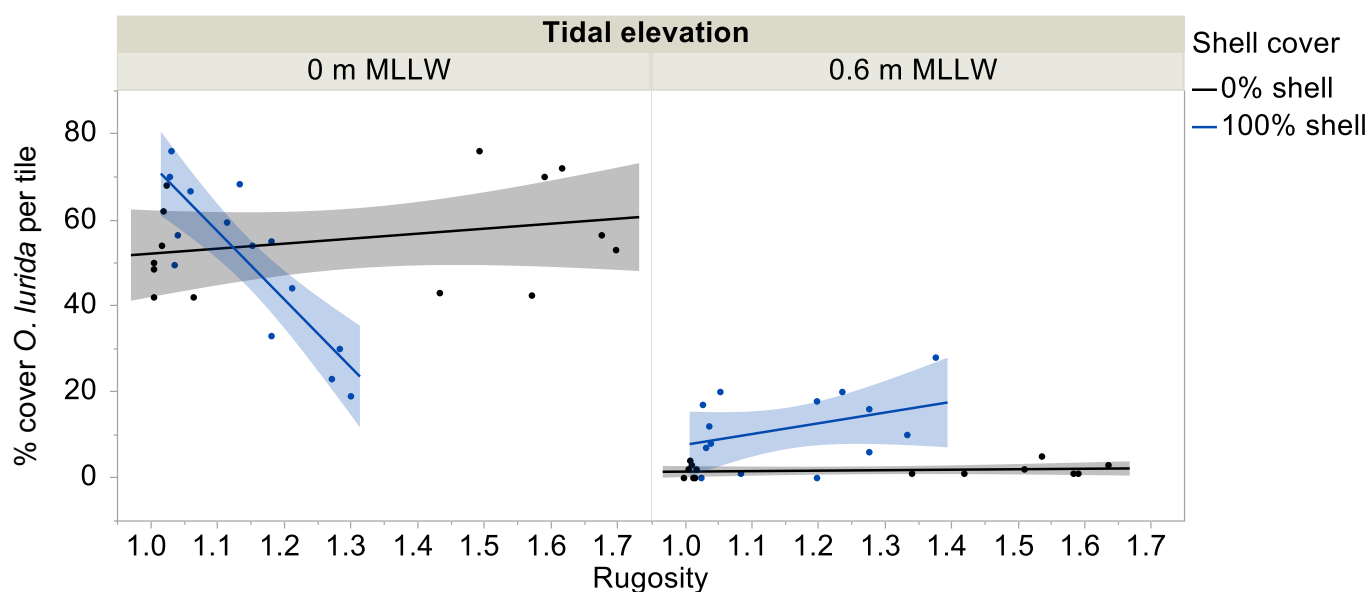


Figure 39. Percent cover of *O. lurida* per tile on tiles deployed from May – September 2018 at GC, San Diego Bay, CA, USA as a function of tidal elevation, shell cover, and rugosity (black = 0% shell, blue = 100% shell). Shaded regions represent 95% confidence fit. At 0 m MLLW, Y (0% shell) = $40.56 + 11.61x$, R^2 (0% shell) = 0.08; Y (100% shell) = $231.3 - 158.1x$, R^2 (100% shell) = 0.73. At 0.6 m MLLW, Y (0% shell) = $0.38 + 1.11x$, R^2 (0% shell) = 0.04; Y (100% shell) = $-17.21 + 24.95x$, R^2 (100% shell) = 0.14.

Table 26. Three-way ANCOVA test statistics for effects of tidal elevation, shell cover, and rugosity on percent cover of *C. gigas* on tiles deployed from May – September 2018 at GC, San Diego Bay, CA, USA. Bold indicates significant difference.

Source	Nparm	DF	Sum of Squares	F Ratio	Prob > F
Tidal elevation	1	1	25838.312	202.5105	<0.0001
Shell cover	1	1	7439.322	58.3065	<0.0001
Tidal elevation*Shell cover	1	1	2091.857	16.3951	0.0002
Rugosity	1	1	3477.416	27.2546	<0.0001
Tidal elevation*Rugosity	1	1	1732.046	13.5751	0.0006
Shell cover*Rugosity	1	1	925.997	7.2576	0.0097
Tidal elevation*Shell cover*Rugosity	1	1	1607.688	12.6004	0.0009

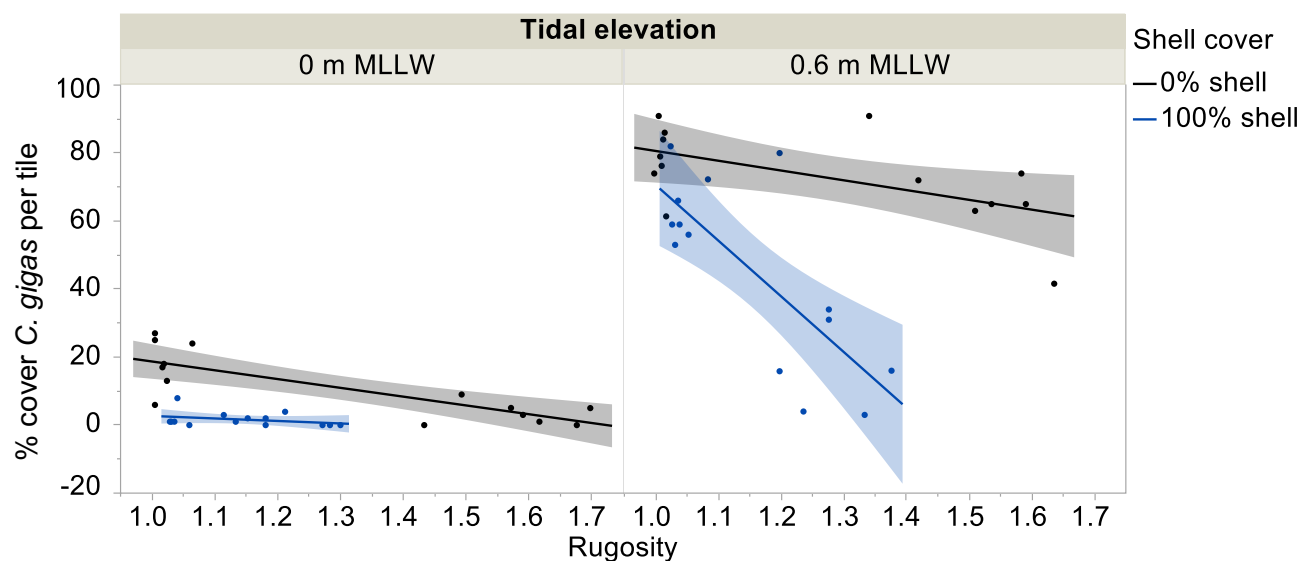


Figure 40. Percent cover of *C. gigas* per tile on tiles deployed from May – September 2018 at GC, San Diego Bay, CA, USA as a function of tidal elevation, shell cover, and rugosity (black = 0% shell, blue = 100% shell). Shaded regions represent 95% confidence fit. At 0 m MLLW, Y (0% shell) = $44.56 - 25.85x$, R^2 (0% shell) = 0.64; Y (100% shell) = $10.05 - 7.35x$, R^2 (100% shell) = 0.11. At 0.6 m MLLW, Y (0% shell) = $109.4 - 28.76x$, R^2 (0% shell) = 0.34; Y (100% shell) = $234.3 - 163.7x$, R^2 (100% shell) = 0.58.

Table 27. Three-way ANCOVA test statistics for effects of tidal elevation, shell cover, and rugosity on percent cover of *O. lurida* - *C. gigas* on tiles deployed from May – September 2018 at GC, San Diego Bay, CA, USA. Bold indicates significant difference.

Source	Nparm	DF	Sum of Squares	F Ratio	Prob > F
Tidal elevation	1	1	86169.475	333.2162	<0.0001
Shell cover	1	1	6249.430	24.1665	<0.0001
Tidal elevation*Shell cover	1	1	8342.974	32.2622	<0.0001
Rugosity	1	1	756.188	2.9242	0.0937
Tidal elevation*Rugosity	1	1	7517.616	29.0705	<0.0001
Shell cover*Rugosity	1	1	59.075	0.2284	0.6349
Tidal elevation*Shell cover*Rugosity	1	1	8221.143	31.7911	<0.0001

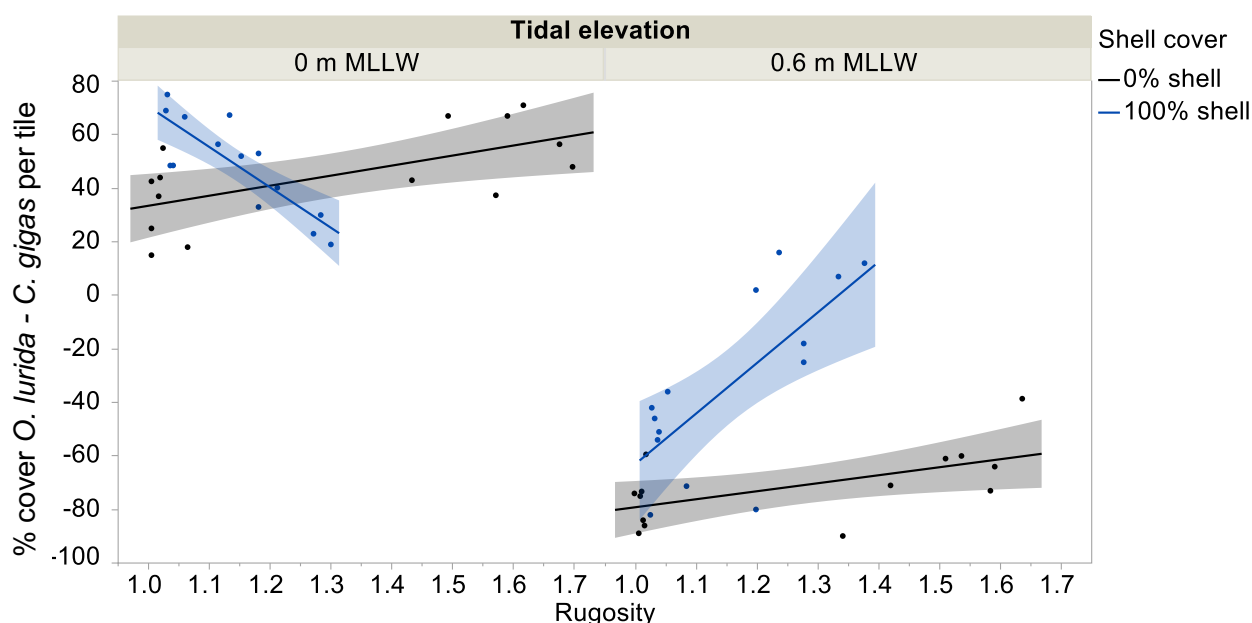


Figure 41. Percent cover of *O. lurida* - *C. gigas* on tiles deployed from May – September 2018 at GC, San Diego Bay, CA, USA as a function of tidal elevation, shell cover, and rugosity (black = 0% shell, blue = 100% shell). Shaded regions represent 95% confidence fit. At 0 m MLLW, Y (0% shell) = $-4 + 37.46x$, R^2 (0% shell) = 0.40; Y (100% shell) = $221.2 - 150.8x$, R^2 (100% shell) = 0.69. At 0.6 m MLLW, Y (0% shell) = $-109 + 29.87x$, R^2 (0% shell) = 0.34; Y (100% shell) = $-251.5 + 188.7x$, R^2 (100% shell) = 0.52.

Table 28. Three-way ANCOVA test statistics for effects of tidal elevation, shell cover, and rugosity on percent cover of live and dead *O. lurida* - *C. gigas* per tile on tiles deployed from May – September 2018 at GC, San Diego Bay, CA, USA. Bold indicates significant difference.

Source	Nparm	DF	Sum of Squares	F Ratio	Prob > F
Tidal elevation	1	1	123229.00	414.2040	<0.0001
Shell cover	1	1	11476.82	38.5765	<0.0001
Tidal elevation*Shell cover	1	1	4374.07	14.7024	0.0004
Rugosity	1	1	2183.74	7.3401	0.0093
Tidal elevation*Rugosity	1	1	4440.49	14.9256	0.0003
Shell cover*Rugosity	1	1	113.11	0.3802	0.5404
Tidal elevation*Shell cover*Rugosity	1	1	5411.94	18.1909	<0.0001

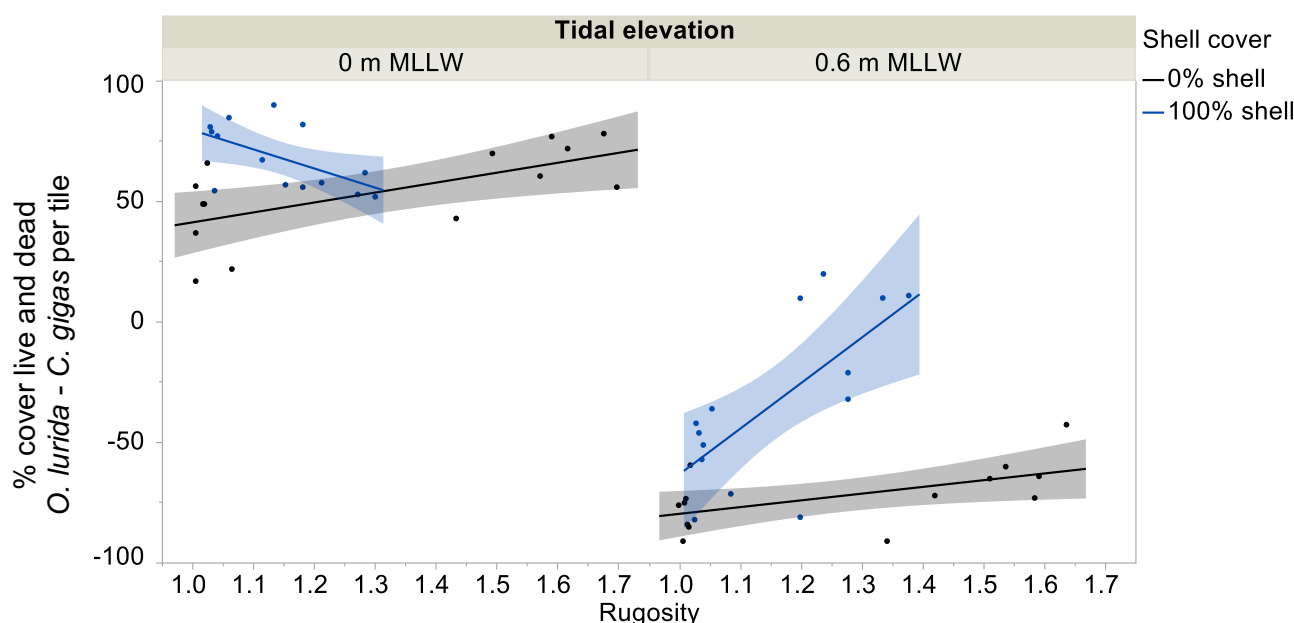


Figure 42. Percent cover of live and dead *O. lurida* - *C. gigas* per tile on tiles deployed from May – September 2018 at GC, San Diego Bay, CA, USA as a function of tidal elevation, shell cover, and rugosity (black = 0% shell, blue = 100% shell). Shaded regions represent 95% confidence fit. At 0 m MLLW, Y (0% shell) = $0.24 + 41.17x$, R^2 (0% shell) = 0.42; Y (100% shell) = $159.9 - 79.26x$, R^2 (100% shell) = 0.32. At 0.6 m MLLW, Y (0% shell) = $-107.5 + 27.91x$, R^2 (0% shell) = 0.32; Y (100% shell) = $-252 + 189x$, R^2 (100% shell) = 0.48.

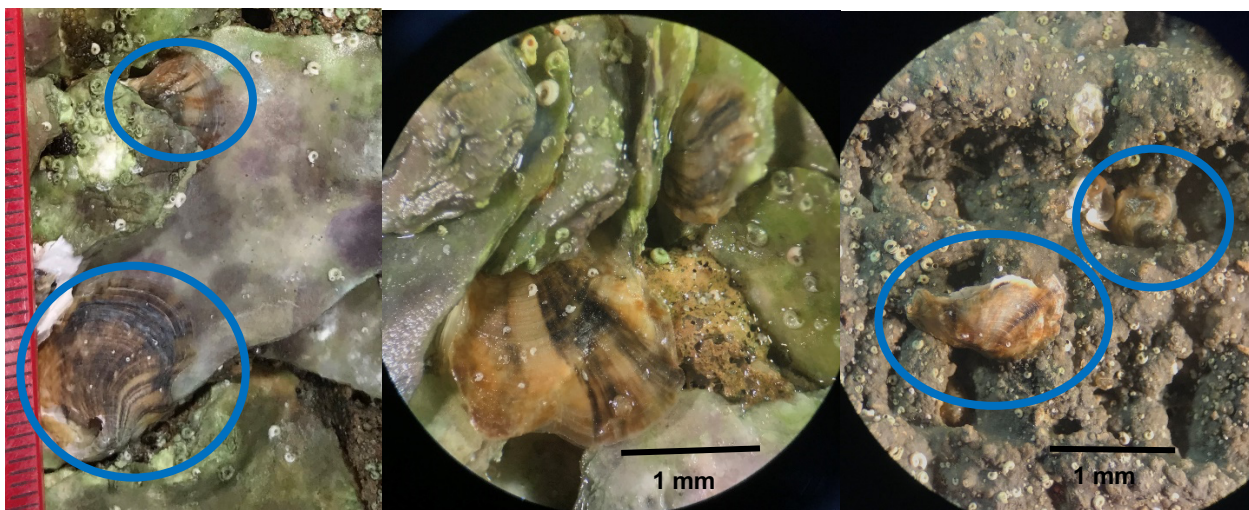


Figure 43. *O. lurida* at 0.6 m MLLW at CI. Left: Macroscopic view of *O. lurida* on Full. Middle: Microscopic view of two *O. lurida* found in crevices formed by shell on Full. Right: Microscopic view of *O. lurida* with umbo in the crevices found on Rough.

Table 29. One-way ANOVA p-values for effects of treatment on overall, native, and non-indigenous species richness on tiles deployed from May – September 2018 per site (CI in Newport Bay, E Street and GC in San Diego Bay, CA, USA) and tidal elevation (0 and 0.6 m MLLW). Bold indicates significant difference.

	Overall Community Composition					
	CI		E Street		GC	
	0 m MLLW	0.6 m MLLW	0 m MLLW	0.6 m MLLW	0 m MLLW	0.6 m MLLW
Overall species richness	0.0002	<0.0001	0.0038	0.3125	0.0003	0.0034
Native species richness	0.0053	<0.0001	0.0011	0.0405	0.0115	0.1632
Non-indigenous species richness	0.0356	<0.0001	0.0011	0.0106	0.0491	0.0189

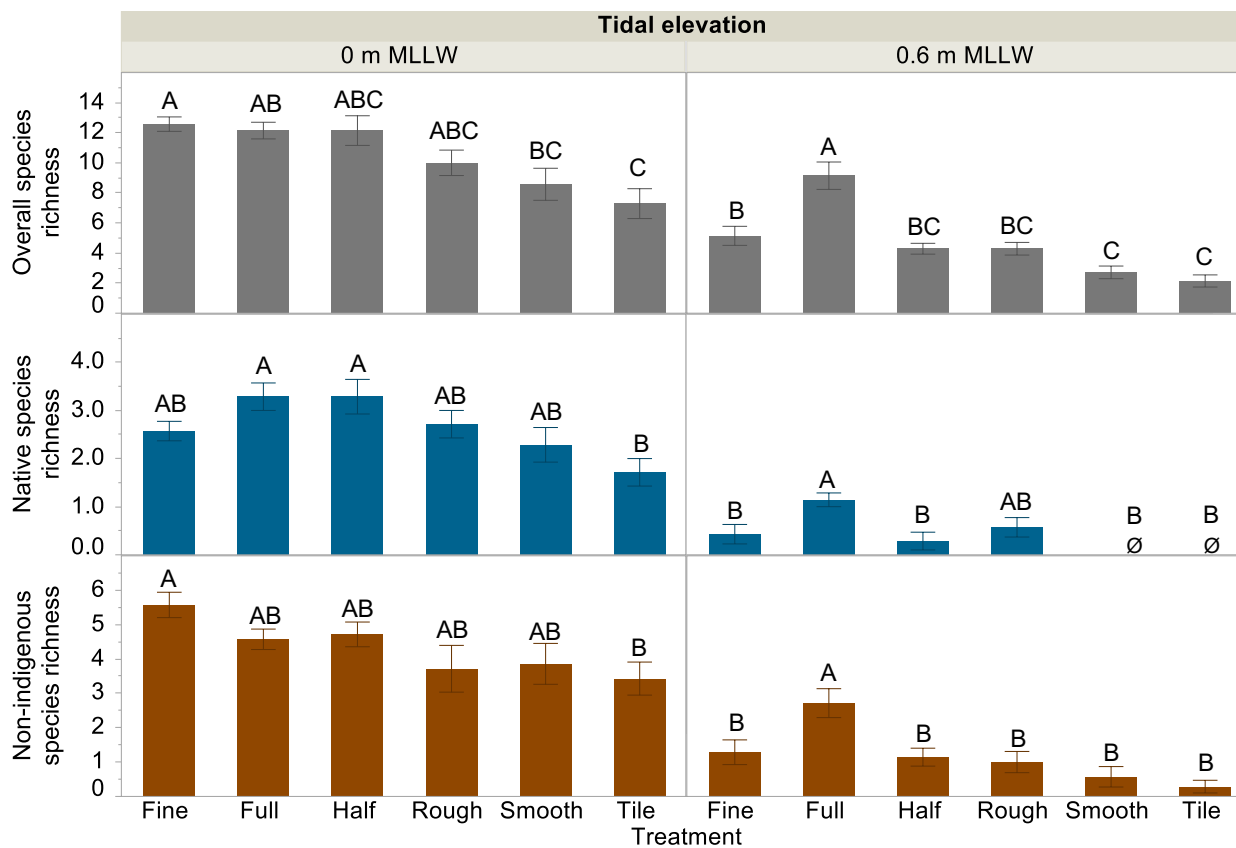


Figure 44. Overall, native, and non-indigenous species richness on the bottom of tiles deployed from May – September 2018 to CI, Newport Bay, CA, USA, as a function of treatment. Error bars = 1 SE. Different letters above bars indicate statistically significant differences based upon post-hoc Tukey HSD tests.

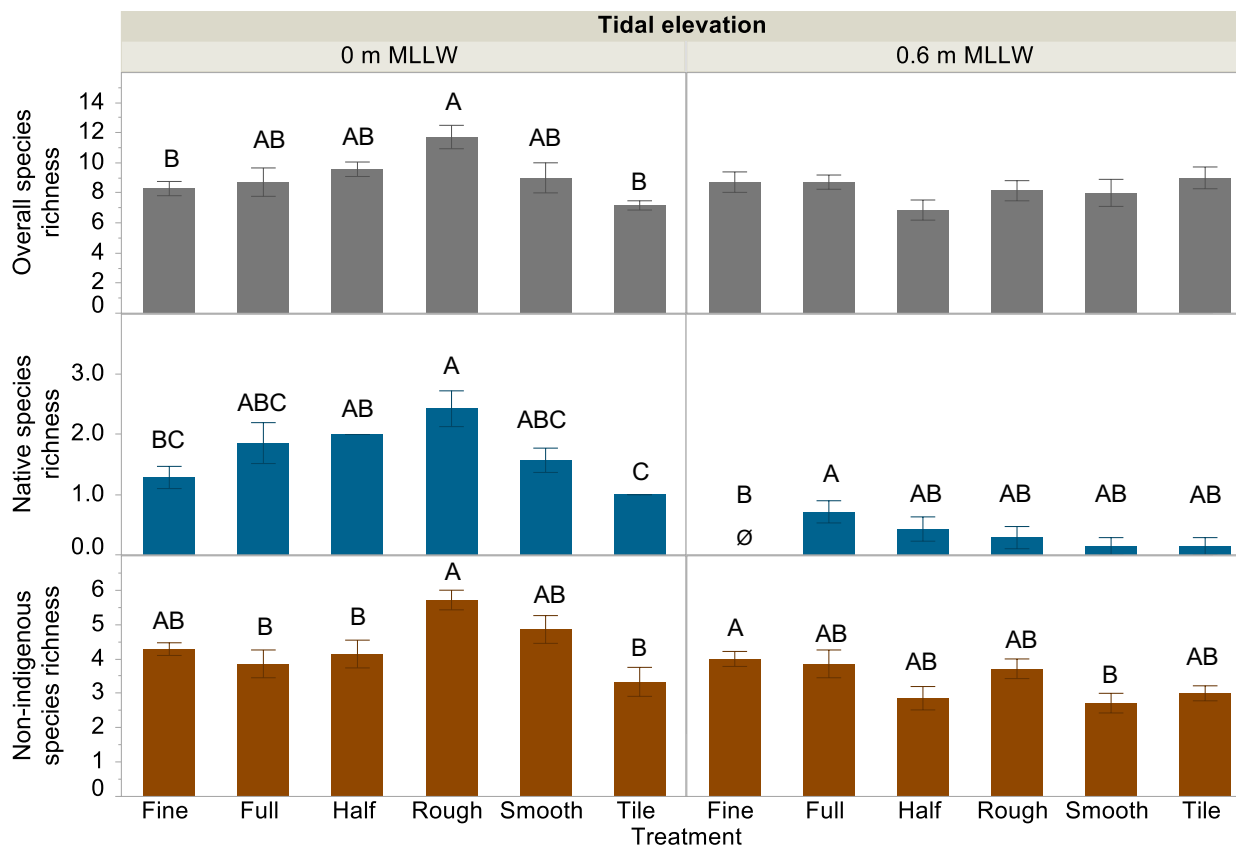


Figure 45. Overall, native, and non-indigenous species richness on the bottom of tiles deployed from May – September 2018 to E Street, San Diego Bay, CA, USA, as a function of treatment. Error bars = 1 SE. Different letters above bars indicate statistically significant differences based upon post-hoc Tukey HSD tests.

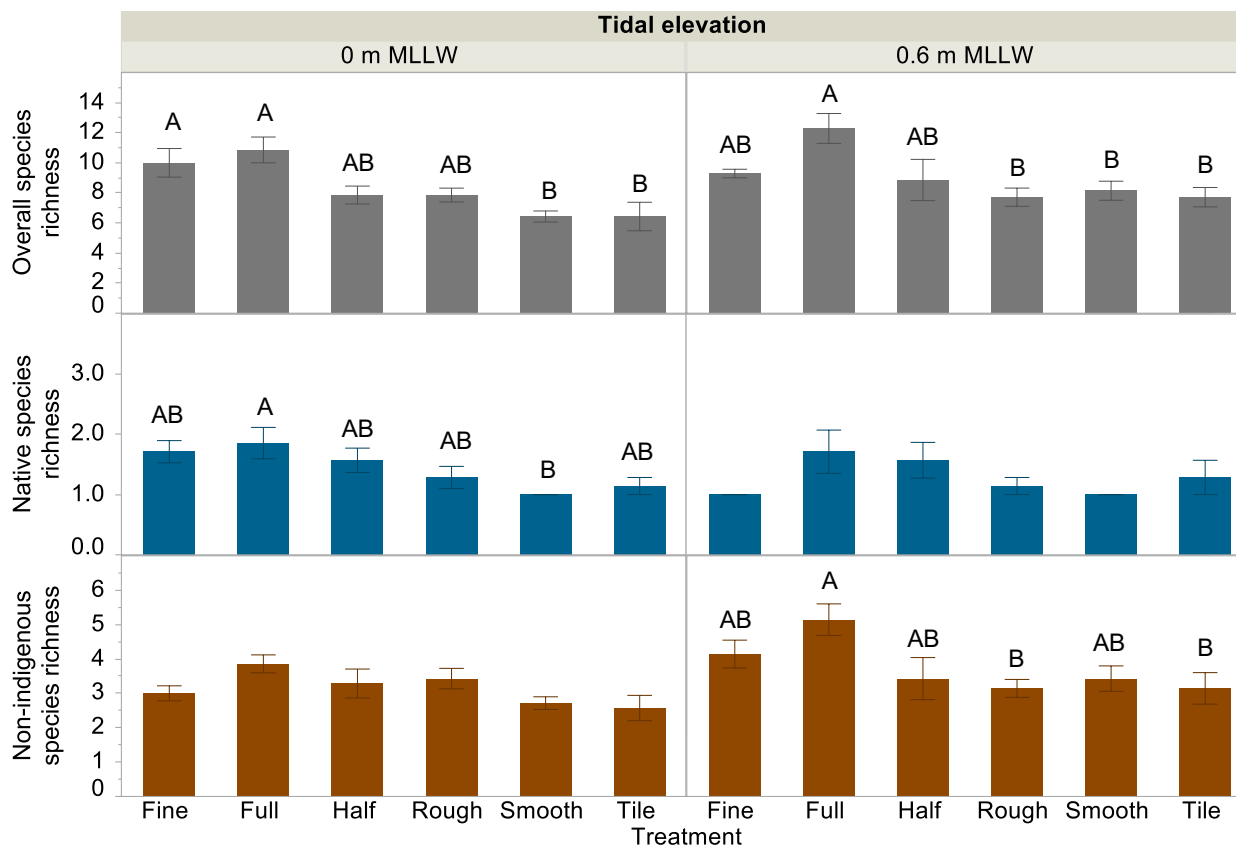


Figure 46. Overall, native, and non-indigenous species richness on the bottom of tiles deployed from May – September 2018 to GC, San Diego Bay, CA, USA, as a function of treatment. Error bars = 1 SE. Different letters above bars indicate statistically significant differences based upon post-hoc Tukey HSD tests.

Table 30. Three-way PERMANOVA test statistics effects of site, tidal elevation, and treatment on overall community composition from tiles deployed from May – September 2018 to ES, San Diego Bay, GC, San Diego Bay, and CI, Newport Bay, CA, USA. Bold indicates significant difference.

Source	df	SS	MS	Pseudo-F	P(perm)	Unique perms
Site	2	236.11	118.06	46.469	0.0001	9899
Tidal elevation	1	98.635	98.635	38.825	0.0001	9909
Treatment	5	40.784	8.1569	3.2107	0.0001	9820
Site*Tidal elevation	2	72.986	36.493	14.364	0.0001	9885
Site*Treatment	10	48.376	4.8376	1.9042	0.0001	9783
Tidal elevation*Treatment	5	24.552	4.9104	1.9328	0.0001	9819
Site*Tidal elevation*Treatment	10	39.274	3.9274	1.5459	0.0003	9770
Res	215	546.21	2.5405			
Total	250	1108				

Non-metric MDS

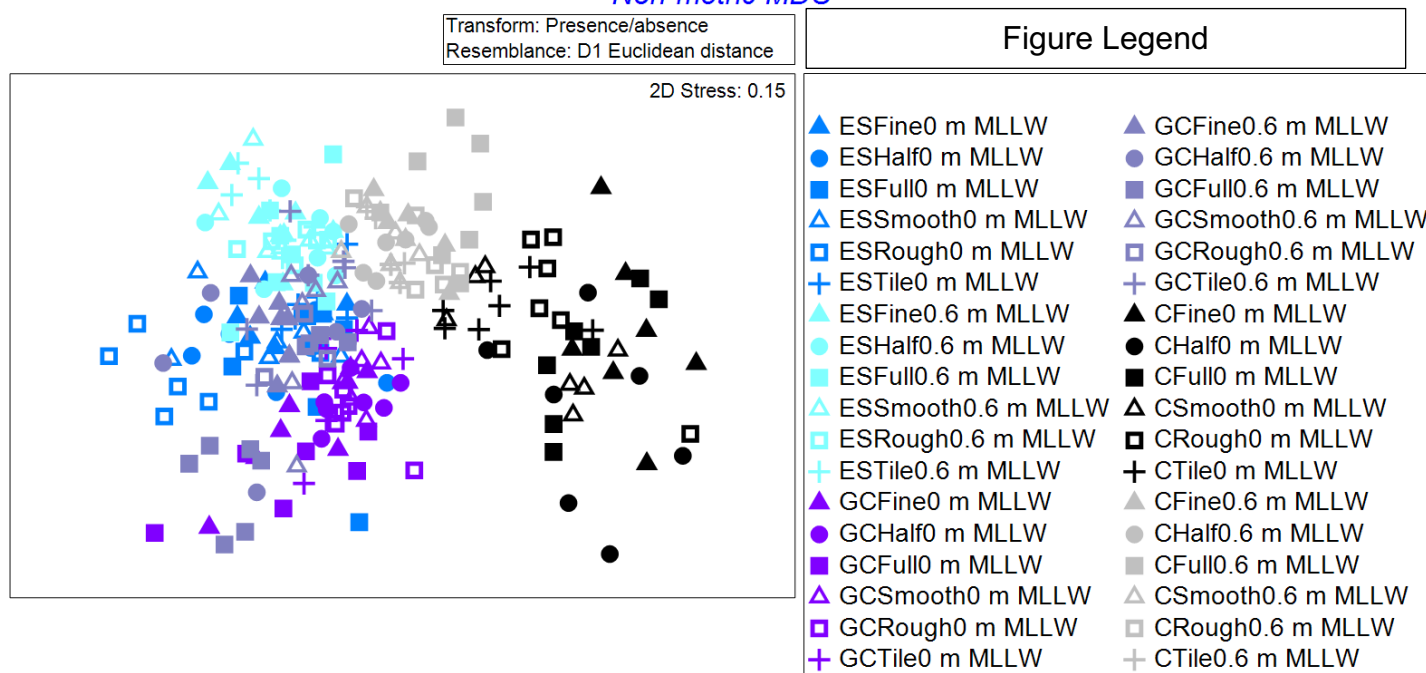


Figure 47. Non-metric multidimensional scaling (nMDS) plot of overall community composition on tiles of site, tidal elevation, and treatment on tiles deployed from May – September 2018 to ES, San Diego Bay, GC, San Diego Bay, and CI, Newport Bay, CA, USA as a function of site, tidal elevation, and treatment. Colors represent sites (blue = ES, purple = GC, black = CI, labeled “C” in the figure legend), shades represent tidal elevations (0 m MLLW = darker, 0.6 m MLLW = lighter), shape fill represents shell presence on treatments (filled = shelled, unfilled = no shell), and similar shapes represent similar rugosity treatments (triangle = low rugosity, square = high rugosity). Stress coefficient = 0.15.

Table 31. Three-way PERMANOVA test statistics effects of site, tidal elevation, and treatment on native community composition from tiles deployed from May – September 2018 to ES, San Diego Bay, GC, San Diego Bay, and CI, Newport Bay, CA, USA.. Bold indicates significant difference.

Source	df	SS	MS	Pseudo-F	P(perm)	Unique perms
Site	2	16.802	8.401	26.451	0.0001	9916
Tidal elevation	1	28.531	28.531	89.83	0.0001	9773
Treatment	5	8.1704	1.6341	5.145	0.0001	9905
Site*Tidal elevation	2	16.118	8.0591	25.374	0.0001	9944
Site*Treatment	10	6.2961	0.62961	1.9824	0.0006	9864
Tidal elevation*Treatment	5	7.1461	1.4292	4.4999	0.0001	9901
Site*Tidal elevation*Treatment	10	6.5996	0.65996	2.0779	0.0005	9870
Res	215	68.286	0.1761			
Total	250	158.17				

Non-metric MDS

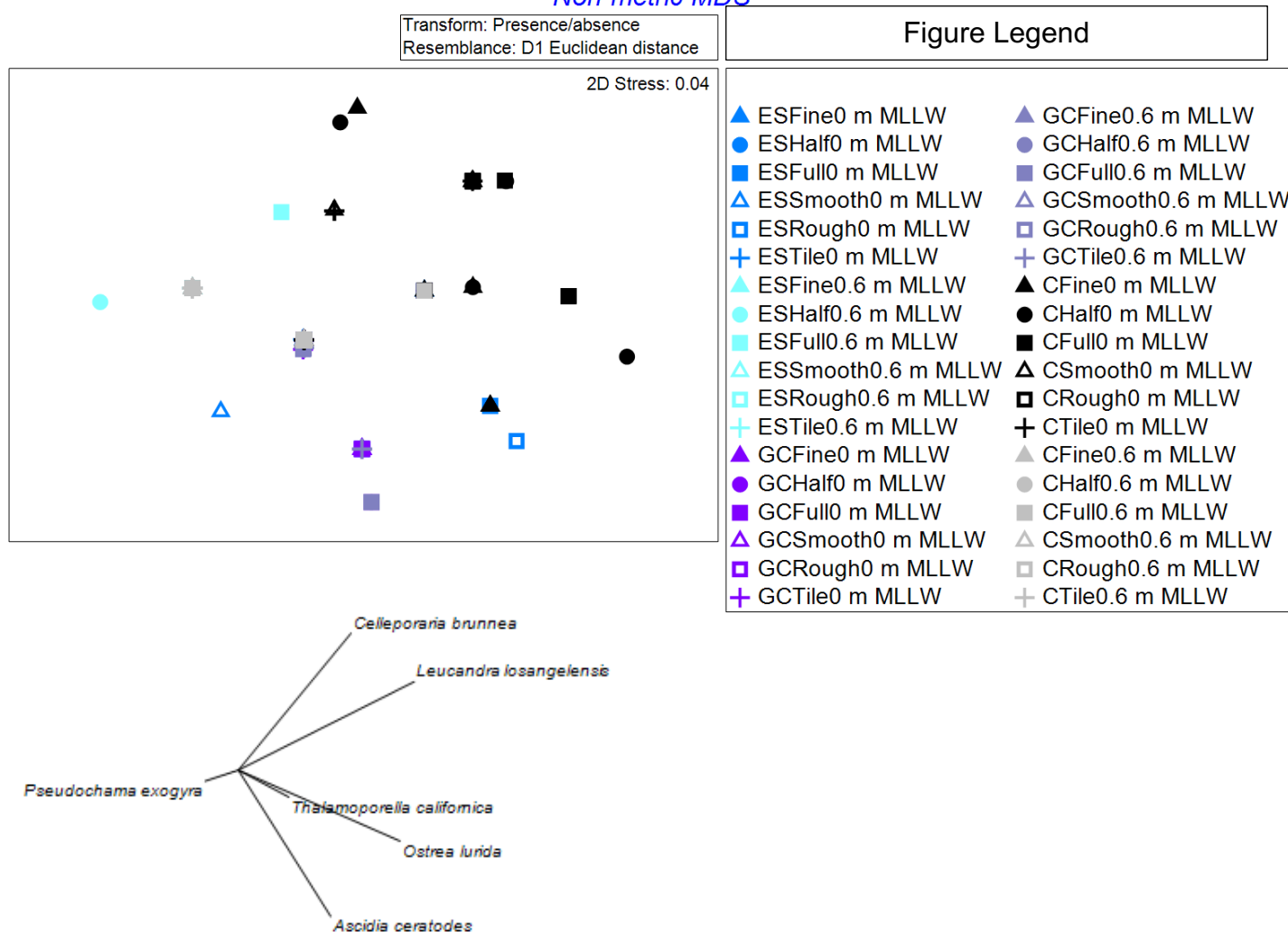


Figure 48. Non-metric multidimensional scaling (nMDS) plot of native community composition on tiles of site, tidal elevation, and treatment on tiles deployed from May – September 2018 to ES, San Diego Bay, GC, San Diego Bay, and CI, Newport Bay, CA, USA as a function of site, tidal elevation, and treatment. Colors represent sites (blue = ES, purple = GC, black = CI, labeled “C” in the figure legend), shades represent tidal elevations (0 m MLLW = darker, 0.6 m MLLW = lighter), shape fill represents shell presence on treatments (filled = shelled, unfilled = no shell), and similar shapes represent similar rugosity treatments (triangle = low rugosity, square = high rugosity). Stress coefficient = 0.04. Biplot rays show the species driving the differences between communities.

Table 32. Three-way PERMANOVA test statistics for effects of site, tidal elevation, and treatment on NIS community composition from tiles deployed from May – September 2018 to ES, San Diego Bay, GC, San Diego Bay, and CI, Newport Bay, CA, USA. Bold indicates significant difference.

Source	df	SS	MS	Pseudo-F	P(perm)	Unique perms
Site	2	159.14	79.569	83.18	0.0001	9920
Tidal elevation	1	29.209	29.209	30.534	0.0001	9917
Treatment	5	15.29	3.058	3.1968	0.0001	9858
Site*Tidal elevation	2	34.549	17.275	18.058	0.0001	9917
Site*Treatment	10	15.44	1.544	1.614	0.0042	9843
Tidal elevation*Treatment	5	8.8638	1.7728	1.8532	0.0059	9860
Site*Tidal elevation*Treatment	10	14.995	1.4995	1.5676	0.0061	9844
Res	215	205.67	0.95659			
Total	250	483.55				

Non-metric MDS

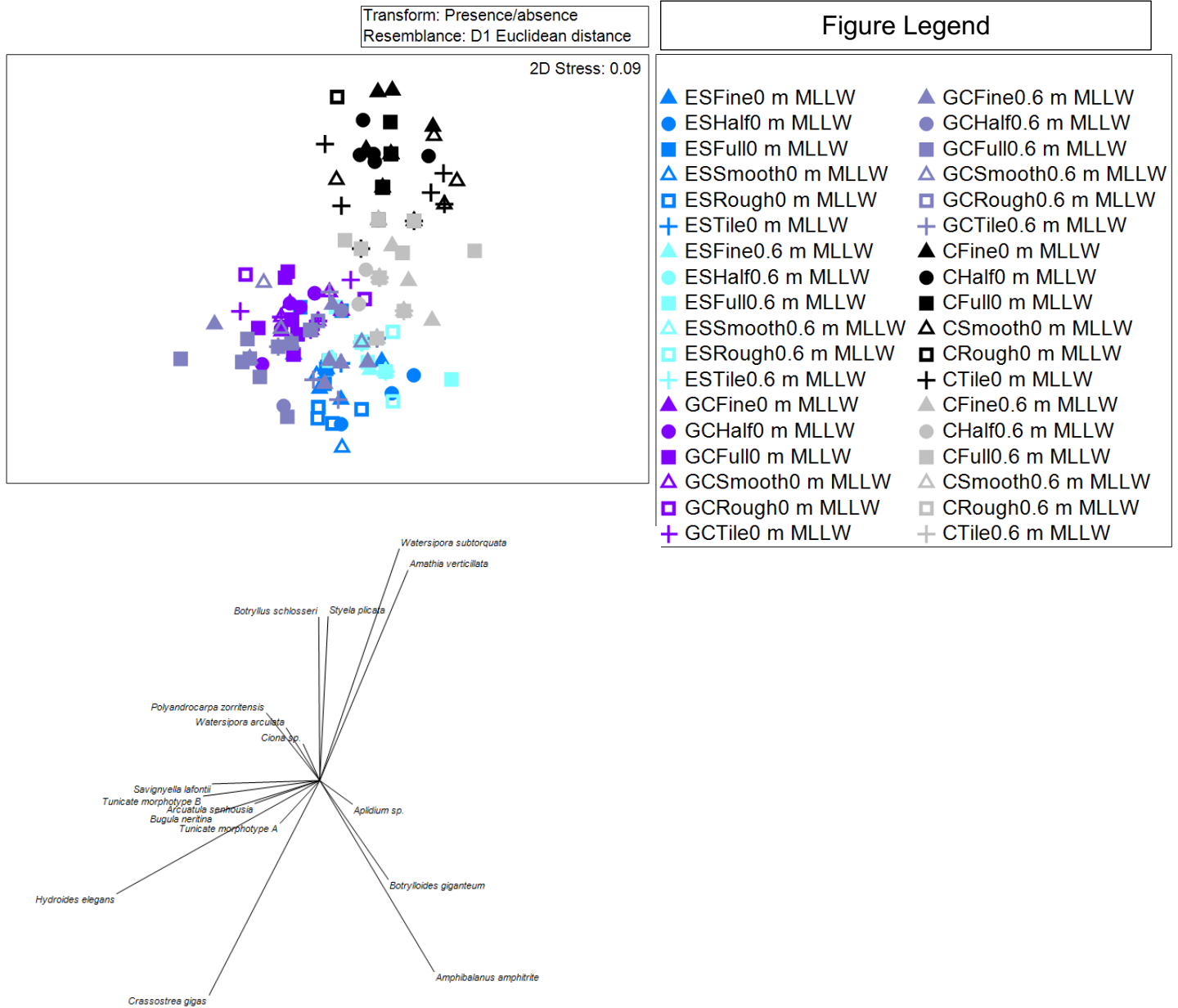


Figure 49. Non-metric multidimensional scaling (nMDS) plot of NIS community composition as a function of site, tidal elevation, and treatment on tiles deployed from May – September 2018 to ES, San Diego Bay, GC, San Diego Bay, and CI, Newport Bay, CA, USA as a function of site, tidal elevation, and treatment. Colors represent sites (blue = ES, purple = GC, black = CI, labeled “C” in the figure legend), shades represent tidal elevations (0 m MLLW = darker, 0.6 m MLLW = lighter), shape fill represents shell presence on treatments (filled = shelled, unfilled = no shell), and similar shapes represent similar rugosity treatments (triangle = low rugosity, square = high rugosity). Stress coefficient = 0.09. Biplot rays show the species driving the differences between communities.

Table 33. Three-way PERMANOVA test statistics for effects of site, tidal elevation, and treatment on overall tunicate abundance from tiles deployed from May – September 2018 to ES, San Diego Bay, GC, San Diego Bay, and CI, Newport Bay, CA, USA. Bold indicates significant difference.

Source	df	SS	MS	Pseudo-F	P(perm)	Unique perms
Site	2	37630	18815	35.387	0.0001	9957
Tidal elevation	1	21260	21260	39.984	0.0001	9955
Treatment	5	25184	5036.8	9.4731	0.0001	9910
Site*Tidal elevation	2	7270.6	3635.3	6.8371	0.0002	9953
Site*Treatment	10	16603	1660.3	3.1226	0.0001	9895
Tidal elevation*Treatment	5	6865.5	1373.1	2.5825	0.0016	9919
Site*Tidal elevation*Treatment	10	12127	1212.7	2.2807	0.0003	9895
Res	216	1.1485x10 ⁵	531.7			
Total	251	2.4179x10 ⁵				

Non-metric MDS

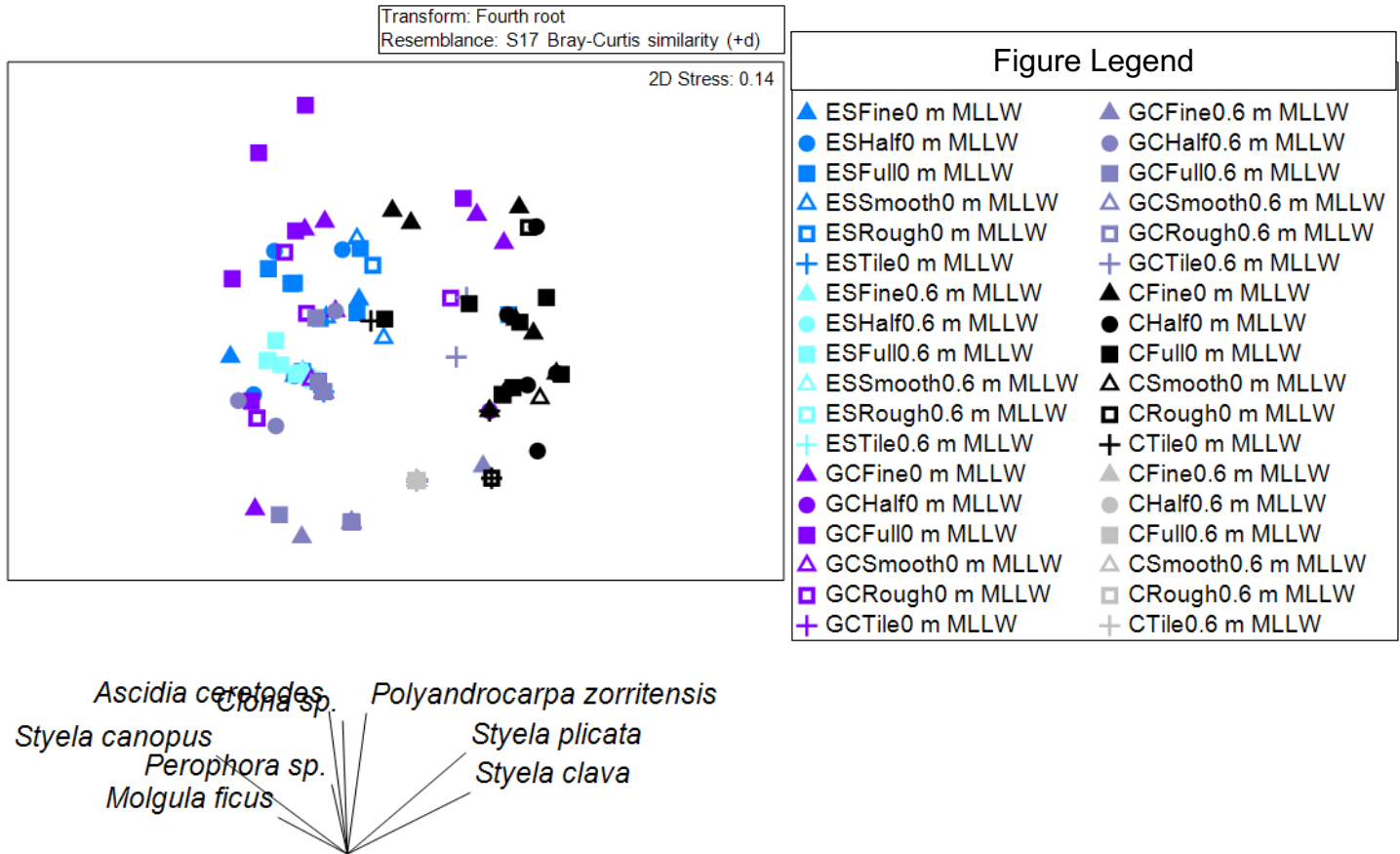


Figure 50. Non-metric multidimensional scaling (nMDS) plot of overall tunicate abundance on the bottom of tiles as a function of site, tidal elevation, and treatment on tiles deployed from May – September 2018 to ES, San Diego Bay, GC, San Diego Bay, and CI, Newport Bay, CA, USA as a function of site, tidal elevation, and treatment. Colors represent sites (blue = ES, purple = GC, black = CI, labeled “C” in the figure legend), shades represent tidal elevations (0 m MLLW = darker, 0.6 m MLLW = lighter), shape fill represents shell presence on treatments (filled = shelled, unfilled = no shell), and similar shapes represent similar rugosity treatments (triangle = low rugosity, square = high rugosity). Stress coefficient = 0.14. Biplot rays show the species driving the differences between communities.

Table 34. Three-way ANOVA test statistics for effects of site, tidal elevation, and treatment on square root transformed abundance of *Ascidia ceratodes* per tile on tiles deployed from May – September 2018 to CI, Newport Bay, ES, San Diego Bay, and GC, San Diego Bay, CA, USA. Bold indicates significant difference.

Source	Nparm	DF	Sum of Squares	F Ratio	Prob > F
Site	2	2	1.1342821	2.0586	0.1301
Tidal elevation	1	1	6.7559929	24.5227	<0.0001
Site*Tidal elevation	2	2	0.3907995	0.7093	0.4932
Treatment	5	5	4.4395683	3.2229	0.0079
Site*Treatment	10	10	6.6517567	2.4144	0.0097
Tidal elevation* Treatment	5	5	4.2023720	3.0507	0.0111
Site*Tidal elevation*Treatment	10	10	6.1501004	2.2323	0.0171

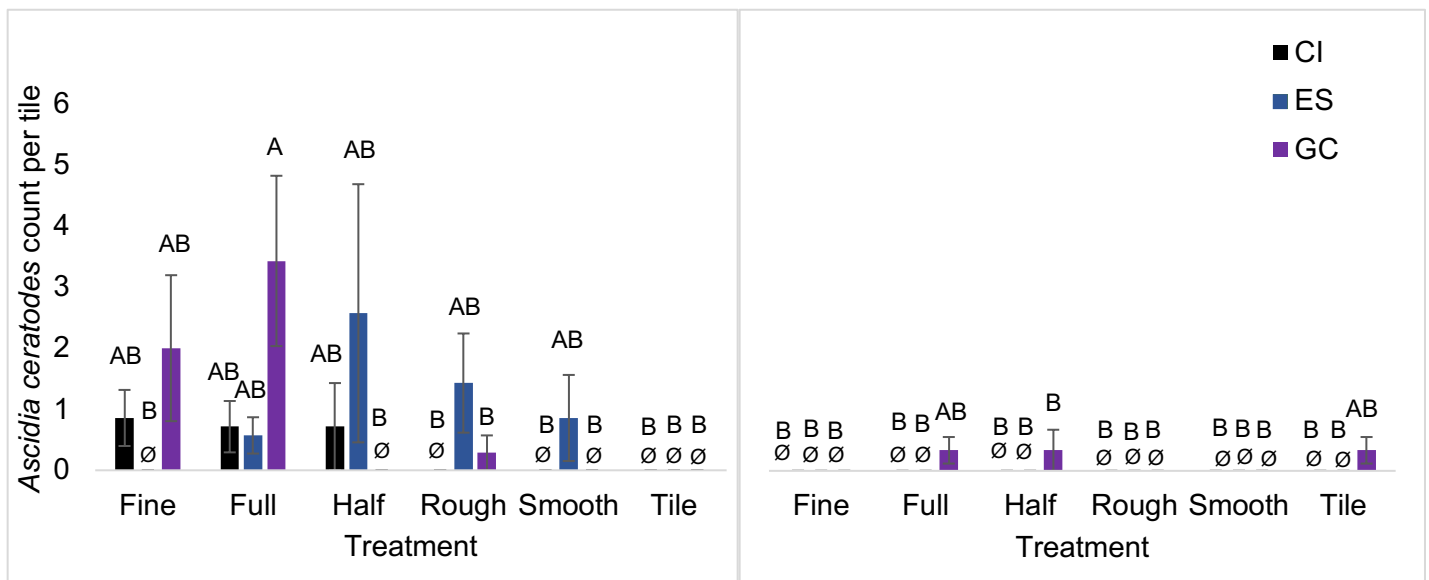


Figure 51. Abundance of *Ascidia ceratodes* per tile on tiles deployed from May – September 2018 to Newport and San Diego Bays, CA, USA, as a function of site, treatment, and tidal elevation (black = CI, blue = ES, purple = GC). Error bars = 1 SE. Different letters above bars indicate statistically significant differences based upon post-hoc Tukey HSD tests.

Table 35. Three-way ANOVA test statistics for effects of site, tidal elevation, and treatment on log transformed abundance of non-indigenous tunicates per tile on tiles deployed from May – September 2018 at all sites (CI in Newport Bay, E Street and GC in San Diego Bay, CA, USA). Bold indicates significant difference.

Source	Nparm	DF	Sum of Squares	F Ratio	Prob > F
Site	2	2	13.149788	11.2000	<0.0001
Tidal elevation	1	1	43.711945	74.4609	<0.0001
Site*Tidal elevation	2	2	5.320812	4.5319	0.0118
Treatment	5	5	72.657889	24.7537	<0.0001
Site*Treatment	10	10	16.021925	2.7292	0.0035
Tidal elevation* Treatment	5	5	12.530497	4.2690	0.0010
Site*Tidal elevation*Treatment	10	10	17.776372	3.0281	0.0013

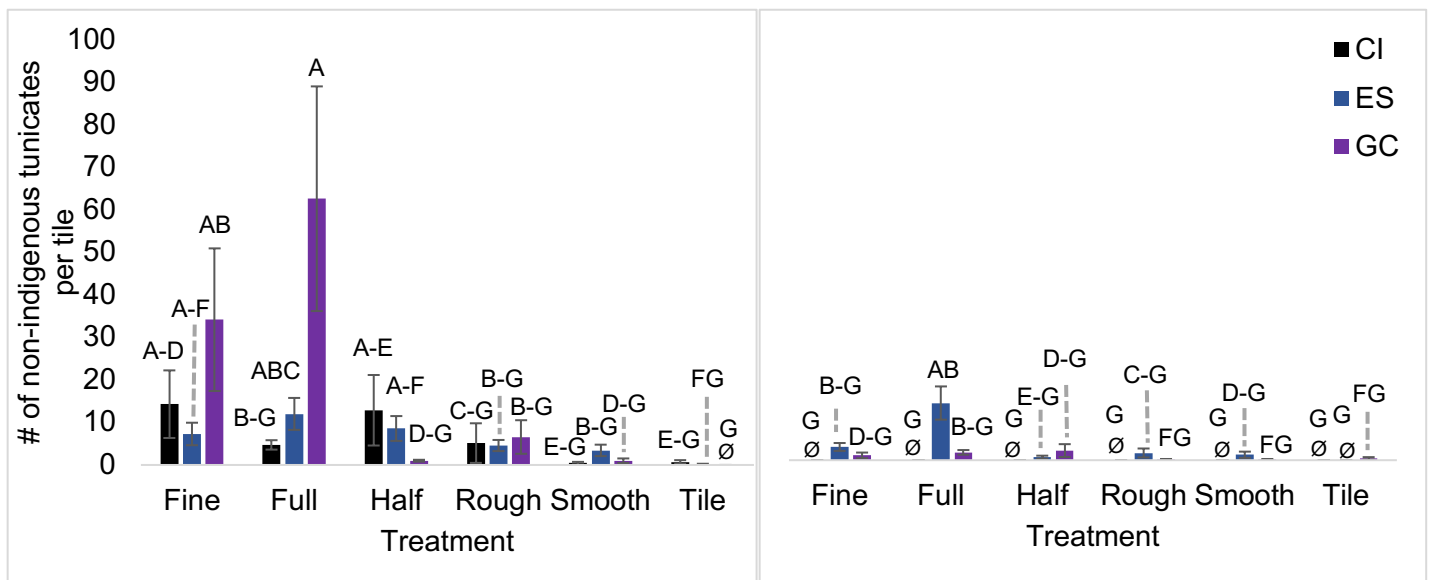


Figure 52. Abundance of non-indigenous tunicates per tile on tiles deployed from May – September 2018 to Newport and San Diego Bays, CA, USA, as a function of site, treatment, and tidal elevation (black = CI, blue = ES, purple = GC). Error bars = 1 SE. Different letters above bars indicate statistically significant differences based upon post-hoc Tukey HSD tests.

Table 36. Three-way ANOVA test statistics for effects of site, tidal elevation, and treatment on square root transformed biomass of algae per tile on tiles Newport and San Diego Bays, CA, USA. Bold indicates significant difference.

Source	Nparm	DF	Sum of Squares	F Ratio	Prob > F
Site	2	2	1.9611311	13.6514	<0.0001
Tidal elevation	1	1	0.0081595	0.1136	0.7364
Site*Tidal elevation	2	2	2.0812925	14.4879	<0.0001
Treatment	5	5	2.1269005	5.9221	<0.0001
Site*Treatment	10	10	1.6722960	2.3282	0.0127
Tidal elevation* Treatment	5	5	0.2911689	0.8107	0.5431
Site*Tidal elevation*Treatment	10	10	1.5970974	2.2235	0.0176

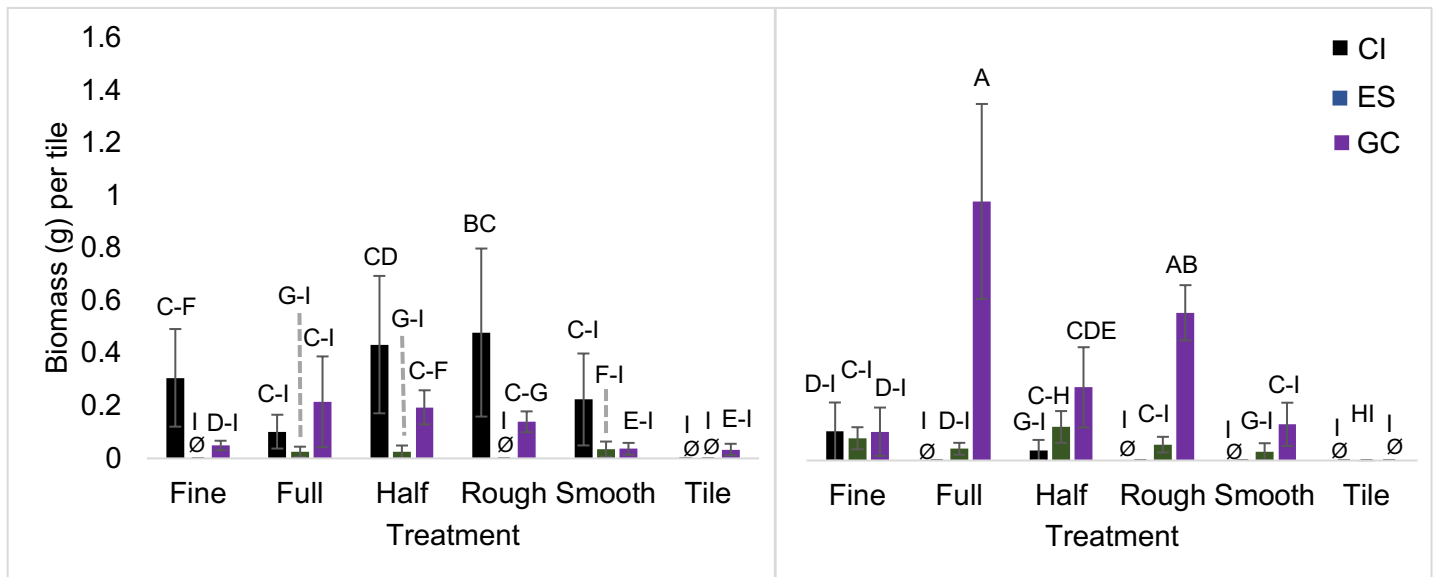


Figure 53. Algal biomass (g) per tile on tiles deployed from May – September 2018 to Newport and San Diego Bays, CA, USA, as a function of site, treatment, and tidal elevation (black = CI, blue = ES, purple = GC). Error bars = 1 SE. Different letters above bars indicate statistically significant differences based upon post-hoc Tukey HSD tests.

Table 37. Three-way ANCOVA test statistics for effects of site, tidal elevation, and treatment on square root- transformed biomass of *Amathia verticillata* per tile on tiles deployed from May – September 2018 at all sites (CI in Newport Bay, E Street and GC in San Diego Bay, CA, USA). Bold indicates significant difference.

Source	Nparm	DF	Sum of Squares	F Ratio	Prob > F
Site	2	2	3.1749743	79.6132	<0.0001
Tidal elevation	1	1	1.3434987	67.3771	<0.0001
Site*Tidal elevation	2	2	2.4927873	62.5072	<0.0001
Treatment	5	5	0.0390170	0.3913	0.8545
Site*Treatment	10	10	0.0926105	0.4644	0.9115
Tidal elevation* Treatment	5	5	0.0257286	0.2581	0.9354
Site*Tidal elevation*Treatment	10	10	0.0413693	0.2075	0.9955

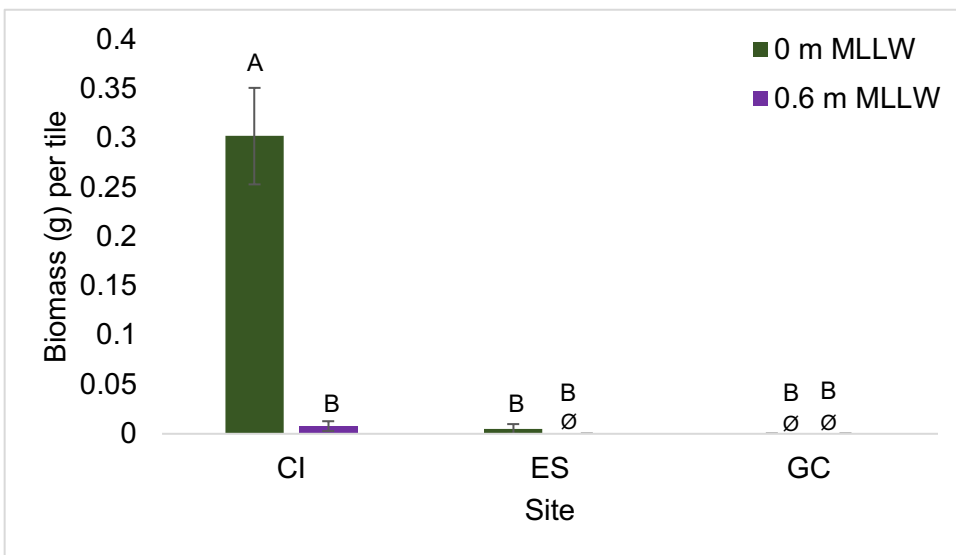


Figure 54. *Amathia verticillata* biomass (g) per tile on tiles deployed from May – September 2018 to Newport and San Diego Bays, CA, USA, as a function of site, treatment, and tidal elevation (green = 0 m MLLW, purple = 0.6 m MLLW). Error bars = 1 SE. Different letters above bars indicate statistically significant differences based upon post-hoc Tukey HSD tests.

Table 38. Space-dominating fauna found in high percent cover on tiles deployed from May – September 2018 to CI, Newport Bay, ES, San Diego Bay, and GC, San Diego Bay, CA, USA. Newport Bay and San Diego Bay, CA, USA. The bottom of one terracotta tile was lost at ES at 0 m MLLW, so total number of tiles reflects this change. Number of tiles includes the count of tiles that detected percent cover of the species as the numerator and the number of tiles possible as the denominator (84 per site), # points per site is the number of times the species was counted in percent cover surveys across tiles, and % cover divides the # points by the total number of points available (# points per site ÷ (83 tiles for ES, 84 tiles for CI and GC x 100 points quantified per tile) = overall % cover). Red font denotes where species did not occupy $\geq 1\%$ cover but is shown for comparison to other sites where it was a space-dominating species.

Species	Provenance	Site	Number of tiles	# points/site	Overall % cover
<i>Crassostrea gigas</i>	Non-indigenous	CI	5/84	7	<1%
		ES	82/83	2313	28%
		GC	72/84	2893	34%
<i>Ostrea lurida</i>	Native	CI	50/84	277	3%
		ES	48/83	958	12%
		GC	71/84	2475	29%
Spirorbid worm	Cryptogenic	CI	75/84	1835	22%
		ES	30/83	50	1%
		GC	30/84	92	1%
<i>Amphibalanus amphitrite</i>	Non-indigenous	CI	4/84	4	<1%
		ES	65/83	1188	14%
		GC	4/84	4	<1%
<i>Watersipora subtorquata</i>	Non-indigenous	CI	45/84	364	4%
		ES	0/83	0	0%
		GC	0/84	0	0%
<i>Botryllus schlosseri</i>	Non-indigenous	CI	19/84	366	4%
		ES	0/83	0	0%
		GC	3/84	14	<1%
<i>Leucandra losangelensis</i>	Native	CI	30/84	182	2%
		ES	12/83	50	1%
		GC	28/84	107	1%

Table 39. Three-way ANCOVA test statistics for effects of tidal elevation, shell cover, and rugosity on percent cover of spirorbid worms per tile on tiles deployed from May – September 2018 to CI, Newport Bay, CA, USA. Bold indicates significant difference.

Source	Nparm	DF	Sum of Squares	F Ratio	Prob > F
Tidal elevation	1	1	17451.691	157.8182	<0.0001
Shell cover	1	1	1402.796	12.6857	0.0008
Tidal elevation *Shell cover	1	1	518.416	4.6881	0.0354
Rugosity	1	1	843.897	7.6315	0.0081
Tidal elevation*Rugosity	1	1	713.037	6.4481	0.0144
Shell cover*Rugosity	1	1	448.368	4.0547	0.0497
Tidal elevation*Shell cover*Rugosity	1	1	123.200	1.1141	0.2965

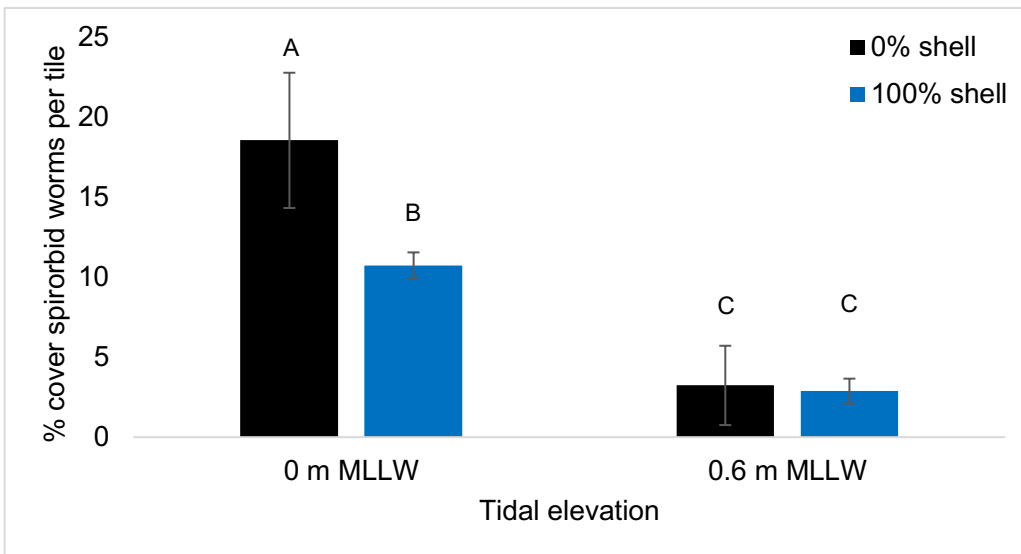


Figure 55. Percent cover of spirorbid worms per tile on tiles deployed from May – September 2018 to CI, Newport Bay, CA, USA as a function of tidal elevation, shell cover, and rugosity (black = 0% shell, blue = 100% shell). Error bars = 1 SE. Different letters above bars indicate statistically significant differences based upon post-hoc Tukey HSD tests.

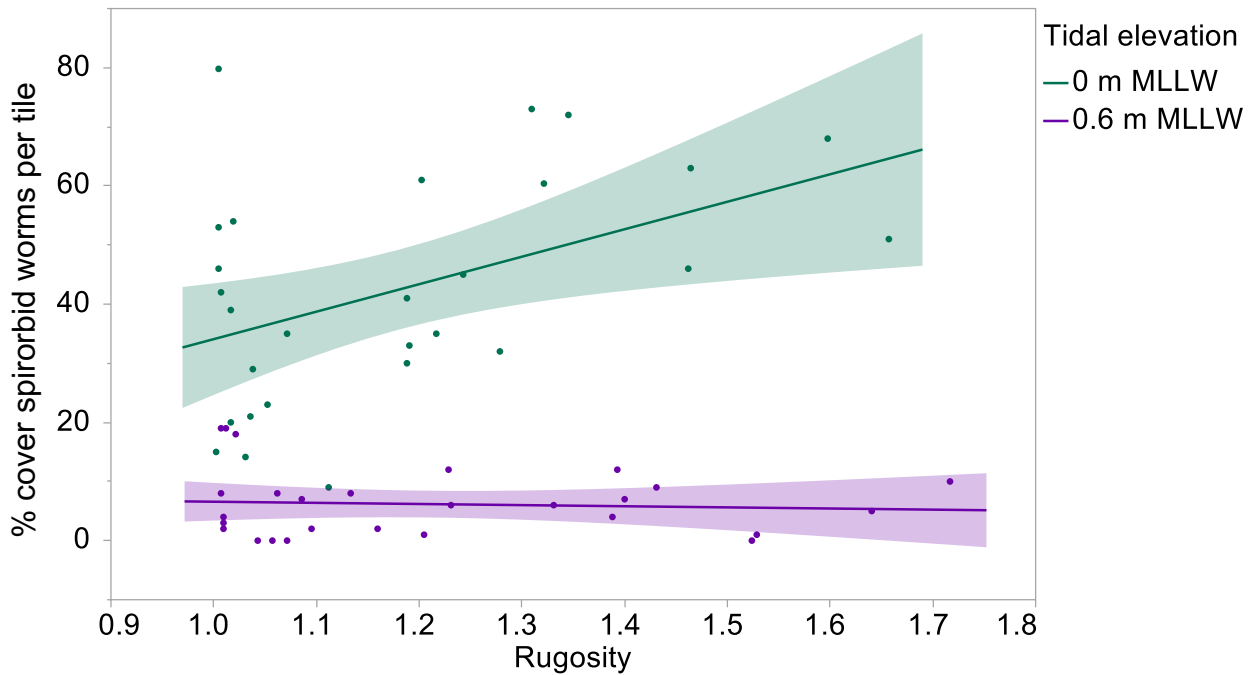


Figure 56. Percent cover of spirorbid worms per tile on tiles deployed from May – September 2018 at CI, Newport Bay, CA, USA as a function of rugosity, shell cover, and tidal elevation (green = 0 m MLLW, purple = 0.6 m MLLW). Shaded regions represent 95% confidence fit. Y (0 m MLLW) = $-12.41 + 46.49x$, R^2 (0 m MLLW) = 0.21; Y (0.6 m MLLW) = $8.49 - 1.91x$, R^2 (0.6 m MLLW) = 0.01.

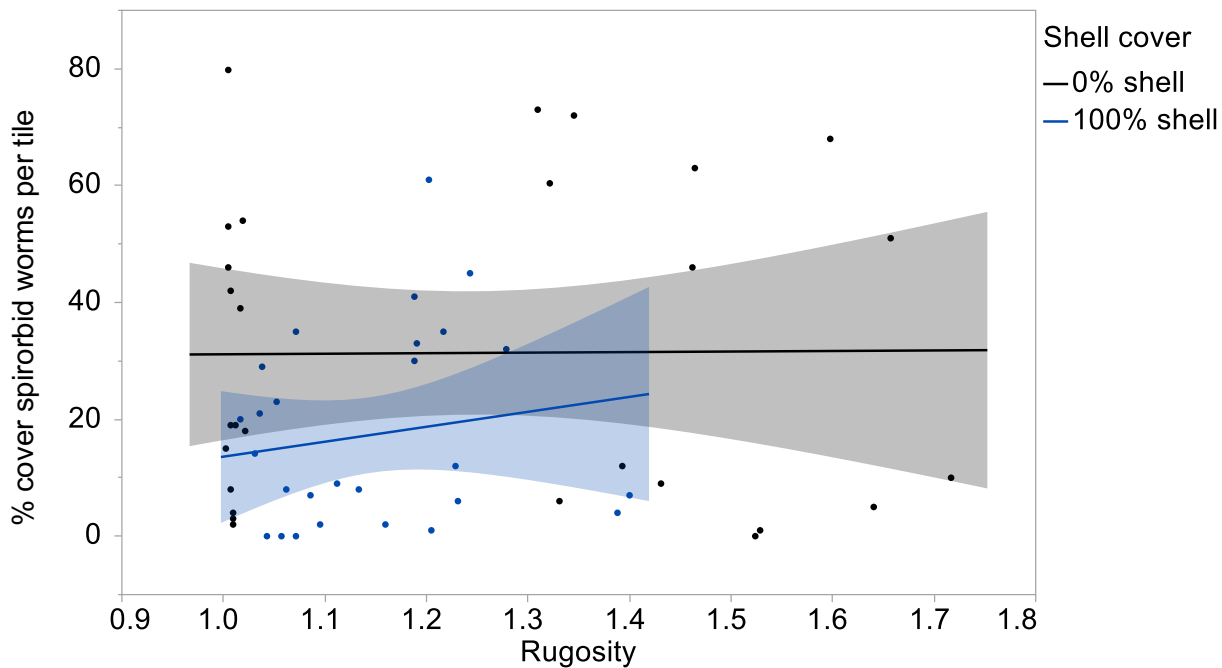


Figure 57. Percent cover of spirorbid worms per tile on tiles deployed from May – September 2018 at CI, Newport Bay, CA, USA as a function of tidal elevation, shell cover, and rugosity (black = 0% shell, blue = 100% shell). Shaded regions represent 95% confidence fit. Y (0% shell) = $30.19 + 0.94x$, R^2 (0% shell) = 0.00; Y (100% shell) = $-11.97 + 25.58x$, R^2 (100% shell) = 0.03.

Table 40. Three-way ANCOVA test statistics for effects of tidal elevation, shell cover, and rugosity on percent cover of spirorbid worms per tile on tiles deployed from May – September 2018 at ES, San Diego Bay, CA, USA. Bold indicates significant difference.

Source	Nparm	DF	Sum of Squares	F Ratio	Prob > F
Tidal elevation	1	1	1.5918357	1.6227	0.2089
Shell cover	1	1	0.2228978	0.2272	0.6358
Tidal elevation *Shell cover	1	1	0.3206257	0.3268	0.5702
Rugosity	1	1	0.8098740	0.8256	0.3681
Tidal elevation*Rugosity	1	1	0.1959233	0.1997	0.6570
Shell cover*Rugosity	1	1	7.6332245	7.7811	0.0075
Tidal elevation*Shell cover*Rugosity	1	1	0.9910944	1.0103	0.3199

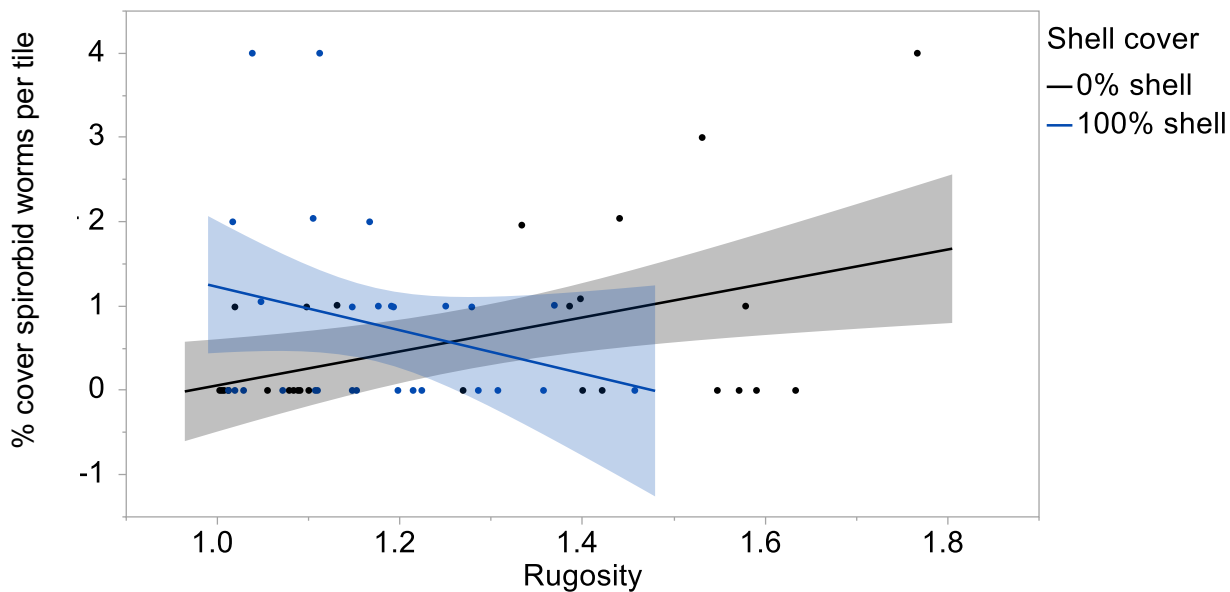


Figure 58. Percent cover of spirorbid worms per tile on tiles deployed from May – September 2018 at ES, San Diego Bay, CA, USA as a function of tidal elevation, shell cover, and rugosity (black = 0% shell, blue = 100% shell). Shaded regions represent 95% confidence fit. Y (0% shell) = $-1.95 + 2.01x$, R^2 (0% shell) = 0.22; Y (100% shell) = $3.80 - 2.6x$, R^2 (100% shell) = 0.07.

Table 41. Three-way ANCOVA test statistics for effects of tidal elevation, shell cover, and rugosity on log transformed percent cover of spirorbid worms per tile on tiles deployed from May – September 2018 at GC, San Diego Bay, CA, USA. Bold indicates significant difference.

Source	Nparm	DF	Sum of Squares	F Ratio	Prob > F
Tidal elevation	1	1	2.4172361	4.8596	0.0323
Shell cover	1	1	1.4888443	2.9932	0.0900
Tidal elevation *Shell cover	1	1	0.2790503	0.5610	0.4575
Rugosity	1	1	0.6823496	1.3718	0.2473
Tidal elevation*Rugosity	1	1	0.6350248	1.2766	0.2641
Shell cover*Rugosity	1	1	1.4340377	2.8830	0.0960
Tidal elevation*Shell cover*Rugosity	1	1	0.6052495	1.2168	0.2755

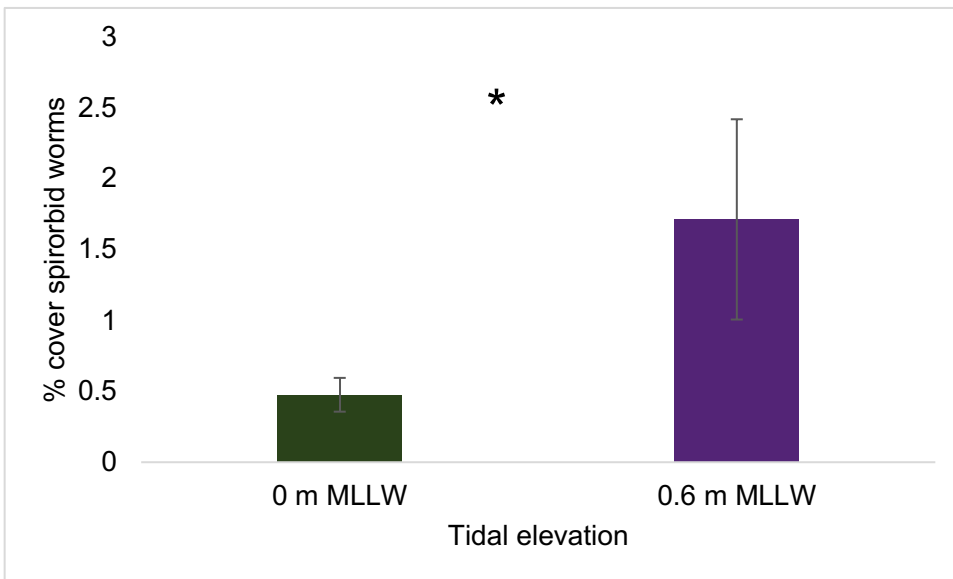


Figure 59. Percent cover of spirorbid worms per tile on tiles deployed from May – September 2018 at GC, San Diego Bay, CA, USA as a function of tidal elevation, shell cover, and rugosity. Error bars = 1 SE. Symbol between bars indicate statistically significant differences.

Table 42. Three-way ANCOVA test statistics for effects of tidal elevation, shell cover, and rugosity on percent cover of square root transformed *Amphibalanus amphitrite* per tile on tiles deployed from May – September 2018 at ES, San Diego Bay, CA, USA. Bold indicates significant difference.

Source	Nparm	DF	Sum of Squares	F Ratio	Prob > F
Tidal elevation	1	1	55.083528	30.4939	<0.0001
Shell cover	1	1	63.156212	34.9629	<0.0001
Tidal elevation *Shell cover	1	1	18.927115	10.4779	0.0022
Rugosity	1	1	34.277966	18.9761	<0.0001
Tidal elevation*Rugosity	1	1	19.859555	10.9941	0.0017
Shell cover*Rugosity	1	1	3.557283	1.9693	0.1670
Tidal elevation*Shell cover*Rugosity	1	1	1.997160	1.1056	0.2983

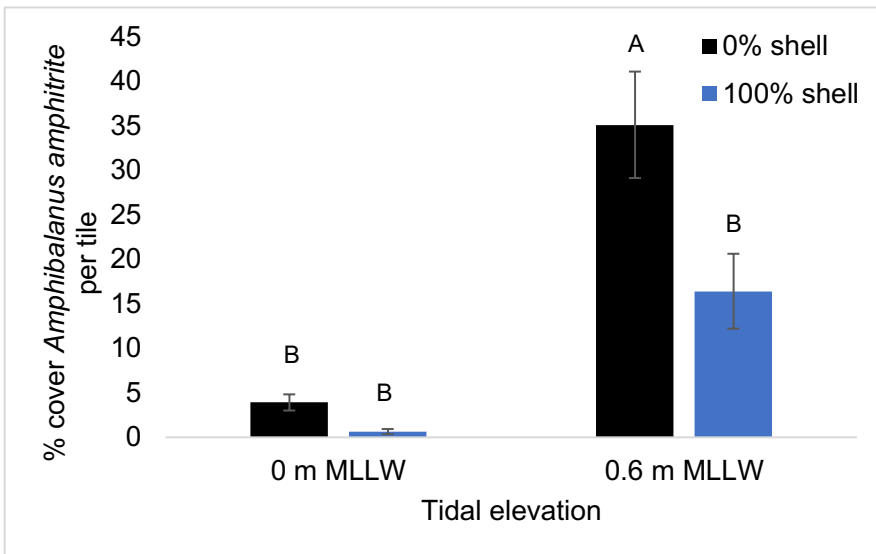


Figure 60. Percent cover of *Amphibalanus amphitrite* per tile on tiles deployed from May – September 2018 at ES, San Diego Bay, CA, USA as a function of tidal elevation, shell cover, and rugosity (black = 0% shell, blue = 100% shell). Error bars = 1 SE. Different letters above bars indicate statistically significant differences based upon post-hoc Tukey HSD tests.

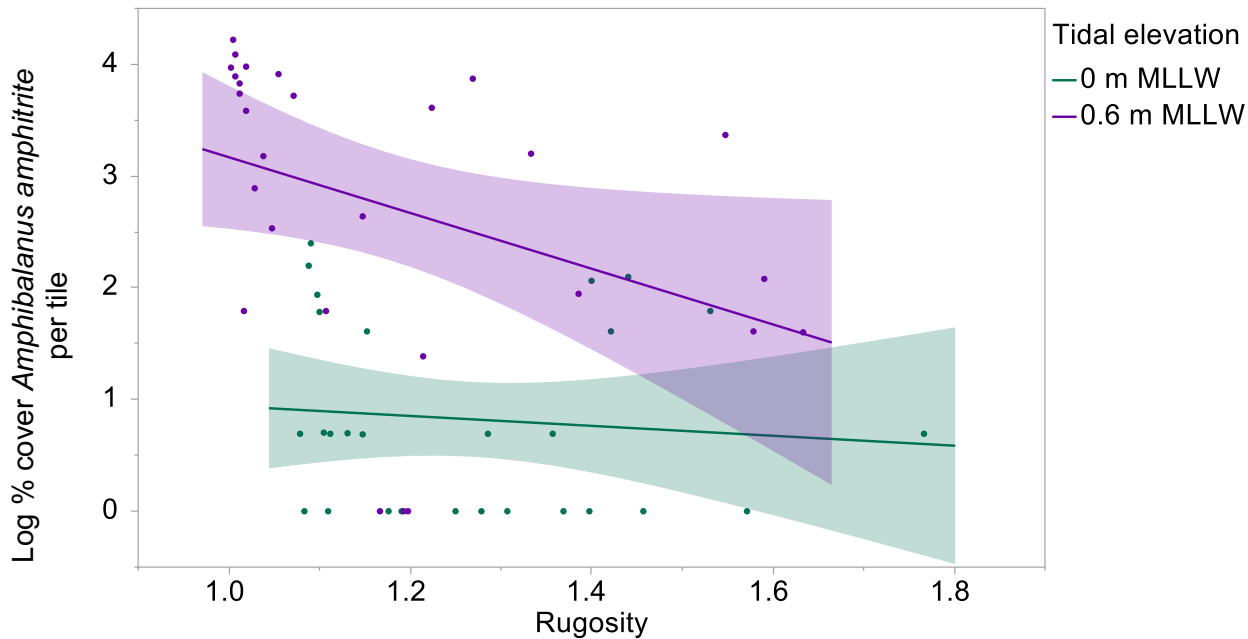


Figure 61. Log transformed percent cover of *Amphibalanus amphitrite* per tile on tiles deployed from May – September 2018 at ES, San Diego Bay, CA, USA as a function of tidal elevation, shell cover, and rugosity (green = 0 m MLLW, purple = 0.6 m MLLW). Shaded regions represent 95% confidence fit. Y (0 m MLLW) = $1.86 - 0.61x$, R^2 (0 m MLLW) = 0.01; Y (0.6 m MLLW) = $10.98 - 5.58x$, R^2 (0.6 m MLLW) = 0.20.

Table 43. Three-way ANCOVA test statistics for effects of tidal elevation, shell cover, and rugosity on percent cover of live and dead *Amphibalanus amphitrite* per tile on tiles deployed from May – September 2018 at ES, San Diego Bay, CA, USA. Bold indicates significant difference.

Source	Nparm	DF	Sum of Squares	F Ratio	Prob > F
Tidal elevation	1	1	11139.184	171.3406	<0.0001
Shell cover	1	1	1945.767	29.9294	<0.0001
Tidal elevation *Shell cover	1	1	1150.324	17.6940	0.0001
Rugosity	1	1	941.724	14.4854	0.0004
Tidal elevation*Rugosity	1	1	724.612	11.1458	0.0016
Shell cover*Rugosity	1	1	9.930	0.1527	0.6977
Tidal elevation*Shell cover*Rugosity	1	1	10.585	0.1628	0.6884

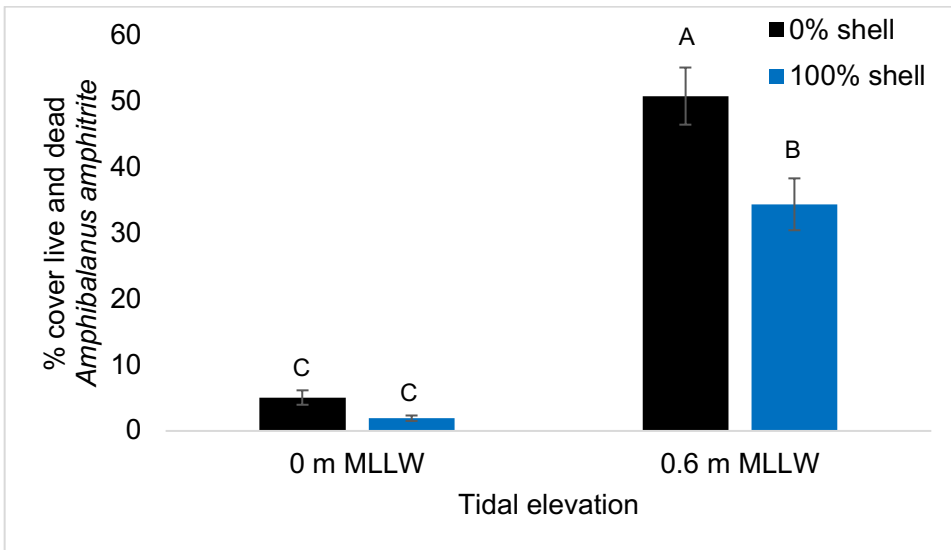


Figure 62. Percent cover of live and dead *Amphibalanus amphitrite* per tile on tiles deployed from May – September 2018 at ES, San Diego Bay, CA, USA as a function of tidal elevation, shell cover, and rugosity (black = 0% shell, blue = 100% shell). Error bars = 1 SE. Different letters above bars indicate statistically significant differences based upon post-hoc Tukey HSD tests.

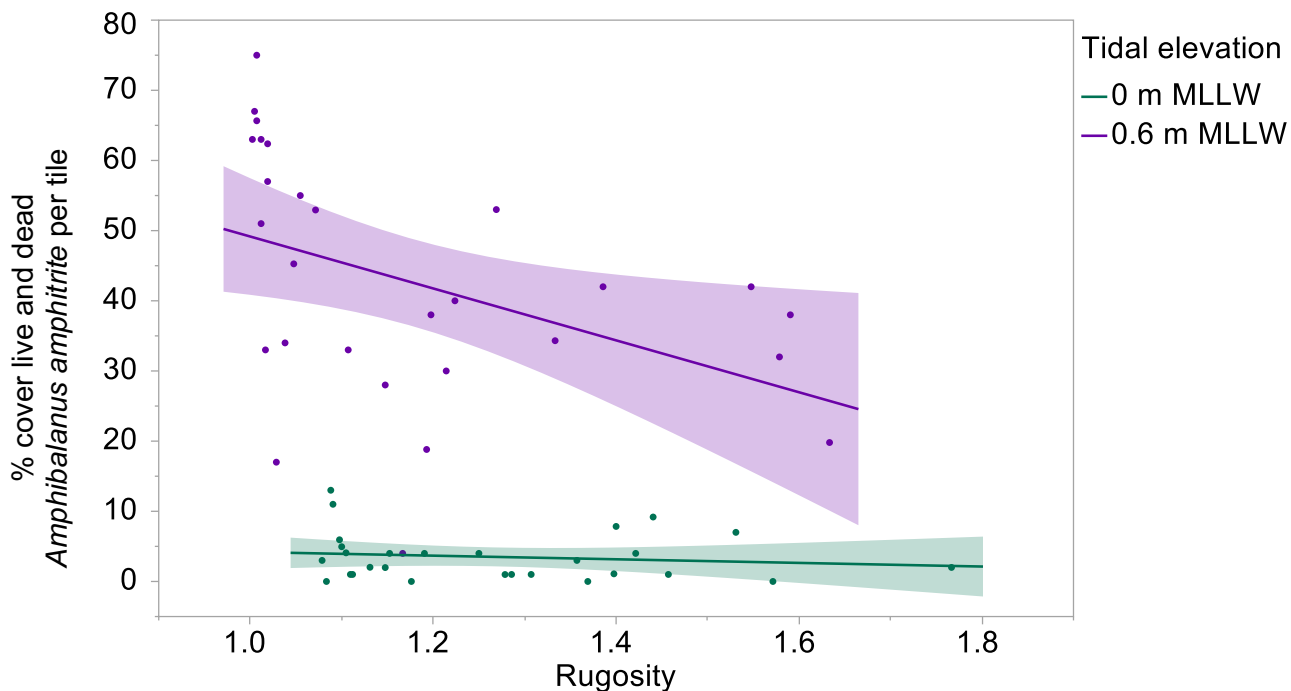


Figure 63. Percent cover of *Amphibalanus amphitrite* live and dead per tile on tiles deployed from May – September 2018 at ES, San Diego Bay, CA, USA as a function of tidal elevation, shell cover, and rugosity (green = 0 m MLLW, purple = 0.6 m MLLW). Shaded regions represent 95% confidence fit. Y (0 m MLLW) = $6.78 - 2.58x$, R^2 (0 m MLLW) = 0.02; Y (0.6 m MLLW) = $86.16 - 37x$, R^2 (0.6 m MLLW) = 0.18.

Table 44. Three-way ANCOVA test statistics for effects of tidal elevation, shell cover, and rugosity on square root transformed percent cover of *Watersipora subtorquata* per tile on tiles deployed from May – September 2018 to CI, Newport Bay, CA, USA,. Bold indicates significant difference.

Source	Nparm	DF	Sum of Squares	F Ratio	Prob > F
Tidal elevation	1	1	79.576181	201.0679	<0.0001
Shell cover	1	1	0.285987	0.7226	0.3995
Tidal elevation *Shell cover	1	1	0.001632	0.0041	0.9491
Rugosity	1	1	0.590150	1.4912	0.2280
Tidal elevation*Rugosity	1	1	0.476466	1.2039	0.2780
Shell cover*Rugosity	1	1	0.004855	0.0123	0.9123
Tidal elevation*Shell cover*Rugosity	1	1	0.000068	0.0002	0.9896

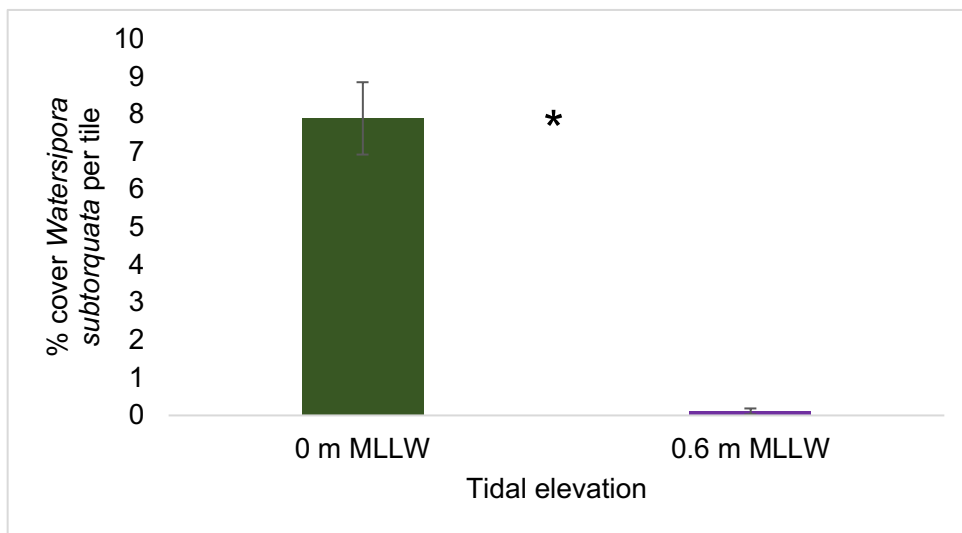


Figure 64. Percent cover of *Watersipora subtorquata* per tile on tiles deployed from May – September 2018 to CI, Newport Bay, CA, USA as a function of tidal elevation, shell cover, and rugosity. Error bars = 1 SE. Symbol between bars indicate statistically significant differences.

Table 45. Two-way ANCOVA test statistics for effects of shell cover and rugosity on percent cover of log transformed *Botryllus schlosseri* per tile on tiles deployed from May – September 2018 to 0 m MLLW at CI, Newport Bay, CA, USA. Bold indicates significant difference.

Source	Nparm	DF	Sum of Squares	F Ratio	Prob > F
Shell cover	1	1	0.5334435	0.2590	0.6144
Rugosity	1	1	9.8176803	4.7668	0.0367
Shell cover*Rugosity	1	1	3.4764633	1.6879	0.2035

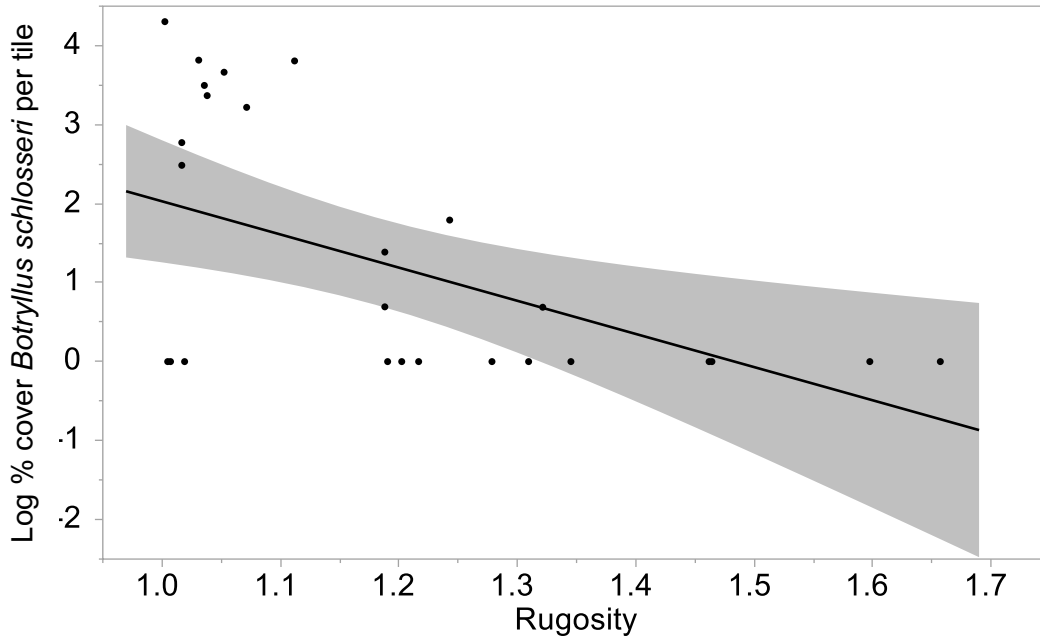


Figure 65. Log transformed percent cover of *Botryllus schlosseri* per tile on tiles deployed from May – September 2018 at CI, Newport Bay, CA, USA as a function of shell cover and rugosity. Shaded regions represent 95% confidence fit. $Y = 6.23 - 4.20x$, $R^2 = 0.25$.

Table 46. Three-way ANCOVA test statistics for effects of site, shell cover, and rugosity on log transformed percent cover of *Leucandra losangelensis* per tile on tiles deployed from May – September 2018 to 0 m MLLW at CI, Newport Bay, ES, San Diego Bay, and GC, San Diego Bay, CA, USA. Bold indicates significant difference.

Source	Nparm	DF	Sum of Squares	F Ratio	Prob > F
Site	2	2	11.477971	8.7177	0.0004
Shell cover	1	1	6.917435	10.5078	0.0018
Site*Shell cover	2	2	3.177230	2.4131	0.0967
Rugosity	1	1	2.078750	3.1577	0.0798
Site*Rugosity	2	2	0.602020	0.4572	0.6349
Shell cover*Rugosity	1	1	0.191763	0.2913	0.5911
Site*Shell cover*Rugosity	2	2	0.371973	0.2825	0.7547

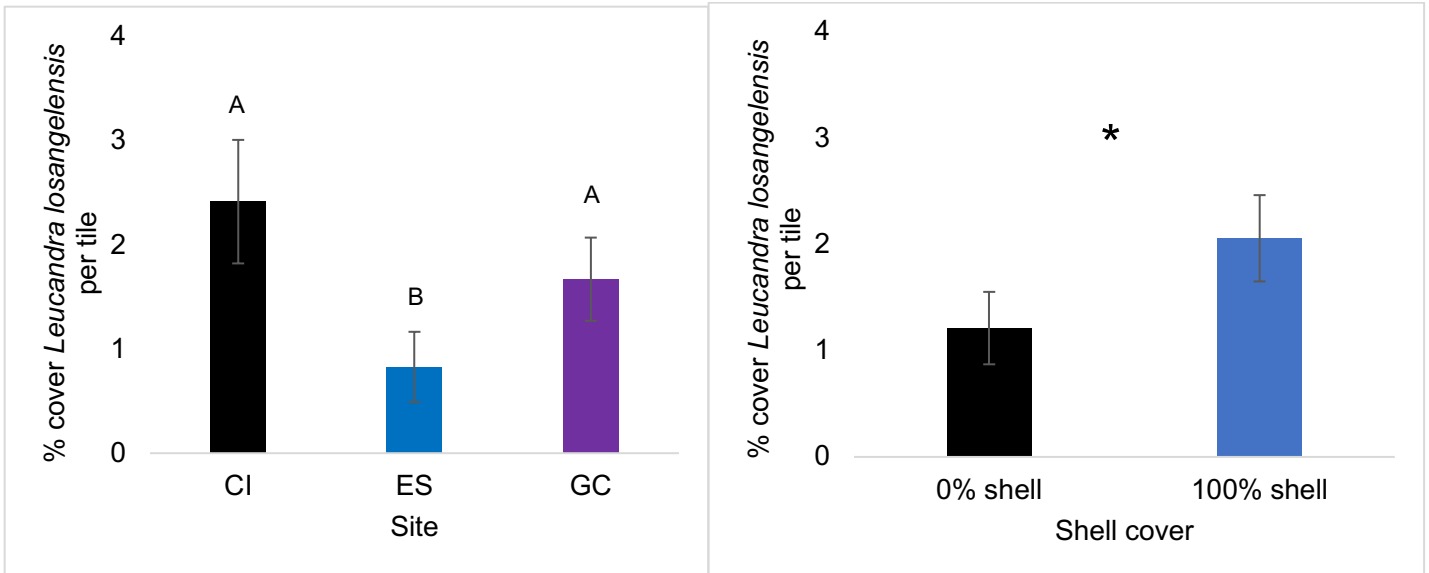


Figure 66. Percent cover of *Leucandra losangelensis* per tile on tiles deployed from May – September 2018 to 0 m MLLW at CI, Newport Bay, ES, San Diego Bay, and GC, San Diego Bay, CA, USA as a function of site, shell cover, and rugosity (black = CI, blue = ES, purple = GC). Error bars = 1 SE. Different letters above bars indicate statistically significant differences based upon post-hoc Tukey HSD tests. Symbol between bars indicate statistically significant differences.

APPENDIX B

SUPPLEMENTARY MATERIAL

Table A1. Three-way ANOVA test statistics for effects of site, tidal elevation, and treatment on rank-averaged pre-deployment rugosity on the top of tiles deployed from May – September 2018 to CI, Newport Bay, ES, San Diego Bay, and GC, San Diego Bay, CA, USA. Bold indicates significant difference.

Source	Nparm	DF	Sum of Squares	F Ratio	Prob > F
Site	2	2	2095.5	1.8366	0.1618
Tidal elevation	1	1	4080.1	7.1520	0.0081
Site*Tidal elevation	2	2	14187.1	12.4342	<0.0001
Treatment	5	5	1158832.3	406.2609	<0.0001
Site*Treatment	10	10	14154.6	2.4812	0.0078
Tidal elevation*Treatment	5	5	4533.4	1.5893	0.1643
Site*Tidal elevation*Treatment	10	10	11981.2	2.1002	0.0256

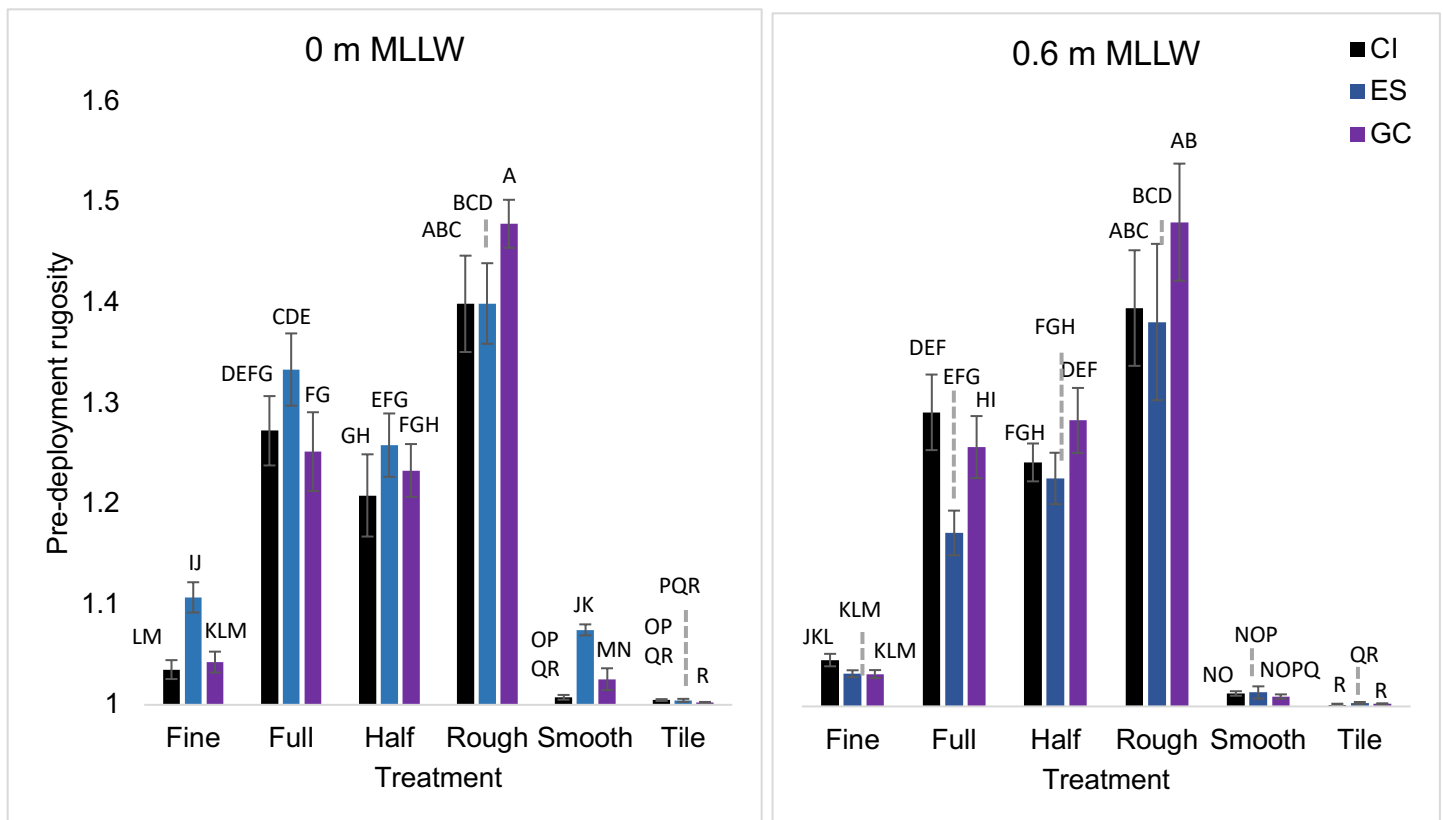


Figure A1. Top pre-deployment rugosity on tiles deployed from May – September 2018 to CI, Newport Bay, ES, San Diego Bay, and GC, San Diego Bay, CA, USA as a function of site, tidal elevation, and treatment (black = CI, Newport Bay, blue = ES, San Diego Bay, purple = GC, San Diego Bay). Error bars = 1 SE. Different letters above bars indicate statistically significant differences based upon post-hoc Tukey HSD tests.

Table A2. Three-way ANOVA test statistics for effects of site, tidal elevation, and treatment on rank-averaged pre-deployment rugosity on the bottom of tiles deployed from May – September 2018 to CI, Newport Bay, ES, San Diego Bay, and GC, San Diego Bay, CA, USA. Bold indicates significant difference.

Source	Nparm	DF	Sum of Squares	F Ratio	Prob > F
Site	2	2	7783.6	11.7281	<0.0001
Tidal elevation	1	1	5619.4	16.9345	<0.0001
Site*Tidal elevation	2	2	11273.7	16.9870	<0.0001
Treatment	5	5	1205317.8	726.4576	<0.0001
Site*Treatment	10	10	10288.7	3.1006	0.0010
Tidal elevation*Treatment	5	5	4319.1	2.6032	0.0261
Site*Tidal elevation*Treatment	10	10	16588.3	4.9990	<0.0001

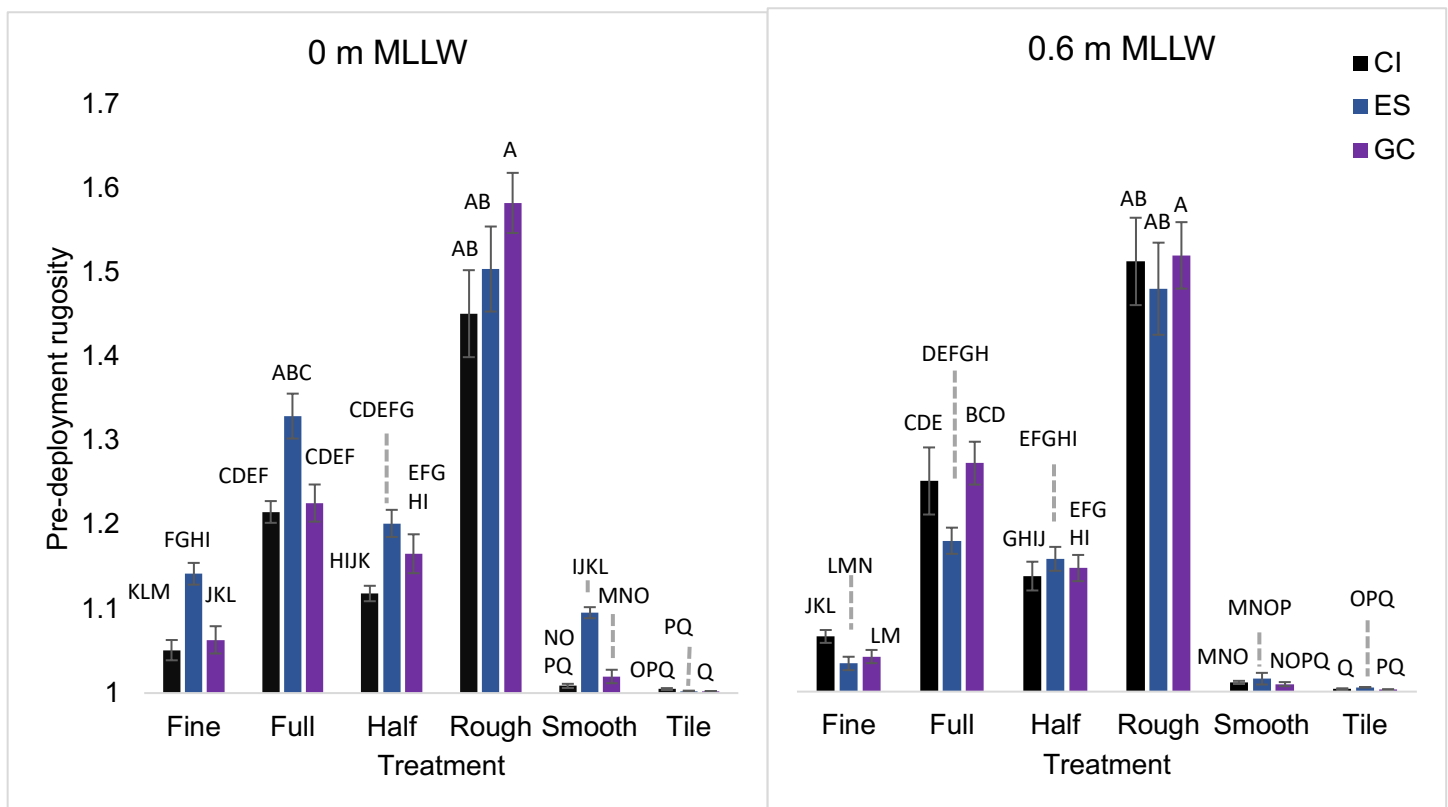


Figure A2. Bottom pre-deployment rugosity on tiles deployed from May – September 2018 to CI, Newport Bay, ES, San Diego Bay, and GC, San Diego Bay, CA, USA as a function of site, tidal elevation, and treatment (black = CI, Newport Bay, blue = ES, San Diego Bay, purple = GC, San Diego Bay). Error bars = 1 SE. Different letters above bars indicate statistically significant differences based upon post-hoc Tukey HSD tests.

Table A3. Three-way ANOVA test statistics for effects of site, tidal elevation, and treatment on pre-deployment percent cover of shell on the top of tiles deployed from May – September 2018 to CI, Newport Bay, ES, San Diego Bay, and GC, San Diego Bay, CA, USA. Bold indicates significant difference.

Source	Nparm	DF	Sum of Squares	F Ratio	Prob > F
Site	2	2	829.00	10.1787	<0.0001
Tidal elevation	1	1	73.14	1.7961	0.1830
Site*Tidal elevation	2	2	58.62	0.7197	0.4892
Treatment	2	2	119554.33	1467.925	<0.0001
Site*Treatment	4	4	553.52	3.3982	0.0117
Tidal elevation*Treatment	2	2	19.48	0.2391	0.7877
Site*Tidal elevation*Treatment	4	4	284.76	1.7482	0.1447

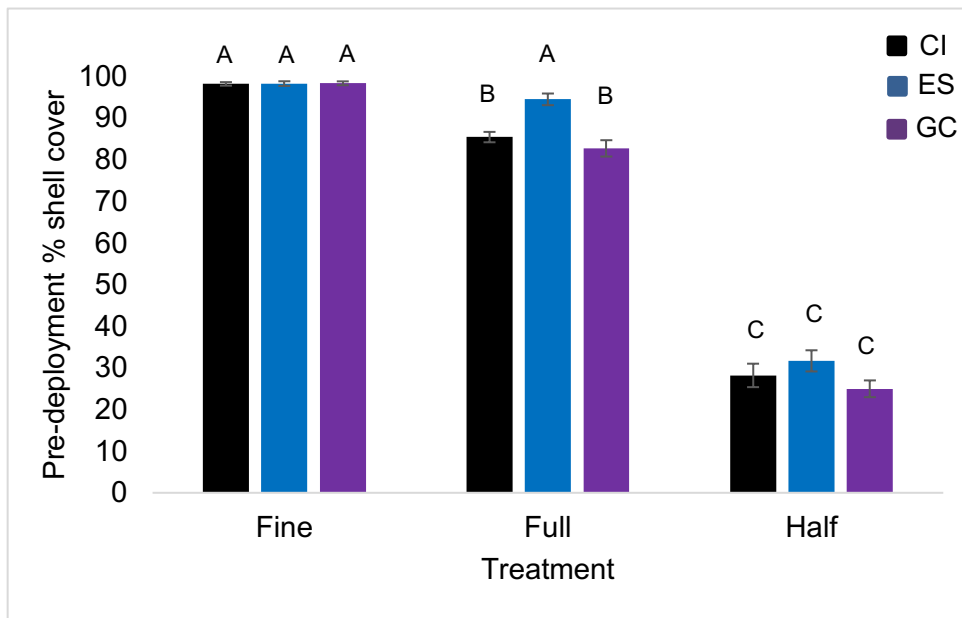


Figure A3. Top pre-deployment percent cover of shell on tiles deployed from May – September 2018 to CI, Newport Bay, ES, San Diego Bay, and GC, San Diego Bay, CA, USA as a function of site, tidal elevation, and treatment (black = CI, Newport Bay, blue = ES, San Diego Bay, purple = GC, San Diego Bay). Error bars = 1 SE. Different letters above bars indicate statistically significant differences based upon post-hoc Tukey HSD tests.

Table A4. Three-way ANOVA test statistics for effects of site, tidal elevation, and treatment on pre-deployment percent cover of shell on the bottom of tiles deployed from May – September 2018 to CI, Newport Bay, ES, San Diego Bay, and GC, San Diego Bay, CA, USA. Bold indicates significant difference.

Source	Nparm	DF	Sum of Squares	F Ratio	Prob > F
Site	2	2	74.412	0.7354	0.4817
Tidal elevation	1	1	12.845	0.2539	0.6154
Site*Tidal elevation	2	2	108.920	1.0764	0.3444
Treatment	2	2	80273.756	793.3212	<0.0001*
Site*Treatment	4	4	614.846	3.0382	0.0204*
Tidal elevation*Treatment	2	2	81.581	0.8062	0.4492
Site*Tidal elevation*Treatment	4	4	214.078	1.0578	0.3811

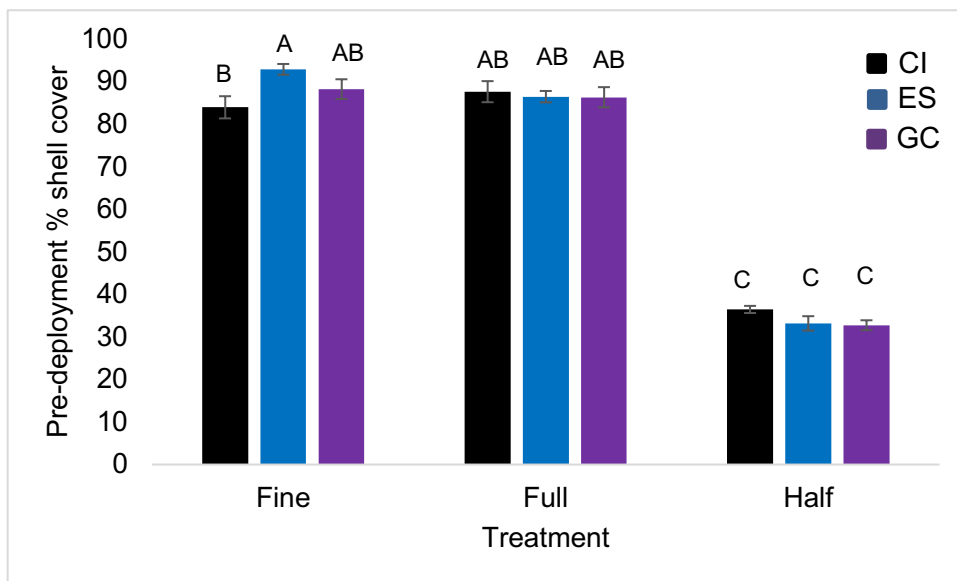


Figure A4. Bottom pre-deployment percent cover of shell on tiles deployed from May – September 2018 to CI, Newport Bay, ES, San Diego Bay, and GC, San Diego Bay, CA, USA as a function of site, tidal elevation, and treatment (black = CI, Newport Bay, blue = ES, San Diego Bay, purple = GC, San Diego Bay). Error bars = 1 SE. Different letters above bars indicate statistically significant differences based upon post-hoc Tukey HSD tests.

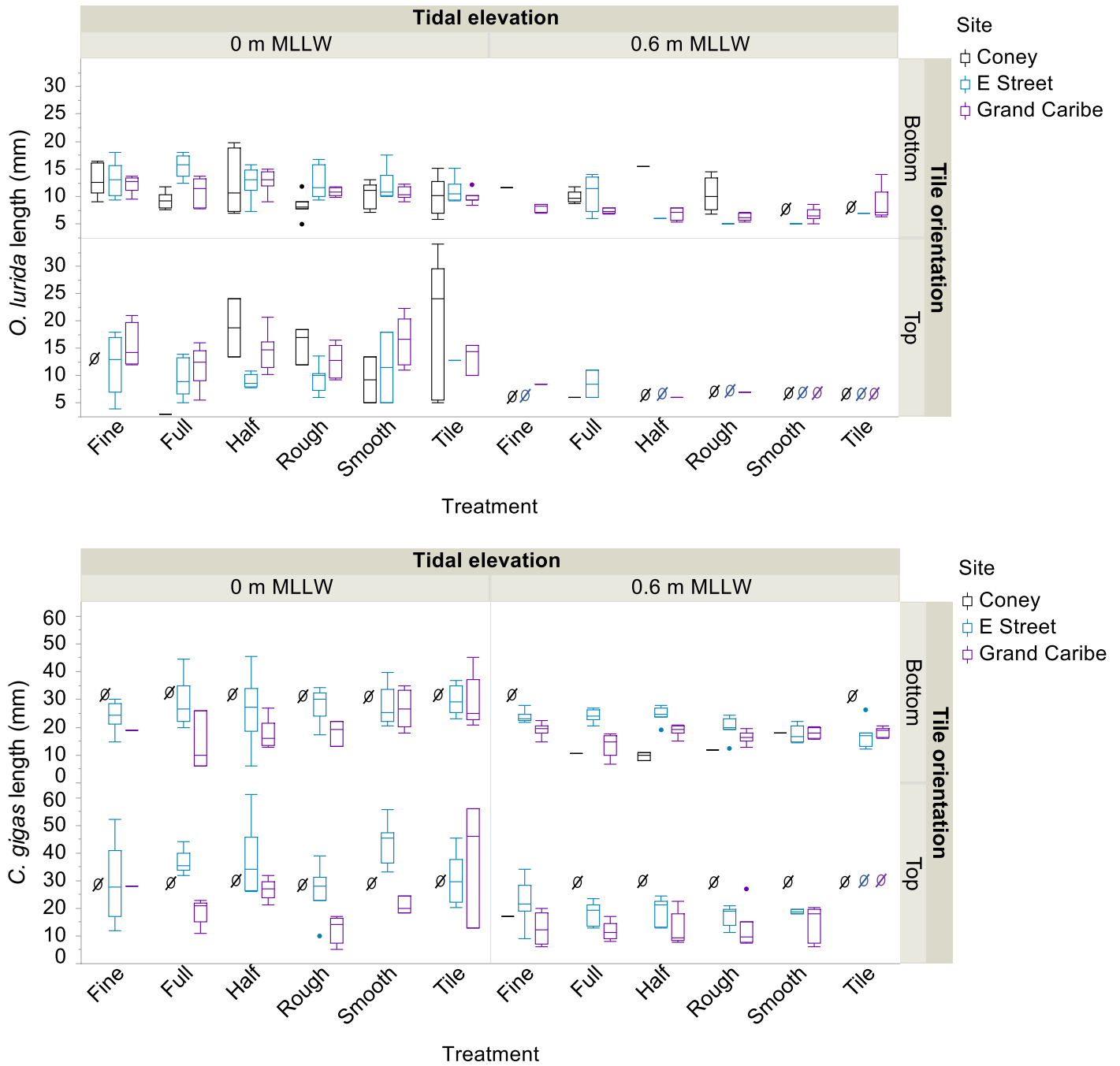


Figure A5. Length of *O. lurida* (top) and *C. gigas* (bottom) on tiles deployed from May – September 2018 to Newport and San Diego Bays, CA, USA as a function of site, tidal elevation, tile orientation, and treatment (black = CI, Newport Bay, blue = ES, San Diego Bay, purple = GC, San Diego Bay). The boxplot displays the median and upper and lower quartile range, the whiskers show the maximum and maximum of the dataset, and the dots represent outliers. Zero with a slash from right to left = no oysters.

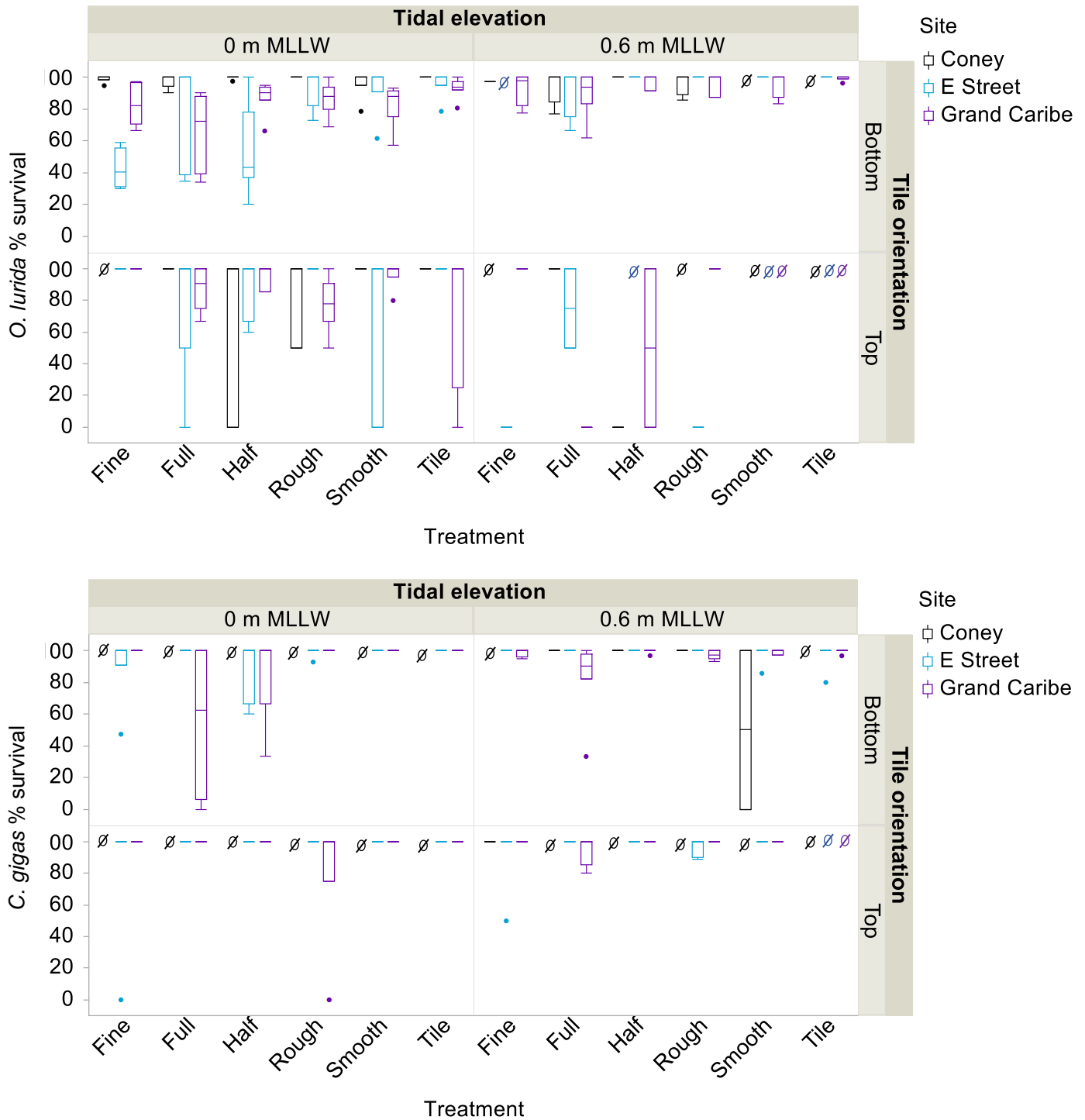


Figure A6. Percent survival of *O. lurida* and *C. gigas* on tiles deployed from May – September 2018 to Newport and San Diego Bays, CA, USA as a function of site, tidal elevation, tile orientation, and treatment (black = CI, Newport Bay, blue = ES, San Diego Bay, purple = GC, San Diego Bay). Zero with a slash from right to left = no data. The boxplot displays the median and upper and lower quartile range, the whiskers show the maximum and maximum of the dataset, and the dots represent outliers.

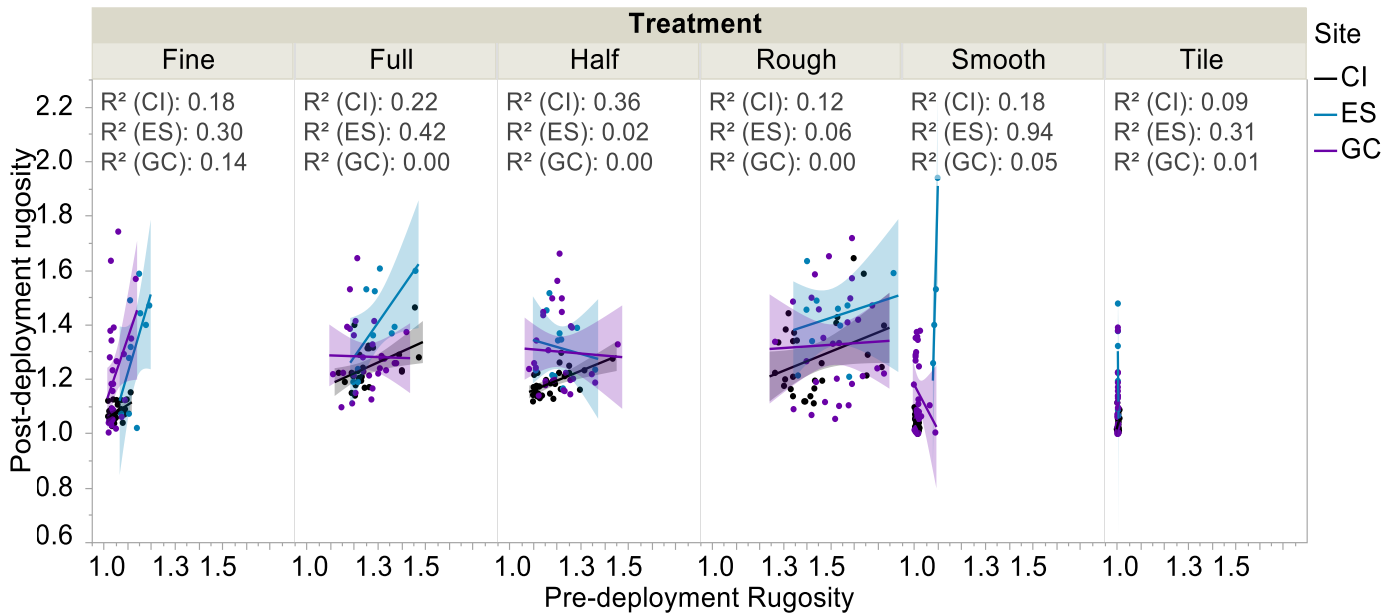


Figure A7. Correlation between pre-deployment rugosity and post-deployment rugosity on tiles deployed from May – September 2018 to Newport and San Diego Bays, CA, USA as a function of site, tidal elevation, and treatment (black = CI, Newport Bay, blue = ES, San Diego Bay, purple = GC, San Diego Bay). Shaded regions represent confidence fit.

Table A5. Non-comprehensive literature review of biomass methods across different algae and fauna.

Citation	Study organism	Rinse	Temperature	Time	Notes
Aikins and Kikuchi, 2001	Three species of macroalgae	Freshwater	Unknown	Unknown	
Bell and Hall 1997	Three seagrass species	Not specific	60°C	24 hours	
Birch et al., 1981	Algae (<i>Cladophora</i>)	Freshwater	70°C	Unknown	
Bishop and Kelher, 2013	Detritus	Unknown	60°C	Dried to consistent weight	
Bullivant 1968	Zoobotryon (<i>Amathia verticillate</i>)	Deionized water	Hotplate at 55 °C	~12 hours (overnight)	
Burkholder and Almodovar, 1974	Mixed algae from mangrove roots	Unknown	100°C	Unknown	
Chock and Mathieson, 1982	Spartina and other intertidal seaweeds	Freshwater	105°C	24 hours	
Congdon and McComb, 1981	<i>Zostrea</i> , seasonal distribution of macroscopic algae and benthic angiosperms	Unknown	80°C	72 hours	

Citation	Study organism	Rinse	Temperature	Time	Notes
Copertino et al., 2009	Turf algae	Not specific	60°C	48 hours	
Fong et al., 1998	<i>Enteromorpha intestinalis</i>	Rinsed in estuary water to get mud and large inverts off; briefly rinsed in freshwater before going in oven	Unknown	~24 hours (or until constant weight)	Spun in salad spinner to get uniform wet weight
Gubelit and Berezina, 2010	Filamentous algae, drift algae	Freshwater	Unknown	Dried to consistent weight	
Hauxwell et al., 1998	Macroalga <i>Cladophora vagabunda</i>	Unknown	60°C	Unknown	Initial algal wet weights were converted to dry weights using a conversion factor (2.5) determined from differences between final wet and dry measurements
Hernandez et al., 1997	Ulva and other green algae	Tap water	60°C	Unknown	
Kamer and Fong, 2000	<i>Enteromorpha intestinalis</i>	Deionized water	60°C	Dried to consistent weight	Spun in salad spinner to remove water
Pederson and Peterson 2001	Bryozoans (at least two species)	Freshwater; not specific	60°C	24 hours	Used method in Bell and Hall 1997
Rodriguez and Stoner, 1990	Multiple macroalgae species	Unknown	70-80°C	Dried to consistent weight	Separated algal species and dried them separately
Twilley et al., 1985	Mixed algae from saltwater pond	Rinsed in estuary water to remove epiphytic material, sorted by species	60°C	Dried to consistent weight	

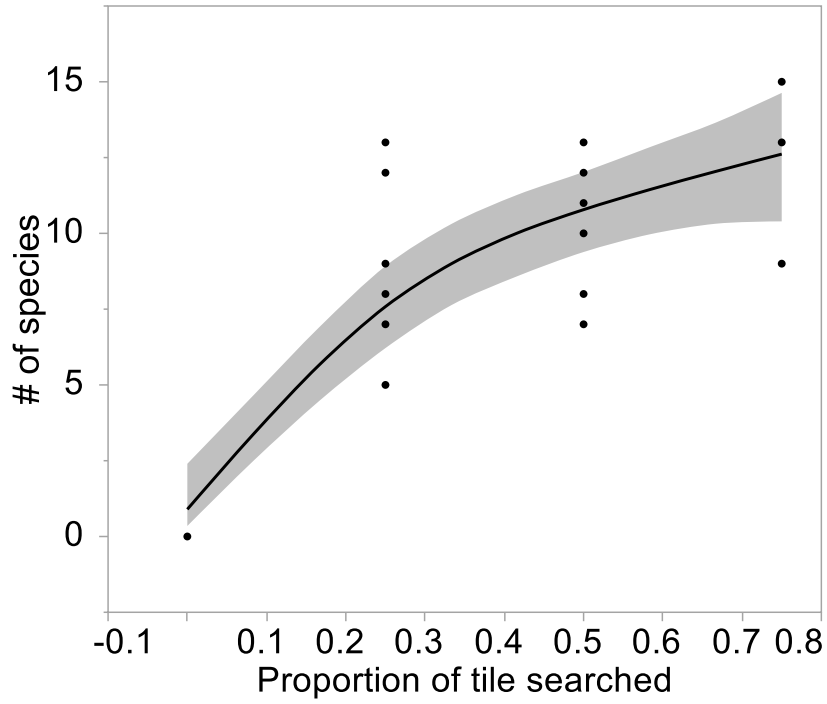


Figure A8. Species area curve exploring the effect of proportion of tile searched on number of species found on Smooth at 0 m MLLW deployed from May – September 2018 to ES, San Diego Bay, CA, USA. Shaded regions represent 95% confidence fit. Line is cubic spline (fits a polynomial line piecewise), lambda = 1.3.

Tidal elevation		0 m MLLW															0.6 m MLLW																										
Site		Coney					E Street					Grand Caribe					Coney					E Street					Grand Caribe																
Treatment		Fi	Fu	H	R	S	T	Fi	Fu	H	R	S	T	Fi	Fu	H	R	S	T	Fi	Fu	H	R	S	T	Fi	Fu	H	R	S	T	Fi	Fu	H	R	S	T	Fi	Fu	H	R	S	T
Algae	Other																																										
Folliculinidae																																											
Animal tube	Unknown																																										
Eggs, other																																											

*All bryozoan identifications are by Megan McCuller via photographs and her notes on identification follow. Bryozoan morphotype A = Candidae or Pomocellaria, but scutum shape was unclear and no ovicells were seen. Bryozoan morphotype B = Cyclostomata, likely *Diaperoforma californica*, but cyclostomes were difficult to identify with small pieces missing brood chambers and oeciostomes. Bryozoan morphotype C = Microporella. Bryozoan morphotype D = Candidae or Aspiscellaria; ovicells were porous, proximal-most spine appeared cervicorn, but was unable to tell scutum shape.

***Ciona sp.* = *Ciona savignyi* or *Ciona robusta*. Both are introduced species to southern California but were indistinguishable after preservation in formalin. Tunicate morphotype A = *Diplosoma listerianum*, *Didemnum vexillum*, or *Symplegma reptans*. Tunicate morphotype B = *Styela canopus* and *Styela clava*. May include some *Molgula ficus* and *Microcosmus squamiger*. Tunicates were very small specimen (< 3 mm). All are introduced species to southern California.

Table A7. Pairwise PERMANOVA test statistics for effects of site, tidal elevation, and treatment on overall community composition on tiles deployed from May – September 2018 to ES, San Diego Bay, GC, San Diego Bay, and CI, Newport Bay, CA, USA. Bold indicates significant difference.

		Overall Community Composition					
		ES		GC		CI	
Treatment 1	Treatment 2	0 m MLLW	0.6 m MLLW	0 m MLLW	0.6 m MLLW	0 m MLLW	0.6 m MLLW
Fine	Half	ns	0.0203	0.0068	ns	0.0316	ns
Fine	Full	ns	ns	ns	0.0013	0.0105	0.0038
Fine	Smooth	ns	ns	0.003	ns	0.005	0.0006
Fine	Rough	0.0028	ns	0.0432	0.0083	0.0117	ns
Fine	Tile	ns	0.0279	0.0082	0.0362	0.0015	0.001
Half	Full	ns	ns	0.019	ns	ns	0.001
Half	Smooth	ns	ns	0.0027	ns	ns	0.0184
Half	Rough	0.0174	ns	ns	ns	ns	ns
Half	Tile	0.0023	ns	0.0241	ns	0.0015	0.0025
Full	Smooth	ns	ns	0.0038	0.0152	0.0049	0.0002
Full	Rough	0.0039	ns	ns	0.0125	0.0068	0.0005
Full	Tile	ns	0.0449	0.0055	0.0028	0.0011	0.0008
Smooth	Rough	0.0043	ns	ns	ns	ns	0.0015
Smooth	Tile	0.0155	ns	ns	ns	ns	ns
Rough	Tile	0.0016	ns	ns	0.0119	0.0219	0.0005

Table A8. Pairwise PERMANOVA test statistics for effects of site, tidal elevation, and treatment on native community composition on tiles deployed from May – September 2018 to ES, San Diego Bay, GC, San Diego Bay, and CI, Newport Bay, CA, USA. Bold indicates significant difference.

		Native Community Composition					
		ES		GC		CI	
Treatment 1	Treatment 2	0 m MLLW	0.6 m MLLW	0 m MLLW	0.6 m MLLW	0 m MLLW	0.6 m MLLW
Fine	Half	ns	ns	0.0055	ns	0.0477	ns
Fine	Full	ns	ns	ns	ns	ns	ns
Fine	Smooth	ns	ns	0.0215	ns	ns	ns
Fine	Rough	0.0443	ns	ns	ns	ns	ns
Fine	Tile	ns	ns	0.0243	ns	0.0035	ns
Half	Full	ns	ns	0.0475	ns	ns	0.0215
Half	Smooth	ns	ns	ns	ns	ns	ns
Half	Rough	ns	ns	ns	ns	ns	ns
Half	Tile	0.016	ns	0.066	ns	0.0038	ns
Full	Smooth	ns	ns	ns	ns	ns	0.0006
Full	Rough	ns	ns	ns	ns	ns	ns
Full	Tile	ns	ns	ns	ns	0.0041	0.0007
Smooth	Rough	ns	ns	ns	ns	ns	ns
Smooth	Tile	ns	ns	ns	ns	ns	ns
Rough	Tile	0.0009	ns	ns	ns	0.0081	ns

Table A9. Pairwise PERMANOVA test statistics for effects of site, tidal elevation, and treatment on non-indigenous community composition on tiles deployed from May – September 2018 to ES, San Diego Bay, GC, San Diego Bay, and CI, Newport Bay, CA, USA. Bold indicates significant difference.

		Non-indigenous Community Composition					
		ES		GC		CI	
Treatment 1	Treatment 2	0 m MLLW	0.6 m MLLW	0 m MLLW	0.6 m MLLW	0 m MLLW	0.6 m MLLW
Fine	Half	ns	0.022	ns	ns	ns	ns
Fine	Full	ns	ns	ns	0.0112	0.034	0.0233
Fine	Smooth	ns	0.0214	ns	ns	0.0183	ns
Fine	Rough	ns	ns	ns	0.0341	0.0108	ns
Fine	Tile	ns	ns	ns	ns	0.003	ns
Half	Full	ns	ns	ns	ns	ns	0.0017
Half	Smooth	ns	ns	0.033	ns	ns	ns
Half	Rough	ns	ns	ns	ns	ns	ns
Half	Tile	ns	ns	ns	ns	ns	ns
Full	Smooth	ns	ns	ns	ns	0.0463	0.0016
Full	Rough	0.0036	ns	ns	0.0061	ns	0.0085
Full	Tile	0.0296	ns	0.0151	0.0037	0.0119	0.0008
Smooth	Rough	ns	ns	ns	ns	ns	ns
Smooth	Tile	0.0051	ns	ns	ns	ns	ns
Rough	Tile	0.0033	ns	ns	0.0123	ns	ns

Table A10. Species found in soft-body samples deployed from May – September 2018 to ES, San Diego Bay, GC, San Diego Bay, and CI, Newport Bay, CA, USA.

Species/morphotype	Provenance
<i>Ascidia ceratodes</i>	Native
<i>Ciona sp.</i>	Non-indigenous
<i>Molgula ficus</i>	Non-indigenous
<i>Polyandrocarpa zorritensis</i>	Non-indigenous
<i>Styela canopus</i>	Non-indigenous
<i>Styela clava</i>	Non-indigenous
<i>Styela plicata</i>	Non-indigenous
<i>Perophora sp.</i>	Cryptogenic
Sea anemone	Cryptogenic

Table A11. Number of tunicates on tiles from each site, tidal elevation, tile orientation, and treatment deployed from May – September 2018 to ES, San Diego Bay, GC, San Diego Bay, and CI, Newport Bay, CA, USA.

Site	Tidal elevation	Tile orientation	Fine	Full	Half	Rough	Smooth	Tile	Grand total
ES	0 m MLLW	Bottom	52	84	60	32	24	1	253
		Top	3	2	0	1	0	0	6
	0.6 m MLLW	Bottom	22	95	5	12	9	0	143
		Top	0	0	0	0	0	0	0
GC	0 m MLLW	Bottom	239	761	7	46	7	0	1060
		Top	3	6	2	5	9	21	46
	0.6 m MLLW	Bottom	8	13	16	1	1	3	42
		Top	0	0	0	0	0	0	0
CI	0 m MLLW	Bottom	101	33	91	37	3	5	270
		Top	3	1	1	0	0	0	5
	0.6 m MLLW	Bottom	0	0	0	0	0	0	0
		Top	0	0	0	0	0	0	0

Table A12. Pairwise PERMANOVA test statistics for effects of site, tidal elevation, and treatment on overall tunicate abundance from tiles deployed from May – September 2018 to ES, San Diego Bay, GC, San Diego Bay, and CI, Newport Bay, CA, USA. Bold indicates significant difference. ID = insufficient data for comparisons, ns = non-significant ($p > 0.05$).

Treatment 1	Treatment 2	Tunicate abundance					
		ES		GC		CI	
		0 m MLLW	0.6 m MLLW	0 m MLLW	0.6 m MLLW	0 m MLLW	0.6 m MLLW
Fine	Half	ns	0.0203	0.0047	ns	ns	ID
Fine	Full	ns	0.0109	ns	ns	ns	ID
Fine	Smooth	ns	0.0389	0.0027	ns	0.0035	ID
Fine	Rough	ns	ns	ns	ns	0.0184	ID
Fine	Tile	0.022	0.0008	0.0005	ns	0.0053	ID
Half	Full	ns	0.0006	0.0062	ns	ns	ID
Half	Smooth	ns	ns	ns	ns	ns	ID
Half	Rough	ns	ns	ns	ns	ns	ID
Half	Tile	0.0095	ns	ns	ns	ns	ID
Full	Smooth	ns	0.0035	0.0031	0.0140	0.0068	ID
Full	Rough	ns	0.0019	ns	0.0205	0.0195	ID
Full	Tile	0.0009	0.0008	0.0007	0.0353	0.007	ID
Smooth	Rough	ns	ns	ns	ns	ns	ID
Smooth	Tile	0.0198	ns	ns	ns	ns	ID
Rough	Tile	0.0052	ns	0.0039	ns	ns	ID

Table A13. Number of tiles with biomass from each site, tidal elevation, and treatment deployed from May – September 2018 to ES, San Diego Bay, GC, San Diego Bay, and CI, Newport Bay, CA, USA.

Site	Tidal elevation	Fine	Full	Half	Rough	Smooth	Tile
ES	0 m MLLW	0	2	1	0	2	0
	0.6 m MLLW	6	3	7	6	2	1
GC	0 m MLLW	5	3	6	6	3	2
	0.6 m MLLW	3	6	5	6	3	0
CI	0 m MLLW	7	7	7	7	7	6
	0.6 m MLLW	2	2	2	1	0	1

Table A14. Species found in biomass samples from tiles deployed from May – September 2018 to ES, San Diego Bay, GC, San Diego Bay, and CI, Newport Bay, CA, USA.

Species/morphotype	Provenance
<i>Thalamoporella californica</i>	Native
<i>Amathia verticillata</i>	Non-indigenous
<i>Botuloides schlosseri</i>	Non-indigenous
<i>Bugula neritina</i>	Non-indigenous
Algae	Cryptogenic
Bryozoan sp. A	Cryptogenic

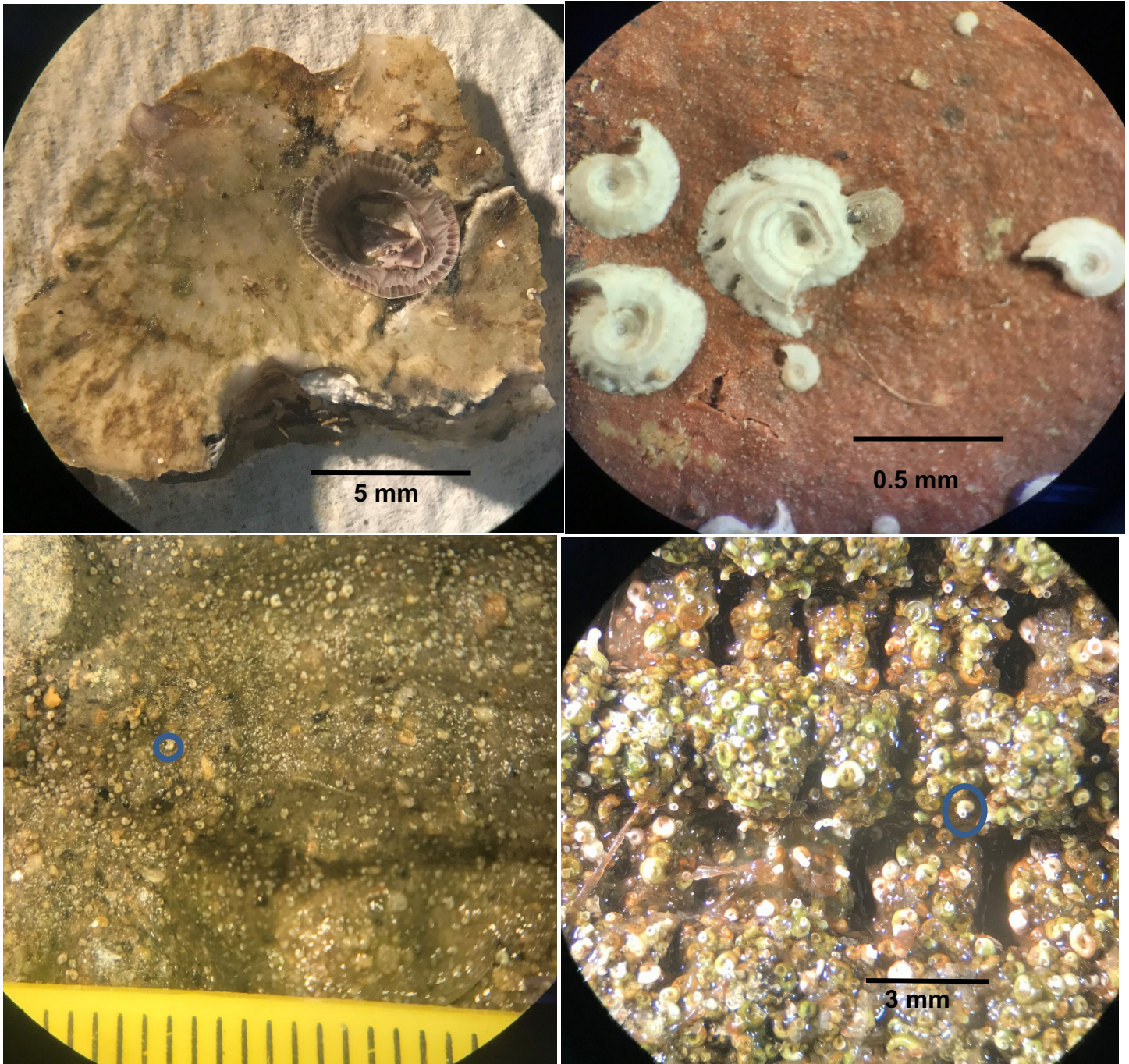


Figure A9. Micro-rugosity provided by species that recruited to tiles deployed to ES, San Diego Bay and CI, Newport Bay, CA, USA from May – September 2018. Top left: Underside of *Crassostrea gigas* that overgrew *Amphibalanus amphitrite* on Tile treatment at ES. Top right: *O. lurida* settling in the crevice of a spirorbid worm settler on a terracotta settlement tile deployed to 0 m MLLW at CI. Bottom left: Microscopic spirorbid worms that recruited to the bottom of tiles at 0.6 m MLLW at CI. Tile treatment shown is Rough; one spirorbid worm circled in blue. Bottom right: Micro-rugosity provided by spirorbid worms on tiles deployed to 0 m MLLW at CI. Tile treatment shown is Rough; one spirorbid worm circled in blue.

REFERENCES

- Aguilera, M. A. (2018). Artificial defences in coastal marine ecosystems in Chile: Opportunities for spatial planning to mitigate habitat loss and alteration of the marine community structure. *Ecological Engineering*, 120, 601–610. <https://doi.org/10.1016/j.ecoleng.2017.04.021>
- Aikins, S., & Kikuchi, E. (2011). Studies on habitat selection by amphipods using artificial substrates within an estuarine environment. *Hydrobiologia*, 457(1), 77–86. <https://doi.org/10.1023/A:1012261116232>
- Airoldi, L., & Bulleri, F. (2011). Anthropogenic disturbance can determine the magnitude of opportunistic species responses on marine urban infrastructures. *PLoS ONE*, 6(8), e22985. <https://doi.org/10.1371/journal.pone.0022985>
- Airoldi, L., Turon, X., Perkol-Finkel, S., & Rius, M. (2015). Corridors for aliens but not for natives: Effects of marine urban sprawl at a regional scale. *Diversity and Distributions*, 21(7), 755–768. <https://doi.org/10.1111/ddi.12301>
- Anderson, M. J., & Underwood, A. J. (1994). Effects of substratum on the recruitment and development of an intertidal estuarine fouling assemblage. *Journal of Experimental Marine Biology and Ecology*, 184(2), 217–236. [https://doi.org/10.1016/0022-0981\(94\)90006-X](https://doi.org/10.1016/0022-0981(94)90006-X)
- Bailey, S. A., Duggan, I. C., & Jenkins, P. T. (2005). Invertebrate resting stages in residual ballast sediment of transoceanic ships. *Canadian Journal of Fisheries and Aquatic Sciences*, 62(5), 1090–1103. <https://doi.org/10.1139/f05-024>
- Barnes, B. B., Luckenbach, M. W., & Kingsley-Smith, P. R. (2010). Oyster reef community interactions: The effect of resident fauna on oyster (*Crassostrea spp.*) larval recruitment. *Journal of Experimental Marine Biology and Ecology*, 391(1–2), 169–177. <https://doi.org/10.1016/j.jembe.2010.06.026>
- Barrett, E. M. (1963). *The California oyster industry* California Department of Fish and Game, Fisheries Bulletin 123, 1-103.
- Beck, M. W., Brumbaugh, R. D., Airoldi, L., Carranza, A., Coen, L. D., Crawford, C., Defeo, O., Edgar, G. J., Hancock, B., Kay, M. C., Lenihan, H. S., Luckenbach, M. W., Toropova, C. L., Zhang, G., & Guo, X. (2011). Oyster reefs at risk and recommendations for conservation, restoration, and management. *BioScience*, 61(2), 107–116. <https://doi.org/10.1525/bio.2011.61.2.5>
- Bell, J. J. (2005). Influence of occupant microhabitat on the composition of encrusting communities on gastropod shells. *Marine Biology*, 147(3), 653–661. <https://doi.org/10.1007/s00227-005-1587-8>
- Bell, S. S., & Hall, M. O. (1997). Drift macroalgal abundance in seagrass beds: Investigating large-scale associations with physical and biotic attributes. *Marine Ecology Progress Series*, 147, 277–283. <https://doi.org/doi.org/10.3354/meps147277>
- Berntsson, K. M., Jonsson, P. R., Lejhall, M., & Gatenholm, P. (2000). Analysis of behavioural rejection of micro-textured surfaces and implications for recruitment by the barnacle *Balanus improvisus*. *Journal of Experimental Marine Biology and Ecology*, 251(1), 59–83. [https://doi.org/10.1016/S0022-0981\(00\)00210-0](https://doi.org/10.1016/S0022-0981(00)00210-0)

- Birch, P., Gordon, D., & McComb, A. (1981). Nitrogen and phosphorus nutrition of *Cladophora* in the Peel-Harvey estuarine system, Western Australia. *Botanica Marina*, 24(7), 381–387. <https://doi.org/10.1515/botm.1981.24.7.381>
- Bishop, M. J., & Kelaher, B. P. (2013). Replacement of native seagrass with invasive algal detritus: Impacts to estuarine sediment communities. *Biological Invasions*, 15(1), 45–59. <https://doi.org/10.1007/s10530-012-0267-0>
- Bishop, M. J., & Peterson, C. H. (2006). Direct effects of physical stress can be counteracted by indirect benefits: Oyster growth on a tidal elevation gradient. *Oecologia*, 147(3), 426–433. <https://doi.org/10.1007/s00442-005-0273-3>
- Blum, J. C., Chang, A. L., Liljeström, M., Schenk, M. E., Steinberg, M. K., & Ruiz, G. M. (2007). The non-native solitary ascidian *Ciona intestinalis* (L.) depresses species richness. *Journal of Experimental Marine Biology and Ecology*, 342(1), 5–14. <https://doi.org/10.1016/j.jembe.2006.10.010>
- Bozek, C. M., & Burdick, D. M. (2005). Impacts of seawalls on saltmarsh plant communities in the Great Bay Estuary, New Hampshire USA. *Wetlands Ecology and Management*, 13(5), 553–568. <https://doi.org/10.1007/s11273-004-5543-z>
- Bonnot, P. (1935). The California oyster industry. *California Fish and Game*, 21(1), 65–80.
- Bracewell, S. A., Spencer, M., Marrs, R. H., Iles, M., & Robinson, L. A. (2012). Cleft, crevice, or the inner thigh: 'Another place' for the establishment of the invasive barnacle *Austrominius modestus* (Darwin, 1854). *PLOS ONE*, 7(11), e48863. <https://doi.org/10.1371/journal.pone.0048863>
- Bracewell, S. A., Robinson, L. A., Firth, L. B., & Knights, A. M. (2013). Predicting free-space occupancy on novel artificial structures by an invasive intertidal barnacle using a removal experiment. *PLOS ONE*, 8(9), e74457. <https://doi.org/10.1371/journal.pone.0074457>
- Buhle, E. R., & Ruesink, J. L. (2009). Impacts of invasive oyster drills on Olympia oyster (*Ostrea lurida* Carpenter 1864) recovery in Willapa Bay, Washington, United States. *Journal of Shellfish Research*, 28(1), 87–96. <https://doi.org/10.2983/035.028.0115>
- Bulleri, F., Russell, B. D., & Connell, S. D. (2012). Context-dependency in the effects of nutrient loading and consumers on the availability of space in marine rocky environments. *PLoS ONE*, 7(3), 9.
- Bullivant, J. S. (1968). The rate of feeding of the bryozoan, *Zoobotryon verticillatum*. *New Zealand Journal of Marine and Freshwater Research*, 2(1), 111–134. <https://doi.org/10.1080/00288330.1968.9515230>
- Burkholder, P. R., & Almodóvar, L. R. (1973). Studies on mangrove algal communities in Puerto Rico. *Florida Scientist* 36(1), 66–74.
- Burt, J., Bartholomew, A., & Sale, P. F. (2011). Benthic development on large-scale engineered reefs: A comparison of communities among breakwaters of different age and natural reefs. *Eco-engineering*, 37(2), 191–198. <https://doi.org/10.1016/j.ecoleng.2010.09.004>

- Carleton, J. H., & Sammarco, P. W. (1987). Effects of substratum irregularity on success of coral settlement: Quantification by comparative geomorphological techniques. *Bulletin of Marine Science*, 40(1), 85–98.
- CDFW (California Department of Fish and Wildlife) Office of Spill Prevention and Response & Marine Invasive Species Program. (2014). *Introduced aquatic species in California bays and harbors 2011 survey*. 36.
- Chapman, M. G., & Blockley, D. J. (2009). Engineering novel habitats on urban infrastructure to increase intertidal biodiversity. *Oecologia*, 161(3), 625–635. <https://doi.org/10.1007/s00442-009-1393-y>
- Chapman, J. W., & Carlton, J. T. (1991). A test of criteria for introduced species: The global invasion by the isopod *Synidotea laevidorsalis* (Miers, 1881). *Journal of Crustacean Biology*, 11(3), 386–400. <https://doi.org/10.2307/1548465>
- Chauvin, J. M. (2018). *Wave attenuation by constructed oyster reef breakwaters* (Publication No. 4752) [Master's thesis, Louisiana State University and Agricultural and Mechanical College]. LSU Digital Commons.
- Chock, J. S., & Mathieson, A. C. (1983). Variations of New England estuarine seaweed biomass. *Botanica Marina*, 26(2). <https://doi.org/10.1515/botm.1983.26.2.87>
- Chowdhury, M. S. N., Walles, B., Sharifuzzaman, S. M., Shahadat Hossain, M., Ysebaert, T., & Smaal, A. C. (2019). Oyster breakwater reefs promote adjacent mudflat stability and salt marsh growth in a monsoon dominated subtropical coast. *Scientific Reports*, 9(1), 8549. <https://doi.org/10.1038/s41598-019-44925-6>
- Coe, W. R. (1931). Sexual rhythm in the California oyster (*Ostrea lurida*). *Science, New Series*, 74(1914), 247–249.
- Cohen, A. N., Harris, L. H., Bingham, B. L., Carlton, J. T., Chapman, J. W., Lambert, C. C., Lambert, G., Ljubenkov, J. C., Murray, S. N., Rao, L. C., Reardon, K., & Schwindt, E. (2005). Rapid assessment survey for exotic organisms in southern California bays and harbors, and abundance in port and non-port areas. *Biological Invasions*, 7(6), 995–1002. <https://doi.org/10.1007/s10530-004-3121-1>
- Cohen, A., & Weinstein, A. (2008). Exotic oyster survey, removal and research in San Francisco Bay. *Annual Progress Report. San Francisco Estuary Institute, Oakland, CA*, 1-26.
- Coombes, M. A., Viles, H. A., Naylor, L. A., & La Marca, E. C. (2017). Cool barnacles: Do common biogenic structures enhance or retard rates of deterioration of intertidal rocks and concrete? *Science of The Total Environment*, 580, 1034–1045. <https://doi.org/10.1016/j.scitotenv.2016.12.058>
- Congdon, R. A., & McComb, A. J. (1981). The vegetation of the Blackwood River Estuary, south-west Australia. *The Journal of Ecology*, 69(1), 1–16. <https://doi.org/10.2307/2259812>
- Connell, S. D. (2001). Urban structures as marine habitats: An experimental comparison of the composition and abundance of subtidal epibiota among pilings, pontoons and rocky reefs. *Marine Environmental Research*, 52(2), 115–125. [https://doi.org/10.1016/S0141-1136\(00\)00266-X](https://doi.org/10.1016/S0141-1136(00)00266-X)

- Copertino, M. S., Cheshire, A., & Kildea, T. (2009). Photophysiology of a turf algal community: Integrated responses to ambient light and standing biomass. *Journal of Phycology*, 45(2), 324–336. <https://doi.org/10.1111/j.1529-8817.2009.00664.x>
- Crisp, D. J., & Barnes, H. (1954). The orientation and distribution of barnacles at settlement with particular reference to surface contour. *The Journal of Animal Ecology*, 23(1), 142. <https://doi.org/10.2307/1664>
- Crooks, J. A., Crooks, K. R., & Crooks, A. J. (2015). Observations of the non-native Pacific oyster (*Crassostrea gigas*) in San Diego County, California. *California Department of Fish and Game*, 101, 101–107.
- Dean, T. A. (1981). Structural aspects of sessile invertebrates as organizing forces in an estuarine fouling community. *Journal of Experimental Marine Biology and Ecology*, 53(2), 163–180. [https://doi.org/10.1016/0022-0981\(81\)90017-4](https://doi.org/10.1016/0022-0981(81)90017-4)
- Dennis, H. D., Evans, A. J., Banner, A. J., & Moore, P. J. (2018). Reefcrete: Reducing the environmental footprint of concretes for eco-engineering marine structures. *Eco-engineering*, 120, 668–678. <https://doi.org/10.1016/j.ecoleng.2017.05.031>
- Diederich, S. (2005). Differential recruitment of introduced Pacific oysters and native mussels at the North Sea coast: Coexistence possible? *Journal of Sea Research*, 53(4), 269–281. <https://doi.org/10.1016/j.seares.2005.01.002>
- Dimick, R. E., Eglund, G., & Long, J. B. (1941). Native oyster investigations of Yaquina Bay, Oregon: progress report II, covering the period July 4, 1939 to September 30, 1941. *The Fish Commission of the State of Oregon*.
- Dittel, A., Epifanio, C. E., & Natunewicz, C. (1996). Predation on mud crab megalopae, *Panopeus herbstii* H. Milne Edwards: Effect of habitat complexity, predator species and postlarval densities. *Journal of Experimental Marine Biology and Ecology*, 198(2), 191–202. [https://doi.org/10.1016/0022-0981\(96\)00003-2](https://doi.org/10.1016/0022-0981(96)00003-2)
- Dubois, S., Commito, J. A., Olivier, F., & Retière, C. (2006). Effects of epibionts on *Sabellaria alveolata* (L.) biogenic reefs and their associated fauna in the Bay of Mont Saint-Michel. *Estuarine, Coastal and Shelf Science*, 68(3), 635–646. <https://doi.org/10.1016/j.ecss.2006.03.010>
- Ellis, J. I., Clark, D., Atalah, J., Jiang, W., Taiapa, C., Patterson, M., Sinner, J., & Hewitt, J. (2017). Multiple stressor effects on marine infauna: Responses of estuarine taxa and functional traits to sedimentation, nutrient and metal loading. *Scientific Reports*, 7(1), 12013. <https://doi.org/10.1038/s41598-017-12323-5>
- Eschweiler, N., & Christensen, H. T. (2011). Trade-off between increased survival and reduced growth for blue mussels living on Pacific oyster reefs. *Journal of Experimental Marine Biology and Ecology*, 403(1), 90–95. <https://doi.org/10.1016/j.jembe.2011.04.010>
- Firth, L. B., Browne, K. A., Knights, A. M., Hawkins, S. J., & Nash, R. (2016). Eco-engineered rock pools: A concrete solution to biodiversity loss and urban sprawl in the marine environment. *Environmental Research Letters*, 11(9), 094015. <https://doi.org/10.1088/1748-9326/11/9/094015>

- Floerl, O., Pool, T. K., & Inglis, G. J. (2004). Positive interactions between nonindigenous species facilitate transport by human vectors. *Ecological Applications*, 14(6), 1724–1736. <https://doi.org/10.1890/03-5399>
- Fofonoff, P. W., Ruiz, G. M., Steves, B., Simkanin, C., & Carlton, J. T. (2018). *NEMESIS Database Species Summary*. National Exotic Marine and Estuarine Species Information System. <http://invasions.si.edu/nemesis/>
- Fong, P., Boyer, K. E., & Zedler, J. B. (1998). Developing an indicator of nutrient enrichment in coastal estuaries and lagoons using tissue nitrogen content of the opportunistic alga, *Enteromorpha intestinalis* (L. Link). *Journal of Experimental Marine Biology and Ecology*, 231(1), 63–79. [https://doi.org/10.1016/S0022-0981\(98\)00085-9](https://doi.org/10.1016/S0022-0981(98)00085-9)
- Foster, M. S., Nigg, E. W., Kiguchi, L. M., Hardin, D. D., & Pearse, J. S. (2003). Temporal variation and succession in an algal-dominated high intertidal assemblage. *Journal of Experimental Marine Biology and Ecology*, 289(1), 15–39. [https://doi.org/10.1016/S0022-0981\(03\)00035-2](https://doi.org/10.1016/S0022-0981(03)00035-2)
- Fuentes, C. M., Whitcraft, C. R., & Zacherl, D. C. (2020). Adaptive restoration reveals potential effect of tidal elevation on oyster restoration outcomes. *Wetlands*, 40(1), 93–99. <https://doi.org/10.1007/s13157-019-01166-7>
- Gilbert, C. H. (1889). Report on certain investigations regarding the planting of oysters in southern California; Alamitos Bay and Newport Bay, California. *US Fish Comm. Bull*, 9, 95–97.
- Gittman, R. K., Fodrie, F. J., Popowich, A. M., Keller, D. A., Bruno, J. F., Currin, C. A., Peterson, C. H., & Piehler, M. F. (2015). Engineering away our natural defenses: An analysis of shoreline hardening in the US. *Frontiers in Ecology and the Environment*, 13(6), 301–307. <https://doi.org/10.1890/150065>
- Glasby, T. M., Connell, S. D., Holloway, M. G., & Hewitt, C. L. (2007). Nonindigenous biota on artificial structures: Could habitat creation facilitate biological invasions? *Marine Biology*, 151(3), 887–895. <https://doi.org/10.1007/s00227-006-0552-5>
- Green, D. S., & Crowe, T. P. (2013). Physical and biological effects of introduced oysters on biodiversity in an intertidal boulder field. *Marine Ecology Progress Series*, 482, 119–132. <https://doi.org/10.3354/meps10241>
- Green, D. S., & Crowe, T. P. (2014). Context- and density-dependent effects of introduced oysters on biodiversity. *Biological Invasions*, 16(5), 1145–1163. <https://doi.org/10.1007/s10530-013-0569-x>
- Griggs, G. B. (2009). The effects of armoring shorelines—The California experience. In *Puget Sound Shorelines and the Impacts of Armoring—Proceedings of a State of the Science Workshop*, 77-84.
- Griggs, G., & Patsch, K. (2019). The protection/hardening of California’s coast: Times are changing. *Journal of Coastal Research*, 35(5), 1051–1061. <https://doi.org/10.2112/JCOASTRES-D-19A-00007.1>
- Groth, S. (2010). Memorandum. *Oregon Department of Fish and Wildlife Marine Resources Program*, 8.

- Gubelit, Y. I., & Berezina, N. A. (2010). The causes and consequences of algal blooms: The *Cladophora glomerata* bloom and the Neva estuary (eastern Baltic Sea). *Marine Pollution Bulletin*, 61(4–6), 183–188. <https://doi.org/10.1016/j.marpolbul.2010.02.013>
- Guy, C., Blight, A., Smyth, D., & Roberts, D. (2018). The world is their oyster: Differences in epibiota on sympatric populations of native *Ostrea edulis* and non-native *Crassostrea gigas* (*Magallana gigas*) oysters. *Journal of Sea Research*, 140, 52–58. <https://doi.org/10.1016/j.seares.2018.07.002>
- Hanlon, N., Firth, L. B., & Knights, A. M. (2018). Time-dependent effects of orientation, heterogeneity and composition determines benthic biological community recruitment patterns on subtidal artificial structures. *Eco-engineering*, 122, 219–228. <https://doi.org/10.1016/j.ecoleng.2018.08.013>
- Hauxwell, J., McClelland, J., Behr, P. J., & Valiela, I. (1998). Relative importance of grazing and nutrient controls of macroalgal biomass in three temperate shallow estuaries. *Estuaries*, 21(2), 347. <https://doi.org/10.2307/1352481>
- Henderson, H., Garrity, N., & Zacherl, D. (2015). *San Diego Bay native oyster restoration plan*. 152. Technical report.
- Henderson, H., Garrity, N., & Zacherl, D. (2018). *San Diego Bay native oyster restoration project basis of design*. 61. Unpublished technical report.
- Hernandez, I., Peralta, G., Perez-Llorens, J. L., & Niell, F. X. (1998). Biomass and dynamics of growth of *Ulva* species in Palmones River estuary. *Oceanographic Literature Review*, 3(45), 522–523. <https://doi.org/doi.org/10.1111/j.0022-3646.1997.00764.x>
- Hill, J. M., & Weissburg, M. J. (2013). Habitat complexity and predator size mediate interactions between intraguild blue crab predators and mud crab prey in oyster reefs. *Marine Ecology Progress Series*, 488, 209–219. <https://doi.org/10.3354/meps10386>
- Hittell, J. S. (1882). *The commerce and industries of the Pacific coast of North America*. AL Bancroft & Company.
- Holliday, J. E. (1996). Effects of surface orientation and slurry coating on settlement of Sydney rock, *Saccostrea commercialis*, oysters on PVC slats in a hatchery. *Aquacultural Engineering*, 15(3), 159–168. [https://doi.org/10.1016/0144-8609\(95\)00012-7](https://doi.org/10.1016/0144-8609(95)00012-7)
- Hopkins, A. E. (1935). Attachment of larvae of the Olympia oyster, *Ostrea lurida*, to plane surfaces. *Ecology*, 16(1), 82–87. <https://doi.org/10.2307/1932859>
- Jones, C. G., Lawton, J. H., & Shachak, M. (1994). Organisms as ecosystem engineers. *Oikos*, 69(3), 373–386.
- Kamer, K., & Fong, P. (2000). A fluctuating salinity regime mitigates the negative effects of reduced salinity on the estuarine macroalga, *Enteromorpha intestinalis* (L.) link. *Journal of Experimental Marine Biology and Ecology*, 254(1), 53–69. [https://doi.org/10.1016/S0022-0981\(00\)00262-8](https://doi.org/10.1016/S0022-0981(00)00262-8)
- Keller, R. P., Drake, J. M., Drew, M. B., & Lodge, D. M. (2011). Linking environmental conditions and ship movements to estimate invasive species transport across the global shipping network. *Diversity and Distributions*, 17(1), 93–102. <https://doi.org/10.1111/j.1472-4642.2010.00696.x>

- Kerckhof, F., Norro, A., Jacques, T., & Degraer, S. (2009). "Early colonisation of a concrete offshore windmill foundation by marine biofouling on the Thornton Bank (southern North Sea)" in S. Degraer & R. Brabant (Ed.). *Offshore wind farms in the Belgian part of the North Sea: State of the art after two years of environmental monitoring* (pp. 39–51). Royal Belgian Institute for Natural Sciences, Management Unit of the North Sea Mathematical Models.
- Knight-Jones, P., Knight-Jones, E. W., & Dales, R. P. (2009). Spirorbidae (Polychaeta Sedentaria) from Alaska to Panama. *Journal of Zoology*, 189(4), 419–458. <https://doi.org/10.1111/j.1469-7998.1979.tb03973.x>
- Kornbluth, A., Perog, B.D., Crippen, S., Zacherl., D.C., Quintana, B., & Wasson, K. (2021). [Mapping of oysters on the Pacific coast of North America: A coastwide collaboration to inform enhanced conservation.] Unpublished raw data.
- Kornis, M. S., Bilkovic, D. M., Davias, L. A., Giordano, S., & Breitburg, D. L. (2018). Shoreline hardening affects nekton biomass, size structure, and taxonomic diversity in nearshore waters, with responses mediated by functional species groups. *Estuaries and Coasts*, 41(S1), 159–179. <https://doi.org/10.1007/s12237-017-0214-5>
- Lai, S., Loke, L. H. L., Hilton, M. J., Bouma, T. J., & Todd, P. A. (2015). The effects of urbanisation on coastal habitats and the potential for ecological engineering: A Singapore case study. *Ocean & Coastal Management*, 103, 78–85. <https://doi.org/10.1016/j.ocecoaman.2014.11.006>
- Lambert, C. C., & Lambert, G. (1998). Non-indigenous ascidians in southern California harbors and marinas. *Marine Biology*, 130(4), 675–688. <https://doi.org/10.1007/s002270050289>
- Latta, M., & Boyer, K. (2015). *San Francisco Bay living shorelines: Nearshore linkages project summary of key findings two years post-installation* (pp. 1–38). Annual report.
- Leclerc, J.-C., Viard, F., Sepúlveda, E. G., Díaz, C., Hinojosa, J. N., Araneda, K. P., Silva, F., & Brante, A. (2020). Habitat type drives the distribution of non-indigenous species in fouling communities regardless of associated maritime traffic. *Diversity and Distributions*, 26(1), 62–75.
- Loke, L. H. L., Bouma, T. J., & Todd, P. A. (2017). The effects of manipulating microhabitat size and variability on tropical seawall biodiversity: Field and flume experiments. *Journal of Experimental Marine Biology and Ecology*, 492, 113–120. <https://doi.org/10.1016/j.jembe.2017.01.024>
- Light, S. F. (2007). *The Light and Smith manual: Intertidal invertebrates from central California to Oregon* (4th ed.). University of California Press. Liversage, K. (2017). First evidence of biogenic habitat from tubeworms providing a near-absolute habitat requirement for high-intertidal *Ulva* macroalgae. *PLOS ONE*, 12(5), e0176952. <https://doi.org/10.1371/journal.pone.0176952>
- Luckhurst, B. E., & Luckhurst, K. (1978). Analysis of the influence of substrate variables on coral reef fish communities. *Marine Biology*, 49(4), 317–323. <https://doi.org/10.1007/BF00455026>
- MacKenzie, C. L. (1997). The history, present condition, and future of the molluscan fisheries of North and Central America and Europe. Volume 1: Atlantic and Gulf coasts. *US Department of Commerce. Seattle, Washington, USA.*

- Marins, F. O., Novaes, R. L. M., Rocha, R. M., & Junqueira, A. O. R. (2010). Non indigenous ascidians in port and natural environments in a tropical Brazilian bay. *Zoologia (Curitiba)*, 27(2), 213–221. <https://doi.org/10.1590/S1984-46702010000200009>
- Markert, A., Wehrmann, A., & Kröncke, I. (2009). Recently established *Crassostrea*-reefs versus native *Mytilus*-beds: Differences in ecosystem engineering affects the macrofaunal communities (Wadden Sea of Lower Saxony, southern German Bight). *Biological Invasions*, 12(1), 15. <https://doi.org/10.1007/s10530-009-9425-4>
- Marques, F., Takalaga, H. K., Perog, B. D., & Zacherl, D. C. (2021). [Recruitment of native and non-indigenous oysters to treatments with shell and rugosity over one year]. Unpublished raw data.
- Masucci, G. D., & Reimer, J. D. (2019). Expanding walls and shrinking beaches: Loss of natural coastline in Okinawa Island, Japan. *PeerJ*, 7, e7520. <https://doi.org/10.7717/peerj.7520>
- McKinney, F. K., & McKinney, M. J. (2002). Contrasting marine larval settlement patterns imply habitat-seeking behaviours in a fouling and a cryptic species (phylum Bryozoa). *Journal of Natural History*, 36(4), 487–500. <https://doi.org/10.1080/00222930010013755>
- Molnar, J. L., Gamboa, R. L., Revenga, C., & Spalding, M. D. (2008). Assessing the global threat of invasive species to marine biodiversity. *Frontiers in Ecology and the Environment*, 6(9), 485–492.
- Morley, S. A., Toft, J. D., & Hanson, K. M. (2012). Ecological effects of shoreline armoring on intertidal habitats of a Puget Sound urban estuary. *Estuaries and Coasts*, 35(3), 774–784. <https://doi.org/10.1007/s12237-012-9481-3>
- Morris, R. L., Bilkovic, D. M., Boswell, M. K., Bushek, D., Cebrian, J., Goff, J., Kibler, K. M., La Peyre, M. K., McClenachan, G., Moody, J., Sacks, P., Shinn, J. P., Sparks, E. L., Temple, N. A., Walters, L. J., Webb, B. M., & Swearer, S. E. (2019). The application of oyster reefs in shoreline protection: Are we over-engineering for an ecosystem engineer? *Journal of Applied Ecology*, 56(7), 1703–1711. <https://doi.org/10.1111/1365-2664.13390>
- Morris, R. L., Chapman, M. G., Firth, L. B., & Coleman, R. A. (2017). Increasing habitat complexity on seawalls: Investigating large- and small-scale effects on fish assemblages. *Ecology and Evolution*, 7(22), 9567–9579. <https://doi.org/10.1002/ece3.3475>
- Murray, C. C., Pakhomov, E. A., & Therriault, T. W. (2011). Recreational boating: A large unregulated vector transporting marine invasive species. *Diversity and Distributions*, 17(6), 1161–1172. <https://doi.org/10.1111/j.1472-4642.2011.00798.x>
- NOAA (National Oceanic and Atmospheric Administration). (2015). *Guidance for Considering the Use of Living Shorelines*. Available online at: https://www.habitatblueprint.noaa.gov/wp-content/uploads/2018/01/NOAA-Guidance-for-Considering-the-Use-of-Living-Shorelines_2015
- Ostalé-Valriberas, E., Sempere-Valverde, J., Coppa, S., García-Gómez, J. C., & Espinosa, F. (2018). Creation of microhabitats (tidepools) in ripraps with climax communities as a way to mitigate negative effects of artificial substrate on marine biodiversity. *Ecological Engineering*, 120, 522–531. <https://doi.org/10.1016/j.ecoleng.2018.06.023>
- Pederson, E., & Peterson, M. (2002). Bryozoans as ephemeral estuarine habitat and a larval transport mechanism for mobile benthos and young fishes in the north-central Gulf of Mexico. *Marine Biology*, 140(5), 935–947.

- Perkol-Finkel, S., Hadary, T., Rella, A., Shirazi, R., & Sella, I. (2018). Seascape architecture—incorporating ecological considerations in design of coastal and marine infrastructure. *Eco-engineering*, 120, 645–654. <https://doi.org/10.1016/j.ecoleng.2017.06.051>
- Perkol-Finkel, S., & Sella, I. (2014). Ecologically active concrete for coastal and marine infrastructure: innovative matrices and designs. *From Sea to Shore—Meeting the Challenges of the Sea*. 1139-1149. <https://doi.org/10.1680/fsts597571139>
- Perkol-Finkel, S., & Sella, I. (2015). Harnessing urban coastal infrastructure for ecological enhancement. In *Proceedings of the Institution of Civil Engineers-Maritime Engineering* (Vol. 168, No. 3, pp. 102-110). Thomas Telford Ltd. <https://doi.org/10.1680/jmaen.15.00017>
- Perog, B. D., Frantz, D. T., Bowers, C. M., Wolfe, M. L., & Zacherl, D. C. [Bay-wide abundance estimates and recruitment strength of native and non-native oysters (*Ostrea lurida*, *Crassostrea gigas*) in San Diego Bay, CA]. Unpublished technical report. California State University, Fullerton.
- Polson, M. P., Hewson, W. E., Eernisse, D. J., Baker, P. K., & Zacherl, D. C. (2009). You say *Conchaphila*, I say *Lurida*: Molecular evidence for restricting the Olympia oyster (*Ostrea lurida* Carpenter 1864) to temperate western North America. *Journal of Shellfish Research*, 28(1), 11–21. <https://doi.org/10.2983/035.028.0102>
- Polson, M. P., & Zacherl, D. C. (2009). Geographic distribution and intertidal population status for the Olympia Oyster, *Ostrea lurida* Carpenter 1864, from Alaska to Baja. *Journal of Shellfish Research*, 28(1), 69–77. <https://doi.org/10.2983/035.028.0113>
- Pomerat, C. M., & Weiss, C. M. (1946). The influence of texture and composition of surface on the attachment of sedentary marine organisms. *The Biological Bulletin*, 91(1), 57–65. <https://doi.org/10.2307/1538033>
- Raith, M., Zacherl, D. C., Pilgrim, E. M., & Eernisse, D. J. (2015). Phylogeny and species diversity of gulf of California oysters (Ostreidae) inferred from mitochondrial DNA. *American Malacological Bulletin*, 33(2), 263. <https://doi.org/10.4003/006.033.0206>
- Rittschof, D., Branscomb, E. S., & Costlow, J. D. (1984). Settlement and behavior in relation to flow and surface in larval barnacles, *Balanus amphitrite* Darwin. *Journal of Experimental Marine Biology and Ecology*, 82(2), 131–146. [https://doi.org/10.1016/0022-0981\(84\)90099-6](https://doi.org/10.1016/0022-0981(84)90099-6)
- Robinson, T. B., Havenga, B., Van der Merwe, M., & Jackson, S. (2017). Mind the gap – context dependency in invasive species impacts: A case study of the ascidian *Ciona robusta*. *NeoBiota*, 32, 127–141.
- Rodriguez, A. B., Fodrie, F. J., Ridge, J. T., Lindquist, N. L., Theuerkauf, E. J., Coleman, S. E., Grabowski, J. H., Brodeur, M. C., Gittman, R. K., & Keller, D. A. (2014). Oyster reefs can outpace sea-level rise. *Nature Climate Change*, 4(6), 493–497. <https://doi.org/10.1038/NCLIMATE2216>
- Rodriguez, C., & Stoner, A. W. (1990). The epiphyte community of mangrove roots in a tropical estuary: Distribution and biomass. *Aquatic Botany*, 36(2), 117–126. [https://doi.org/10.1016/0304-3770\(90\)90076-W](https://doi.org/10.1016/0304-3770(90)90076-W)
- Rodriguez, L., & Zacherl, D. C. (2021) [The effect of *Amathia verticillata* on Olympia oyster recruitment in]. Unpublished raw data.

- Ruesink, J. (2007). Biotic resistance and facilitation of a non-native oyster on rocky shores. *Marine Ecology Progress Series*, 331, 1–9. <https://doi.org/10.3354/meps331001>
- Ruiz, G. M., Fofonoff, P. W., Carlton, J. T., Wonham, M. J., & Hines, A. H. (2000). Invasion of coastal marine communities in North America: Apparent patterns, processes, and biases. *Annual Review of Ecology and Systematics*, 31(1), 481–531. <https://doi.org/10.1146/annurev.ecolsys.31.1.481>
- Russell, R., Wood, S. A., Allison, G., & Menge, B. A. (2006). Scale, environment, and trophic status: The context dependency of community saturation in rocky intertidal communities. *The American Naturalist*, 167(6), E158–E170. <https://doi.org/10.1086/504603>
- Rzhavsky, A. (1994). On the morphoecology of spirorbid tubes (Polychaeta: Spirorbidae). *Ophelia*, 39, 177–182. <https://doi.org/10.1080/00785326.1994.10429542>
- SAGE (Systems Approach to Geomorphic Engineering). (n.d.). SAGE living shorelines brochure. Retrieved March 5, 2021, from <http://sagecoast.org/info/information.html>
- Sawyer, K. M. (2011). *Settlement preference and the timing of settlement of the Olympia oyster, Ostrea lurida, in Coos Bay, Oregon* [Master's thesis, University of Oregon]. Scholars' Bank.
- Schaefer, M. B. (1937). Attachment of the larvae of *Ostrea gigas*, the Japanese oyster, to plane surfaces. *Ecology*, 18(4), 523–527. <https://doi.org/10.2307/1930578>
- Scyphers, S. B., Powers, S. P., & Heck, K. L. (2015). Ecological value of submerged breakwaters for habitat enhancement on a residential scale. *Environmental Management*, 55(2), 383–391. <https://doi.org/10.1007/s00267-014-0394-8>
- Seitz, R., Lipcius, R., Olmstead, N., Seebo, M., & Lambert, D. (2006). Influence of shallow-water habitats and shoreline development on abundance, biomass, and diversity of benthic prey and predators in Chesapeake Bay. *Marine Ecology Progress Series*, 326, 11–27. <https://doi.org/10.3354/meps326011>
- Sella, I., & Perkol-Finkel, S. (2015). Blue is the new green—ecological enhancement of concrete based coastal and marine infrastructure. *Ecological engineering*, 84, 260–272. <https://doi.org/10.1016/j.ecoleng.2015.09.016>
- Sheehan, E. V., Bridger, D., & Attrill, M. J. (2015). The ecosystem service value of living versus dead biogenic reef. *Estuarine, Coastal and Shelf Science*, 154, 248–254. <https://doi.org/10.1016/j.ecss.2014.12.042>
- Smith, C. S., Puckett, B., Gittman, R. K., & Peterson, C. H. (2018). Living shorelines enhanced the resilience of saltmarshes to Hurricane Matthew (2016). *Ecological Applications*, 28(4), 871–877. <https://doi.org/10.1002/eap.1722>
- Smith, C. S., Rudd, M. E., Gittman, R. K., Melvin, E. C., Patterson, V. S., Renzi, J. J., Wellman, E. H., & Silliman, B. R. (2020). Coming to terms with living shorelines: A scoping review of novel restoration strategies for shoreline protection. *Frontiers in Marine Science*, 7. <https://doi.org/10.3389/fmars.2020.00434>

- Strain, E. M. A., Morris, R. L., Coleman, R. A., Figueira, W. F., Steinberg, P. D., Johnston, E. L., & Bishop, M. J. (2018). Increasing microhabitat complexity on seawalls can reduce fish predation on native oysters. *Eco-engineering*, *120*, 637–644. <https://doi.org/10.1016/j.ecoleng.2017.05.030>
- Strain, E. M. A., Steinberg, P. D., Vozzo, M., Johnston, E. L., Abbiati, M., Aguilera, M. A., Airoldi, L., Aguirre, J. D., Ashton, G., Bernardi, M., Brooks, P., Chan, B. K. K., Cheah, C. B., Chee, S. Y., Coutinho, R., Crowe, T., Davey, A., Firth, L. B., Fraser, C., ... Bishop, M. J. (2021). A global analysis of complexity–biodiversity relationships on marine artificial structures. *Global Ecology and Biogeography*, *30*(1), 140–153. <https://doi.org/10.1111/geb.13202>
- Strain, E. M. A., Cumbo, V. R., Morris, R. L., Steinberg, P. D., & Bishop, M. J. (2020). Interacting effects of habitat structure and seeding with oysters on the intertidal biodiversity of seawalls. *PLOS ONE*, *15*(7), e0230807. <https://doi.org/10.1371/journal.pone.0230807>
- Summerhayes, S. A., Bishop, M. J., Leigh, A., & Kelaher, B. P. (2009). Effects of oyster death and shell disarticulation on associated communities of epibiota. *Journal of Experimental Marine Biology and Ecology*, *379*(1–2), 60–67. <https://doi.org/10.1016/j.jembe.2009.08.006>
- Susick, K., Scianni, C., & Mackie, J. A. (2020). Artificial structure density predicts fouling community diversity on settlement panels. *Biological Invasions*, *22*(2), 271–292. <https://doi.org/10.1007/s10530-019-02088-5>
- Tamburri, M. N., Zimmer, R. K., & Zimmer, C. A. (2007). Mechanisms reconciling gregarious larval settlement with adult cannibalism. *Ecological Monographs*, *77*(2), 255–268. <https://doi.org/10.1890/06-1074>
- Thomsen, M. S., Wernberg, T., Olden, J. D., Griffin, J. N., & Silliman, B. R. (2011). A framework to study the context-dependent impacts of marine invasions. *Journal of Experimental Marine Biology and Ecology*, *400*(1), 322–327. <https://doi.org/10.1016/j.jembe.2011.02.033>
- Thomsen, M., Solgaard, McGlathery, K. J., & Tyler, A. C. (2006). Macroalgal distribution patterns in a shallow, soft-bottom lagoon, with emphasis on the nonnative *Gracilaria vermiculophylla* and *Codium fragile*. *Estuaries and Coasts*, *29*(3), 465–473. <https://doi.org/10.1007/BF02784994>
- Tolley, S. G., & Volety, A. K. (2005). The role of oysters in habitat use of oyster reefs by resident fishes and decapod crustaceans. *Journal of Shellfish Research*, *24*(4), 1007–1012. [https://doi.org/10.2983/0730-8000\(2005\)24\[1007:TROOIH\]2.0.CO;2](https://doi.org/10.2983/0730-8000(2005)24[1007:TROOIH]2.0.CO;2)
- Torres, R. F., Marks, A., Bowers, C. M., Henderson, H. D., & Zacherl, D. C. (2021). [Settlement and recruitment patterns of native and non-indigenous oysters in San Diego Bay, California]. Unpublished raw data. California State University, Fullerton.
- Tracy, B., Larson, K., Ashton, G., Gretchen, G., Chang, A., & Ruiz, G. (2017). Northward range expansion of three non-native ascidians on the west coast of North America. *BioInvasions Records*, *6*(3), 203–209. <https://doi.org/10.3391/bir.2017.6.3.04>
- Tracy, B., & Reyns, N. (2014). Spatial and temporal patterns of native and invasive ascidian assemblages in a Southern California embayment. *Aquatic Invasions*, *9*(4), 441–455. <https://doi.org/10.3391/ai.2014.9.4.03>

- Trimble, A. C., Ruesink, J. L., & Dumbauld, B. R. (2009). Factors preventing the recovery of a historically overexploited shellfish species, *Ostrea lurida* Carpenter 1864. *Journal of Shellfish Research*, 28(1), 97–106. <https://doi.org/10.2983/035.028.0116>
- Tronske, N. B., Parker, T. A., Henderson, H. D., Burnaford, J. L., & Zacherl, D. C. (2018). Densities and zonation patterns of native and non-indigenous oysters in southern California bays. *Wetlands*, 38(6), 1313–1326. <https://doi.org/10.1007/s13157-018-1055-0>
- Twilley, R., Kemp, W., Staver, K., Stevenson, J., & Boynton, W. (1985). Nutrient enrichment of estuarine submersed vascular plant communities. 1. Algal growth and effects on production of plants and associated communities. *Marine Ecology Progress Series*, 23, 179–191. <https://doi.org/10.3354/meps023179>
- Tyrrell, M. C., & Byers, J. E. (2007). Do artificial substrates favor nonindigenous fouling species over native species? *Journal of Experimental Marine Biology and Ecology*, 342(1), 54–60. <https://doi.org/10.1016/j.jembe.2006.10.014>
- USDN/NFECS (U.S. Department of the Navy, Naval Facilities Engineering Command Southwest) & Port of San Diego. (2013). *San Diego Bay Integrated Natural Resources Management Plan, Final September 2013*.
- Vaselli, S., Bulleri, F., & Benedetti-Cecchi, L. (2008). Hard coastal-defence structures as habitats for native and exotic rocky-bottom species. *Marine Environmental Research*, 66(4), 395–403. <https://doi.org/10.1016/j.marenvres.2008.06.002>
- Viola, S. M., Page, H. M., Zaleski, S. F., Miller, R. J., Doheny, B., Dugan, J. E., Schroeder, D. M., & Schroeter, S. C. (2018). Anthropogenic disturbance facilitates a non-native species on offshore oil platforms. *Journal of Applied Ecology*, 55(4), 1583–1593. <https://doi.org/10.1111/1365-2664.13104>
- Vozzo, M. L., Mayer-Pinto, M., Bishop, M. J., Cumbo, V. R., Bugnot, A. B., Dafforn, K. A., Johnston, E. L., Steinberg, P. D., & Strain, E. M. A. (2021). Making seawalls multifunctional: The positive effects of seeded bivalves and habitat structure on species diversity and filtration rates. *Marine Environmental Research*, 165, 105243. <https://doi.org/10.1016/j.marenvres.2020.105243>
- Wagner, E., Dumbauld, B., Hacker, S., Trimble, A., Wisheart, L., & Ruesink, J. (2012). Density-dependent effects of an introduced oyster, *Crassostrea gigas*, on a native intertidal seagrass, *Zostera marina*. *Marine Ecology Progress Series*, 468, 149–160. <https://doi.org/10.3354/meps09952>
- Walters, L., & Wethey, D. (1996). Settlement and early post-settlement survival of sessile marine invertebrates on topographically complex surfaces: The importance of refuge dimensions and adult morphology. *Marine Ecology Progress Series*, 137, 161–171. <https://doi.org/10.3354/meps137161>
- Wasson, K. (2010). Informing Olympia oyster restoration: Evaluation of factors that limit populations in a California estuary. *Wetlands*, 30(3), 449–459. <https://doi.org/10.1007/s13157-010-0056-4>
- Wasson, K., Hughes, B. B., Berriman, J. S., Chang, A. L., Deck, A. K., Dinnel, P. A., Endris, C., Espinoza, M., Dudas, S., Ferner, M. C., Grosholz, E. D., Kimbro, D., Ruesink, J. L., Trimble, A. C., Vander Schaaf, D., Zabin, C. J., & Zacherl, D. C. (2016). Coast-wide recruitment dynamics of Olympia oysters reveal limited synchrony and multiple predictors of failure. *Ecology*, 97(12), 3503–3516. <https://doi.org/10.1002/ecy.1602>

- Wasson, K., Zabin, C. J., Bedinger, L., Cristina Diaz, M., & Pearse, J. S. (2001). Biological invasions of estuaries without international shipping: The importance of intraregional transport. *Biological Conservation*, 102(2), 143–153. [https://doi.org/10.1016/S0006-3207\(01\)00098-2](https://doi.org/10.1016/S0006-3207(01)00098-2)
- Whalan, S., Wahab, M. A. A., Sprungala, S., Poole, A. J., & Nys, R. de. (2015). Larval settlement: The role of surface topography for sessile coral reef invertebrates. *PLOS ONE*, 10(2), e0117675. <https://doi.org/10.1371/journal.pone.0117675>
- White, J. M., Buhle, E. R., Ruesink, J. L., & Trimble, A. C. (2009). Evaluation of Olympia oyster (*Ostrea lurida* Carpenter 1864) status and restoration techniques in Puget Sound, Washington, United States. *Journal of Shellfish Research*, 28(1), 107–112. <https://doi.org/10.2983/035.028.0101>
- Wilkie, E. M., Bishop, M. J., & O'Connor, W. A. (2012). Are native *Saccostrea glomerata* and invasive *Crassostrea gigas* oysters' habitat equivalents for epibenthic communities in south-eastern Australia? *Journal of Experimental Marine Biology and Ecology*, 10. <https://doi.org/10.1016/j.jembe.2012.03.018>
- Wood, V. 2018. *The effect of sedimentation on oysters (Ostrea lurida) adjacent to eelgrass beds (Zostera marina)* (Publication No. 10981447) [Master's thesis, California State University, Fullerton]. ProQuest.
- Zacherl, D.C. (2021). [Settlement and recruitment of *Ostrea lurida* and *Crassostrea gigas* in southern California]. Unpublished raw data. California State University, Fullerton.
- Zacherl, D. C. & Perog, B. D. (2019). [San Diego Bay Native Oyster Restoration Project final report: Recruitment of oysters onto baycrete structures in San Diego Bay]. Unpublished technical report. California State University, Fullerton.
- Zacherl, D. C., Moreno, A., & Crossen, S. (2015). Exploring restoration methods for the Olympia oyster *Ostrea lurida* Carpenter, 1864: Effects of shell bed thickness and shell deployment methods on shell cover, oyster recruitment, and oyster density. *Journal of Shellfish Research*, 34(3), 819–830. <https://doi.org/10.2983/035.034.0311>
- Zu Ermgassen, P. S. E., Spalding, M. D., Blake, B., Coen, L. D., Dumbauld, B., Geiger, S., Grabowski, J. H., Grizzle, R., Luckenbach, M., McGraw, K., Rodney, W., Ruesink, J. L., Powers, S. P., & Brumbaugh, R. (2012). Historical ecology with real numbers: Past and present extent and biomass of an imperilled estuarine habitat. *Proceedings of the Royal Society B: Biological Sciences*, 279(1742), 3393–3400. <https://doi.org/10.1098/rspb.2012.0313>
- Zwerschke, N., Emmerson, M. C., Roberts, D., & O'Connor, N. E. (2016). Benthic assemblages associated with native and non-native oysters are similar. *Marine Pollution Bulletin*, 111(1–2), 305–310. <https://doi.org/10.1016/j.marpolbul.2016.06.094>